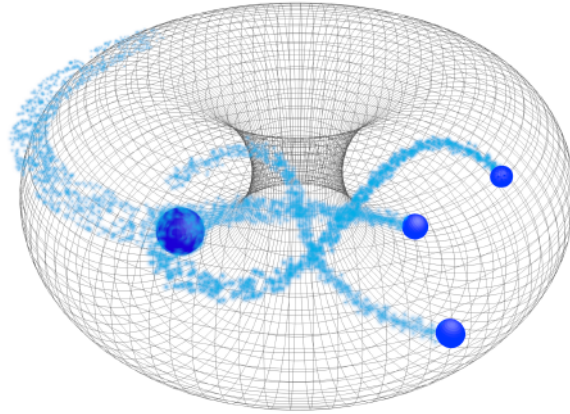


Topological states of matter in frustrated quantum magnetism



Dissertation

eingereicht von

Alexander Wietek, M.Sc. M.Sc.

zur Erlangung des akademischen Grades
“Doctor of Philosophy (Ph.D.)”

Leopold-Franzens-Universität Innsbruck
Fakultät für Mathematik, Informatik und Physik



Betreut von: Univ.-Prof. Dr. Andreas M. Läuchli

Oktober 2017

Abstract / Zusammenfassung

Frustrated quantum magnets may exhibit fascinating collective phenomena. The main goal of this dissertation is to provide conclusive evidence for the emergence of novel phases of matter like quantum spin liquids in local quantum spin models. After a general introduction to frustrated magnetism, spin liquids and the numerical methods employed in part I comprising chapters 1 and 2 we present the main results of the thesis in part II.

We develop novel algorithms for large-scale Exact Diagonalization computations in chapter 3. So-called *sublattice coding methods* for efficient use of lattice symmetries in the procedure of diagonalizing the Hamiltonian matrix are proposed. Furthermore, we suggest a randomized distributed memory parallelization strategy. Benchmarks of computations on various supercomputers with system size up to 50 spin-1/2 particles have been performed.

Results concerning the emergence of a chiral spin liquid in a frustrated kagome Heisenberg antiferromagnet are presented in chapter 4. We confirm previous findings obtained via DMRG calculations using Exact Diagonalization and propose that the chiral spin liquid phase in this model is well described by Gutzwiller-projected wave functions. Also, the stability and extent of this phase are discussed.

In an extended Heisenberg model on the triangular lattice, we establish another chiral spin liquid phase in chapter 5 amongst several magnetically ordered phases. We discuss the special case of the Heisenberg J_1 - J_2 model with nearest and next-nearest neighbor interactions and present a scenario where the critical point of phase transition from the 120° Néel to a putative \mathbb{Z}_2 spin liquid is described by a Dirac spin liquid.

A generalization of the $SU(2)$ Heisenberg model with $SU(N)$ degrees of freedom on the triangular lattice with an additional ring-exchange term is discussed in chapter 6. We present our contribution to the project and the final results that suggest a series of chiral spin liquid phases in an extended parameter range for $N = 3, \dots, 10$.

Finally, we present preliminary data from a Quantum Monte Carlo study of an $SU(N)$ version of the J - Q model on a square lattice in chapter 7. We study this model for $N = 2, \dots, 10$ and multi-column representations of $SU(N)$ and establish the phase boundary between the Néel ordered phase and the disordered phases for $J, Q \geq 0$. The disordered

phase in the four-column representation is expected to be a two-dimensional analog of the Haldane phase for the spin-1 Heisenberg chain.

Deutsche Zusammenfassung

Frustrierte Quantenmagnete können faszinierende kollektive Phänomene aufweisen. Das Ziel dieser Dissertation ist es schlüssigen Nachweis für die Emergenz neuer Materiezustände wie Quantenspinflüssigkeiten in lokalen Quantenspinmodellen zu erbringen. Nach einer allgemeinen Einleitung in frustrierten Magnetismus, Spinflüssigkeiten und die verwendeten numerischen Methoden in Teil I, bestehend aus Kapitel 1 und 2 stellen wir die wichtigsten Ergebnisse dieser Arbeit in Teil II vor.

Wir entwickeln neue Algorithmen für skalierbare Exakte Diagonalisierung in Kapitel 3. So genannte *Untergitterkodierungsmethoden* zur effizienten Nutzung von Gittersymmetrien im Vorgang der Diagonalisierung der Hamiltonmatrix werden vorgeschlagen. Desweiteren stellen wir eine randomisierte Parallelisierungsstrategie für verteilte Speichersysteme vor. Benchmarks mit Systemgrößen bis zu 50 Spin-1/2 Teilchen wurden auf mehreren Supercomputern durchgeführt.

Ergebnisse zur Emergenz von chiralen Spinflüssigkeiten in einem erweiterten Heisenberg Antiferromagneten auf dem Kagome-Gitter werden in Kapitel 4 vorgestellt. Wir bestätigen vorangegangene DMRG Studien mithilfe der Exakten Diagonalisierung und zeigen auf, dass diese chirale Spinflüssigkeit gut mithilfe Gutzwiller-projizierter Wellenfunktionen beschrieben werden kann. Desweiteren werden die Stabilität und die Ausdehnung dieser Phase behandelt.

In einem erweiterten Heisenbergmodell auf dem Dreiecksgitter bringen wir den Nachweis einer weiteren chiralen Spinflüssigkeitsphase zwischen mehreren magnetisch geordneten Phasen in Kapitel 5. Wir besprechen den Spezialfall des Heisenberg J_1 - J_2 Modells mit nächster- und übernächster-Nachbar Wechselwirkung und stellen ein Szenario vor, bei welchem der kritische Punkt des Phasenübergangs zwischen der 120° Néel geordneten und der mutmaßlichen \mathbb{Z}_2 Spinflüssigkeit durch eine Dirac Spinflüssigkeit beschrieben wird.

Eine Verallgemeinerung des $SU(2)$ Heisenberg Modells mit $SU(N)$ Freiheitsgraden auf dem Dreiecksgitter mit zusätzlichem Ringaustauschterm wird in Kapitel 6 diskutiert. Wir stellen unseren Beitrag zum Projekt und die endgültigen Ergebnisse vor, welche eine Reihe von chiralen Spinflüssigkeitsphasen in einer ausgedehnten Parameterregion für $N = 3, \dots, 10$.

Zuletzt stellen wir vorläufige Daten einer Quanten Monte Carlo Studie zu einer $SU(N)$ Version des J - Q Modells auf dem Quadratgitter vor. Wir untersuchen dieses Modell für $N = 2, \dots, 10$ und Darstellungen mit mehreren Spalten von $SU(N)$ und stellen den Phasenübergangspunkt von der Néel geordneten zur ungeordneten Phase für $J, Q \geq 0$ fest. Es wird erwartet, dass die ungeordnete Phase in der vier-Spalten Darstellung ein zweidimensionales Analogon zur Haldane Phase der Spin-1 Heisenberg Kette ist.

Acknowledgements

First things first. During my doctoral studies, I learned that scientific work and writing a Ph.D. thesis is quite an undertaking. Luckily, I received support from many people who I would like to explicitly mention here and to whom I want to express my sincere gratitude.

As my supervisor, Andreas Läuchli introduced me to the exciting world of physics research. I am deeply grateful for his scientific advice and the interesting projects he pointed out to me. I greatly enjoyed the frequent scientific discussions that have always been very inspiring for me, his friendly and forthcoming attitude and his ongoing support. Moreover, I would like to thank Andreas for giving me the opportunity to visit many conferences and workshops. Thank you very much!

I am very happy to have had such amazing working colleagues, which lightened up the everyday life at the Institute for Theoretical Physics. It has been a pleasure to share an office with Michael Schuler all the time. Discussing, working and developing software together has had very positive impact on this thesis. My work benefited a lot all the discussions with Antoine Sterdyniak, Louis-Paul Henry, and Thomas Lang, to whom I could always turn to for scientific questions. I would also like to thank Carlo Krimphoff, Lars Bonnes, Elke Stenico, Andreas Parteli, Christian Romen, Michael Rader and Clemens Ganahl for making the time at the institute so enjoyable.

I had the great opportunity to visit Syngé Todo at the University of Tokyo for six months, which has been nothing short of an amazing experience. I would like to thank Syngé Todo for accepting me as an exchange student, for introducing me to the Quantum Monte Carlo technique and for his scientific advice. Working in his group broadened my horizon both scientifically as well as personally. I benefited a lot from discussions with Hidemaro Suwa and would like to thank also the other members of the lab, especially Kai Shimagaki, Toshiki Horita and Fumihiro Ishikawa for showing me a good time in Tokyo. Furthermore, I would once again like to thank Andreas Läuchli for his financial support during that time and acknowledge the financial support from the Marietta Blau Stipendium.

The good times I shared with my friends and family mean a lot to me and I would

like to sincerely thank all of them. I feel very lucky to have received so much help and understanding, especially by my parents. Most of all I would like to thank my wonderful wife, Christina Kurzthaler, who always had an open ear for my smaller and sometimes bigger troubles. Her ongoing support and encouragement have made everything, be it research or everyday life, so much easier and so much more delightful.

Contents

Abstract / Zusammenfassung	iv
Acknowledgements	vi
I. Preliminaries	1
1. Introduction	3
1.1. Frustrated Magnetism	9
1.1.1. Magnetic order	9
1.1.2. Mechanisms of Disorder	14
1.1.3. Order-by-Disorder principle	18
1.2. Quantum Spin Liquids	20
1.2.1. Gapless and gapped phases	20
1.2.2. Resonating Valence Bond Liquids	23
1.2.3. Parton construction and mean-field theory	26
1.2.4. Chiral Spin Liquids	30
1.2.5. Dirac Spin Liquids	33
2. Methods	35
2.1. Exact Diagonalization	35
2.1.1. Representing Hilbert spaces and operators	36
2.1.2. The Lanczos algorithm	37
2.1.3. Symmetries and symmetry-adapted wave functions	41
2.2. Variational Monte Carlo	47
2.2.1. Markov Chain Monte Carlo	48
2.2.2. Stochastic sampling of quantum wave functions	49
2.2.3. Coefficients of Gutzwiller projected wave functions	50

II. Research projects	53
3. Symmetries and Parallelization for Large-Scale Exact Diagonalization	55
3.1. Introduction	55
3.2. Sublattice Coding techniques	57
3.3. Distributed and hybrid memory parallelization	64
3.4. Benchmarks	69
3.5. Conclusion	71
4. Nature of chiral spin liquids on the kagome lattice	73
4.1. Introduction	73
4.2. Model	75
4.3. Energy spectroscopy	77
4.4. Parton construction and overlaps	78
4.5. Conclusion	82
5. Chiral Spin Liquid and Quantum Criticality in Extended $S = 1/2$ Heisenberg Models on the Triangular Lattice	83
5.1. Introduction	83
5.2. Model	85
5.3. Phase diagram	86
5.4. Chiral Spin Liquids	87
5.5. Spin disordered state in the $J_1 - J_2$ Heisenberg model	90
5.6. Conclusion	92
6. Chiral Spin Liquids in Triangular-Lattice $SU(N)$ Fermionic Mott Insulators with Artificial Gauge Fields	93
6.1. Construction of the $SU(N)$ chiral spin liquid	94
7. $SU(N)$ J-Q model on the square lattice with multi-column representations	103
7.1. Introduction	103
7.2. Model	105
7.3. Strange correlator of $SU(N)$ Heisenberg chains	106
7.4. Spin disordered states in Q -only model	109
7.5. Conclusion and Outlook	110
8. Conclusion and Outlook	113

Appendices	117
A. Representation theory for space groups	121
B. Tower of States analysis	123
References	133
List of Publications	155
Eidesstattliche Erklärung	157

I

Preliminaries

A beginning is the time for taking the most delicate care that the balances are correct.

FRANK HERBERT, *Dune*

Microscopic particles like electrons, neutrons, and protons build up the matter that surrounds us in everyday life. While the fundamental physical laws that describe the interaction between electrons and the atomic nuclei are as of today well understood, predicting the behavior of many particles interacting with each other remains a great challenge. The behavior of a macroscopic amount of non-interacting particles can be deduced from averaging over the behavior of single particles. Often, also weakly interacting particles behave as if they are essentially non-interacting. Strong interactions, on the other hand, may lead to exciting collective phenomena. Understanding the emergence of macroscopic behavior from strongly interacting microscopic constituents is a challenging, yet fascinating, task.

The ratio between kinetic and interaction energy of microscopic particles is set by temperature. Low temperatures decrease the kinetic energy of particles, thus making interaction effects more pronounced, as can prominently be observed in ferromagnetic materials. While the spin degrees of freedom strongly fluctuate at high temperatures, they collectively align in the same direction once cooled down below the Curie temperature. In particular, the tendency to align in the same direction is due to the exchange interaction of the spin degrees of freedom. This order-to-disorder transition in ferromagnets can be explained by Landau's theory of symmetry breaking. The disordered state is symmetric under spin rotations, while the ordered state chooses a preferred direction and the symmetry is not respected by the state of the system. The principle of symmetry breaking explains most known phase transitions and is a major cornerstone in the theory of condensed matter physics.

However, there are phases of matter whose theoretical description is beyond Landau's

1. Introduction

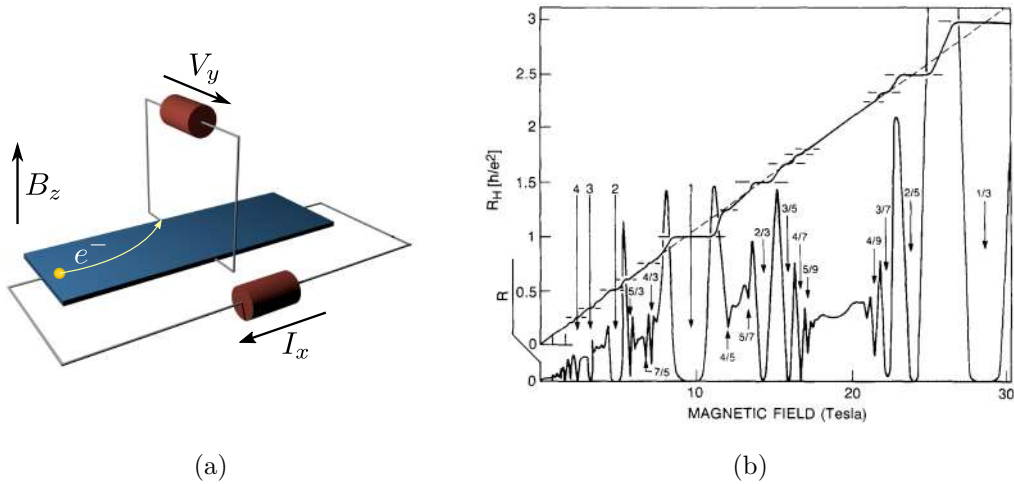


Figure 1.1.: The Fractional Quantum Hall effect. a) Sketch of the experimental setup for measuring Hall effects, B_z denotes the magnetic field, I_x the applied current and V_y the measured Hall voltage b) Measurements of the low-temperature Hall resistance $R_H (= R_{xy})$ and the diagonal resistivity R from [3]. Plateaux appear at fractional values of the filling fraction ν .

theory. The fractional quantum Hall effect, short FQHE, discovered experimentally by Tsui, Stormer and Gossard in 1982 [1] is understood to exhibit a novel kind of ordering. The FQHE is a variant of the Hall effect, where electrons are confined to two dimensions at low temperatures and high magnetic fields, as can be realized in GaAs-AlGaAs heterojunctions [1, 2]. The Hall resistance is defined by

$$R_{xy} = \frac{V_y}{I_x}, \quad (1.0.1)$$

where V_y is the Hall voltage and I_x the applied current. It exhibits plateaux at certain quantized values

$$R_{xy} = \frac{1}{\nu} \frac{2\pi\hbar}{e^2}, \quad (1.0.2)$$

which depends on fundamental physical constants as the elementary charge e and Plank's constant \hbar , cf. Fig. 1.1. ν is called the filling fraction and sets the plateau of the Hall resistance. Integer filling fractions $\nu = 1, 2, 3, \dots$ constitute the integer quantum Hall effect and fractional filling fractions $\nu = \frac{1}{3}, \frac{1}{5}, \frac{2}{3}, \dots$ constitute the fractional quantum Hall effect, respectively. Phase transitions between different filling fractions are observed when tuning the applied magnetic field. The electrons are strongly interacting via the Coulomb force and form collective many-body quantum states with intriguing properties in FQHE plateaux. Firstly, different FQHE plateaux share the same symmetry properties. A phase transition between these plateaux cannot be explained by Landau's theory of phase

transitions, instead, the novel concept of topological order was introduced [4]. Different phases in the FQHE are understood to have different topological orders which cannot be adiabatically connected without observing a phase transition.

Topologically ordered phases exhibit a wide variety of exciting phenomena. One of which is the fractionalization of quasiparticles. Elementary excitations of FQHE states may have a charge which is a fraction of the elementary charge of an electron. Thus, while the microscopic constituents are electrons with exactly one elementary charge, emergent quasiparticles may have, e.g. $1/3$ of the elementary charge. This charge fractionalization has already been observed in experiments [5]. Another theoretically predicted property of the quasiparticles is non-trivial statistical behavior. If two bosons or fermions are interchanged their many-body wave function attains a phase of 0 or π respectively due to (anti-)symmetry. Emergent quasiparticles of topologically ordered phases in two dimensions may exhibit a different behavior. The phase for interchanging may be different from 0 or π . In this case, the quasiparticles are called *anyons*. More generally, the process of interchanging or braiding topological quasiparticles may act nontrivially on the space of degenerate states with a given number of quasiparticles in which case the quasiparticles are called non-Abelian anyons.

The discovery of novel phases of matter has in the past often given rise to new technologies. The impact of, for example, semiconductors or liquid crystal devices is hard to overestimate. Since topological order is a completely new paradigm of phases of matter, naturally the question arises what technologies such states can be used for. Although technological breakthroughs are hard to predict, it has been suggested that topological states of matter can be used to implement fault-tolerant quantum computation or quantum memory devices [6]. Many approaches to quantum computation, like trapped ions [7, 8] suffer the problem that small local disturbances to the physical system cause decoherence since information is stored locally in those systems. The approaches to topological quantum computation circumvent this problem by encoding the information globally over the entire system. Changing the state of the system with local perturbations is exponentially suppressed in the system size, thus information can be stored robustly. The implementation of quantum gates for performing computations can be achieved by using the statistical properties of non-Abelian anyons.

Apart from the FQHE also different physical systems are expected to exhibit phase transitions that are beyond Landau's theory. In the context of high-temperature superconductivity of cuprates [9] like La_2CuO_4 it was found that the system can approximately be described by the Hubbard model [10]

$$H = -t \sum_{\substack{\langle i,j \rangle \\ \alpha=\uparrow,\downarrow}} (c_{i\alpha}^\dagger c_{j\alpha} + \text{H.c.}) + U \sum_i n_{i,\uparrow} n_{i,\downarrow}, \quad (1.0.3)$$

where $c_{i\alpha}^\dagger$, $c_{i\alpha}$ are electron creation and annihilation operators, $n_{i,\alpha} = c_{i,\alpha}^\dagger c_{i,\alpha}$, $\langle i, j \rangle$ denotes the sum over nearest neighbour pairs and t and U are the hopping and on-site repulsion

1. Introduction

strength. Compounds like La_2CuO_4 are expected to be close to half-filling, i.e. the number of up or down spin fermions is exactly half the number of lattice sites. In the strong coupling, or Mott-insulating limit $t \ll U$ the effective low energy model is given by a quantum Heisenberg model of the form

$$H = J \sum_{\langle i,j \rangle} \mathbf{S}_i \cdot \mathbf{S}_j, \quad (1.0.4)$$

The coupling constant is given by $J = t^2/U$ and $\mathbf{S}_i = (S_i^x, S_i^y, S_i^z)^T$ denotes spin operators at position i . Anderson proposed in 1987 that the ground state of the Heisenberg model Eq. (1.0.4) could be a so-called *resonating valence bond*, short RVB state under certain circumstances which would yield an explanation for high temperature superconductivity [11]. The RVB state is an example of a so-called *quantum spin liquid* state which is, apart from the FQHE states, another class of states that may exhibit topological order. We will discuss these states in more detail in section 1.2.

The Heisenberg model Eq. (1.0.4) and extensions thereof have been studied in a plethora of situations. The physics of the system Eq. (1.0.4) depends strongly on the sign of the coupling constant J . For $J < 0$ the model is called *ferromagnetic* and it becomes energetically favorable for neighboring spins to align in the same direction. Similarly, the model is called *antiferromagnetic* for $J > 0$ and neighboring spins are energetically favored to align in the opposite direction.

A famous exact analytical solution by Hans Bethe [12] is known for the case of local spin-1/2 on a chain lattice. In most cases, an analytical solution is not known. Until today an analytical solution of the two-dimensional quantum spin-1/2 Heisenberg antiferromagnet on a square lattice has not been found. Yet, analytical approximations like linear spin-wave theory [13] or numerical techniques like Exact Diagonalization[14] or Quantum Monte Carlo [15] have by now firmly established that the ground state of this system is magnetically ordered. We will discuss magnetic ordering in more detail in section 1.1.1.

In many situations, magnetic materials which are described by models like Eq. (1.0.4) are disordered at high temperatures and ordered at low temperatures. This need not necessarily be the case, as certain mechanisms may prevent a system to develop magnetic order at low temperatures or even in the ground state. Famous materials not ordering at even lowest experimental accessible temperatures include Herbertsmithite $\text{ZnCu}_3(\text{OH})_6\text{Cl}_2$ [16] or organic Mott insulators like $\text{EtMe}_3\text{Sb}[\text{Pd}(\text{dmit})_2]_2$ [17, 18] or $\kappa\text{-(BEDT-TTF)}_2\text{Cu}_2(\text{CN})_3$ [19, 20]. The main ingredients preventing magnetic ordering are a low spin quantum number of the magnetic ions, reduced dimension of the effective interactions at low temperatures, and geometrical frustration. We will describe the effect of these mechanisms in detail in section 1.1.2. The material Herbertsmithite Fig. 1.2, for example, fulfills these criteria very well: the local magnetic Cu^{2+} ions with spin-1/2 are aligned in two-dimensional layers which form a highly frustrated kagome geometry. Indeed neutron scattering experiments show absence of magnetic ordering at lowest experimentally attainable temperatures [16].

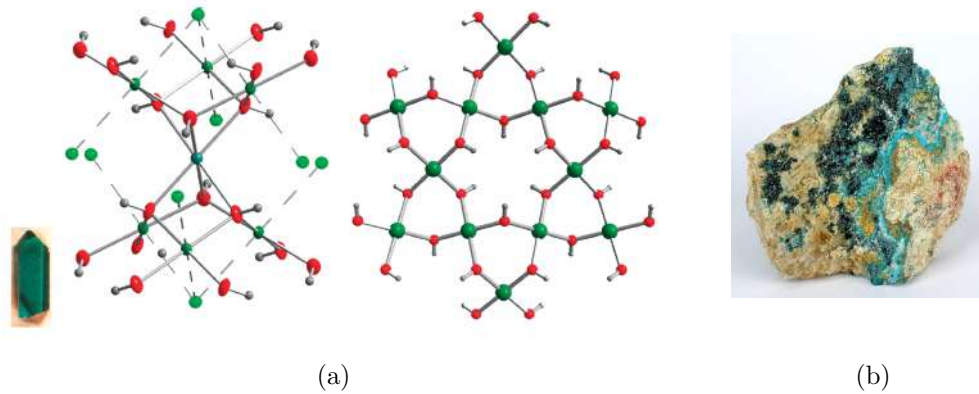


Figure 1.2.: Herbertsmithite $\text{ZnCu}_3(\text{OH})_6\text{Cl}_2$. a) schematic crystal structure. Reprinted with permission from [21]. Copyright 2017 American Chemical Society. Blue, green, bright green, red, and gray spheres represent Zn, Cu, Cl, O, and H atoms, respectively [21]. The magnetic Cu^{2+} ions form two-dimensional kagome planes which are weakly coupled amongst each other. b) Naturally occurring Herbertsmithite (blue crystal) in a rock compound (from Wikimedia Commons, photograph by Rob Lavinsky, iRocks.com – CC-BY-SA-3.0)

The nature of disordered states in low-dimensional frustrated quantum magnets is a highly interesting topic. In many cases, these disordered states are expected to differ drastically from trivial paramagnetic phases with a low degree of quantum entanglement. Indeed, some of these states may exhibit topological order similar to the FQHE. Such states are called *Quantum Spin Liquids*. Many of them have been proposed as the ground state of frustrated quantum antiferromagnets. Prominently, Anderson’s RVB liquid has been proposed as the ground state of the triangular lattice spin $1/2$ Heisenberg antiferromagnet [22]. Similarly, so-called *chiral spin liquids* have been envisioned as the ground state for certain frustrated models [23]. Chiral spin liquids are a direct analog of FQHE wave functions for spin systems [24]. Whereas, the ground state of the triangular lattice spin- $1/2$ Heisenberg antiferromagnet is by now understood to be magnetically ordered [25], the nature ground state of the model on the kagome lattice is still highly debated and suggested to be a quantum spin liquid [26–40]. We will discuss quantum spin liquids in detail in section 1.2.

There are several exactly solvable models which can be proven to stabilize a quantum spin liquid ground state, famously Kitaev’s Toric Code [41], Kitaev’s honeycomb model [42], or quantum dimer models [31, 43]. Also recently exact parent Hamiltonians for chiral spin liquids have been found [44–46]. The interactions between the particles in those models are nevertheless often not realistic to be realized in an experimental setup. It is thus an important question whether simpler models might give rise to the emergence

1. Introduction

of quantum spin liquids.

In absence of exact analytical solutions, one has to employ other methods for studying quantum spin systems. Frustrated quantum magnets are strongly correlated phases of matter where the interactions between particles dominate the physics of the system. Therefore, many standard analytical techniques like perturbation theory from a non-interacting limit or mean-field approaches often fail to predict the correct behavior. Numerical methods, on the other hand, have proven as valuable tools to gain insight to strongly correlated electron systems. Amongst the most prominent numerical methods for studying quantum spin systems are Exact Diagonalization, Quantum Monte Carlo, Variational Monte Carlo [47], density matrix renormalization group, short DMRG [48], or tensor network algorithms [49]. Each of the methods comes with its advantages and disadvantages and some are particularly suited for certain problems. In the course of this thesis the Exact Diagonalization, Variational Monte Carlo and Quantum Monte Carlo methods have been developed and applied. We give a short description of these methods in section 2.1, section 2.2.

1.1. Frustrated Magnetism

*That's what the world is, after all:
an endless battle of contrasting memories.*

HARUKI MURAKAMI, 1Q84

Frustrated quantum magnets are currently studied intensely by both experimentalists and theoreticians. On the experimental side, many materials are studied for their intriguing properties. A detailed survey of those and the experimental methods for investigating their physical properties can be found in Ref. [50]. Here we give a short introduction to the theoretical aspects. We describe how the principle of spontaneous symmetry breaking manifests itself in quantum magnets as magnetic order in section 1.1.1. Interesting phenomena such as the emergence of quantum spin liquids may occur when the system is disordered even at lowest temperatures. There are several mechanisms preventing the system from ordering when cooled down which we explain in section 1.1.2. Often, these mechanisms lead to a massive degeneracy of ground states. The order-by-disorder principle discussed in section 1.1.3 may favor certain submanifold of these states due to thermal or quantum fluctuations and therefore give rise to unexpected emergent states of matter.

1.1.1. Magnetic order

Patterns of magnetic ordering are energetically favorable in many spin systems. Consider the ferromagnetic Ising model

$$H_{\text{Ising}} = J \sum_{\langle i,j \rangle} \sigma_i \cdot \sigma_j + h \sum_i \sigma_i, \quad (1.1.1)$$

where $\sigma_i = \pm 1$ are classical Ising spins with $J < 0$ and h denotes an external magnetic field. For $h = 0$ the ferromagnetic states $|\uparrow \cdots \uparrow\rangle$ and $|\downarrow \cdots \downarrow\rangle$ with all spins aligned in the same direction are the ground states. The system in the ground state at $h = 0$ is magnetically ordered. Thermal fluctuations favor entropy and the system becomes a disordered paramagnetic state at high temperatures.

Magnetic order is an instance of spontaneous symmetry breaking. The Ising model Eq. (1.1.1) at $h = 0$ is invariant under global spin flips, $\sigma_i \rightarrow -\sigma_i$, thus possesses a discrete \mathbb{Z}_2 symmetry. In two or more dimensions the model exhibits an order-to-disorder transition at finite temperature [51]. In the ordered phase this symmetry is not respected by the equilibrium ground states and the magnetization order parameter

$$\langle m \rangle = \frac{1}{N} \sum_j \langle \sigma_j \rangle, \quad (1.1.2)$$

attains a finite value in the thermodynamic limit in the sense that

$$\lim_{h \rightarrow 0} \lim_{N \rightarrow \infty} \langle m \rangle \neq 0. \quad (1.1.3)$$

1. Introduction

Here, $\langle \dots \rangle$ denotes a classical ensemble average and N the number of lattice sites. The degeneracy of the ground state is twofold, thus discrete in the thermodynamic limit.

Another fundamental model describing magnetic materials is the quantum Heisenberg model

$$H = \sum_{i,j} J_{ij} \mathbf{S}_i \cdot \mathbf{S}_j + h \sum_j e^{-i\mathbf{Q}\cdot\mathbf{r}_j} S_j^z + \text{H.c.}, \quad (1.1.4)$$

where $\mathbf{S}_i = (S_i^x, S_i^y, S_i^z)^T$ are quantum mechanical SU(2) spin operators and J_{ij} are coupling constants. \mathbf{r}_j denotes the position of the i -th spin and \mathbf{Q} defines an ordering vector. The Heisenberg model Eq. (1.1.4) is invariant under continuous global SU(2) spin rotations for vanishing external field $h = 0$, i.e.

$$\left[H, \sum_i S_i^\alpha \right] = 0 \quad \text{at} \quad h = 0, \quad (1.1.5)$$

for $\alpha = x, y, z$. The ordered magnetization with ordering vector \mathbf{Q} is defined by

$$\langle m^{\mathbf{Q}} \rangle = \frac{1}{N} \sum_j e^{-i\mathbf{Q}\cdot\mathbf{r}_j} \langle S_j^z \rangle, \quad (1.1.6)$$

where $\langle \dots \rangle = \frac{1}{\mathcal{Z}} \text{Tr}(e^{-\beta H} \dots)$ denotes the quantum statistical average at inverse temperature β and partition function $\mathcal{Z} = \text{Tr}(e^{-\beta H})$. The ordered magnetization $\langle m^{\mathbf{Q}} \rangle$ is not invariant under the SU(2) symmetry group of spin rotations and can, therefore, be used as an order parameter to detect spontaneous symmetry breaking,

$$\lim_{h \rightarrow 0} \lim_{N \rightarrow \infty} \langle m^{\mathbf{Q}} \rangle \neq 0. \quad (1.1.7)$$

The phenomenology of spontaneous symmetry breaking of a continuous symmetry is more diverse than in the discrete case. In the thermodynamic limit, the ground state becomes infinitely degenerate due to the continuous nature of the symmetry group [52, 53].

There are certain characteristic phenomena when approaching the thermodynamic limit in systems breaking a continuous symmetry. Ferromagnetic Heisenberg models with $J_{ij} < 0$ for all i and j always admit the fully polarized ground state

$$|\text{ferro}\rangle = |\uparrow\uparrow \dots \uparrow\rangle, \quad (1.1.8)$$

with all spins aligned in one direction. Yet, the ground state is at least $(2SN + 1)$ degenerate where S denotes the local value of the spin. This is because the multiplet with total spin $SN(SN + 1)$ can be generated by rotating the fully polarized state in Eq. (1.1.8).

The situation is quite different for antiferromagnetic models $J_{ij} > 0$. The simple analog of the fully polarized state in Eq. (1.1.8) would be the classical *Néel state* [54]

$$|\text{Néel}\rangle = |\uparrow\downarrow\uparrow\downarrow \dots\rangle. \quad (1.1.9)$$

Even for an antiferromagnetic Ising model this state is only the ground state if the lattice is bipartite and antiferromagnetic interactions only connect sites between the two disjoint sublattices. This is not the case for frustrated geometries, cf. section 1.1.2. Moreover, this state is not an eigenstate of the antiferromagnetic Heisenberg model. For a two-site spin-1/2 Heisenberg interaction the eigenstates and eigenvalues are given by

$$\mathbf{S}_1 \cdot \mathbf{S}_2 |S = 0, m = 0\rangle = -\frac{3}{4} |S = 0, m = 0\rangle = -\frac{3}{4} (|\uparrow\downarrow\rangle - |\downarrow\uparrow\rangle) \quad (1.1.10)$$

$$\mathbf{S}_1 \cdot \mathbf{S}_2 \begin{cases} |S = 1, m = 1\rangle \\ |S = 1, m = 0\rangle \\ |S = 1, m = -1\rangle \end{cases} = +\frac{1}{4} \begin{cases} |S = 1, m = 1\rangle \\ |S = 1, m = 0\rangle \\ |S = 1, m = -1\rangle \end{cases} = +\frac{1}{4} \begin{cases} |\uparrow\uparrow\rangle \\ |\uparrow\downarrow\rangle + |\downarrow\uparrow\rangle \\ |\downarrow\downarrow\rangle \end{cases} \quad (1.1.11)$$

The ground state with energy $-\frac{3}{4}$ is a rotationally invariant spin singlet. The fact that the ground state has total spin zero is not only true for the two site interaction but for generic bipartite antiferromagnetic Heisenberg models on a finite lattice. This is known as Marshall's theorem and has been mathematically proven in Refs. [55, 56]. This result only holds for finite size geometries. In order to break the SU(2) symmetry, a set of higher spin- S states approaches the ground state energy. This set of states is called the *Anderson tower of states* and is characteristic for spontaneous breaking of a continuous symmetry. The excitation energy of these states is proportional to $S(S+1)/N$, thus collapses linearly to the ground state energy for $N \rightarrow \infty$. A typical finite size spectrum obtained from Exact Diagonalization of the Heisenberg spin-1/2 square lattice antiferromagnet on 32 lattice sites is shown in Fig. 1.3. Quantum numbers such as total spin, quasimomentum and point group representations of the states occurring in the tower of states can actually be predicted for a given magnetic order and give a strong evidence that a certain order is realized by the system. The method of extracting these quantum numbers is explained in appendix B and more detailed in Ref. [57].

Spontaneous symmetry breaking in the sense of Eq. (1.1.7) implies *long-range order* of the spin correlation functions

$$\lim_{|r_i - r_j| \rightarrow \infty} \langle \mathbf{S}_i \cdot \mathbf{S}_j \rangle \neq 0. \quad (1.1.12)$$

For translationally invariant systems, the static magnetic structure factor

$$\mathcal{S}(\mathbf{k}) = \sum_j e^{i\mathbf{k} \cdot (\mathbf{r}_j - \mathbf{r}_0)} \langle \mathbf{S}_j \cdot \mathbf{S}_0 \rangle, \quad (1.1.13)$$

is the Fourier-transform of the spin correlation function. Long-range order implies the divergence of the structure factor at an ordering wave vector \mathbf{Q} .

Every pattern of magnetic ordering on regular lattice has one or several characteristic ordering vectors \mathbf{Q} . Ferromagnetic order is peaked at $\mathbf{Q} = \Gamma \equiv \mathbf{0}$ whereas a square lattice Néel antiferromagnetic order is peaked at $\mathbf{Q} = M \equiv (\pi, \pi)$. The ordering vector

1. Introduction

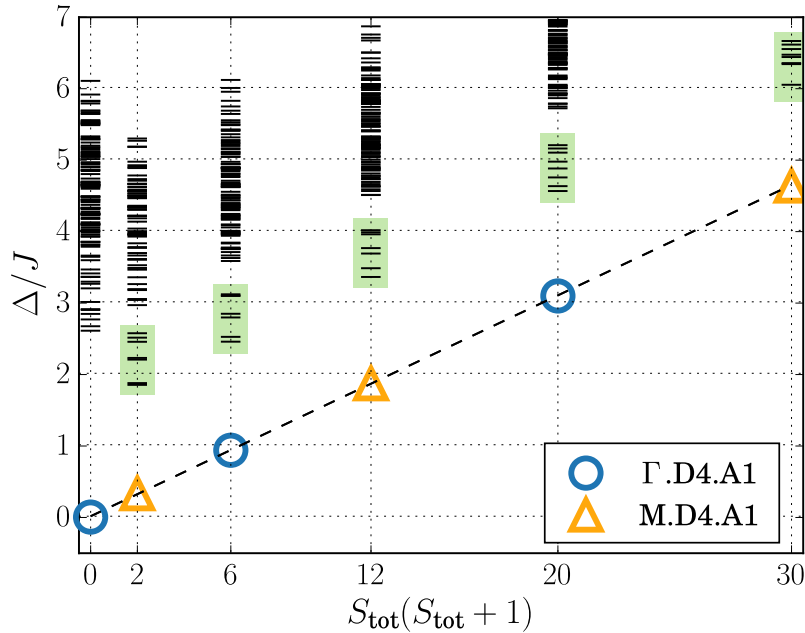


Figure 1.3.: Many-body energy spectrum of the 32 site spin-1/2 Heisenberg antiferromagnet on a square lattice geometry. States are differentiated by their total spin quantum number $S(S + 1)$. The quasimomentum of the states in the Anderson tower is given by Γ and M with $D4$ point group representation $A1$. For details on the representation theory and quantum numbers of space groups see appendix A. The levels with the green background are the magnon (Goldstone mode) levels and exhibit a linear dispersion relation.

Q does not uniquely define an ordering pattern. Thus, there can be multiple ordering patterns with the same ordering vector. Ref. [58] gives a classification of possible patterns of magnetic orderings and presents their prominent features, including the peaks of the structure factor in reciprocal space. Fig. 1.4 shows the spin correlations of the 120° Néel ordered ground state of the triangular lattice spin-1/2 Heisenberg antiferromagnet on a 36 site lattice and its corresponding static spin structure factor in reciprocal space.

A hallmark feature in systems breaking a continuous symmetry is the occurrence of gapless low-energy modes. These modes are called Goldstone modes [59, 60] and are a general phenomenon occurring in many branches of physics. For spin systems, they are called *magnons* or *spin waves*. The Goldstone theorem states that these gapless modes necessarily need to exist once a continuous symmetry is spontaneously broken. We state the theorem in the form presented in Ref. [61] where also an elementary proof is given.

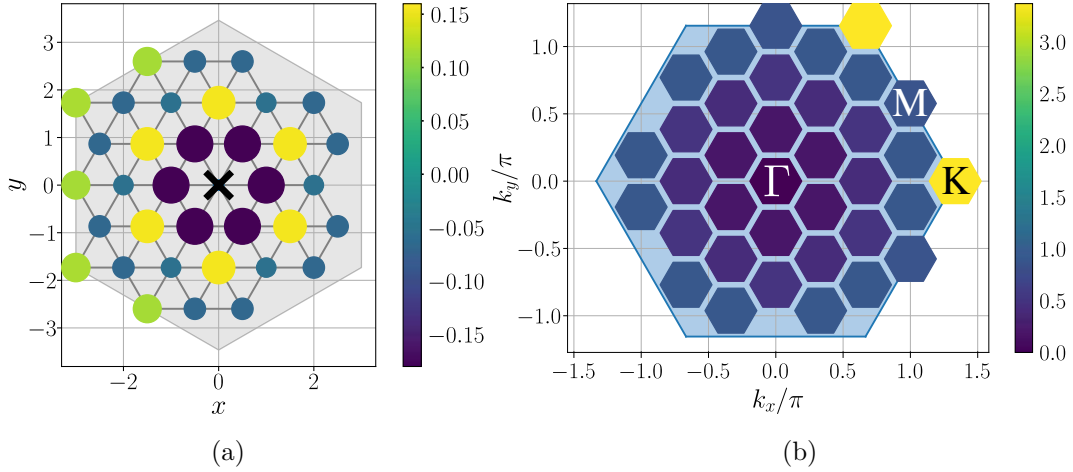


Figure 1.4.: Spin correlations $\langle \mathbf{S}_i \cdot \mathbf{S}_0 \rangle$ (a) and structure factor $\mathcal{S}(\mathbf{k})$ (b) for the ground state of the antiferromagnetic spin-1/2 Heisenberg nearest neighbour model on a 36 site triangular lattice. The black cross in (a) marks the spin \mathbf{S}_0 . The ground state is 120° Néel ordered [25] and shows a peak in the structure factor at the K point in the Brillouin zone.

Theorem (Goldstone's theorem). *Consider the generic Heisenberg Hamiltonian*

$$H = \sum_{ij} J_{ij} \mathbf{S}_i \cdot \mathbf{S}_j, \quad (1.1.14)$$

satisfying the following locality condition

$$\frac{1}{N} |J_{ij}| |\mathbf{r}_i - \mathbf{r}_j| < \infty. \quad (1.1.15)$$

If the spin structure factor Eq. (1.1.13) diverges at some finite wave vector \mathbf{Q}

$$\lim_{\mathbf{k} \rightarrow \mathbf{Q}} \mathcal{S}(\mathbf{k}) \rightarrow \infty, \quad (1.1.16)$$

then there exists an eigenstate with momentum \mathbf{k} , whose energy $E(\mathbf{k})$ vanishes at \mathbf{Q}

$$\lim_{\mathbf{k} \rightarrow \mathbf{Q}} E(\mathbf{k}) = 0. \quad (1.1.17)$$

The magnon modes can already be detected in finite size spectra, cf. Fig. 1.3. Their behavior can be approximated by linear spin wave theory (see e.g. Refs. [52, 62, 63]) and allow for the prediction of many physical properties of magnetically ordered states.

1. Introduction

1.1.2. Mechanisms of Disorder

The equilibrium behavior of a physical system in statistical mechanics system is determined by its free energy functional

$$F = E - TS, \quad (1.1.18)$$

where E is the internal energy, T the temperature and S the entropy of the system. In equilibrium, the state minimizing the free energy is realized. At higher temperatures, states with higher entropy are favored, at lower temperatures states with lower energy are favored. Ordered states are often minimizing energy constraints and are consequently often realized in a ground state. Temperature tends to introduce disorder to the system. In the infinite temperature limit, the equilibrium state becomes equidistributed in phase space. For spin systems, this state is a featureless paramagnetic state.

Temperature is not the only physical mechanism that induces fluctuations in spin systems. There are several other mechanisms that increase the entropy of states even at low or zero temperature. These mechanisms may give rise to the emergence of fascinating new phenomena such as quantum spin liquids. We will now discuss the most important disorder mechanisms for frustrated quantum spin systems.

Quantum fluctuations

Disorder can be introduced by going from classical spin models to quantum mechanical spin models. Such a transition can be observed in the spin-1/2 anisotropic Heisenberg model

$$H = J_z \sum_{\langle i,j \rangle} S_i^z S_j^z + \frac{J_{xy}}{2} \sum_{\langle i,j \rangle} S_i^+ S_j^- + S_i^- S_j^+. \quad (1.1.19)$$

Consider a classical Néel state

$$|\text{Néel}\rangle = |\uparrow\downarrow\uparrow\downarrow\dots\rangle. \quad (1.1.20)$$

In the classical Ising limit $J_{xy} = 0$ on a bipartite lattice this state is the ground state of Eq. (1.1.19) for $J_z > 0$. When turning on the quantum mechanical exchange interaction for $J_{xy} > 0$ this state is not an eigenstate anymore, since the exchange term introduces spin flips like

$$(S_i^+ S_j^- + S_i^- S_j^+) |\dots \uparrow_i \dots \downarrow_j \dots\rangle = |\dots \downarrow_i \dots \uparrow_j \dots\rangle. \quad (1.1.21)$$

The true ground state in Eq. (1.1.19) must, therefore, be a superposition of multiple spin configurations with locally fluctuating spins.

This effect is most pronounced in the $S = 1/2$ case. An exchange term turns a fully polarized state $|\uparrow\downarrow\rangle$ to the oppositely polarized state $|\downarrow\uparrow\rangle$. For higher spin, the effect of the exchange term is less pronounced since applying the off-diagonal term to a fully polarized state

$$(S_i^+ S_j^- + S_i^- S_j^+) |\dots (S)_i \dots (-S)_j \dots\rangle \propto |\dots (S-1)_i \dots (-S+1)_j \dots\rangle, \quad (1.1.22)$$

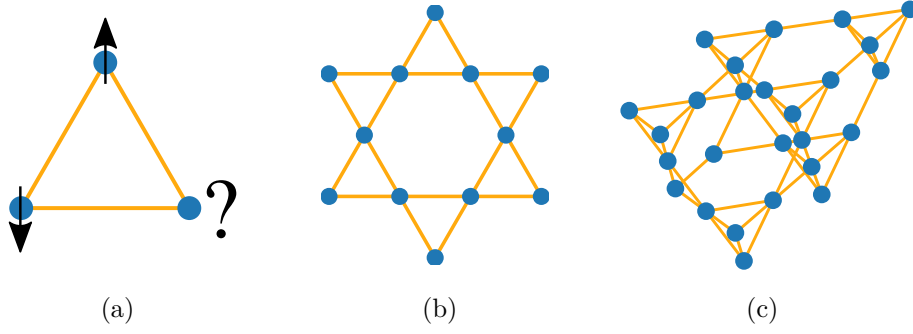


Figure 1.5.: Geometrically frustrated lattice geometries. The triangle (a) shows the basic dilemma leading to frustration in antiferromagnetic models. Local interactions cannot be simultaneously be minimized. The kagome (b) and the pyrochlore (c) lattice both give rise to high degrees of frustration.

does not fully invert the local polarization. Processes reverting the local polarization only occur at $2S$ -th order in perturbation theory. Hence, higher spin S yields less fluctuations in the local spin polarization. Indeed, the large- S limit of the quantum Heisenberg model can be proven to correspond to the classical Heisenberg model in a mathematically rigorous way [64].

For the square anisotropic spin-1/2 Heisenberg model in the classical Ising limit $J_{xy} = 0$ we know that the model exhibits long-range order at low but finite temperatures due to Onsager's solution [51]. Yet, in the isotropic Heisenberg case, the system is disordered at any finite temperature [65]. So perturbing a classical system with terms introducing quantum fluctuations may result in an order-to-disorder transition. In one dimension the Ising model at exactly $T = 0$ is long-range ordered whereas the Heisenberg case exhibits algebraically decaying correlation functions according to the exact Bethe ansatz solution [12].

Geometric Frustration

As in real life, frustration occurs in physical systems if too many constraints cannot be simultaneously satisfied. The most basic example in physics is the antiferromagnetic Ising model

$$H = J \sum_{\langle i,j \rangle} \sigma_i \cdot \sigma_j, \quad J > 0, \quad \sigma_i = \pm 1, \quad (1.1.23)$$

on the triangular lattice. Fig. 1.5a illustrates the dilemma. Out of the 2^3 possible spin configurations on a single triangle, six states are of energy $-J$ and two are of energy $3J$. The ground state is thus sixfold degenerate. This is a typical effect if not all local energy constraints can be simultaneously minimized. For spin systems, triangular geometries may give rise to frustration. Besides the triangular lattice geometry, prominent lattice

1. Introduction

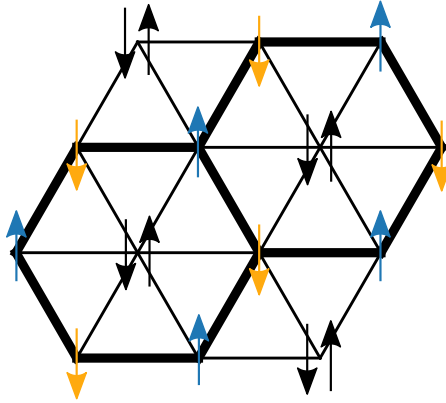


Figure 1.6.: A subset of ground states of the triangular lattice Ising antiferromagnet. The direction of the spins in the middle of the hexagons can be freely chosen without altering the energy of the state. Redrawn freely from [66].

geometries with a high degree of geometric frustration are the two-dimensional kagome and the three-dimensional pyrochlore lattice shown in Fig. 1.5. The ground state degeneracy can even become an extensive thermodynamic quantity. On an extended triangular lattice consider a state where on a hexagonal sublattice all energy constraints are minimized as in Fig. 1.6. Then the direction of each third spin in the middle of the hexagon can be freely chosen. This gives rise to a degeneracy of $D = 2^{N/3}$ states, where N is the number of sites. A measure of the ground state degeneracy is given by the entropy at zero temperature S_0 , the *residual entropy*. Since the states in Fig. 1.6 are a subset of all degenerate ground states we have a simple estimation for the residual entropy of the triangular lattice Ising antiferromagnet,

$$S_0/N > \frac{1}{3} \log 2 \approx 0.231049. \quad (1.1.24)$$

The ground state degeneracy thus becomes an extensive thermodynamic quantity. We see that geometric frustration induces large fluctuations even at zero temperature. Similar counting arguments have also been performed for Heisenberg models [67].

For the square lattice Ising model, an exact analytical solution was found by Onsager [51]. Following his work, several other authors found solutions to Ising models on the honeycomb, triangular and kagome lattice [68–71]. All unfrustrated cases, i.e. the (anti-)ferromagnetic square and honeycomb geometry and the ferromagnetic triangular and kagome geometries have been proven to exhibit an order-disorder transition at a finite critical temperature $T_c > 0$. The frustrated cases, on the other hand, do not order even at zero temperature. The residual entropies have been computed exactly. For the triangular

lattice [68] is given by

$$S_0/N = \frac{2}{\pi} \int_0^{\pi/3} \log(2 \cos(\omega)) d\omega \approx 0.3383, \quad (1.1.25)$$

and for the kagome lattice [71] by

$$S_0/N = \frac{1}{24\pi^2} \int_0^{2\pi} \int_0^{2\pi} \log[21 - 4(\cos(\omega_1) + \cos(\omega_2) + \cos(\omega_1 + \omega_2))] d\omega_1 d\omega_2 \approx 0.50183. \quad (1.1.26)$$

The kagome lattice may, therefore, be regarded as being more frustrated than the triangular lattice geometry.

Dimensionality

Lower dimensionality may introduce additional fluctuations to a system. Systems exhibiting a global continuous symmetry like SU(2) spin rotational symmetry in Heisenberg models Eq. (1.1.14) become disordered at dimensions $d \leq 2$. A nice heuristic scaling argument for this has been given by John Cardy [72]. Consider an ordered state like a ferromagnet with a domain of linear length l where the local magnetic moment is rotated 180° in the center with respect to the ferromagnetic state. Since we have continuous degrees of freedom we can perform this rotation gradually. The energy cost between two neighboring spins is of the order $\mathcal{O}(l^{-2})$. In d dimensions, a domain of length l has $\mathcal{O}(l^d)$ local interactions. Thus the energy cost of such a domain is of the order $\mathcal{O}(l^{d-2})$. On the other hand allowing for domain walls increases the entropy. For minimizing the free energy,

$$F = E - TS, \quad (1.1.27)$$

it is therefore favorable to have states with several domain walls which yield a higher entropy in $d \leq 2$, whereas such states become energetically unfavorable in $d > 2$.

This heuristic argument can be made very precise in the sense of a rigorous mathematical proof for several systems. First works [65, 73, 74] showed the absence of long-range order in bosonic superfluids, fermionic superconductors, and spin systems in $d \leq 2$. For Heisenberg spin systems with mild locality assumptions on the range of interactions, the precise statement is given by the Mermin-Wagner theorem [65]. We state the theorem from Ref. [61].

Theorem (Mermin-Wagner theorem). *For the quantum Heisenberg model*

$$H = \sum_{i,j} J_{ij} \mathbf{S}_i \cdot \mathbf{S}_j - h \sum_j e^{-i\mathbf{Q} \cdot \mathbf{r}_j} S_j^z + H.c., \quad (1.1.28)$$

1. Introduction

satisfying the locality condition Eq. (1.1.15) there can be no spontaneous symmetry breaking in one dimension for $T \geq 0$ or in two dimensions at finite temperature $T > 0$,

$$\lim_{h \rightarrow 0} \lim_{N \rightarrow \infty} \langle m^{\mathbf{Q}} \rangle = 0. \quad (1.1.29)$$

The theorem has been generalized to various different systems. A review on these generalizations is given by Ref. [75].

From a field theoretical perspective, spontaneous symmetry breaking of a continuous symmetry implies the emergence of massless Goldstone bosons. It has been shown [76] that in two space time dimensions the correlation functions of these fields are infrared divergent and thus the theory is ill-defined. This can be seen as the generic underlying principle that forbids the emergence of long-range order in lower dimensions.

The Mermin-Wagner theorem does not make statements about the two-dimensional case at zero temperature and the three-dimensional case. The question about the behavior of the two-dimensional spin-1/2 Heisenberg antiferromagnet on a square lattice at exactly zero temperature thus remains unanswered by the Mermin-Wagner theorem. Several analytical and numerical studies have investigated this question. A first numerical Exact Diagonalization study [14] on lattices up to 18 sites indicated that the ground state is indeed long-range ordered. This has been supported by spin-wave calculations [13] who predicted the behavior of the spin correlation function

$$|\langle \mathbf{S}_i \cdot \mathbf{S}_j \rangle| - (\tilde{m})^2 \sim \frac{1}{|\mathbf{r}_i - \mathbf{r}_j|}, \quad (1.1.30)$$

where $\tilde{m} \equiv \langle m^{(\pi,\pi)} \rangle$ is the staggered magnetization with wave vector $\mathbf{Q} = (\pi, \pi)$, cf. Eq. (1.1.6). This was finally confirmed by statistically exact Quantum Monte Carlo simulations [15] which found a value of

$$\tilde{m} = 0.30 \pm 0.02. \quad (1.1.31)$$

This corresponds to 60% of the staggered magnetization of the classical ground state. A review of the physics of the two-dimensional spin 1/2 Heisenberg model is given by [77]. For spin $S \geq 1$ a mathematical proof showed that at $T = 0$ long-range order is established [78].

In three dimensions the spin-1/2 Heisenberg antiferromagnetic model on the cubic lattice exhibits a finite temperature phase transition from an ordered to a disordered phase. This has been demonstrated by a QMC study [79] finding a critical temperature

$$T_c/J = 0.946 \pm 0.001. \quad (1.1.32)$$

1.1.3. Order-by-Disorder principle

Quantum or thermal fluctuations usually introduce disorder to a system. Under special circumstances, they can also have the opposite effect and order the system. Although

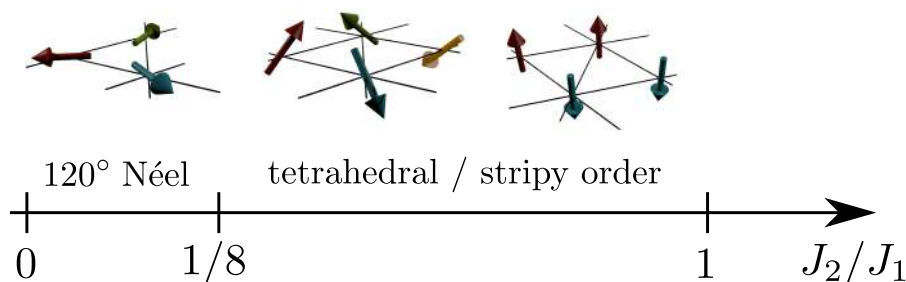


Figure 1.7.: Ground states of the classical triangular lattice antiferromagnetic Heisenberg model with additional next-nearest neighbor interactions Eq. (1.1.33). For $1/8 < J_2/J_1 < 1$ the tetrahedral and stripy states are degenerate.

several types of states may be degenerate ground states in the classical regime, the fluctuations around different types can be unequal in behavior. Introducing thermal or quantum fluctuations then selects the type of states whose fluctuations provide the largest entropy or lowest zero-point energy. This somehow paradoxical effect is called *order-by-disorder* mechanism.

A typical example of quantum fluctuations ordering a system can be found in the frustrated antiferromagnetic triangular lattice Heisenberg model with nearest and next-nearest neighbor interactions [80]

$$\mathcal{H} = J_1 \sum_{\langle i,j \rangle} \mathbf{S}_i \cdot \mathbf{S}_j + J_2 \sum_{\langle\langle i,j \rangle\rangle} \mathbf{S}_i \cdot \mathbf{S}_j. \quad (1.1.33)$$

For $0 < J_2/J_1 < 1/8$ the classical ground state is 120° Néel ordered whereas for $1/8 < J_2/J_1 < 1$ two types of states are degenerate: a collinear state where states are ordered ferromagnetically in one direction of the triangular lattice and antiferromagnetically along the other two directions and a tetrahedral state where four spins are aligned in a way that they form a regular tetrahedron, cf. Fig. 1.7. Quantum fluctuations can now be taken into account via spin-wave theory around the classically ordered states. The correction to the ground state energy yields a lower energy for the stripy ordered state than the tetrahedral state. By numerically evaluating ground state properties of the model one can show that indeed stripy order is realized for $J_2/J_1 \gtrsim 0.18$ [81, 82]. We will discuss an extended version of this model in detail in chapter 5.

Several other examples of quantum and thermal fluctuations leading to the realization of a subset of degenerate configurations have been discussed in the literature [67, 83–87]. The order-by-disorder mechanism can be understood as a generic guiding principle how specific states are selected amongst a highly degenerate ground state manifold and therefore as an unconventional mechanism for the emergence of order.

1.2. Quantum Spin Liquids

*What if someone said
Promise lies ahead
Hopes are high in certain scientific circles*

DREAM THEATER, The Great Debate

Discovering and understanding novel phases of matter is one of the main objectives of condensed matter physics. Often, experimental discovery precedes the theoretical understanding. The FQHE, for example, was first discovered experimentally by Tsui, Stormer and Gossard in 1982 [1] and important theoretical ideas such as the Laughlin wave function [88] have been proposed a posteriori. *Quantum Spin Liquid* phases, on the other hand, are envisioned by theoreticians and direct experimental proof of their existence is still missing. They are disordered states of matter and may exhibit fascinating phenomena such as the emergence of quasiparticles described by gauge theories. Thus, they substantially differ from a featureless disordered paramagnetic state. There are many experimental candidate systems in frustrated magnetism for which quantum spin liquid behavior could be a plausible explanation [89], although a satisfactory proof of their existence in nature has as of today not been given. Here we want to give a very short introduction to these novel phases which is tailored to the needs of this thesis. More comprehensive reviews have been given by Refs. [89–91].

We discuss the implications of a gap in the excitation spectrum of a system in section 1.2.1. We then introduce the resonating valence bond state in section 1.2.2, which has been amongst the first proposed spin liquid states. A general construction principle for spin liquids generalizing the RVB state called the parton construction is presented in section 1.2.3. We then discuss how this construction is applied to yield two types of spin liquids: the chiral spin liquid in section 1.2.4 which is closely related to the FQHE and Dirac spin liquids in section 1.2.5 which are envisioned to be gapless states without long-range order.

1.2.1. Gapless and gapped phases

Long-range order in systems with a continuous symmetry like the Heisenberg model Eq. (1.1.14) implies gapless excitations according to Goldstone’s theorem, cf. section 1.1.1. The converse is not necessarily true. Quantum critical states at continuous phase transitions usually exhibit algebraically decaying correlations

$$\langle \mathbf{S}_i \cdot \mathbf{S}_j \rangle \sim |\mathbf{r}_i - \mathbf{r}_j|^{-\eta}, \quad (1.2.1)$$

while having a gapless excitation spectrum. Also extended phases may show this kind of behavior. The most prominent example thereof is the spin-1/2 Heisenberg chain, whose

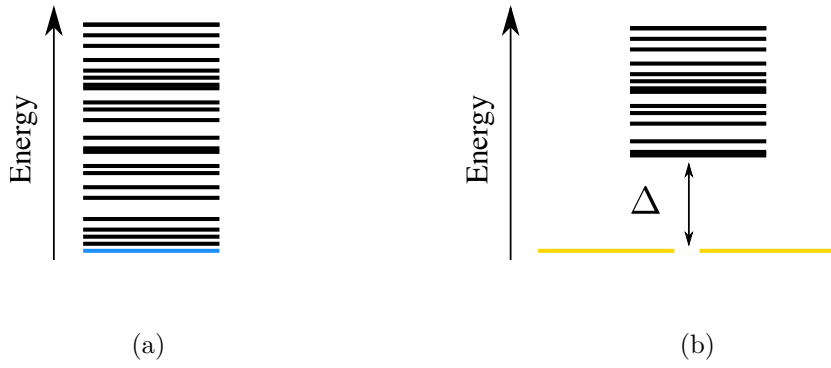


Figure 1.8.: Gapless (a) and gapped (b) excitation spectra. Long-range ordered phases are necessarily gapless. Other gapless states include critical states, the spin-1/2 Heisenberg chain [12] and algebraic spin liquids [92, 93]. Gapped phases are necessarily short-ranged and for half-odd integer spin the ground state must be degenerate with periodic boundary conditions according to the Lieb-Schultz-Mathis-Hastings theorem [94, 95].

spin correlation function also decays algebraically over distance according to the Bethe ansatz solution [12]. Also in higher dimensions, such states have been proposed. One example is the so-called Dirac or algebraic spin liquid [92, 93], which we will discuss in more detail in section 1.2.5. On the other hand, gapped phases necessarily exhibit exponentially decaying correlation functions [96],

$$\langle \mathbf{S}_i \cdot \mathbf{S}_j \rangle \sim \exp(-|\mathbf{r}_i - \mathbf{r}_j|/\xi). \quad (1.2.2)$$

The ground state of a gapped phase can be degenerate. This degeneracy may be caused by symmetry breaking a discrete symmetry. An example of such a phase would be valence bond solid states shown in Fig. 1.9. Valence bond solids are spin singlets, thus do not break rotational $SU(2)$ symmetry. Yet, they break discrete lattice symmetries, like translation or rotation symmetry. Such a state is for example realized as a phase in the so-called J-Q models [97].

More excitingly, the degeneracy below the gap may be due to topological ordering. A remarkable exactly solvable model that illustrates this mechanism is given by Kitaev's toric code model [41],

$$H = - \sum_s A_s - \sum_p B_p, \quad (1.2.3)$$

where

$$A_s = \prod_{j \in \text{star}(s)} \sigma_j^x, \quad B_p = \prod_{j \in \text{plaq}(s)} \sigma_j^z. \quad (1.2.4)$$

Here, σ_j^x and σ_j^z denote the Pauli matrices. $\text{star}(s)$ is the set of lattice sites in the “star” of position s and $\text{plaq}(s)$ is the set of lattice sites at the boundary of “plaquette” p , cf.

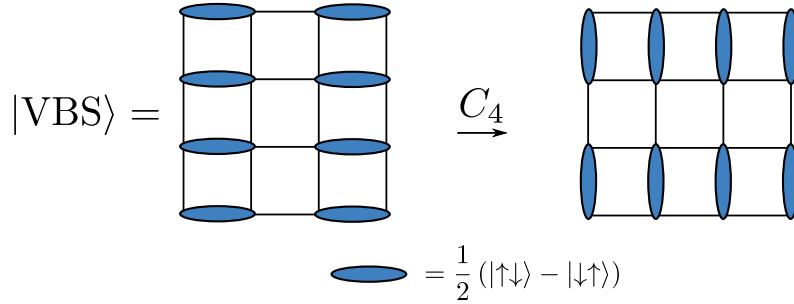


Figure 1.9.: Valence Bond solids are regular coverings of a lattice with two spins paired up in a singlet. They are not invariant under lattice symmetries such as rotational or translational symmetry.

Fig. 1.10. Although this model is not realistic for actual materials in perfectly illustrates many of the aspects of topological order. We will not discuss the details of the solution here, but we refer the reader to the original article [41]. The gapped ground state is an equal weight superposition of all possible loop configurations on the square lattice (the language of loops can be directly translated to spin configurations, cf. Fig. 1.10b), which is sometimes called a *loop soup*. Therefore, it does not break any lattice symmetries. With periodic boundary conditions, there are 4 kinds of loop configurations that cannot be continuously deformed into each other. They differ by having an even/odd number of incontractible loops along the two periodic directions. These four kinds of loop configurations are mutually orthogonal and thus yield a four-fold degenerate ground state. The four-fold degeneracy for periodic boundary conditions stems from the fact that a torus allows for incontractible loops along both periodicity directions.

The excitations of the toric code can also be exactly analyzed and the phase for exchanging particles can be explicitly computed and it turns out that these obey anyonic statistics. The toric code can be regarded as a Hamiltonian implementation of a \mathbb{Z}_2 lattice gauge theory [98] which admits a deconfined phase in two dimensions. Short-range correlations, ground state degeneracy dependent on the topology (e.g. periodic boundary conditions) of the lattice, anyonic braiding statistics and the relation to deconfined phases of lattice gauge theories are typical hallmark features of quantum spin liquids. The toric code exhibits what is called \mathbb{Z}_2 topological order. There are also other \mathbb{Z}_2 topologically ordered states, as for example the nearest-neighbor RVB states, discussed in section 1.2.2 on a triangular lattice [31, 99]. A different kind of topological order is realized in chiral spin liquids which we will discuss in section 1.2.4.

Interestingly, there are certain restrictions on the nature of the gapped, short-range ordered phases. The statement is known as the *Lieb-Schultz-Mattis-Hastings theorem* [94, 95]. Assuming half-odd integer spin per unit cell with periodic boundary conditions and certain technical assumptions on the geometry of the finite lattice (see [94, 95] for the exact

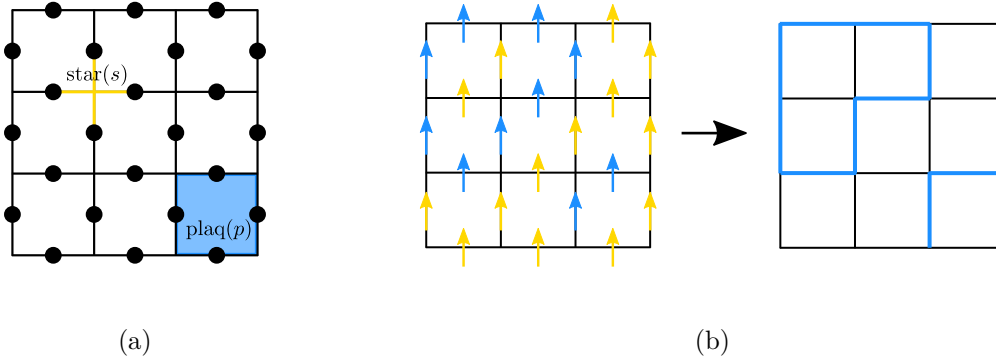


Figure 1.10.: The toric code model. The spins are placed on the links connecting the sites of a square lattice. The terms A_s and B_p as in Eq. (1.2.4) are defined on the “stars” and “plaquettes” as shown in (a). The language of spins can be translated into the language of loops and strings as shown in (b). A string segment is present if the corresponding spin points up.

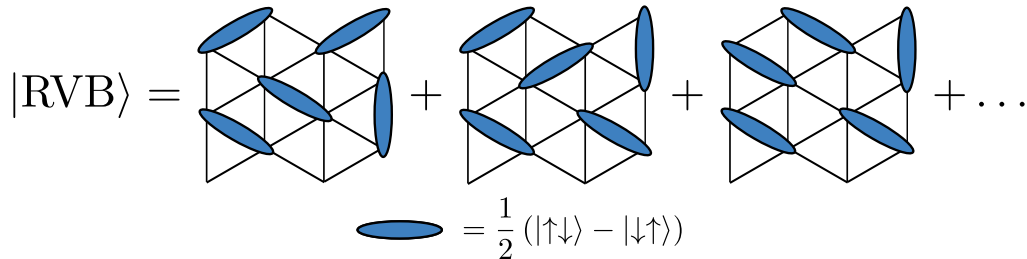
prerequisites) the theorem states that a gapped system cannot have a unique ground state in the thermodynamic limit. Instead, there must be degenerate ground states below the gap. The prerequisites of the Lieb-Schultz-Mattis-Hastings theorem are fulfilled by the extended Heisenberg models we investigate in chapters 4 and 5. The toric code, on the other hand, does not fulfill these conditions since its unit cell consists out of two spin-1/2 degrees of freedom. Nevertheless, it is an example of a gapped, topologically ordered phase.

1.2.2. Resonating Valence Bond Liquids

The behavior of frustrated low dimensional quantum magnets may in many ways differ from their classical unfrustrated counterparts. Due to the mechanisms discussed in section 1.1.2 magnetic ordering may be suppressed even at zero temperature. Instead of symmetry breaking phases novel states of matter can emerge.

A fundamental building block of quantum spin models in magnetism is the Heisenberg bond between two neighboring spins $J(\mathbf{S}_i \cdot \mathbf{S}_j)$. In the antiferromagnetic case $J > 0$, its energy is minimized by the singlet state in contrast to the Néel state for classical interaction. Given a disjoint covering of a lattice with dimers (i.e. pairs of two sites) we can define a state that is just a tensor product of singlets on these dimers, cf. Fig. 1.11. we will call such a state a *valence bond configuration*, similar to the regular valence bond solid in Fig. 1.9. Heisenberg bonds on lattice sites connected by a dimer are energetically minimized whereas other bonds are not minimized. Hence, such states are reasonable variational wave functions for quantum magnets. Importantly, these states are manifestly singlet states and are thus spin rotational $SU(2)$ symmetric.

1. Introduction



$$|\text{RVB}\rangle = \text{[Diagram 1]} + \text{[Diagram 2]} + \text{[Diagram 3]} + \dots$$

$$\text{[Oval]} = \frac{1}{2} (|\uparrow\downarrow\rangle - |\downarrow\uparrow\rangle)$$

Figure 1.11.: Valence bond configurations in an RVB state on the triangular lattice. The RVB state proposed by [22] is an equal weight superposition of nearest-neighbor valence bond configurations. More general RVB states may include valence bond configurations with longer range singlet pairs and non-uniform weights [11].

In a seminal paper [22], Anderson proposed that a superposition of valence bond configurations yields an extremely low variational energy for the triangular spin-1/2 Heisenberg model. He considered the equal weight superposition of all dimer configurations where dimers connect nearest neighbor bonds. This state is called a *resonating valence bond liquid*, short RVB liquid and schematically shown in Fig. 1.11. As a superposition of all possible nearest-neighbor valence bond configurations, it is not only SU(2) symmetric but also symmetric under space group symmetries. The state is a truly quantum mechanical state and does not possess a classical equivalent. Anderson found that the RVB state had lower variational energy than spin-wave estimations on the energy of the Néel state. The energy estimate for the RVB state given by [22] is

$$E_{\text{RVB}} \approx -(0.54 \pm 0.01) NJ, \quad (1.2.5)$$

where N denotes the number of sites and J the coupling constant. We compare this energy to the actual ground state energy from numerical Exact Diagonalization on a 48 site cluster obtained in the course of this thesis, cf. section 3.4. The precise energy on this cluster is given in table 3.1

$$E_0 = -0.5586 NJ. \quad (1.2.6)$$

The variational energy of the RVB state is therefore extremely close to the actual ground state energy. Nevertheless, numerical studies later on provided conclusive evidence that the system breaks SU(2) symmetry and exhibits 120° Néel order [25, 80, 100]. Therefore the question arises whether this state can be realized as the ground state of a local spin Hamiltonian. Although a toy model exactly realizing the above RVB state has for example been given by Rokhsar and Kivelson [43], the question whether the RVB state is realized in more realistic models remains open until today. It is now understood that RVB states

on non-bipartite two-dimensional lattices may exhibit fractionalized excitations with \mathbb{Z}_2 topological order [31, 99] similar to the toric code model Eq. (1.2.3) [41].

The valence bond configurations (not necessarily nearest-neighbors) span the space of singlet states on a lattice [101, 102] and thus, every singlet wave function can be expressed as a linear combination of them. In order to extend the idea of the RVB state Anderson [11] proposed to investigate a certain subset of possible superpositions of valence bond configurations. For constructing these states we first consider a fermionic Hilbert space of up and down electrons on the lattice. Thus a typical configuration in this Hilbert space is given by

$$|\psi\rangle = |\uparrow\downarrow, \emptyset, \uparrow, \downarrow\rangle, \quad (1.2.7)$$

where double site occupancies $\uparrow\downarrow$ and vacancies \emptyset are allowed in contrast to pure spin configurations. The operator which sets the part of a many-body wave function with double site occupancy to zero is given by

$$P_{\text{GW}} = \prod_i (1 - n_{i,\uparrow} n_{i,\downarrow}), \quad (1.2.8)$$

where $n_{i,\sigma} = c_{i\sigma}^\dagger c_{i\sigma}$ for fermionic creation and annihilation operators $c_{i\sigma}^\dagger$ and $c_{i\sigma}$, $\sigma = \uparrow\downarrow$. The operator P_{GW} in Eq. (2.2.24) is called Gutzwiller projection [103, 104]. Anderson now proposed to apply the Gutzwiller projection to BCS wave functions from the BCS theory of superconductivity of the form

$$|\psi_{\text{BCS}}\rangle = \prod_{\mathbf{k} \in \text{B.Z.}} (u_{\mathbf{k}} + v_{\mathbf{k}} c_{\mathbf{k}\uparrow}^\dagger c_{-\mathbf{k}\downarrow}^\dagger) |0\rangle, \quad (1.2.9)$$

where $u_{\mathbf{k}}, v_{\mathbf{k}}$ serve as variational parameters and

$$c_{\mathbf{k}\sigma}^\dagger = \frac{1}{\sqrt{N}} \sum_{i=1}^N e^{i\mathbf{k}\cdot\mathbf{r}_i} c_{i\sigma}^\dagger, \quad (1.2.10)$$

are fermionic creation operators in reciprocal space. The following computation shows how the Gutzwiller projected BCS state $P_{\text{GW}} |\psi_{\text{BCS}}\rangle$ is related to the RVB state

$$P_{\text{GW}} |\psi_{\text{BCS}}\rangle \propto P_{\text{GW}} \prod_{\mathbf{k} \in \text{B.Z.}} \left(1 + \frac{v_{\mathbf{k}}}{u_{\mathbf{k}}} c_{\mathbf{k}\uparrow}^\dagger c_{-\mathbf{k}\downarrow}^\dagger \right) |0\rangle \quad (1.2.11)$$

$$= P_{\text{GW}} \exp \left[\sum_{\mathbf{k}} \frac{v_{\mathbf{k}}}{u_{\mathbf{k}}} c_{\mathbf{k}\uparrow}^\dagger c_{-\mathbf{k}\downarrow}^\dagger \right] |0\rangle \quad (1.2.12)$$

$$= \left(\sum_{\mathbf{k}} \frac{v_{\mathbf{k}}}{u_{\mathbf{k}}} c_{\mathbf{k}\uparrow}^\dagger c_{-\mathbf{k}\downarrow}^\dagger \right)^{N/2} |0\rangle \quad (1.2.13)$$

$$= \left(\sum_{i,j} a_{ij} c_{i\uparrow}^\dagger c_{j\downarrow}^\dagger \right)^{N/2} |0\rangle, \quad (1.2.14)$$

1. Introduction

where

$$a_{ij} = \sum_{\mathbf{k} \in \text{B.Z.}} \frac{v_{\mathbf{k}}}{u_{\mathbf{k}}} e^{i\mathbf{k}(r_i - r_j)}. \quad (1.2.15)$$

The second equality uses the fact that $\exp(f^\dagger) = 1 + f^\dagger$ for fermionic operators f^\dagger , the third equality projects to the correct particle number in the Taylor expansion of the exponential function. If $a_{ij} = a_{ji}$ the operator

$$a_{ij}(c_{i\uparrow}^\dagger c_{j\downarrow}^\dagger + c_{j\uparrow}^\dagger c_{i\downarrow}^\dagger) = a_{ij}(c_{i\uparrow}^\dagger c_{j\downarrow}^\dagger - c_{i\downarrow}^\dagger c_{j\uparrow}^\dagger) \quad (1.2.16)$$

in Eq. (1.2.14) creates a singlet state on the sites i and j with coefficient a_{ij} . We see that the state in Eq. (1.2.14) is again a superposition of dimer coverings on the lattice, but now with different coefficients a_{ij} defined by $u_{\mathbf{k}}$ and $v_{\mathbf{k}}$ via Eq. (1.2.15). It may, therefore, be regarded as a generalization of the initially proposed state in [22] and is thus also called an RVB state.

1.2.3. Parton construction and mean-field theory

The Gutzwiller projection operator Eq. (1.2.8) transforms a fermionic wave function defined on a fermionic Hilbert space into a spin wave function on the subspace with no double-occupancies or vacancies. As in the case of the triangular lattice spin-1/2 Heisenberg models, cf. section 1.2.2, these Gutzwiller projected wave functions may yield low variational energies and may even be realized as a ground state of pure spin systems without charge degrees of freedom. A generic Heisenberg model

$$H = \sum_{i,j} J_{ij} \mathbf{S}_i \cdot \mathbf{S}_j, \quad (1.2.17)$$

may be considered as a low-energy effective Hamiltonian in the Mott-insulating regime $t_{ij} \ll U$ of a Hubbard model of type

$$H_{\text{Hubbard}} = \sum_{i,j,\sigma} (t_{ij} c_{i\sigma}^\dagger c_{j\sigma} + \text{H.c.}) + U \sum_i n_{i\uparrow} n_{i\downarrow}. \quad (1.2.18)$$

The spin operators \mathbf{S}_i on site i are introduced by

$$\mathbf{S}_i = \frac{1}{2} \sum_{\alpha\beta} c_{i\alpha}^\dagger \boldsymbol{\sigma}_{\alpha\beta} c_{i\beta}, \quad (1.2.19)$$

where $\alpha, \beta = \downarrow, \uparrow$. The coupling constants J_{ij} are related to the original hopping t_{ij} and on-site repulsion U terms via $J_{ij} = 4|t_{ij}|^2/U$. The effective Heisenberg model can be defined on the smaller Hilbert space of spin configurations with no double-occupancies or vacancies. It is thus a simplification of the original Hubbard model.

Starting from a pure spin model like Eq. (1.2.17) we can also take the opposite direction. We introduce fermionic operators as in Eq. (1.2.19) to the Heisenberg model Eq. (1.2.17) and investigate the resulting fermionic problem [105]

$$H = \sum_{i,j,\alpha,\beta} -\frac{J_{ij}}{2} c_{i\alpha}^\dagger c_{j\alpha} c_{j\beta}^\dagger c_{i\beta} + \sum_{i,j} \frac{J_{ij}}{2} \left(n_i - \frac{1}{2} n_i n_j \right), \quad (1.2.20)$$

where

$$n_i = c_{i\uparrow}^\dagger c_{i\uparrow} + c_{i\downarrow}^\dagger c_{i\downarrow}, \quad (1.2.21)$$

is the number operator of fermions per site. The fermionic operators $c_{i\alpha}^\dagger$ introduced via Eq. (1.2.19) are then called *parton* or *spinon* operators. Several authors also use to call the parton operators Abrikosov fermions or the decomposition Eq. (1.2.19) slave-boson approach [105]. Now, the Hilbert space is enlarged and we are actually considering a different problem. In order to describe the same model we have to enforce the constraint of single site occupancy

$$n_i = 1. \quad (1.2.22)$$

The parton Hamiltonian Eq. (1.2.20) together with the single site occupation constraint Eq. (1.2.22) are now completely equivalent to the original Heisenberg model Eq. (1.2.17). The single site occupancy constraint Eq. (1.2.22) turns the second term in Eq. (1.2.20) into a constant. We are thus left with the following Hamiltonian for the partons

$$H_{\text{parton}} = \sum_{i,j,\alpha,\beta} -\frac{J_{ij}}{2} c_{i\alpha}^\dagger c_{j\alpha} c_{j\beta}^\dagger c_{i\beta}. \quad (1.2.23)$$

The Hamiltonian Eq. (1.2.23) has an interesting fundamental property: local U(1) gauge symmetry [106]. It is invariant under the local gauge transformations

$$c_{i\alpha}^\dagger \rightarrow e^{i\theta_i} c_{i\alpha}^\dagger. \quad (1.2.24)$$

This symmetry is not present the original Hubbard model Eq. (1.2.18) since the hopping terms $c_{i\alpha}^\dagger c_{j\alpha}$ are only invariant under global phase transformations. The local gauge symmetry Eq. (1.2.24) is therefore an emergent property of the system in the Mott insulating regime [106].

Generic ansatz wave functions from Gutzwiller projection

The equivalence between the original spin model Eq. (1.2.17) and the parton Hamiltonian Eq. (1.2.23) together with the constraint Eq. (1.2.22) gives rise to a principle of constructing variational ansatz wave functions generalizing the RVB approach. The problem in exactly solving Eq. (1.2.23) are the four-fermion operators. In a mean-field approach, we can replace $c_{i\alpha}^\dagger c_{j\alpha}$ with its vacuum expectation values $\chi_{ij} \equiv \langle c_{i\alpha}^\dagger c_{j\alpha} \rangle$ or the operators $c_{i\alpha}^\dagger c_{j\beta}^\dagger$

1. Introduction

with $\Delta_{ij} \equiv \langle c_{i\uparrow}^\dagger c_{j\downarrow}^\dagger \rangle$. Furthermore, we replace the constraint Eq. (1.2.22) by a relaxing this constraint to be valid only on average

$$\langle n_i \rangle = 1. \quad (1.2.25)$$

This condition can be realized by adding a chemical potential term of the form

$$\sum_i \mu_i (n_i - 1) \quad (1.2.26)$$

to the parton Hamiltonian Eq. (1.2.23) and adjusting the chemical potential μ_i . In summary, the Hamiltonian Eq. (1.2.23) can be approximated by a generic quadratic mean-field Hamiltonian of the form [105]

$$H_{\text{mean}} = \sum_{i,j,\alpha} (\chi_{ij} c_{i\alpha}^\dagger c_{j\alpha} + \text{H.c.}) + \sum_{i,j} (\Delta_{ij}^* c_{i\uparrow}^\dagger c_{j\downarrow}^\dagger + \text{H.c.}) + \sum_i \mu_i (n_i - 1). \quad (1.2.27)$$

The numbers χ_{ij} , Δ_{ij} and μ_i define the hopping, pairing and chemical potential amplitudes, respectively. Since the mean-field Hamiltonian is quadratic in the parton operators it is exactly solvable in the extended Hilbert space. In general the non-interacting mean-field ground state $|\psi_0^{\text{mf}}\rangle$ will be given by a filled Fermi sea or a BCS type wave function, depending on whether or not the pairing amplitudes Δ_{ij} are non-zero. In order to create an ansatz wave function for the ground state of the original spin model Eq. (1.2.17) we can again set the coefficients of configurations with double site occupancy or vacancies to zero via Gutzwiller projection Eq. (1.2.8)

$$|\psi_{\text{GPWF}}\rangle = P_{\text{GW}} |\psi_0^{\text{mf}}\rangle. \quad (1.2.28)$$

We will call such a state a *Gutzwiller projected parton wave function*, short GPWF.

The previously defined RVB states in Eq. (1.2.14) are a special case of these GPWFs. Fourier transforming Eq. (1.2.27) with a translationally invariant ansatz χ_{ij} and Δ_{ij} yields a BCS type mean-field Hamiltonian of the form

$$H = \sum_{\mathbf{k},\sigma} \chi_{\mathbf{k}} c_{\mathbf{k}\sigma}^\dagger c_{\mathbf{k}\sigma} + \sum_{\mathbf{k}} (\Delta_{\mathbf{k}}^* c_{\mathbf{k}\uparrow}^\dagger c_{-\mathbf{k}\downarrow}^\dagger + \text{H.c.}), \quad (1.2.29)$$

whose solution after Bogoliubov transformation is given by the BCS state in Eq. (1.2.9).

The coefficients of these ansatz wave functions in the parton construction can be computed as a Slater determinant. We will discuss the numerical evaluation of properties and coefficients of these wave functions in section 2.2.3. It turns out that studying these wave functions can be done numerically in a computationally efficient way [47].

The manipulations and approximations leading from Eq. (1.2.17) to Eq. (1.2.27) are actually quite crude. First of all, the Hilbert space is enlarged and a fermionic model

Eq. (1.2.20) is introduced. From Eq. (1.2.23) to Eq. (1.2.27) we replace the single occupancy constraint Eq. (1.2.22) by its relaxed average version Eq. (1.2.25). The parameters χ_{ij} and Δ_{ij} may then be chosen to satisfy self-consistency equations,

$$\langle c_{i\alpha}^\dagger c_{j\alpha} \rangle = \chi_{ij}, \quad \langle c_{i\uparrow}^\dagger c_{j\downarrow}^\dagger \rangle = \Delta_{ij}, \quad (1.2.30)$$

and the chemical potentials μ_i may be adjusted to satisfy the average constraint Eq. (1.2.25). The resulting quadratic mean-field Hamiltonian can then be analyzed and parton mean-field phase diagrams can be worked out. Yet, the predictive power of such an approach is limited and necessarily needs to be complemented with different approaches. Often, variational energies are computed using Variational Monte Carlo, cf. section 2.2.3 or overlaps with numerically precise ground states from Exact Diagonalization can be calculated.

Fluctuations around mean-field theory

For taking into account fluctuations around the zeroth-order mean-field theory of the parton Hamiltonian Eq. (1.2.27) we introduce the path integral formulation. The partition function can be written as [105]

$$\mathcal{Z} = \int \mathcal{D}c_i \mathcal{D}\mu_i \mathcal{D}\chi_{ij} \exp \left\{ i \int dt \mathcal{L} - \sum_i \mu_i(t)(n_i - 1) \right\}, \quad (1.2.31)$$

where the Lagrangian \mathcal{L} is given by

$$\mathcal{L} = \sum_i c_i^\dagger i \partial_t c_i - \sum_{i,j,\sigma} -\frac{J_{ij}}{2} \left[(c_{i\sigma}^\dagger c_{j\sigma} \chi_{ji} + \text{H.c.}) - |\chi_{ij}|^2 \right], \quad (1.2.32)$$

with the Hubbard-Stratonovich fields χ_{ij} . The path integral formulation also allows deriving effective theories for specific ansätze for in section 1.2.4 and section 1.2.5.

We emphasize that in Eq. (1.2.31) the chemical potentials $\mu_i(t)$ are now explicitly time-dependent. This reproduces the original single occupancy constraint Eq. (1.2.22) since functional integration over the μ_i fields yields

$$\int \mathcal{D}\mu_i \exp \left\{ i \int dt \mu_i(n_i - 1) \right\} = \delta(n_i - 1). \quad (1.2.33)$$

Eq. (1.2.31) and Eq. (1.2.32) are therefore again equivalent to the original spin system Eq. (1.2.17).

The fluctuating fields χ_{ij} can now be decomposed into amplitude fluctuations $\bar{\chi}_{ij}$ and phase fluctuations a_{ij} ,

$$\chi_{ij} = \bar{\chi}_{ij} e^{ia_{ij}}. \quad (1.2.34)$$

According to [105] the amplitude fluctuations should be gapped and $\bar{\chi}_{ij}$ may, therefore, be regarded as a constant. Still, phase fluctuations a_{ij} are assumed as dynamical fields.

1. Introduction

The effective Hamiltonian is then given by

$$H = \sum_{i,j,\sigma} (\bar{\chi}_{ij} c_{i\sigma}^\dagger c_{j\sigma} e^{ia_{ij}} + \text{H.c.}) + \sum_i \mu_i (n_i - 1). \quad (1.2.35)$$

The system now exhibits a gauge structure. Gauge transformations of the type

$$c_{i\sigma}^\dagger \rightarrow e^{i\theta_i} c_{i\sigma}^\dagger, \quad a_{ij} \rightarrow a_{ij} + \theta_j - \theta_i, \quad (1.2.36)$$

leave the Hamiltonian Eq. (1.2.35) invariant. Eq. (1.2.35) now describes a lattice gauge theory with U(1) lattice gauge fields a_{ij} and μ_i .

Let us compare the two effective Hamiltonians Eq. (1.2.27) and Eq. (1.2.35). A common feature for both is that we have to make an ansatz for the coefficients χ_{ij} or $\bar{\chi}_{ij}$ respectively. Apart from this Eq. (1.2.27) describes free partons which are essentially uncorrelated. Consequently, this approximation cannot correctly describe the strong correlations present in Heisenberg systems. Correlations are taken into account via the gauge fields in Eq. (1.2.35). The only approximation made when passing from the Heisenberg model to Eq. (1.2.35) is to assume a constant amplitude in the Hubbard-Stratonovich fields χ_{ij} , because amplitude fluctuations are expected to be gapped [105]. It is thus conjectured that the lattice gauge theory Eq. (1.2.35) may correctly describe strongly correlated phases of Heisenberg spin systems. Phases of the lattice gauge theory Eq. (1.2.35) correspond to phases of the original spin model.

A central question in the study of gauge theories is whether the matter fields (in our case the partons) are confined or deconfined. Particles are said to be confined if the energy cost for separating them diverges at large distances. A typical example of this is quark confinement in quantum chromodynamics. An example of deconfinement is quantum electrodynamics in $3 + 1$ dimensions where the potential energy between two electrons is given by the Coulomb interaction and two electrons can be separated by an arbitrary distance with finite energy cost. For spin systems, we may now ask the same question whether two partons can be separated by an arbitrary distance at finite energy cost. Deconfined phases of lattice gauge theories such as Eq. (1.2.35) are essentially quantum spin liquids.

1.2.4. Chiral Spin Liquids

One of the first proposed parton ansätze was the *chiral spin liquid*, short CSL state [23].

The word "chiral" refers to the violation of parity symmetry (i.e. spatial reflection symmetry) and time reversal symmetry. A quantity that measures the breaking of these two symmetries is the so-called *scalar chirality* operator,

$$\mathbf{S}_i \cdot (\mathbf{S}_j \times \mathbf{S}_k). \quad (1.2.37)$$

A reflection symmetry reverses the orientation of a path $i \rightarrow j \rightarrow k$ whereas time reversal symmetry transforms the spin operators as $\mathbf{S}_i \rightarrow -\mathbf{S}_i$, thus changing the sign in

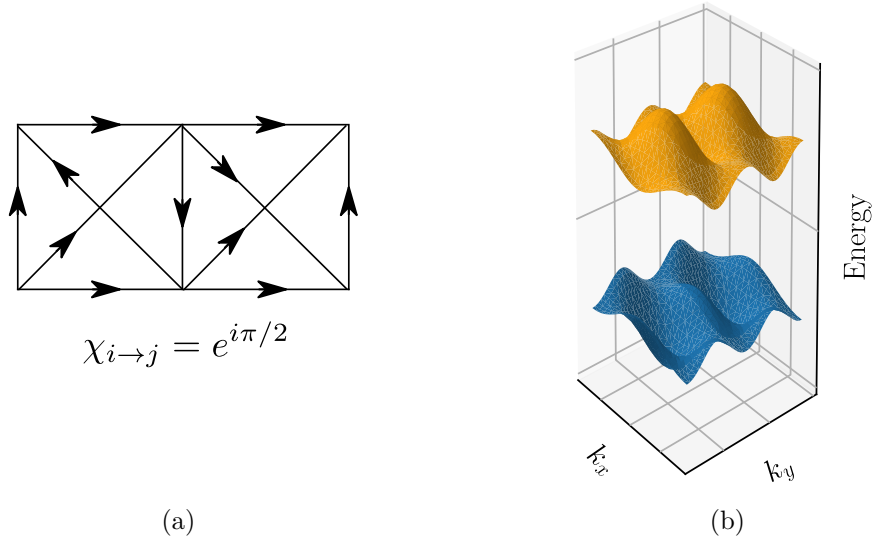


Figure 1.12.: Parton ansatz for chiral spin liquids as proposed by [23]. The hopping amplitudes in (a) are chosen such that there is π flux through the squares and $\pi/2$ flux through triangles. The band structure of this parton ansatz features two bands separated by a gap with Chern number ± 1 .

Eq. (1.2.37). Certain magnetic orderings may also not be parity or time reversal symmetry invariant like the tetrahedral order in Fig. 1.7.

In contrast to chiral magnetic orderings, a CSL is a chiral gapped quantum state of matter whose low-energy degrees of freedom are described by an effective Chern-Simons theory. We will explain the latter statement in more detail below. One way of constructing this phase is via a parton ansatz that breaks time-reversal symmetry as proposed by Ref. [23]. Consider complex hopping amplitudes in the parton ansatz Eq. (1.2.27). The hopping terms are then chosen such that we obtain a band structure where the valence band has non-zero Hall conductivity $\sigma_{xy} \neq 0$,

$$j_y = \sigma_{xy} E_x, \quad (1.2.38)$$

where j_y denotes the Hall current as a response to the applied electric field E_x . The famous TKNN formula [107] tells us that the Hall conductivity is quantized and proportional to the integer Chern number of the occupied bands. Ref. [23] proposed to choose a parton ansatz with a gapped band structure where the bands have non-zero Chern number. The specific ansatz proposed by Ref. [23] is shown in Fig. 1.12. The unit cell of the square lattice is enlarged to two sites and the fluxes of the χ_{ij} are chosen such that there is π flux through the squares and $\pi/2$ flux through triangles. The band structure of this ansatz consists of two bands separated by a finite gap with Chern number ± 1 . The ground state of the free parton Hamiltonian is obtained by filling up the valence band with spin up and spin

1. Introduction

down partons. The ansatz itself is not translationally invariant. Nevertheless, there are still gauge degrees of freedom for choosing a phase locally, i.e. the gauge transformation,

$$c_{i\alpha}^\dagger \rightarrow e^{i\theta_i} c_{i\alpha}^\dagger, \quad (1.2.39)$$

leaves the ansatz invariant. A translation in the x -direction followed by the gauge transformation,

$$c_{i\alpha}^\dagger \rightarrow (-1)^{i_x} c_{i\alpha}^\dagger, \quad (1.2.40)$$

restores the original ansatz. Thus, the projected wave function is translationally invariant. Nevertheless, the flux through elementary plaquettes or triangles cannot be altered by a gauge transformation like Eq. (1.2.39). Hence, the state with $\pi/2$ -flux through the triangles is not gauge-equivalent to the state with $-\pi/2$ -flux. Time-reversal symmetry is thus explicitly broken by this state.

Since the parton band structure is gapped, an effective theory of the gauge fields a_{ij} and μ_i in the parton mean-field Hamiltonian Eq. (1.2.35) can be obtained by integrating out the parton fields in the path integral formulation Eq. (1.2.31). The resulting theory is a pure gauge theory. Taking the proper continuum limit it can be shown that the effective action is given by [23]

$$S = \int d^3x \frac{1}{2} \sigma_{xy} a_\mu \partial_\nu a_\lambda \epsilon_{\mu\nu\lambda} + \mathcal{O}(1/g^2), \quad \mu = 0, 1, 2. \quad (1.2.41)$$

Here a_0 and $a_{1,2}$ denote the continuum limits of the lattice gauge fields μ_i and a_{ij} respectively and the neglected terms are of order $1/g^2$, where g is proportional to the gap of the parton spectrum. The action Eq. (1.2.41) is called a Chern-Simons theory.

Chern-Simons theory prominently occurs in the theory of the fractional quantum Hall effect also as a low-energy effective field theory describing the plateaux of the Hall resistivity. Chiral spin liquids can, therefore, be considered as a spin analog of FQHE wave function. Response functions and quasiparticle statistics are encoded in the effective Chern-Simons theory Eq. (1.2.41). The Chern-Simons theory for the ansatz in Fig. 1.12 supports semionic statistics, i.e. braiding two parton excitations yields a statistical phase of $\pi/2$. We will study analogous states for triangular and kagome lattices in chapters 4 to 6. Semionic spinon statistics implies a twofold degenerate ground state for periodic boundary conditions [108]. This degeneracy can be observed well in numerical Exact Diagonalization studies.

Historically, the first construction of the CSL phase by Kalmeyer and Laughlin [24] is in close analogy to the Laughlin wave functions of the fractional quantum Hall effect. For a given spin configuration $|\sigma_1 \dots \sigma_N\rangle$ with $S_{\text{tot}}^z = 0$ let (x_i, y_i) be the positions of the $N/2$ up spins $|\uparrow\rangle$. The chiral spin liquid wave function as defined by Ref. [24] is given by its coefficients $\langle \sigma_1 \dots \sigma_N | \text{CSL} \rangle$ in the S^z basis,

$$\langle \sigma_1 \dots \sigma_N | \text{CSL} \rangle = \prod_{j < k} (z_j - z_k)^2 \exp \left\{ -\frac{1}{4l_0^2} \sum_{i=1}^{N/2} |z_i|^2 \right\}, \quad (1.2.42)$$

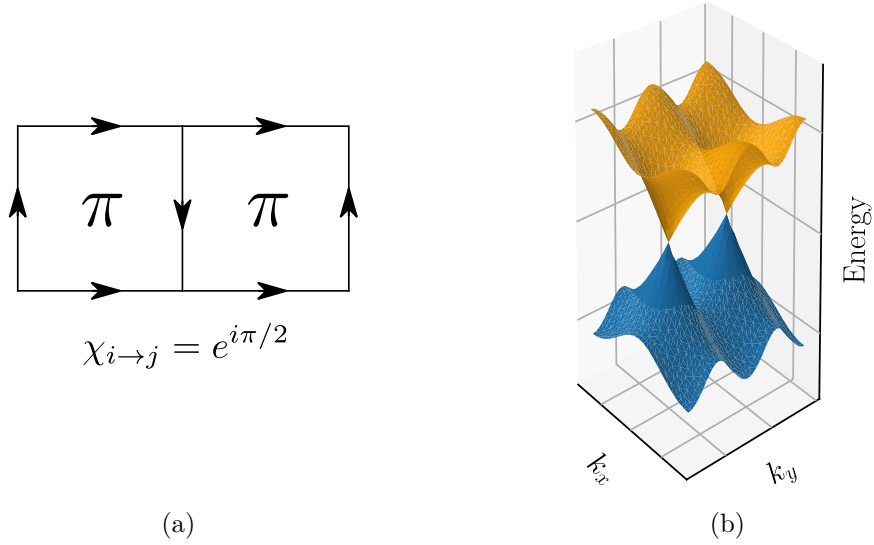


Figure 1.13.: Dirac spin liquids. (a) parton ansatz of the π -flux state in [92, 93]. The phases in the hopping parameters χ_{ij} are chosen that each plaquette has π -flux. (b) band structure of the π -flux parton ansatz. There are gapless excitations at the Fermi level with two distinct Dirac cones.

where $z_i = x_i + iy_i$ is the complex coordinate of the i -th up spin and l_0 is called the magnetic length. This corresponds to the bosonic Laughlin state [88] at filling fraction $\nu = 1/2$ of the fractional Quantum Hall effect.

This CSL state Eq. (1.2.42) can be proven to be a singlet state [109], which is not obvious at first sight. Spin correlations,

$$\langle \text{CSL} | \mathbf{S}_i \cdot \mathbf{S}_j | \text{CSL} \rangle, \quad (1.2.43)$$

can be computed numerically and have been shown to decay exponentially with distance. Quasihole wave functions can be regarded as excitations of the CSL wave function. Their semionic statistics can then directly be proven [109]. It is understood, that the Kalmeyer-Laughlin construction [24] yields the same CSL phase as the parton construction by Ref. [23].

1.2.5. Dirac Spin Liquids

Another prominent type of mean field parton ansätze are Dirac spin liquids, sometimes also called U(1) or algebraic spin liquids. Their parton band structure contains Dirac cones at the Fermi level, similar to the graphene band structure. This kind of ansatz has first been proposed by [92, 93]. The specific choice in [92, 93] is called the π -flux state. Its mean field parameters and band structure are shown in Fig. 1.13.

1. Introduction

In contrast to the chiral spin liquid ansatz in Fig. 1.12 the parton band structure is gapless. Consequently, the partons cannot safely be integrated out as for the chiral spin liquids. The effective low energy theory of the ansatz is described by 2×2 fermions, two for spin up/down times two for the Dirac cones of the band structure, which are coupled to the $U(1)$ gauge fields a_{ij} and μ_i in Eq. (1.2.35). The behavior of such gauge theories is not fully understood as of today. It is therefore not clear whether the gapless excitations are stable with respect to the gauge fluctuations. It has been shown that the Dirac spin liquid indeed exhibits gapless excitations with algebraically decaying correlation functions [110]. It is thus an example of a gapless state without long-range order. The Dirac spin liquid has been proposed as a wave function able to describe deconfined criticality [111], thus a wave function describing a quantum critical point. Another proposal suggests that the Dirac spin liquid may actually yield an extended phase in two dimensions [112], at least if the number of Dirac cones or the number of flavors (up/down) is increased. This can be viewed as an analogy to the Heisenberg spin-1/2 chain in one dimension.

Similar states have been proposed on the kagome and the triangular lattice [36, 113] for describing spin liquid phases whose nature is still debated.

Set the controls for the heart of the sun.

PINK FLOYD

2.1. Exact Diagonalization

Solving the stationary Schrödinger equation,

$$H|\psi\rangle = E|\psi\rangle, \quad (2.1.1)$$

of nonrelativistic quantum mechanics amounts to computing all eigenstates $|\psi\rangle$ and energies E of the Hamiltonian H . For problems without an exact analytical solution, the diagonalization of the Hamiltonian could be performed numerically. This method to numerically compute properties of a quantum system is called *Exact Diagonalization* (ED). Since eigenvectors and eigenvalues of matrices can be obtained up to high precision with modern algorithms, ED is a powerful and reliable numerical tool. Computing every single eigenvalue and eigenstate of the Hamiltonian completely solves the stationary Schrödinger equation, such that all physical quantities can in principle be derived from this solution. This numerical procedure is called *full diagonalization*. In order to diagonalize the Hamiltonian this way, a variety of numerical algorithms can be employed [114]. Although there are many differences between those, the computational effort of these methods is of the order $\mathcal{O}(D^3)$, where D is the linear dimension of the matrix. On present-day supercomputers matrices with linear dimension up to approximately $N \approx 10^6$ can be fully diagonalized.

For quantum many-body systems the Hilbert spaces \mathcal{H} are typically fermionic or bosonic Fock spaces or tensor products of local spin systems. The dimension of these kinds of Hilbert spaces increases exponentially with the number of particles considered. Thus, full diagonalizations become infeasible if the particle number is too large. If one is only interested in the ground state or several low-lying excitations iterative methods can be applied

2. Methods

that yield approximate eigenvalues at the boundary of the spectrum. The most prominent iterative algorithm for computing extremal eigenvalues and eigenvectors of Hermitian matrices is the Lanczos algorithm [115], which we will discuss in section 2.1.2. For sparse matrices, the complexity of the computation for achieving a fixed precision may effectively reduce to $\mathcal{O}(D)$. This allows for computations with orders of magnitude larger Hilbert spaces. For ED in condensed matter systems Hilbert space dimensions of $D \approx 10^{11}$ can currently be attained.

In this chapter, we introduce the basic principles of the ED method. In section 2.1.1 we explain how to represent Hilbert spaces and operators in a computer. We discuss basic principles and some practical issues about the Lanczos algorithm in section 2.1.2. Symmetries and the use of symmetry adapted wave functions for block diagonalization of matrices are discussed in section 2.1.3. We present novel algorithms for working with symmetry adapted wave functions and efficient distributed memory parallelization in chapter 3. There, we also present benchmarks for our implementation of these ideas.

2.1.1. Representing Hilbert spaces and operators

The first step towards practical numerical computations is to choose a basis of the Hilbert space. For spin systems with local dimension d we may choose the canonical basis of tensor products of local spins. Spin configurations are represented by an integer value via its d -ary representation. For instance, the spin-1/2 state of four particles $|\uparrow\uparrow\downarrow\uparrow\rangle$ is encoded as

$$|\uparrow\uparrow\downarrow\uparrow\rangle \rightarrow |1101\rangle \rightarrow (1101)_2 = (13)_{10}. \quad (2.1.2)$$

In general, we encode a spin configuration $|\sigma\rangle = |\sigma_1, \dots, \sigma_N\rangle$ on N lattice sites by

$$\text{int}(|\sigma\rangle) \equiv \sum_{k=1}^N \sigma_k d^{N-k}, \quad (2.1.3)$$

where d denotes the local dimension of the Hilbert space. Bases of fermionic or bosonic Hilbert spaces may be encoded correspondingly.

Given a basis $|\sigma_n\rangle$, $n = 1, \dots, D$, of the Hilbert space we can compute the matrix elements $\langle\sigma_n|H|\sigma_m\rangle$ of the Hamiltonian. For example, we can compute the matrix elements of a spin exchange term on a spin-1/2 state

$$\frac{1}{2}(S_2^+ S_3^- + S_2^- S_3^+) |(13)_{10}\rangle = \frac{1}{2}(S_2^+ S_3^- + S_2^- S_3^+) |\uparrow\uparrow\downarrow\uparrow\rangle = \frac{1}{2} |\uparrow\downarrow\uparrow\uparrow\rangle = \frac{1}{2} |(11)_{10}\rangle. \quad (2.1.4)$$

Thus, we have

$$\langle(11)_{10}|\frac{1}{2}(S_2^+ S_3^- + S_2^- S_3^+)|(13)_{10}\rangle = \frac{1}{2}. \quad (2.1.5)$$

We can then store all the elements in a numerical $D \times D$ matrix for full diagonalization. In case we want to apply iterative methods we may also store the elements in a sparse-matrix format or compute matrix-vector products on-the-fly without storing any matrix elements.

2.1.2. The Lanczos algorithm

Iterative methods drastically reduce the computational effort in computing extremal eigenvalues and eigenvectors,

$$A|v\rangle = \lambda|v\rangle, \quad (2.1.6)$$

of large matrices $A \in \mathbb{C}^{D \times D}$, where D is the dimension of the matrix. Typically a series of matrix-vector multiplications is performed to yield improving approximations to eigenvalues and eigenvectors. Krylov subspace methods such as the Lanczos algorithm [115] for Hermitian matrices are powerful and efficient iterative methods.

We give a short rationale for this kind of algorithms where we restrict ourselves to the case when A is Hermitian, $A^\dagger = A$. The Rayleigh coefficient of a matrix A is defined as

$$r_A(|v\rangle) \equiv \frac{\langle v|A|v\rangle}{\langle v|v\rangle}, \quad (2.1.7)$$

for all vectors $|v\rangle \in V \equiv \mathbb{C}^D$. The Rayleigh coefficient evaluated at an eigenvector $|\lambda\rangle$ yields the corresponding eigenvalue λ ,

$$r_A(|\lambda\rangle) = \lambda. \quad (2.1.8)$$

Minimizing the Rayleigh coefficient corresponds to finding a minimal eigenvalue λ_0 of the matrix A

$$\lambda_0 = \min_{v \in V} r_A(|v\rangle). \quad (2.1.9)$$

The minimal eigenvalue can be approximated by minimizing the Rayleigh coefficient in an n -dimensional subspace

$$V_n = \text{span}\{|v_1\rangle, \dots, |v_n\rangle\} \subseteq V. \quad (2.1.10)$$

To further improve the approximation we can apply the gradient descent method. The direction of steepest descent for Hermitian matrices A is given by

$$-\nabla r_A(|v\rangle) = \frac{2}{\langle v|v\rangle} (r_A(|v\rangle)|v\rangle - A|v\rangle). \quad (2.1.11)$$

The Krylov space of order n of a matrix A and a starting vector $|V_1\rangle$ is defined as

$$\mathcal{K}_n(A, |v_1\rangle) \equiv \text{span}\{|v_1\rangle, A|v_1\rangle, \dots, A^n|v_1\rangle\}. \quad (2.1.12)$$

The direction of steepest descent Eq. (2.1.11) in the n -th Krylov space $\mathcal{K}_n(A, |v_1\rangle)$ is an element of the next $(n+1)$ -th Krylov space $\mathcal{K}_{n+1}(A, |v_1\rangle)$. Thus, minimizing the Rayleigh coefficient in higher order Krylov spaces increases the accuracy of the approximation in Eq. (2.1.9) by means of the gradient descent method.

2. Methods

In general the vectors $|v_1\rangle, A|v_1\rangle, \dots, A^n|v_1\rangle$ are not orthonormal. The Lanczos method [115] iteratively constructs an orthonormal basis of the Krylov spaces. Given an orthonormal basis $|v_1\rangle, |v_2\rangle, \dots, |v_n\rangle$ of the n -th Krylov space we can use Gram-Schmidt orthogonalization to construct an orthonormal basis of the $(n+1)$ -th Krylov space. The next $(n+1)$ -th orthonormal basis vector is given by

$$|v_{n+1}\rangle = \frac{|\hat{v}_{n+1}\rangle}{\|\hat{v}_{n+1}\|}, \text{ where } |\hat{v}_{n+1}\rangle = A|v_n\rangle - \sum_{i=0}^n \langle v_n|A|v_i\rangle |v_i\rangle. \quad (2.1.13)$$

Using the orthogonality of the vectors $|v_k\rangle$ and the hermiticity $A^\dagger = A$, this procedure simplifies to (see e.g. [116])

$$|v_{n+1}\rangle = \frac{|\hat{v}_{n+1}\rangle}{\|\hat{v}_{n+1}\|} \text{ with } |\hat{v}_{n+1}\rangle = A|v_n\rangle - \langle v_n|A|v_n\rangle |v_n\rangle - \|\hat{v}_n\| |v_{n-1}\rangle. \quad (2.1.14)$$

The prescription Eq. (2.1.14) is called the *Lanczos recursion*. The vectors $|v_k\rangle$ are called the *Lanczos vectors*. We introduce the usual abbreviations found in literature,

$$\alpha_k \equiv \langle v_k|A|v_k\rangle, \quad \beta_k \equiv \|\hat{v}_k\|. \quad (2.1.15)$$

With these abbreviations the Lanczos recursion reads

$$|v_{n+1}\rangle = \frac{|\hat{v}_{n+1}\rangle}{\beta_{n+1}}, \text{ where } |\hat{v}_{n+1}\rangle = A|v_n\rangle - \alpha_n |v_n\rangle - \beta_n |v_{n-1}\rangle. \quad (2.1.16)$$

By defining the matrix of Lanczos vectors

$$V_n = (v_1 | \dots | v_n), \quad (2.1.17)$$

we can write the recursion Eq. (2.1.16) as [116]

$$AV_n = V_n T_n + |\hat{v}_{n+1}\rangle e_k^T, \quad (2.1.18)$$

where e_k is the k -th canonical basis vector of \mathbb{R}^k and the matrix T_n , called the n -th T-matrix, is a tridiagonal matrix given by

$$T_n = \begin{pmatrix} \alpha_1 & \beta_1 & 0 & \dots & 0 \\ \beta_1 & \alpha_2 & \beta_2 & 0 & \vdots \\ 0 & \beta_2 & \ddots & & \\ & & & \ddots & 0 \\ \vdots & & & \ddots & \alpha_{n-1} & \beta_{n-1} \\ 0 & \dots & 0 & \beta_{n-1} & \alpha_n \end{pmatrix}. \quad (2.1.19)$$

Since $T_n = V_n^\dagger A V_n$, the T-matrix can be interpreted as the projection of the matrix A onto

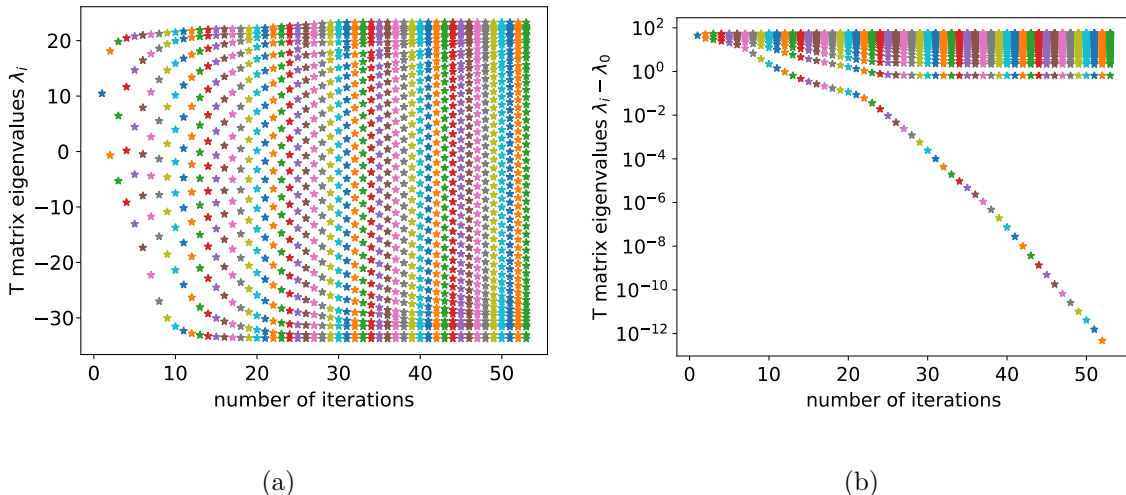


Figure 2.1.: (a) Convergence of the T-matrix eigenvalues. The matrix A diagonalized is the Hamiltonian of the spin-1/2 Heisenberg antiferromagnetic model on a 50 site square lattice in the ground state symmetry sector. The dimension of this sector is $D \approx 3 \cdot 10^{11}$. (b) Logarithmic plot of $\lambda_i - \lambda_0$. The speed of convergence of the ground state energy is exponential and a precision of 10^{-12} is reached after 53 Lanczos iterations.

$\mathcal{K}_n(A, |v_1\rangle)$. The T-matrix T_n thus approximates the matrix A on the n -th Krylov space. By λ_{k,T_n} and $|\lambda_{k,T_n}\rangle$ we denote the eigenvalues and eigenvectors of the n -th T-matrix. The sequence $(\lambda_{k,T_n})_{n \in \mathbb{N}}$ converges to an eigenvalue λ_k of A and the sequence $(V_n |\lambda_{k,T_n}\rangle)_{n \in \mathbb{N}}$ converges to the corresponding eigenvector $|\lambda_k\rangle$. The speed of convergence is typically exponential. Thus, already a small number of iterations yields a good approximation to the eigenvalues and eigenvectors of A . To converge for the minimal eigenvalue in condensed matter systems in this thesis typically 50 – 200 iterations suffice. The T-matrix is then diagonalized by a full diagonalization algorithm. Yet, a detailed analysis of the convergence behavior is subtle and we refer the reader to Refs. [117, 118]. A practical example of this convergence is shown in Fig. 2.1 for a matrix A of dimension $D \approx 3 \cdot 10^{11}$.

There are several practical issues concerning the Lanczos iteration. First of all, there are several ways of how to actually compute a single Lanczos iteration which are compared in Refs. [119–121]. If the matrix A is not stored in memory, thus matrix-vector multiplications are computed on-the-fly, the main memory requirement of the Lanczos algorithm is the storage of the Lanczos vectors. We make use of two simple variants which require storing either 2 or 3 vectors depending on whether the matrix A is real symmetric or complex Hermitian, cf. algorithm 2.1 and algorithm 2.2.

Another issue concerning the convergence of the Lanczos algorithm is the loss of orthogonality of the Lanczos vectors due to finite precision machine arithmetic. In several

2. Methods

Algorithm 2.1 Real-symmetric Lanczos step [120], only the current Lanczos vector $|v_n\rangle$ and a temporary vector $|w\rangle$ are stored. Applicable, if A is real and symmetric. In the first step $|w\rangle$ is initialized as the zero vector.

if $n = 1$: $|w\rangle \leftarrow 0, \beta_1 \leftarrow 0$

$|w\rangle \leftarrow A|v_n\rangle - \beta_n|w\rangle$

\triangleright r.h.s. $|w\rangle = |v_{n-1}\rangle$

$\alpha_n \leftarrow \langle w|v_n\rangle$

$|w\rangle \leftarrow |w\rangle - \alpha_n|v_n\rangle$

$\beta_{n+1} \leftarrow \sqrt{\langle w|w\rangle}$

Swap $|v_n\rangle \leftrightarrow |w\rangle$

$|v_{n+1}\rangle \leftarrow \frac{1}{\beta_{n+1}}|v_n\rangle$

Algorithm 2.2 Complex-Hermitian Lanczos step, storage of two Lanczos vectors $|v_n\rangle$ and $|v_{n-1}\rangle$ and a temporary vector $|w\rangle$ is required.

if $n = 1$: $\beta_1 \leftarrow 0$

$|w\rangle \leftarrow A|v_n\rangle$

$\alpha_n \leftarrow \langle w|v_n\rangle$

$|w\rangle \leftarrow |w\rangle - \alpha_n|v_n\rangle - \beta_n|v_{n-1}\rangle$

$|v_{n-1}\rangle \leftarrow |v_n\rangle$

$\beta_{n+1} \leftarrow \sqrt{\langle w|w\rangle}$

$|v_{n+1}\rangle \leftarrow \frac{1}{\beta_{n+1}}|w\rangle$

applications an explicit reorthogonalization of the Lanczos vectors is necessary. A survey of these methods is given by Ref. [121]. In practice, if one is only interested in a ground state or first excited state of some specific condensed matter system, it turns out that this reorthogonalization is not necessary. Also, reorthogonalization increases the memory requirements. Therefore, we always employ the simple Lanczos recursion without reorthogonalization in this thesis.

The Lanczos iterations construct the T-matrix which yields approximate eigenvalues λ_{k,T_n} . In case we are interested in approximate eigenvectors of A we have to compute $V_n |\lambda_{k,T_n}\rangle$. In order not to store all Lanczos vectors in V_n we first run the Lanczos algorithm to compute the T-matrix eigenvectors $|\lambda_{k,T_n}\rangle$ and then, in a second run, starting from the same initial vector $|v_1\rangle$, compute the linear combination $V_n |\lambda_{k,T_n}\rangle$. This requires one additional vector to be stored in memory.

2.1.3. Symmetries and symmetry-adapted wave functions

Apart from being most fundamental properties of a system, symmetries can be employed to divide an ED calculation into smaller pieces by block diagonalizing the Hamiltonian. In this chapter, we review the notion of quantum numbers and symmetry-adapted wave functions in a group theoretical setting. For basics on group representation theory in quantum mechanics, we refer to [122]. We then explain how, in principle, numerical calculations in a symmetrized basis can be performed.

Quantum numbers and degenerate eigenstates

A symmetry of a Hamiltonian H is an operator g that commutes with the Hamiltonian,

$$[H, g] = 0. \quad (2.1.20)$$

Denote by $|n, \alpha\rangle$ the eigenfunctions of H satisfying

$$H |n, \alpha\rangle = E_n |n, \alpha\rangle, \quad (2.1.21)$$

where the index α denotes the different degenerate eigenstates with eigenvalue E_n . Due to

$$Hg |n, \alpha\rangle = gH |n, \alpha\rangle = E_n g |n, \alpha\rangle, \quad (2.1.22)$$

the symmetry g leaves the eigenspaces for a given eigenvalue E_n invariant. A group \mathcal{G} of symmetries defines a representation ρ_n on the degenerate eigenspaces via

$$\Gamma^n : g \mapsto \Gamma(g), \quad (2.1.23)$$

where $\Gamma(g)_{\alpha\beta} \equiv (\langle n, \alpha | g | n, \beta \rangle)_{\alpha\beta}$ are matrices with dimension equal to the degeneracy of the eigenvalue E_n . Thus, every degenerate set of eigenvalues can be labeled by irreducible

2. Methods

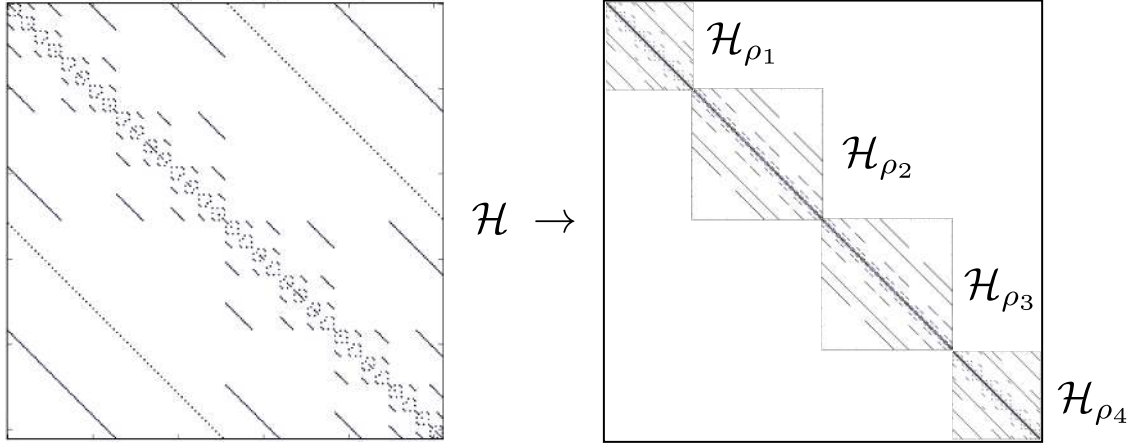


Figure 2.2.: Block diagonalization of a Hamiltonian. The Hilbert space \mathcal{H} is split into subspaces \mathcal{H}_{ρ_i} corresponding to an irreducible representation ρ_i of the symmetry group. The Hamiltonian transformed to the basis of symmetry-adapted wave functions is block diagonal.

representations of the symmetry group, its *quantum numbers*. Common examples are momentum quantum numbers for translational symmetry, total spin quantum numbers for spin rotational SU(2) symmetry for spin systems or parity for inversion symmetry.

A basis of the Hilbert space can be chosen such that the Hilbert space decomposes into a direct sum of subspaces,

$$\mathcal{H} = \bigoplus_{\rho} \mathcal{H}_{\rho}, \quad (2.1.24)$$

where the states in each subspace \mathcal{H}_{ρ} transform according to a given irreducible representation ρ of the symmetry group \mathcal{G} . We will work out how the exact form of these *symmetry-adapted wave functions* and their transformation properties for different kinds of symmetries in the following paragraphs. Importantly, the Hamiltonian does not couple states in different irreducible representation spaces,

$$\rho \neq \sigma \Rightarrow \langle \psi^{\rho} | H | \phi^{\sigma} \rangle = 0 \text{ for } |\psi^{\rho}\rangle \in \mathcal{H}_{\rho} \text{ and } |\phi^{\sigma}\rangle \in \mathcal{H}_{\sigma}. \quad (2.1.25)$$

Consequently, if we group the basis states of a given irreducible representation together we will have block diagonalized the Hamiltonian where every block is labeled by its irreducible representation, as shown in Fig. 2.2. We will now discuss the general block diagonalization principle for several specific symmetries.

Particle number conservation

Particle number conservation is often encountered in spin systems. For SU(2) Heisenberg spin systems like

$$H = \sum_{i,j} J_{ij} \mathbf{S}_i \cdot \mathbf{S}_j, \quad (2.1.26)$$

the total magnetization

$$S_{\text{tot}}^z = \sum_i S_i^z, \quad (2.1.27)$$

is a conserved quantity. Grouping together states of the same S_{tot}^z will therefore block diagonalize the Hamiltonian. The total S_{tot}^z labels the irreducible representations of the continuous U(1) symmetry,

$$g(\theta) = e^{i\theta S_{\text{tot}}^z}, \quad (2.1.28)$$

and the basis states transform according to

$$g(\theta) |\psi\rangle = e^{i\theta n} |\psi\rangle, \text{ if } S_{\text{tot}}^z |\psi\rangle = n |\psi\rangle. \quad (2.1.29)$$

We see that eigenstates in the S^z basis are already symmetry-adapted wave functions. While Eq. (2.1.28) and Eq. (2.1.29) are not necessary to understand and implement particle number conservation, their analogs for space group symmetries are essential for constructing the symmetry-adapted wave functions.

Discrete symmetries

Translational or point group symmetries imply (angular-)momentum conservation. These symmetries form a finite discrete group on finite size lattices. Following the general idea of decomposing the Hilbert space into irreducible representations in Eq. (2.1.24) we can use them to further decompose out Hilbert space into momentum or point group representation sectors. We review how to build the basis of symmetry-adapted wave functions for a discrete symmetry group \mathcal{G} . Detailed derivations can be found in [122]. Let

$$\Gamma^\rho : g \mapsto \Gamma^\rho(g), \quad (2.1.30)$$

be an irreducible representation of the symmetry group \mathcal{G} such that the representation matrices $\Gamma^\rho(g)$ are unitary. Given an arbitrary state $|\psi\rangle \in H$ its projection onto symmetry-adapted wave functions with irreducible representation ρ is given by [122]

$$|\psi_n^\rho\rangle \equiv \frac{1}{N_{\rho,n,\psi}} \sum_{g \in \mathcal{G}} (\Gamma^\rho(g)_{nn})^* g |\psi\rangle, \quad (2.1.31)$$

where $N_{\rho,n,\psi}$ is a normalization constant and $n \in \{1, \dots, d_\rho\}$, where d_ρ is the dimension of the representation Γ^ρ . The symmetry-adapted wave function in Eq. (2.1.31) now

2. Methods

transforms according to the n -th row of the representation Γ^ρ , i.e.

$$g |\psi_n^\rho\rangle = \sum_m \Gamma^\rho(g)_{nm} |\psi_m^\rho\rangle. \quad (2.1.32)$$

symmetry-adapted wave functions from different representations Γ^ρ are mutually orthonormal, i.e.

$$\langle \psi_n^\rho | \psi_m^\eta \rangle = \delta_{\rho\eta} \delta_{nm}. \quad (2.1.33)$$

In case we consider a one-dimensional representation of the symmetry group Eq. (2.1.31) simplifies to

$$|\psi^\rho\rangle \equiv \frac{1}{N_{\rho,\psi}} \sum_{g \in \mathcal{G}} \chi^\rho(g)^* g |\psi\rangle, \quad (2.1.34)$$

with the transformation property

$$g |\psi^\rho\rangle = \chi^\rho(g) |\psi^\rho\rangle, \quad (2.1.35)$$

where $\chi^\rho(g)$ denotes the character of the representation Γ^ρ and $N_{\rho,\psi}$ is a normalization constant.

Example (translational symmetries): We consider a spin-1/2 model on a $L \times L$ square lattice with periodic boundary conditions and lattice constant $a = 1$. The translational symmetry group consists out of L translations in the x -direction times L translations in the y -direction. We thus consider the Abelian symmetry group

$$\mathcal{G} = \mathbb{Z}_L \times \mathbb{Z}_L. \quad (2.1.36)$$

Its one-dimensional irreducible representations can be labeled by the lattice momenta

$$\mathbf{k}_{mn} = (k_m, k_n) = (2\pi m/L, 2\pi n/L), \quad m, n = 0, \dots, L-1 \quad (2.1.37)$$

whose characters are given by the Bloch factors

$$\chi_{\mathbf{k}_{mn}}(t_x^p \cdot t_y^q) = e^{i(k_m \cdot p + k_n \cdot q)}, \quad (2.1.38)$$

where $t_x^p \cdot t_y^q$ denotes a translation by p lattice sites in the x -direction and q lattice sites in the y direction. The symmetry-adapted wave functions are then given by

$$|\psi^{\mathbf{k}_{mn}}\rangle = \frac{1}{N_{\mathbf{k}_{mn},\psi}} \sum_{p,q=1}^L e^{i(k_m \cdot p + k_n \cdot q)} (t_x^p \cdot t_y^q) |\psi\rangle. \quad (2.1.39)$$

For a given finite discrete symmetry group all irreducible representations $\Gamma^\rho(g)$ can in principle be worked out. From the generic Eq. (2.1.31) and Eq. (2.1.34) the symmetry-adapted wave functions are then obtained. Discrete local symmetries like spin flip symmetry for spin-1/2 systems,

$$f = \prod_i \sigma_i^x, \quad (2.1.40)$$

can also be considered within this framework. This symmetry defines a \mathbb{Z}_2 symmetry group with an even and odd parity irreducible representation.

Moreover, if the symmetry group is a direct product of two subgroups $\mathcal{G} = \mathcal{A} \times \mathcal{B}$ the representations of \mathcal{G} are given by tensor products,

$$\Gamma^{(\rho,\nu)}(a \cdot b) = \Gamma^\rho(a) \otimes \Gamma^\nu(b), \quad (2.1.41)$$

of representations $\Gamma^\rho(a)$ and $\Gamma^\nu(b)$ of \mathcal{A} and \mathcal{B} . The characters are simply the product of the characters of \mathcal{A} and \mathcal{B}

$$\chi^{(\rho,\nu)}(a \cdot b) = \chi^\rho(a) \cdot \chi^\nu(b). \quad (2.1.42)$$

This can be applied to construct symmetry-adapted wave functions with a space group \mathcal{S} and a local symmetry group like \mathbb{Z}_2 for spin flip symmetry. Since local symmetries like the spin flip symmetry commute with space group symmetries the symmetry group $\mathcal{G} = \mathcal{S} \times \mathbb{Z}_2$ is a direct product. Hence, the representation matrices and characters of \mathcal{G} are given by Eq. (2.1.41) and Eq. (2.1.42).

For semi-direct products of groups, Eq. (2.1.41) and Eq. (2.1.42) do not hold in general. Space groups are in general only a semi-direct product of the translation group and the point group. We briefly discuss the representation theory of two-dimensional space groups in appendix A.

Computations in the symmetrized basis

From now we only consider one-dimensional representations of the symmetry group. We change the basis from pure spin configurations,

$$|\sigma\rangle = |\sigma_1 \dots \sigma_N\rangle \in \mathcal{H}, \quad (2.1.43)$$

to symmetry-adapted spin configurations,

$$|\sigma^\rho\rangle \in \mathcal{H}_\rho, \quad (2.1.44)$$

as defined in Eq. (2.1.34). For numerical implementations the question arises how to encode the symmetrized basis states $|\sigma^\rho\rangle$ and how to explicitly compute the matrix elements

$$\langle \tau^\rho | H | \sigma^\rho \rangle. \quad (2.1.45)$$

2. Methods

The symmetry group \mathcal{G} decomposes the space of pure spin configurations into disjoint orbits,

$$\text{Orbit}(|\sigma\rangle) = \{g|\sigma\rangle \mid g \in \mathcal{G}\}. \quad (2.1.46)$$

For every irreducible representation an orbit corresponds to a symmetrized state via Eq. (2.1.34). To encode such a symmetrized state we simply choose a single state $|\tilde{\sigma}\rangle \in \text{Orbit}(|\sigma\rangle)$ which unambiguously identifies the symmetrized state. We call the state $|\tilde{\sigma}\rangle$ the *representative* of $\text{Orbit}(|\sigma\rangle)$.

To choose a specific state in $\text{Orbit}(|\sigma\rangle)$ it is canonical to choose the state with the smallest integer encoding,

$$|\tilde{\sigma}\rangle = g_{\sigma}|\sigma\rangle, \quad \text{where } g_{\sigma} = \underset{g \in \mathcal{G}}{\text{argmin}} \text{int}(g|\sigma\rangle). \quad (2.1.47)$$

To compute the matrix elements of the Hamiltonian in Eq. (2.1.45) we decompose the Hamiltonian,

$$H = \sum_k H_k, \quad (2.1.48)$$

as a sum of non-branching terms H_k , i.e. for every single spin configurations $|\sigma\rangle$ there is only one other spin configuration $|\tau\rangle$, such that

$$H_k|\sigma\rangle = h_k|\tau\rangle, \quad (2.1.49)$$

where h_k is in general just a complex number. For instance, a simple spin-1/2 Heisenberg bond $\mathbf{S}_i \cdot \mathbf{S}_j$ does not fulfill the non-branching condition in Eq. (2.1.49) but it can be rewritten as a sum of a spin exchange bond $\frac{1}{2}(S_i^+ S_j^- + S_i^- S_j^+)$ and an Ising bond $S_i^z S_j^z$ which do indeed fulfill the condition Eq. (2.1.49) individually. Applying a non-branching bond on a representative does in general not yield another representative. Put differently, the state $|\tau\rangle$ in

$$|\tau\rangle = H_k|\tilde{\sigma}\rangle \quad (2.1.50)$$

is not necessarily minimal in $\text{Orbit}(|\tau\rangle)$. If g_{τ} is the element of the symmetry group that transforms $|\tau\rangle$ to its representative $|\tilde{\tau}\rangle$, i.e.

$$|\tilde{\tau}\rangle = g_{\tau}|\tau\rangle, \quad (2.1.51)$$

then the matrix element Eq. (2.1.45) is given by

$$\langle \tilde{\tau}^{\rho} | H_k | \tilde{\sigma}^{\rho} \rangle = \chi^{\rho}(g_{\tau}) \frac{N_{\rho, \tau}}{N_{\rho, \sigma}} \langle \tau | H_k | \tilde{\sigma} \rangle. \quad (2.1.52)$$

The right hand side of Eq. (2.1.52) contains the matrix elements in the unsymmetrized basis, the character $\chi^\rho(g_\tau)$ of the representation labeled by ρ evaluated at g_τ and the normalization constants $N_{\rho,\tau}$ and $N_{\rho,\sigma}$. Once a complete set of representatives is known, the Hamiltonian matrix in the symmetrized basis can be constructed via Eq. (2.1.52). If the original Hamiltonian is sparse, also the Hamiltonian in the symmetrized basis is sparse and a Lanczos algorithm can be applied for diagonalization.

2.2. Variational Monte Carlo

According to science history [123], Stanislaw Ulam invented the idea of Monte Carlo simulations while playing the card game Solitaire. Since computing the winning probability is much more interesting than actually playing the game, Ulam came up with an inventive idea to compute this probability. Instead of working out all possible permutations and ways of playing the cards a pretty good guess of the winning probability can be attained by simply playing several times and counting the number of wins. More generally, in case we want to compute a stochastic expectation value of the form

$$\langle f \rangle = \sum_x f(x)p(x), \quad (2.2.1)$$

of a function $f(x)$ with respect to the probability measure $p(x)$. Instead of summing over all microscopic configurations x we could compute the mean value,

$$\overline{\langle f \rangle} = \frac{1}{n} \sum_{i=1}^n f(X_i), \quad (2.2.2)$$

of n microscopic configurations X_i , which are chosen randomly according to the probability distribution $p(x)$. This yields an estimator $\overline{\langle f \rangle}$ for the true value $\langle f \rangle$, according to the law of large numbers. In case the samples X_i are independently distributed an unbiased error estimator is given by

$$\sigma_f^2 = \frac{1}{n-1} \sum_{i=1}^n \left(f(X_i) - \overline{\langle f \rangle} \right)^2. \quad (2.2.3)$$

A refined method of stochastically estimating an expectation value Eq. (2.2.1) is given by the Markov Chain Monte Carlo method, which we briefly review in section 2.2.1. Expectation values of the form

$$\langle \mathcal{O} \rangle = \frac{\langle \psi | \mathcal{O} | \psi \rangle}{\langle \psi | \psi \rangle}, \quad (2.2.4)$$

can be written as a stochastic expectation value as in Eq. (2.2.1). This way, physical properties of variational wave functions $|\psi\rangle$ can be evaluated in a computationally efficient way. We will discuss this *Variational Monte Carlo*, short VMC, method in section 2.2.2. For applying the VMC method we need to compute coefficients of variational wave functions in a given basis. The coefficients of Gutzwiller projected wave functions in the local S^z basis are presented in section 2.2.3.

2. Methods

2.2.1. Markov Chain Monte Carlo

Here, we summarize the basic principles of Markov Chain Monte Carlo methods, short MCMC. For a detailed exposition see e.g. Ref. [124]. The basic idea of MCMC methods is to construct a Markov Chain $(X_i)_{i=1}^{\infty}$ with equilibrium distribution $p(x)$. The stochastic average Eq. (2.2.1) is then approximated by the estimator

$$\overline{\langle f \rangle} = \frac{1}{n} \sum_{i=1}^n f(X_i), \quad (2.2.5)$$

where X_i are now samples from the evolution of the Markov chain $(X_i)_{i=1}^{\infty}$. The samples X_i in the estimator Eq. (2.2.5) are taken once the distribution of the Markov samples X_i has converged to the equilibrium distribution $p(x)$. The balance condition,

$$\sum_y p(x)T(x \rightarrow y) = \sum_y p(y)T(y \rightarrow x), \quad (2.2.6)$$

together with the ergodicity of the Markov chain are necessary and sufficient conditions for the transition kernel $T(x \rightarrow y)$ to yield $p(x)$ as the equilibrium distribution. Each solution to this equation yields a Markov chain suitable for computing the estimator Eq. (2.2.5). The most popular transition kernel fulfilling this condition is the *Metropolis* kernel [125],

$$T(x \rightarrow y) = G(x \rightarrow y)A(x \rightarrow y), \quad (2.2.7)$$

where $G(x \rightarrow y)$ is called the *proposal distribution* and

$$A(x \rightarrow y) = \min \left(1, \frac{p(y) G(y \rightarrow x)}{p(x) G(x \rightarrow y)} \right) \quad (2.2.8)$$

is called the *acceptance rate*. $G(x \rightarrow y)$ encodes the strategy for choosing updates and $A(x \rightarrow y)$ defines a probability, whether or not a proposed update is accepted. This kernel additionally fulfills the more restrictive detailed balance condition,

$$p(x)T(x \rightarrow y) = p(y)T(y \rightarrow x), \quad (2.2.9)$$

for all microscopic x and y . Although this condition is sufficient to ensure convergence to the equilibrium distribution, it is not a necessary condition. Transition kernels not fulfilling the detailed balance condition have also been proposed [126] and can be used for minimizing rejection rates. Since subsequent values X_i of a Markov chain are in general not independent, the estimator σ_f^2 in Eq. (2.2.3) cannot be used to estimate the error of the mean value in Eq. (2.2.2). The correct general error estimator is given by

$$\sigma_{f,\text{dep}}^2 = \sigma_f^2(1 + 2\tau_f) = \frac{1}{n-1} \left[\sum_{i=1}^n \left(f(X_i) - \overline{\langle f \rangle} \right)^2 \right] (1 + 2\tau_f), \quad (2.2.10)$$

where the autocorrelation time τ_f of the quantity f is given by

$$\tau_f \equiv \frac{1}{\langle f^2 \rangle - \langle f \rangle^2} \sum_{t=1}^{\infty} \left(\langle f_1 f_{1+t} \rangle - \langle f \rangle^2 \right). \quad (2.2.11)$$

Hence, in order to estimate the true error Eq. (2.2.10) one can either directly estimate the autocorrelation time [127] or use so-called *binning analysis*.

Binning analysis

We collect the measurements X_i into n_B bins of size B such that $n_B \cdot B = n$, where n is the total number of measurements. In each bin, we compute the bin average

$$f_k^{(B)} = \frac{1}{B} \sum_{i=kB}^{k(B+1)} f(X_i). \quad (2.2.12)$$

In terms of these bin averages the mean estimator Eq. (2.2.2) can be written as

$$\overline{f} = \frac{1}{n_B} \sum_{k=1}^{n_B} f_k^{(B)}. \quad (2.2.13)$$

The main point of binning analysis is to define new error estimators,

$$\sigma_{f,B}^2 = \frac{1}{n_B - 1} \sum_{k=1}^{n_B} \left(f_k^{(B)} - \overline{f} \right)^2, \quad (2.2.14)$$

that converge to the generic error estimator Eq. (2.2.10),

$$\sigma_{f,\text{dep}}^2 = \lim_{B \rightarrow \infty} \sigma_{f,B}^2. \quad (2.2.15)$$

Convergence is reached for bin sizes $B \gg \tau_f$. Thus, one typically investigates the evolution of the error estimator $\sigma_{f,B}^2$ for increasing B , as shown exemplarily in Fig. 2.3. The binning analysis can also be performed by only storing $\mathcal{O}(\log n)$ measurements [128].

2.2.2. Stochastic sampling of quantum wave functions

Evaluating physical quantities of a pure quantum state $|\psi\rangle$ amounts to computing expectation values of the form

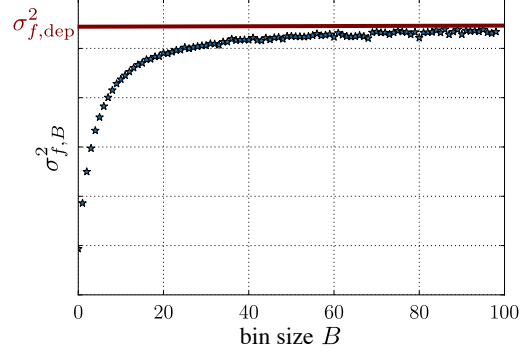
$$\langle \mathcal{O} \rangle = \frac{\langle \psi | \mathcal{O} | \psi \rangle}{\langle \psi | \psi \rangle}. \quad (2.2.16)$$

Once the coefficients $\langle x | \psi \rangle$ of the wave function $|\psi\rangle$ are known in a certain basis $|x\rangle$ of the Hilbert space, Eq. (2.2.16) can in principle be evaluated exactly by computing

$$\langle \mathcal{O} \rangle = \frac{1}{\mathcal{N}} \sum_{x,y} \langle \psi | x \rangle \langle x | \mathcal{O} | y \rangle \langle y | \psi \rangle, \quad (2.2.17)$$

2. Methods

Figure 2.3.: Typical error estimator $\sigma_{f,B}^2$ of a MCMC simulation for increasing bin size B . The error estimator finally reaches a plateau approximating the true error estimator $\sigma_{f,\text{dep}}^2$.



where

$$\mathcal{N} = \sum_x |\langle x|\psi\rangle|^2. \quad (2.2.18)$$

The computational effort scales with the dimension of the Hilbert space. Consequently, these calculations become infeasible for large system sizes. This limitation can be overcome by rewriting Eq. (2.2.17) to a form that allows for stochastic Monte Carlo sampling,

$$\langle \mathcal{O} \rangle = \frac{1}{\mathcal{N}} \sum_{x,y} \langle \psi|x\rangle \langle x|\mathcal{O}|y\rangle \langle y|\psi\rangle = \quad (2.2.19)$$

$$= \sum_y \left(\sum_x \frac{\langle \psi|x\rangle}{\langle \psi|y\rangle} \langle x|\mathcal{O}|y\rangle \right) |\langle y|\psi\rangle|^2 / \mathcal{N} \quad (2.2.20)$$

$$\equiv \sum_y f(y)p(y). \quad (2.2.21)$$

Eq. (2.2.21) now corresponds to a stochastic expectation value of the function

$$f(y) = \sum_x \frac{\langle \psi|x\rangle}{\langle \psi|y\rangle} \langle x|\mathcal{O}|y\rangle, \quad (2.2.22)$$

with respect to the probability measure

$$p(y) = |\langle y|\psi\rangle|^2 / \mathcal{N}. \quad (2.2.23)$$

This can now be evaluated by the Metropolis Monte Carlo algorithm as presented in section 2.2.1. When using the Metropolis transition kernel, only ratios $\langle x|\psi\rangle/\langle y|\psi\rangle$ of the coefficients are needed to evaluate Eq. (2.2.21). Sometimes, these ratios can be computed more efficiently than the coefficients $\langle x|\psi\rangle$ itself, as is the case for Gutzwiller projected wave functions.

2.2.3. Coefficients of Gutzwiller projected wave functions

Gutzwiller projected wave functions, short GPWF, are correlated many electron states. They were introduced by Martin Gutzwiller [103, 129] as variational wave functions for

Hubbard models appearing in the study of high-temperature superconductivity. We already discussed them in section 1.2.2 and section 1.2.3 in the context of the parton construction of spin liquids. Here, we want to discuss how to compute coefficients of these wave functions and how to perform quick Monte Carlo updates via evaluating only ratios of coefficients.

The Gutzwiller projection operator is given by [103, 104]

$$P_{\text{GW}} = \prod_i (1 - n_{i\uparrow}n_{i\downarrow}), \quad (2.2.24)$$

where $n_{i\sigma} = c_{i\sigma}^\dagger c_{i\sigma}$ for fermionic creation and annihilation operators $c_{i\sigma}^\dagger$ and $c_{i\sigma}$, $\sigma = \uparrow\downarrow$. It sets the part of a many-body wave function with double site occupancy to zero. This can be thought of as enforcing a hard-core constraint on a fermionic wave function. A GPWF is now given by applying this projector to an uncorrelated product state wave function

$$|\psi_{\text{GPWF}}\rangle = P_{\text{GW}} |\psi_0\rangle. \quad (2.2.25)$$

$|\psi_0\rangle$ can be chosen as the ground state of the parton mean-field Hamiltonian in Eq. (1.2.27). For simplicity, we consider a simple tight binding parton ansatz without pairing terms,

$$H = \sum_{\substack{i,j \\ \sigma}} t_{ij} c_{i\sigma}^\dagger c_{j\sigma} + \text{H.c.}, \quad (2.2.26)$$

which can be diagonalized

$$a_{i\sigma}^\dagger = \sum_j u_j^i c_{j\sigma}^\dagger \quad (2.2.27)$$

$$H = \sum_{i\sigma} \epsilon_i a_{i\sigma}^\dagger a_{i\sigma}, \quad (2.2.28)$$

where $(u^i)_j$ denotes the i -th eigenvector of the hopping matrix (t_{ij}) with eigenvalue ϵ_i . Its many-body ground state is given by

$$|\psi_0\rangle = \prod_{\substack{\epsilon_i < E_F \\ \sigma}} a_{i\sigma}^\dagger |0\rangle, \quad (2.2.29)$$

where energy levels are filled up to the Fermi energy E_F . To investigate GPWFs [103, 129] numerically, we have to work out their coefficients in a computational basis. We are interested in the coefficients of this wave function at half filling, i.e.

$$N_{\text{up}} = N_{\text{down}} = N/2. \quad (2.2.30)$$

2. Methods

In this case, the coefficients of the ground state wave functions are explicitly given by the following $N \times N$ Slater determinant,

$$\langle \sigma_1 \sigma_2 \dots \sigma_N | \psi_0 \rangle = \det \begin{pmatrix} w_1^\uparrow(1, \sigma_1) & w_1^\uparrow(2, \sigma_2) & \dots & w_1^\uparrow(N, \sigma_N) \\ w_2^\uparrow(1, \sigma_1) & w_2^\uparrow(2, \sigma_2) & \dots & w_2^\uparrow(N, \sigma_N) \\ \vdots & \vdots & \ddots & \vdots \\ w_{N/2}^\uparrow(1, \sigma_1) & w_{N/2}^\uparrow(2, \sigma_2) & \dots & w_{N/2}^\uparrow(N, \sigma_N) \\ w_1^\downarrow(1, \sigma_1) & w_1^\downarrow(2, \sigma_2) & \dots & w_1^\downarrow(N, \sigma_N) \\ w_2^\downarrow(1, \sigma_1) & w_2^\downarrow(2, \sigma_2) & \dots & w_2^\downarrow(N, \sigma_N) \\ \vdots & \vdots & \ddots & \vdots \\ w_{N/2}^\downarrow(1, \sigma_1) & w_{N/2}^\downarrow(2, \sigma_2) & \dots & w_{N/2}^\downarrow(N, \sigma_N) \end{pmatrix}, \quad (2.2.31)$$

where

$$w_k^\uparrow(i, \sigma_i) = \begin{cases} (u^k)_i & \text{if } \sigma_i = \uparrow \\ 0 & \text{if } \sigma_i = \downarrow \end{cases} \quad \text{and} \quad w_k^\downarrow(i, \sigma_i) = \begin{cases} 0 & \text{if } \sigma_i = \uparrow \\ (u^k)_i & \text{if } \sigma_i = \downarrow \end{cases}. \quad (2.2.32)$$

The coefficients of more general GPWFs with pairing terms as in the general case in Eq. (1.2.27) can also be written in terms of Slater determinants, see e.g. [130].

The computational cost of evaluating the determinant in Eq. (2.2.31) is of the order $\mathcal{O}(N^3)$. In a typical Monte Carlo simulation, many of these coefficients have to be evaluated which becomes the bottleneck of the computation. A clever method to speed up these computations was proposed in [47]. The key observation is that in the Metropolis Monte Carlo sampling only ratios of coefficients have to be calculated. If two matrices differ only by one column the ratio of the determinants can be evaluated with $\mathcal{O}(N)$ operations if the inverse matrices are known. If an update is accepted, the inverse matrix has to be recomputed. This can also be done more efficiently with $\mathcal{O}(N^2)$ operations if the inverse of a matrix with only one different column is known. For details on this update procedure see [47].

II

Research projects

Symmetries and Parallelization for Large-Scale Exact Diagonalization

Computer, tea, Earl Grey, hot.

JEAN-LUC PICARD

Abstract

We present novel algorithms for fast and memory-efficient use of discrete symmetries in Exact Diagonalization computations of quantum many-body systems. These techniques allow us to work flexibly in the reduced basis of symmetry-adapted wave functions. Moreover, a parallelization scheme for the Hamiltonian-vector multiplication in the Lanczos procedure for distributed memory machines avoiding load balancing problems is proposed. We show that using these methods systems of up to 50 spin-1/2 particles can be successfully diagonalized.

3.1. Introduction

Exact Diagonalization, short ED, studies have in the past been a reliable source of numerical insight into various problems in quantum many-body physics. The method is versatile, unbiased and capable of simulating systems with a sign problem. The main limitation of ED is the typical exponential scaling of computational effort and memory requirements in the system size. Nevertheless, the number of particles feasible for simulation has steadily increased since the early beginnings [14, 131, 132]. Not only does increasing the number of particles yield better approximations to the thermodynamic limit, but also several interesting simulation clusters with many symmetries become available if more particles can be simulated. Having access to such clusters becomes important if several competing phases

3. Large-Scale Exact Diagonalization

ought to be realized on the same finite size sample. In this work, we present algorithms and strategies for the implementation of a state-of-the-art large-scale ED code and prove that applying these methods systems of up to 50 spin-1/2 particles can be simulated on present day supercomputers. There are two key ingredients making these computations possible:

1. **Efficient use of symmetries.** In section 3.2 we present algorithms to work with symmetry-adapted wave functions in a fast and memory efficient way. These so-called *sublattice coding techniques* allow us to diagonalize the Hamiltonian in every irreducible representation of a discrete symmetry group. The basic idea behind these algorithms goes back to H.Q. Lin [131].
2. **Parallelization of the matrix-vector multiplications** in the Lanczos algorithm for distributed memory machines. We propose a method avoiding load-balancing problems in message-passing and present a computationally fast way of storing the Hilbert space basis in section 3.3.

These ideas have been implemented and tested on various supercomputers. We present results and benchmarks of our implementation in section 3.4.

We refer the reader to section 2.1 for a basic introduction to the ED method. The Lanczos method is reviewed in section 2.1.2 and symmetry-adapted wave functions are discussed in section 2.1.3. In this chapter, we also only consider one-dimensional representations of the symmetry group. We recall some important notions. Consider a generic spin configuration on N lattice sites with local dimension d ,

$$|\boldsymbol{\sigma}\rangle = |\sigma_1, \dots, \sigma_N\rangle, \quad \sigma_i \in \{1, \dots, d\}. \quad (3.1.1)$$

The *symmetry-adapted basis states* $|\boldsymbol{\sigma}^\rho\rangle$ are defined as (cf. Eq. (2.1.34))

$$|\boldsymbol{\sigma}^\rho\rangle \equiv \frac{1}{N_{\rho,\boldsymbol{\sigma}}} \sum_{g \in \mathcal{G}} \chi^\rho(g)^* g |\boldsymbol{\sigma}\rangle, \quad (3.1.2)$$

where \mathcal{G} denotes a discrete symmetry group, ρ a one-dimensional representation of this group, $\chi^\rho(g)$ the character of this representation evaluated at group element g , and $N_{\rho,\boldsymbol{\sigma}}$ denotes the normalization constant of the state $|\boldsymbol{\sigma}^\rho\rangle$. The set of basis state spin configurations $|\boldsymbol{\sigma}\rangle$ is divided into *orbits* (cf. Eq. (2.1.46)),

$$\text{Orbit}(|\boldsymbol{\sigma}\rangle) = \{g |\boldsymbol{\sigma}\rangle \mid g \in \mathcal{G}\}. \quad (3.1.3)$$

The *representative* $|\tilde{\boldsymbol{\sigma}}\rangle$ within each orbit is given by as the element with smallest integer value coding (cf. Eq. (2.1.47)),

$$|\tilde{\boldsymbol{\sigma}}\rangle = g_\sigma |\boldsymbol{\sigma}\rangle, \quad \text{where} \quad g_\sigma = \underset{g \in \mathcal{G}}{\operatorname{argmin}} \operatorname{int}(g |\boldsymbol{\sigma}\rangle). \quad (3.1.4)$$

The matrix element $\langle \tilde{\tau}^\rho | H_k | \tilde{\sigma}^\rho \rangle$ for non-branching terms H_k for two symmetry-adapted basis states with representation ρ is given by (cf. Eq. (2.1.52))

$$\langle \tilde{\tau}^\rho | H_k | \tilde{\sigma}^\rho \rangle = \chi^\rho(g_\tau) \frac{N_{\rho,\tau}}{N_{\rho,\sigma}} \langle \tau | H_k | \tilde{\sigma} \rangle. \quad (3.1.5)$$

In the following we define

$$|\sigma\rangle < |\tau\rangle :\Leftrightarrow \text{int}(|\sigma\rangle) < \text{int}(|\tau\rangle). \quad (3.1.6)$$

3.2. Sublattice Coding techniques

Evaluating the matrix elements $\langle \tilde{\tau}^\rho | H_k | \tilde{\sigma}^\rho \rangle$ in Eq. (3.1.5) for all basis states $|\tilde{\sigma}^\rho\rangle$ and $|\tilde{\tau}^\rho\rangle$ efficiently is the gist of employing symmetries in ED computations. In an actual implementation on the computer we need to perform the following steps:

- Apply the non-branching term H_k on the representative state $|\tilde{\sigma}\rangle$. This yields a possibly non-representative state $|\tau\rangle$. From this, we can compute the factor $\langle \tau | H_k | \tilde{\sigma} \rangle$.
- Find the representative $|\tilde{\tau}\rangle$ of $|\tau\rangle$ and determine the group element g_τ such that $|\tilde{\tau}\rangle = g_\tau |\tau\rangle$. This yields the factor $\chi^\rho(g_\tau)$.
- Know the normalization constants $N_{\rho,\sigma}$ and $N_{\rho,\tau}$. These are usually computed when creating a list of all representatives and stored in a separate list.

The problem of finding the representative $|\tilde{\sigma}\rangle$ of a given state $|\sigma\rangle$ and its corresponding symmetry g_σ turns out to be the computational bottleneck of ED in a symmetrized basis. It is thus desirable to solve this problem fast and memory efficient. There are two straightforward approaches to solving this problem:

- Apply all symmetries directly to $|\tau\rangle$ to find the minimizing group element g_τ ,

$$g_\tau = \underset{g \in \mathcal{G}}{\text{argmin}} \text{int}(g |\tau\rangle). \quad (3.2.1)$$

This method does not have any memory overhead but is computationally slow since all symmetries have to be applied to the given state $|\tau\rangle$.

- For every state $|\sigma\rangle$ we store $|\tilde{\sigma}\rangle$ and g_σ in a lookup table. While this is very fast computationally, the lookup table for storing all representatives grows exponentially in the system size.

The key to solving the representative search problem adequately is to have an algorithm that is almost as fast as a lookup table, where memory requirements are within reasonable bounds. This problem has already been addressed by several authors [131, 132]. The

3. Large-Scale Exact Diagonalization

central idea in these so-called *sublattice coding techniques* is to have a lookup table for the representatives on a sublattice of the original lattice and combine the information of the sublattice representatives to compute the total representative. These ideas were first introduced in [131–133]. In the following paragraphs, we explain the basic idea behind these algorithms and propose a flexible extension to arbitrary geometries and number of sublattices.

Sublattice coding on two sublattices

For demonstration purposes, we consider a simple translationally invariant spin-1/2 system on a six-site chain lattice with periodic boundary conditions. The lattice is divided into two sublattices as in Fig. 3.1. The even sites form the sublattice A and the odd sites form the sublattice B . We enumerate the sites such that the sites 1 to 3 are in sublattice A and the sites 4 to 6 are in sublattice B . We choose the integer representation of a state $|\sigma\rangle$ such that the most significant bits are formed by the spins in sublattice A . The symmetry group we consider consists of the six translations on the chain

$$\mathcal{G} = \{\text{Id}, T, T_2, T_3, T_4, T_5\}, \quad (3.2.2)$$

where T_n denotes the translation by n lattice sites. The splitting of the lattice into two sublattices is stable in the sense that every symmetry element $g \in \mathcal{G}$ either maps the A sublattice to A and the B sublattice to B or the A sublattice to B and the B sublattice to A . We call this property *sublattice stability*. It is both a property of the partition of our lattice into sublattices and the symmetry group. Hence, the symmetry group is composed of two kinds of symmetries

$$\begin{aligned} \mathcal{G}_A &\equiv \{g \in \mathcal{G}; \quad g \text{ maps sublattice } A \text{ onto } A\}, \\ \mathcal{G}_B &\equiv \{g \in \mathcal{G}; \quad g \text{ maps sublattice } B \text{ onto } A\}. \end{aligned} \quad (3.2.3)$$

We denote by $|\sigma\rangle_A$ (resp. $|\sigma\rangle_B$) the state restricted to sublattice A (resp. B) and define the *sublattice representatives*,

$$\begin{aligned} \text{Rep}_A(|\sigma\rangle_A) &\equiv h_A |\sigma\rangle_A, \quad \text{where} \quad h_A = \underset{g \in \mathcal{G}_A}{\text{argmin}} \text{int}(g |\sigma\rangle_A), \\ \text{Rep}_B(|\sigma\rangle_B) &\equiv h_B |\sigma\rangle_B, \quad \text{where} \quad h_B = \underset{g \in \mathcal{G}_B}{\text{argmin}} \text{int}(g |\sigma\rangle_B), \end{aligned} \quad (3.2.4)$$

and the *representative symmetries*,

$$\begin{aligned} \text{Sym}_A(|\sigma\rangle_A) &\equiv \{g \in \mathcal{G}_A; \quad g |\sigma\rangle_A = \text{Rep}_A(|\sigma\rangle_A)\}, \\ \text{Sym}_B(|\sigma\rangle_B) &\equiv \{g \in \mathcal{G}_B; \quad g |\sigma\rangle_B = \text{Rep}_B(|\sigma\rangle_B)\}. \end{aligned} \quad (3.2.5)$$

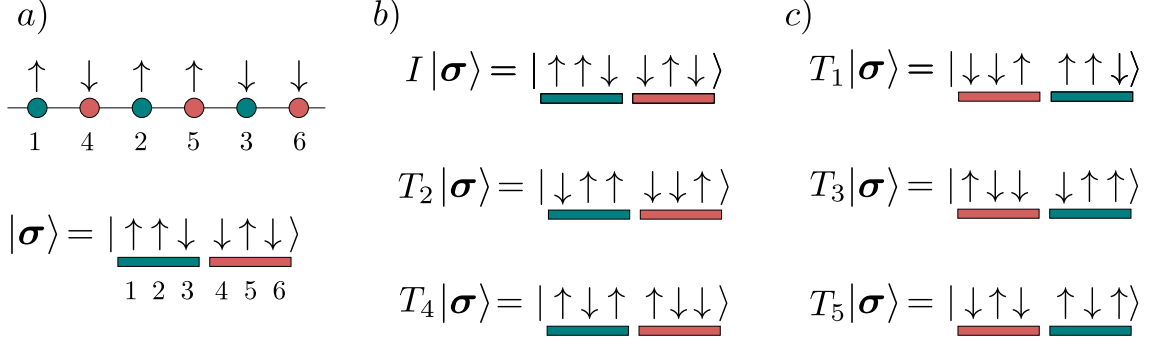


Figure 3.1.: Two sublattice coding of the spin state $|\sigma\rangle$ on a six-site chain lattice and action of translational symmetries. The sites are enumerated such that site 1-3 are on the blue sublattice A , 4-6 on the red sublattice B . The representative state with this enumeration of sites is given by $|\tilde{\sigma}\rangle = T_1|\sigma\rangle = |\downarrow\downarrow\uparrow\uparrow\downarrow\rangle$. Notice, that the symmetries act on real space and thus the transformation of the basis states also depends on the numbering of sites.

Let again $|\tilde{\sigma}\rangle = g_\sigma|\sigma\rangle$, where $|\tilde{\sigma}\rangle$ is the representative of $|\sigma\rangle$. The minimizing symmetry g_σ can only be an element of $\text{Sym}_A(|\sigma\rangle_A)$ if $\text{Rep}_A(|\sigma\rangle_A) \leq \text{Rep}_B(|\sigma\rangle_B)$, or vice versa. Put differently,

$$\text{Rep}_B(|\sigma\rangle_B) < \text{Rep}_A(|\sigma\rangle_A) \quad \Rightarrow \quad g_\sigma \notin \text{Sym}_A(|\sigma\rangle_A). \quad (3.2.6)$$

Otherwise, any symmetry element in $\text{Rep}_B(|\sigma\rangle_B)$ would yield a smaller integer value than g_σ . This is the core idea behind the sublattice coding technique. We store $\text{Rep}_{A,B}(|\sigma\rangle_{A,B})$ for every substate $|\sigma\rangle_{A,B}$ in a lookup table together with $\text{Sym}_{A,B}(|\sigma\rangle_{A,B})$. In a first step, we determine the sublattice representative with smallest most significant bits. Then we apply the representative symmetries to $|\sigma\rangle$ in order to determine the true representative $|\tilde{\sigma}\rangle$. The number of representative symmetries $|\text{Sym}_{A,B}(|\sigma\rangle_{A,B})|$ is typically much smaller than the total number of symmetries $|\mathcal{G}|$. The following example illustrates the idea and shows how to compute the representative given the information about sublattice representatives and representative symmetries.

Example We consider the state $|\sigma\rangle = |\uparrow\uparrow\downarrow\downarrow\uparrow\downarrow\rangle$ on a six-site chain lattice as in Fig. 3.1 a). Notice that the sites are not enumerated from left to right but such that sites 1 to 3 belong to the sublattice A and sites 4 to 6 belong to sublattice B . The states restricted on the sublattices are $|\sigma\rangle_A = |\uparrow\uparrow\downarrow\rangle$ and $|\sigma\rangle_B = |\downarrow\downarrow\uparrow\rangle$. The action of the sublattice symmetries

$$\begin{aligned} \mathcal{G}_A &\equiv \{\text{Id}, T_2, T_4\}, \\ \mathcal{G}_B &\equiv \{T_1, T_3, T_5\}, \end{aligned} \quad (3.2.7)$$

3. Large-Scale Exact Diagonalization

on $|\sigma\rangle$ is shown in Fig. 3.1 b) and c). From this, we compute the sublattice representatives as in Eq. (3.2.4),

$$\begin{aligned}\text{Rep}_A(|\sigma\rangle_A) &= |\downarrow\uparrow\uparrow\rangle, \\ \text{Rep}_B(|\sigma\rangle_B) &= |\downarrow\downarrow\uparrow\rangle,\end{aligned}\tag{3.2.8}$$

whose integer values are given by

$$\begin{aligned}\text{int}(\text{Rep}_A(|\sigma\rangle_A)) &= (011)_2 = 3, \\ \text{int}(\text{Rep}_B(|\sigma\rangle_B)) &= (001)_2 = 1.\end{aligned}\tag{3.2.9}$$

Since $\text{Rep}_B(|\sigma\rangle_B) < \text{Rep}_A(|\sigma\rangle_A)$ the symmetry g_σ yielding the total representative $|\tilde{\sigma}\rangle$ must be contained in

$$\text{Sym}_B(|\sigma\rangle_B) = \{T_1\},\tag{3.2.10}$$

which in this case just contains a single element, namely T_1 . Consequently, the representative $|\tilde{\sigma}\rangle$ is given by

$$|\tilde{\sigma}\rangle = T_1 |\sigma\rangle = |\downarrow\downarrow\uparrow\uparrow\uparrow\downarrow\rangle.\tag{3.2.11}$$

Lookup tables If the quantities $\text{Rep}_{A,B}(|\sigma\rangle_{A,B})$ and $\text{Sym}_{A,B}(|\sigma\rangle_{A,B})$ are now stored in a lookup table, this computation can be done very efficiently. Notice that instead of having to store 2^N entries in the lookup table for the representative we only need four lookup tables of order $\mathcal{O}(2^{N/2})$. On larger system sizes the difference between memory requirements of order $\mathcal{O}(2^N)$ and $\mathcal{O}(2^{N/2})$ is substantial.

To further speed up computations we also create lookup tables to store the action of each symmetry $g \in \mathcal{G}$ on a substate $|\sigma\rangle_A$,

$$\begin{aligned}\text{SymmetryAction}_A(g, |\sigma\rangle_A) &= g |\sigma\rangle_A, \\ \text{SymmetryAction}_B(g, |\sigma\rangle_B) &= g |\sigma\rangle_B.\end{aligned}\tag{3.2.12}$$

With this information, we can efficiently apply symmetries to a given spin configuration by looking up the action of g on the respective substate and combining the results. The memory requirement for these lookup tables is $\mathcal{O}(N_{\text{sym}}2^{N/2})$, where $N_{\text{sym}} = |\mathcal{G}|$. This can be reduced by generalizing the sublattice coding algorithm to multiple sublattices. The memory requirement then scales as $\mathcal{O}(N_{\text{sym}}2^{N/N_{\text{sublat}}})$, where N_{sublat} denotes the number of sublattices.

Generic sublattice coding algorithm

We start by discussing how we subdivide a lattice Λ into N_{sublat} sublattices. The basic requirement is that every symmetry group element either only operates within the sublattices or exchanges sublattices. We do not allow for symmetry elements that split up a sublattice onto different sublattices. Therefore we make the following definition:

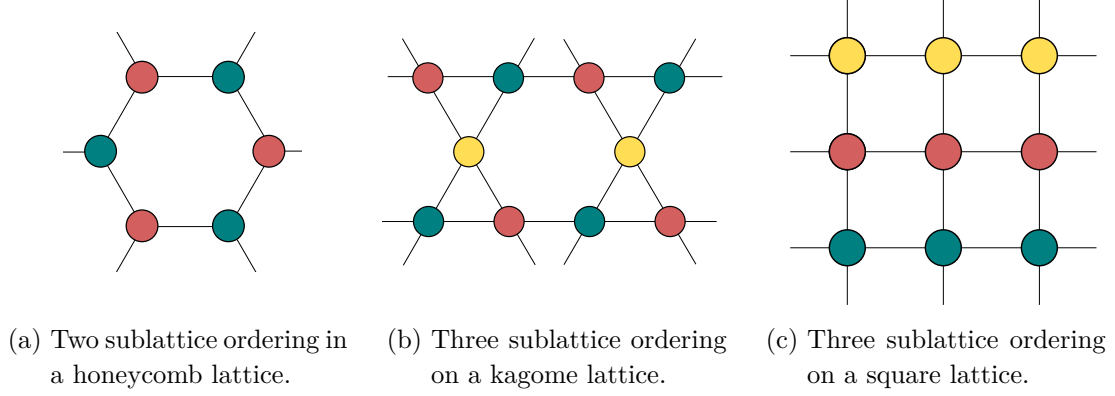


Figure 3.2.: Sublattice orderings for several common lattices. In figures Fig. 3.2a and Fig. 3.2b the sublattices are stable with respect to all spatial symmetries. In figure Fig. 3.2c the sublattices are stable with respect to all translational symmetries, horizontal and vertical reflections, 180° rotations but not with respect to 90° rotations or diagonal reflections.

Definition (Sublattice stability) A decomposition,

$$\Lambda = \bigcup_{X=1}^{N_{\text{sublat}}} \Lambda_X, \quad (3.2.13)$$

of a lattice Λ with symmetry group \mathcal{G} into N_{sublat} disjoint sublattices Λ_X is called *sublattice stable* if every $g \in \mathcal{G}$ maps each Λ_X onto exactly one (possibly different) Λ_Y , i.e. for all $g \in \mathcal{G}$ and all Λ_X there exists a Λ_Y such that

$$g(\Lambda_X) = \Lambda_Y.$$

The set Λ_X is called the *X-sublattice* of Λ .

The notion of *sublattice stability* is illustrated in Fig. 3.2. The sublattices Λ_X are drawn in different colors. A translation by one unit cell in Fig. 3.2a keeps the sublattices of the honeycomb lattice invariant whereas a 60° rotation exchanges the sublattices. For the kagome lattice in Fig. 3.2b a 60° rotation around a hexagon center for example cyclically permutes the three sublattices. One checks that for both Figs. 3.2a and 3.2b all translational as well as all point group symmetries are sublattice stable, so different color sublattices are mapped onto each other. This is different for Fig. 3.2c. Still here all translational symmetries just permute the sublattices, but a 90° rotation splits up a sublattice into different sublattices. Nevertheless, a 180° rotation keeps the sublattices stable, similarly a vertical or horizontal reflection. Therefore, only the reduced point group D2 instead of the full D4 point group for the square lattice fulfills the sublattice stability condition in

3. Large-Scale Exact Diagonalization

this case. D2 and D4 denote the dihedral groups of order 4 and 8 with two- and four-fold rotations and reflections. Note, that for a square lattice a two or four sublattice decomposition for which the full D4 point group is sublattice stable can be chosen instead. The choice of sublattice decomposition in Fig. 3.2c just serves illustrational purposes.

From the definition of sublattice stability, it is clear that the total number of sites N has to be divisible by the number of sublattices N_{sublat} . The numbering of the lattice sites is chosen such that the lattice sites from $(X - 1)N/N_{\text{sublat}} + 1$ to XN/N_{sublat} belong to sublattice X . We choose the most significant bits in the integer representation to be the bits on sublattice 1. Similar as in the previous section we define the following quantities

Definition For every sublattice Λ_X we define the following notions:

- *sublattice symmetries:*

$$\mathcal{G}_X \equiv \{g \in \mathcal{G} \mid g \text{ maps sublattice } X \text{ onto sublattice } 1\}. \quad (3.2.14)$$

- *sublattice representative:*

$$\text{Rep}_X(|\sigma\rangle_X) \equiv h_X |\sigma\rangle_X, \quad \text{where } h_X = \underset{g \in \mathcal{G}_X}{\text{argmin}} \text{int}(g |\sigma\rangle_X), \quad (3.2.15)$$

where $|\sigma\rangle_X$ denotes the substate of $|\sigma\rangle$ restricted on sublattice Λ_X .

- *representative symmetries:*

$$\text{Sym}_X(|\sigma\rangle_X) \equiv \{g \in \mathcal{G}_X \mid g |\sigma\rangle_X = \text{Rep}_X(|\sigma\rangle_X)\}. \quad (3.2.16)$$

- *sublattice symmetry action:*

$$\text{SymmetryAction}_X(g, |\sigma\rangle_X) = g |\sigma\rangle_X. \quad (3.2.17)$$

The symmetries in \mathcal{G}_X map the sublattice X onto the most significant bits. Therefore, the symmetry that minimizes the integer value in the orbit must be contained in the representative symmetries of a minimal sublattice representative, i.e.

$$g_\sigma = \underset{g \in \mathcal{G}}{\text{argmin}} g |\sigma\rangle \Rightarrow g_\sigma \in \bigcup_{\substack{Y, \text{Rep}_Y(|\sigma\rangle_Y) \\ \text{minimal}}} \text{Sym}_Y(|\sigma\rangle_Y). \quad (3.2.18)$$

To find the minimizing symmetry g_σ , we only have to check the symmetries yielding the minimal sublattice representative. The quantities $\text{Rep}_X(|\sigma\rangle_X)$ and $\text{Sym}_X(|\sigma\rangle_X)$ are stored in lookup tables, whose size scales as $\mathcal{O}(2^{N/N_{\text{sublat}}})$. In order to quickly apply the symmetries, we can additionally store $\text{SymmetryAction}_X(g, |\sigma\rangle_X)$ in another lookup table. The memory cost of doing so scales as $\mathcal{O}(N_{\text{sym}} 2^{N/N_{\text{sublat}}})$ and thus requires the most memory. The generic sublattice coding algorithm consists of two parts. The preparation of the lookup tables is shown as pseudocode in algorithm 3.3. The pseudocode of the actual algorithm for finding the representative using the lookup tables is shown in algorithm 3.4.

Algorithm 3.3 Preparation of lookup tables for sublattice coding algorithm

```

for each substate  $|\sigma_X\rangle$  :
  for each sublattice  $X$  :
    compute the sublattice representative Eq. (3.2.15), store it to  $\text{Rep}_X(|\sigma\rangle_X)$ 
    compute the representative symmetries Eq. (3.2.16), store them to  $\text{Sym}_X(|\sigma\rangle_X)$ 
    for each symmetry  $g \in \mathcal{G}$  :
      compute  $g|\sigma\rangle_X$  and store it to  $\text{SymmetryAction}_X(g, |\sigma\rangle_X)$ 
  
```

Algorithm 3.4 Sublattice coding algorithm for finding the representative.

Input: state $|\sigma\rangle$ **Output:** representative $|\tilde{\sigma}\rangle$ and g_σ Determine $\text{MinRep} = \min_X \{\text{Rep}_X(|\sigma\rangle_X)\}$ Set $|\tilde{\sigma}\rangle = +\infty$ **for each** sublattice Y with $\text{Rep}_Y(|\sigma\rangle_Y) = \text{MinRep}$:**for each** symmetry $g \in \text{Sym}_Y(|\sigma\rangle_Y)$:compute $g|\sigma\rangle$ by using the lookup tables $\text{SymmetryAction}_X(g, |\sigma\rangle_X)$ **if** $g|\sigma\rangle < |\tilde{\sigma}\rangle$: $|\tilde{\sigma}\rangle \leftarrow g|\sigma\rangle$ $g_\sigma \leftarrow g$ **return** $|\tilde{\sigma}\rangle, g_\sigma$

Example We consider the same state on a six-site chain lattice as in Fig. 3.1, but now using a three sublattice decomposition in Fig. 3.3. We call the blue sublattice the A sublattice, the red B and the yellow C . Notice, that due to different sublattice structure the labeling of the real space sites is different from the two sublattice case. In the three sublattice case, we are now given the state

$$|\sigma\rangle = |\uparrow\uparrow\downarrow\downarrow\uparrow\downarrow\rangle. \quad (3.2.19)$$

Its substates are

$$|\sigma\rangle_A = |\uparrow\uparrow\rangle, \quad |\sigma\rangle_B = |\downarrow\downarrow\rangle, \quad |\sigma\rangle_C = |\uparrow\downarrow\rangle, \quad (3.2.20)$$

with corresponding sublattice representatives

$$\text{Rep}_A(|\sigma\rangle_A) = |\uparrow\uparrow\rangle, \quad \text{Rep}_B(|\sigma\rangle_B) = |\downarrow\downarrow\rangle, \quad \text{Rep}_C(|\sigma\rangle_C) = |\downarrow\uparrow\rangle, \quad (3.2.21)$$

and representative symmetries

$$\text{Sym}_A(|\sigma\rangle_A) = \{I, T_3\}, \quad \text{Sym}_B(|\sigma\rangle_B) = \{T_2, T_5\}, \quad \text{Sym}_C(|\sigma\rangle_C) = \{T_1\}. \quad (3.2.22)$$

The minimal sublattice representative MinRep as in algorithm 3.4 is given by

$$\text{MinRep} = \text{Rep}_B(|\sigma\rangle_B) = |\downarrow\downarrow\rangle. \quad (3.2.23)$$

3. Large-Scale Exact Diagonalization

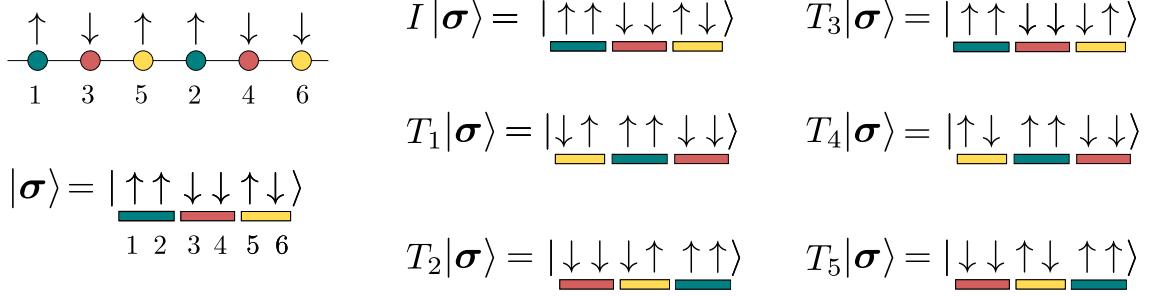


Figure 3.3.: Three sublattice coding of the spin state $|\sigma\rangle$ on a six-site chain lattice and action of translation symmetries. The sites are enumerated such that site 1 and 2 are on sublattice A, 3,4 on B and 5,6 on C. The representative state with this enumeration of sites is given by $|\tilde{\sigma}\rangle = T_2|\sigma\rangle = |\downarrow\downarrow\uparrow\uparrow\rangle$

The minimizing symmetry must now be in $\text{Sym}_B(|\sigma\rangle_B) = \{T_2, T_5\}$. We see that

$$T_2|\sigma\rangle = |\downarrow\downarrow\uparrow\uparrow\rangle < T_5|\sigma\rangle = |\downarrow\uparrow\downarrow\uparrow\rangle. \quad (3.2.24)$$

Therefore, the representative $|\tilde{\sigma}\rangle$ is given by

$$|\tilde{\sigma}\rangle = |\downarrow\downarrow\uparrow\uparrow\rangle, \quad (3.2.25)$$

with the minimizing symmetry $g_\sigma = T_2$. Notice, that this state differs from the one found in the two sublattice example since the labeling of the sites changes the integer representation of a state and thus the definition of the representative. Once a given labeling of sites is fixed the representative is of course unique.

3.3. Distributed and hybrid memory parallelization

For reaching larger system sizes in ED computations a proper balance between memory requirements and computational costs has to be found. There are two major approaches when applying the Lanczos algorithm. The Hamiltonian matrix can either be stored in memory in some sparse-matrix format or generated on-the-fly every time a matrix-vector multiplication is performed. Storing the matrix is usually faster, yet memory requirements are higher. This approach is for example pursued by the software package SPINPACK [134]. A matrix-free implementation of the Lanczos algorithm usually needs more computational time since the matrix generation, especially in a symmetrized basis can be expensive. Of course, the memory cost is drastically reduced since only a few vectors of the size of the Hilbert space have to be stored. It turns out that on current supercomputing infrastructures the main limitation in going to larger system sizes is indeed the memory requirements of the computation. It is thus often favorable to use a slower matrix-free

3.3. Distributed and hybrid memory parallelization

implementation, as done by the software package $\mathcal{H}\Phi$ [135], for example. Due to this reasons, we also choose the matrix-free approach.

The most computational time in the Lanczos algorithm is used in the matrix-vector multiplication. The remaining types of operations are scalar multiplications, dot products of Lanczos vectors or the diagonalization of the T -matrix which are usually of negligible computational cost. Today's largest supercomputers are typically distributed memory machines, where every process only has direct access to a small part of the total memory. It is thus a nontrivial task to distribute data onto several processes and implement communication amongst them once remote memory has to be accessed. Also, when scaling the software to a larger amount of processes load balancing becomes important. The computational work should be evenly distributed amongst the individual processes in order to avoid waiting times in communication. In the following, we explain how we achieve this goal in our implementation using the Message Passing Protocol (MPI) [136].

Matrix-vector multiplication The Hamiltonian can be written a sum of non-branching terms,

$$H = \sum_k H_k, \quad (3.3.1)$$

as in Eq. (2.1.49). To perform the full matrix-vector multiplication we compute the matrix-vector multiplication for the non-branching terms H_k and add up the results,

$$H |\psi\rangle = \sum_k H_k |\psi\rangle. \quad (3.3.2)$$

We denote by

$$\{|\sigma_i\rangle\}, \quad i = 1, \dots, D, \quad (3.3.3)$$

a (possibly symmetry-adapted) basis of the Hilbert space. A wave function $|\psi\rangle$ is represented on the computer by storing its coefficients $\langle\sigma_i|\psi\rangle$. Given an input vector,

$$|\psi_{\text{in}}\rangle = \sum_{i=1}^D \langle\sigma_i|\psi_{\text{in}}\rangle |\sigma_i\rangle, \quad (3.3.4)$$

we want to compute the coefficients $\langle\sigma_i|\psi_{\text{out}}\rangle$ in

$$H_k |\psi_{\text{in}}\rangle = |\psi_{\text{out}}\rangle. \quad (3.3.5)$$

The resulting output vector $|\psi_{\text{out}}\rangle$ is given by

$$\begin{aligned} |\psi_{\text{out}}\rangle &= \sum_{i=1}^D \langle\sigma_i|\psi_{\text{out}}\rangle |\sigma_i\rangle = \sum_{i=1}^D \langle\sigma_i|H_k|\psi_{\text{in}}\rangle |\sigma_i\rangle \\ &= \sum_{i,j=1}^D c_k(\sigma_j) \langle\sigma_j|\psi_{\text{in}}\rangle \langle\sigma_i|\sigma'_j\rangle |\sigma_i\rangle, \end{aligned} \quad (3.3.6)$$

3. Large-Scale Exact Diagonalization

where $c_k(\boldsymbol{\sigma}_j)$ and $|\boldsymbol{\sigma}'_j\rangle$ are given by

$$H_k |\boldsymbol{\sigma}_j\rangle = c_k(\boldsymbol{\sigma}_j) |\boldsymbol{\sigma}'_j\rangle. \quad (3.3.7)$$

Notice, that in a symmetry-adapted basis, evaluating $c_k(\boldsymbol{\sigma}_j)$ requires the evaluation of Eq. (3.1.5), where the sublattice coding technique of section 3.2 can be applied. Clearly, we have

$$\langle \boldsymbol{\sigma}_i | \boldsymbol{\sigma}'_j \rangle = \begin{cases} 1 & \text{if } |\boldsymbol{\sigma}_i\rangle = |\boldsymbol{\sigma}'_j\rangle, \\ 0 & \text{else.} \end{cases} \quad (3.3.8)$$

For parallelizing the multiplication Eq. (3.3.6), we distribute the coefficients in the basis $\{|\boldsymbol{\sigma}_i\rangle\}$ onto the different MPI processes. This means we have a mapping,

$$\text{proc} : |\boldsymbol{\sigma}_i\rangle \rightarrow \{1, \dots, n_{\text{procs}}\}, \quad (3.3.9)$$

that assigns to every basis state of the Hilbert space its MPI process number. Here, n_{procs} denotes the number of MPI processes. In general, $|\boldsymbol{\sigma}_j\rangle$ and $|\boldsymbol{\sigma}'_j\rangle$ are not stored in the same process. Hence, the coefficient $c_k(\boldsymbol{\sigma}_j) \langle \boldsymbol{\sigma}_j | \psi_{\text{in}} \rangle$ has to be sent from the process no. $\text{proc}(|\boldsymbol{\sigma}_j\rangle)$ to process no. $\text{proc}(|\boldsymbol{\sigma}'_j\rangle)$. This makes communication between the processes necessary. This communication is buffered in our implementation, i.e. for every basis state $|\boldsymbol{\sigma}_j\rangle$ we first store the target basis state $|\boldsymbol{\sigma}'_j\rangle$ and the coefficient $c_k(\boldsymbol{\sigma}_j) \langle \boldsymbol{\sigma}_j | \psi_{\text{in}} \rangle$ locally. Once every local basis state has been evaluated, we perform the communication and exchange the information amongst all processes. This corresponds to an `MPI_Alltoallv` call in the MPI standard.

After this communication step, every process has to add the received coefficient to the locally stored coefficient $\langle \boldsymbol{\sigma}'_j | \psi_{\text{out}} \rangle$. For this, we have to search, where the now locally stored coefficient of the basis state $|\boldsymbol{\sigma}'_j\rangle$ is located in memory. Typically, we keep a list of all locally stored basis states defining the position of the coefficients. This list is then searched for the entry $|\boldsymbol{\sigma}'_j\rangle$, which can also be time-consuming and needs to be done efficiently. We are thus facing the following challenges when distributing the basis states of the Hilbert space amongst the MPI processes:

- Every process has to know which process any basis state $|\boldsymbol{\sigma}_i\rangle$ belongs to.
- The storage of the information about the distribution should be memory efficient.
- The distribution of basis states has to be fair, in the sense that every process has a comparable workload in every matrix-vector multiplication.
- The search for a basis state within a process should be done efficiently.

We will now propose a method to address these issues in a satisfactory way.

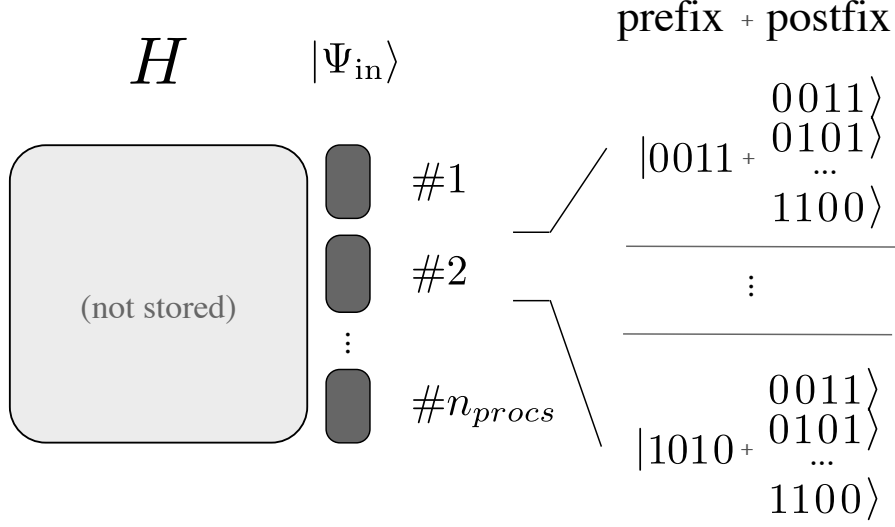


Figure 3.4.: Storage layout of the distributed Hilbert space. The prefixes are randomly distributed amongst the MPI processes using a hash function. States with same prefixes are mapped to the same process. Within a process, the states are ordered lexicographically. The Hamiltonian matrix is not stored.

Distribution of basis states The central point of our parallelization strategy is the proper choice of the distribution function $\text{proc}(\sigma)$ for the basis states in Eq. (3.3.9). We split up every basis state into prefix and postfix sites,

$$|\sigma\rangle = \underbrace{|\sigma_1 \cdots \sigma_{n_{\text{prefix}}}\rangle}_{\text{prefix sites}} \underbrace{|\sigma_{n_{\text{prefix}}+1} \cdots \sigma_{n_{\text{prefix}}+n_{\text{postfix}}}\rangle}_{\text{postfix sites}}, \quad (3.3.10)$$

where n_{prefix} and n_{postfix} denote the number of prefix and postfix sites. We decide that states with the same prefix are stored in the same MPI process. The prefixes are randomly distributed amongst all the processes. We do this by using a hash function that maps the prefix bits onto a random but deterministic MPI process. This hash function can be chosen such that every process has a comparable amount of states stored locally. Moreover, a random distribution of states reduces load balance problems significantly since the communication structure is randomized. This is in stark contrast to distributing the basis states in a linear fashion. Thereby, single processes can often have a multiple of the workload than other processes, thus causing idle time in other processes.

By choosing this kind of random distribution of basis states, we also don't have to store any information about their distribution. This information is all encoded in the hash function. Nevertheless, we store the basis states belonging to a process locally in an array. Finding the index of a given basis state also requires some computational effort. Here, we use the separation between prefix and postfix sites. We store the basis states in an ordered

3. Large-Scale Exact Diagonalization

Algorithm 3.5 Preparation of the distributed and symmetrized Hilbert space

Perform the following steps on every process in parallel (no communication necessary)
 myid denotes the number of the current MPI process
 prepares data structures **Basis**, **Limits** on each process

```

for each prefix spin configuration  $|\sigma_{\text{prefix}}\rangle = |\sigma_1 \cdots \sigma_{n_{\text{prefix}}}\rangle$  :
  if  $\text{proc}(|\sigma_{\text{prefix}}\rangle) \neq \text{myid}$  :
    continue
  else:
    begin = length(Basis)
    for each spin configuration  $|\sigma\rangle$  with prefix  $|\sigma_{\text{prefix}}\rangle$  :
      compute representative  $|\tilde{\sigma}\rangle$  of  $|\sigma\rangle$ 
      if  $|\sigma\rangle = |\tilde{\sigma}\rangle$  :
        append  $|\sigma\rangle$  to Basis
      end = length(Basis)
    if end  $\neq$  begin :
      insert  $(|\sigma_{\text{prefix}}\rangle, \text{begin}, \text{end})$  to Limits
  
```

Algorithm 3.6 Parallel matrix-vector multiply for a non-branching term H_k

Input: input wave function $|\psi_{\text{in}}\rangle$

Output: matrix-vector product $|\psi_{\text{out}}\rangle = H_k |\psi_{\text{in}}\rangle$

▷ Preparation and sending step (communication may be buffered)

for each basis state $|\sigma_j\rangle$ stored locally in **Basis** :

- apply non-branching term H_k and apply sublattice coding technique to compute $c_k(\sigma_j)$ and $|\sigma'_j\rangle$,

$$H_k |\sigma_j\rangle = c_k(\sigma_j) |\sigma'_j\rangle .$$

- compute $c = c_k(\sigma_j) \langle \sigma_j | \psi_{\text{in}} \rangle$
- send the pair $(|\sigma'_j\rangle, c)$ to process no. $\text{proc}(|\sigma'_j\rangle)$

▷ Receiving and search step

for each pair $(|\sigma'_j\rangle, c)$ received :

- determine indices (**begin**, **end**) from **Limits** $(|\sigma'_j\rangle)$
 - determine index i of $|\sigma'\rangle$ by binary search in array **Basis** between (**begin**, **end**)
 - Set $\langle \sigma'_j | \psi_{\text{out}} \rangle [i] \leftarrow c$
-

way. This way, states belonging to the same prefix are aligned in memory as shown in Fig. 3.4. We can store the index of the first and the last states that belong to a given prefix. To find the index of a given state we can now lookup the first and last index of the prefix of this state and perform a binary search for the state between these two indices. This reduces the length of the array we have to perform the binary search on and, hence, reduces the computational effort in finding the index. For implementing this procedure we need two data structures locally stored on each process.

1. An array $\mathbf{Basis}(i)$ storing all the basis states,

$$\mathbf{Basis}(i) = |\sigma_i\rangle, \quad i = 1, \dots, D. \quad (3.3.11)$$

2. An associative array $\mathbf{Limits}(|\sigma_{\text{prefix}}\rangle)$ storing the map

$$\mathbf{Limits}(|\sigma_{\text{prefix}}\rangle) = [\mathbf{begin}(|\sigma_{\text{prefix}}\rangle), \mathbf{end}(|\sigma_{\text{prefix}}\rangle)] \quad (3.3.12)$$

where $\mathbf{begin}(|\sigma_{\text{prefix}}\rangle)$ denotes the index of the first state with prefix $|\sigma_{\text{prefix}}\rangle$ and $\mathbf{end}(|\sigma_{\text{prefix}}\rangle)$ denotes the index of the last state with this prefix in the array $\mathbf{Basis}(i)$, $|\sigma_{\text{prefix}}\rangle = |\sigma_1 \cdots \sigma_{n_{\text{prefix}}}\rangle$.

In algorithm 3.5 we summarize how to prepare these data structures. The parallel matrix-vector multiplication in pseudocode is shown in algorithm 3.6. When working in the symmetry-adapted basis, the lookup tables of the sublattice coding method need to be accessible to every MPI process. One way to achieve this is of course, that every process generates its own lookup tables. However, in present-day supercomputers, several processes will be assigned to the same physical machine sharing the same physical memory. To save memory, the lookup tables are stored only once on a computing node. Its processes can then access the lookup tables via shared memory access. In our code, we use POSIX shared memory functions [137] to implement this hybrid parallelization.

3.4. Benchmarks

In order to assess the power of the methods proposed in the previous sections, we performed test runs to compute ground state energies. We considered the Heisenberg antiferromagnetic spin-1/2 nearest neighbor model on four different lattice geometries: square (48 sites), triangular (48 sites), kagome (48 sites) and square (50 sites). Fig. 3.5 shows the simulation clusters and the sublattice structure we used. The benchmarks were performed on three different supercomputers. The Vienna Scientific Cluster VSC3 is built up from over 2020 nodes with two Intel Xeon E5-2650v2, 2.6 GHz, 8 core processors, the supercomputer Hydra at the Max Planck Supercomputing & Data Facility in Garching with over 3500 nodes with 20 core Intel Ivy Bridge 2.8 GHz processors and the System B Sekirei at the Institute for Solid State Physics of the University of Tokyo with over 1584 nodes

3. Large-Scale Exact Diagonalization

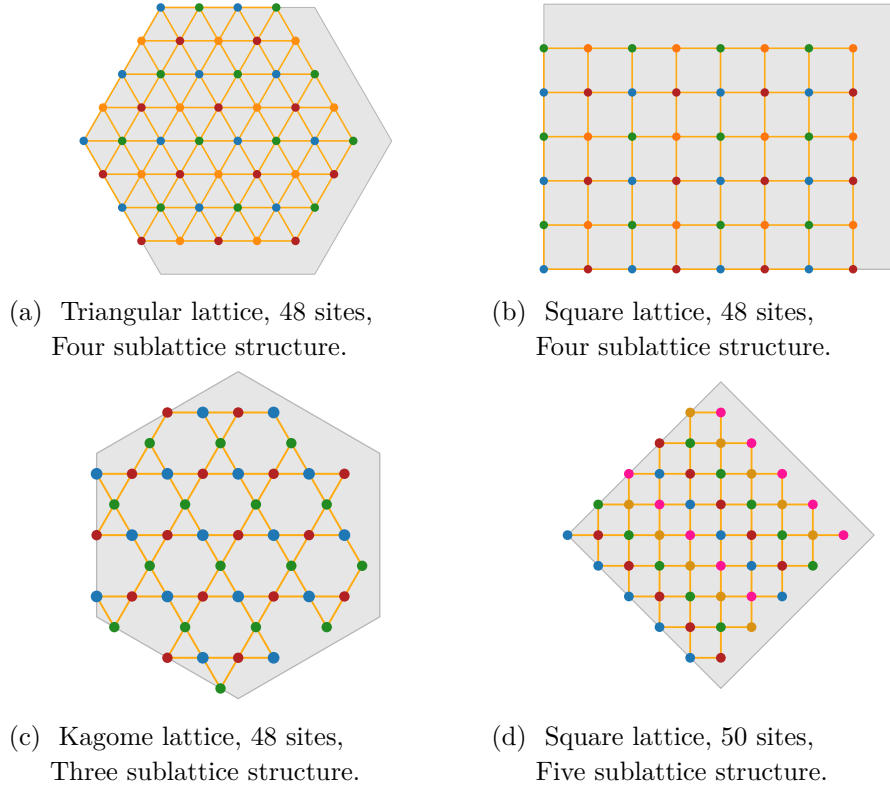


Figure 3.5.: Geometries of Heisenberg spin-1/2 model benchmarks. Different colors show the sublattice structure used for the sublattice coding technique. Grey background shows the Wigner-Seitz cell defining the periodicity of the lattice.

with two Intel Xeon E5-2680v3 12 core 2.5GHz processors. Both the Hydra and Sekirei use InfiniBand FDR interconnect, whereas the VSC3 uses Intel TrueScale Infiniband for network communication.

The benchmarks are summarized in table 3.1. We make use of all translational, certain point group symmetries and spin-flip symmetry. We show the memory occupied by a single lookup table for the symmetries. Since we use a single buffered and blocking all-to-all communication in the implementation it is straightforward to measure the percentage of time spent for MPI communication by taking the time before the communication call and afterward. In order to validate the results of our computation, we compared the results of the unfrustrated square case to Quantum Monte Carlo computations of the ground state energy. We used a continuous time world-line Monte Carlo Code [138] with 10^5 thermalization and 10^6 measurements at temperature $T = 0.01$. The computed energies per site are $E/N = -0.676013 \pm 2 \cdot 10^{-5}$ for the 48 site square cluster and $E/N = -0.67512 \pm 2 \cdot 10^{-5}$ for the 50 site cluster. The actual values computed with ED are within the error bars. The ground state energy of the kagome Heisenberg antiferromagnet on

Geometry computer	Triangular 48 Sekirei	Square 48 VSC3	Kagome 48 Hydra	Square 50 Sekirei
point group	D6	D2	D6	D2
# symmetries	1152	384	384	400
dimension	$2.8 \cdot 10^{10}$	$8.3 \cdot 10^{10}$	$8.4 \cdot 10^{10}$	$3.2 \cdot 10^{11}$
# cores	3456	8192	10240	3456
total memory	2.5 TB	n.A.	n.A.	15.5 TB
memory lookup	151 MB	50 MB	604 MB	17 MB
Time / MVM	399 s	1241 s	258 s	3304 s
% comm. time	39%	77%	48%	39%
g.s. sector	$\Gamma.A1.even$	$\Gamma.A1.even$	$\Gamma.A1.even$	$M.A1.odd$
g.s. energy	-26.8129452715	-32.4473598728	-21.0577870635	-33.7551019315

Table 3.1.: Benchmark results for various problems on three different supercomputer systems described in the main text. The employed symmetries include translational, point group and spinflip symmetry. We show the total memory used by all MPI processes and the memory used by the lookup tables for the sublattice coding technique. We also show the amount of time spent for communication.

48 sites has been previously computed [139] with a specialized code and agrees with our results. We see that the amount of time spent for communication is different for the three supercomputers. On Sekirei, a parallel efficiency of 61% on 3456 cores has been achieved.

3.5. Conclusion

We proposed the generic sublattice coding algorithm for making efficient use of discrete symmetries in large-scale ED computations. The method can be used flexibly on most lattice geometries and only requires a reasonable amount of memory for storing the lookup tables. The parallelization strategy for distributed memory architectures we discussed includes a random distribution of the Hilbert space amongst the parallel processes. Lookup tables of the sublattice coding technique are stored only once per node and are accessed via shared memory. Using these techniques, we showed that computations of spin-1/2 models of up to 50 spins have now become feasible.

Acknowledgements

We thank Synge Todo for making the simulations on Sekirei at the ISSP at the University of Tokyo possible. Further computations for this chapter have been carried out on VSC3 of the Vienna Scientific Cluster, the supercomputer Hydra at the Max Planck Supercomputing & Data Facility in Garching.

Nature of chiral spin liquids on the kagome lattice

This chapter has been published as:

Alexander Wietek, Antoine Sterdyniak, and Andreas M. Läuchli. “Nature of chiral spin liquids on the kagome lattice”. In: *Phys. Rev. B* 92.12 (2015). DOI: 10.1103/PhysRevB.92.125122. arXiv: 1503.03389 [cond-mat.str-el]

The numerical simulations and the development of simulation software has been performed by the author of this thesis. He also wrote substantial parts of the paper.

Abstract

We investigate the stability and the nature of the chiral spin liquids which were recently uncovered in extended Heisenberg models on the kagome lattice. Using a Gutzwiller projected wave function approach – i.e. a parton construction – we obtain large overlaps with ground states of these extended Heisenberg models. We further suggest that the appearance of the chiral spin liquid in the time-reversal invariant case is linked to a classical transition line between two magnetically ordered phases.

4.1. Introduction

The quest for quantum spin liquids [89] is currently a very active endeavour in condensed matter physics. This elusive state of quantum matter comes in various forms and is theoretically intensely studied, however was difficult to pin down in computational studies of *realistic* quantum spin Hamiltonians and hard to characterise unambiguously in experiments on quantum magnets.

The $S = 1/2$ Heisenberg antiferromagnet on the kagome lattice has emerged as one of the paradigmatic systems where quantum spin liquid phases are expected. A plethora of theoretical proposals have been put forward, ranging from valence bond crystals [37, 141–

4. Nature of chiral spin liquids on the kagome lattice

144], algebraic spin liquids [26–29], \mathbb{Z}_2 spin liquids [30–36], to chiral spin liquids [37–40]. Despite tremendous theoretical and computational progress [145–157], the true nature of the ground state and the low-lying excited states of the nearest neighbour Heisenberg model on the kagome lattice is still not settled completely.

Chiral spin liquids (CSL) are a particular family of spin liquids in which time-reversal symmetry (TRS) and parity symmetry are (spontaneously or explicitly) broken [23, 108]. The scalar chirality $\langle \mathbf{S}_i \cdot (\mathbf{S}_j \times \mathbf{S}_k) \rangle$ is non-zero and uniform and manifests the breaking of time-reversal and parity symmetries, analogous to the presence of an orbital magnetic field. In a favorable situation the breaking of these symmetries could conceivably lead to a spin analogue of the Fractional Quantum Hall Effect, although other types of ground states are possible as well [158, 159]. Historically Kalmeyer and Laughlin envisioned such a scenario by considering lattice versions of the bosonic $\nu = 1/2$ Laughlin wave function as candidate ground state wave functions for the triangular lattice Heisenberg model [24, 109].

In two recent papers [160, 161], two forms of chiral spin liquids have been discovered, which are stabilised away from the nearest neighbour Heisenberg model upon adding further neighbour Heisenberg interactions or scalar chirality terms to the Hamiltonian. Both studies numerically demonstrate the required ground state degeneracy and characterize the underlying topological order by computing the modular matrices. For different models CSLs have also been found in Refs. [45, 162, 163].

This breakthrough lays the foundation for further investigations of chiral spin liquids. Several pressing, important questions arise: i) are the two chiral spin liquids phases distinct or are they related? ii) is there a simple physical (lattice-based) picture or a variational wave function that describes the chiral spin liquid? iii) what is the "raison d'être" of these chiral spin liquids, i.e. why are the chiral spin liquids stabilized for the two reported Hamiltonians? Can we come up with some guiding principle which will allow to stabilise CSL on other lattices? In the following we will address each of these questions. In short we find that the two chiral spin liquids are indeed connected. We then demonstrate that appropriate Gutzwiller projected parton wave functions can have large overlaps with the numerically exact ground states of the studied microscopic models. And finally we show that one location of the chiral spin liquids in parameter space coincides largely with a transition line in the phase diagram of the corresponding classical model. The classical transition line lies between coplanar $\mathbf{q} = 0$ magnetic order and a chiral, non-coplanar magnetically ordered phase (*cuboc1* [38]).

4.2. Model

We will consider the following Hamiltonian which unifies the two models studied in Refs. [160, 161]:

$$\begin{aligned}
 H = & J_1 \sum_{\langle i,j \rangle} \mathbf{S}_i \cdot \mathbf{S}_j + J_2 \sum_{\langle\langle i,j \rangle\rangle} \mathbf{S}_i \cdot \mathbf{S}_j + \\
 & J_3 \sum_{\langle\langle\langle i,j \rangle\rangle\rangle} \mathbf{S}_i \cdot \mathbf{S}_j + J_\chi \sum_{i,j,k \in \Delta, \nabla} \mathbf{S}_i \cdot (\mathbf{S}_j \times \mathbf{S}_k).
 \end{aligned}
 \tag{4.2.1}$$

This model includes first, second and third nearest neighbour Heisenberg interactions with coupling constants J_1 , J_2 , J_3 as sketched in Fig. 4.1. The third nearest neighbour Heisenberg interactions are only considered across the hexagons. While these interactions preserve TRS and all the discrete lattice symmetries of the kagome lattice, the additional three-spin scalar chirality interactions on the triangles parametrized by J_χ break explicitly TRS and spatial parity. Note that Hamiltonian Eq. (4.2.1) features SU(2) invariance in spin space. For simplicity we will set $J_1 = 1$ in the following.

In Ref. [161] a CSL phase was found for $0.05\pi \lesssim \arctan |J_\chi/J_1| \lesssim \pi/2$ and $J_2 = J_3 = 0$. In this case, TRS is explicitly broken. Interestingly a two-fold degenerate ground state was found, which furthermore exhibits the expected modular data and entanglement spectrum for a topologically ordered chiral $\nu = 1/2$ Laughlin state-like phase. On the other hand in Ref. [160] a chiral spin liquid with *spontaneous* TRS breaking was discovered for $J_\chi = 0$ and $0.2 \lesssim (J_2 = J_3)/J_1 \lesssim 0.7$. Here the ground state degeneracy is four, which can

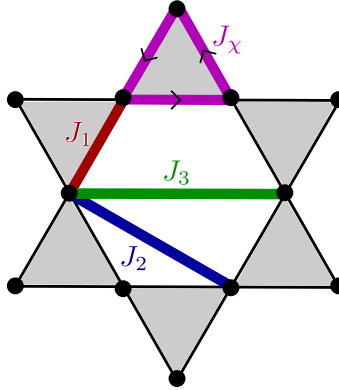


Figure 4.1.: Sketch of the kagome lattice and of the different interaction terms of the Hamiltonian (4.2.1). Heisenberg interactions between first, second and third nearest neighbour are considered. The third nearest neighbour Heisenberg interactions are only considered across the hexagons. Three-spin scalar chirality interactions, breaking time-reversal and parity symmetries, are also considered on grey shaded triangles.

4. Nature of chiral spin liquids on the kagome lattice

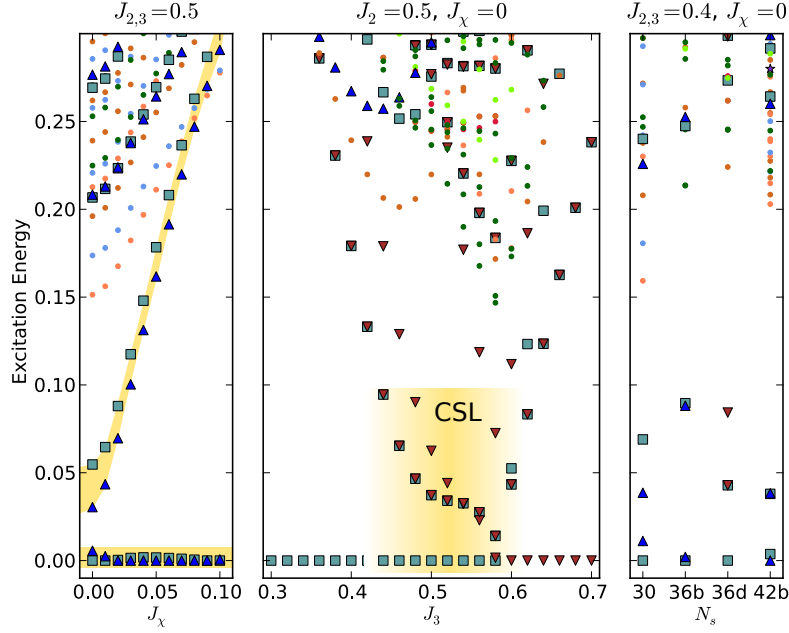


Figure 4.2.: Excitation Spectra from Exact Diagonalization. Different symbols and colors correspond to different momentum/pointgroup symmetry sectors. We use the cluster geometries and notation explained in Ref. [152] **(a)** Effect of J_χ term on spectrum on the 30 sites cluster. The four-fold degeneracy of the ground state is lifted to a two-fold degeneracy which corresponds to one sign of the scalar chirality. **(b)** Scan across the classical transition line for $J_\chi = 0$ on the 36b sites cluster. The four-fold degeneracy of the CSL is only present close to $J_2 = J_3$ (yellow shading). **(c)** Energy spectra for $J_2 = J_3 = 0.4$, $J_\chi = 0$ and various system sizes N_s and geometries. *Turquoise rectangle*: $(0,0)$ $[\Gamma]$ momentum, even under 180° rotation. *Blue up triangle*: $(0,\pi)$ $[M]$ momentum, odd under 180° rotation. *Red down triangle*: $(0,0)$ $[\Gamma]$ momentum, even under 180° rotation, odd under reflection.

be understood as arising from two copies of opposite chirality of a two-fold degenerate $\nu = 1/2$ Laughlin state. Unlike several topological phases as Toric code [41] and double-semion [164] phases that also have a four-fold ground state degeneracy, we will show that in this case time-reversal symmetry is spontaneously broken.

4.3. Energy spectroscopy

To investigate the persistence of this chiral spin liquid at the thermodynamical limit, we studied the model for $J_2 = J_3 = 0.4$ and $J_\chi = 0$ up to 42 sites. The low-energy spectra for different system sizes are shown in Fig. 4.2 c). While the energy splitting between the four ground states has a non-monotonous behaviour, the energy gap between the four lowest energy states and the fifth one increases with the system size. Moreover, the ratio of the energy splitting to the energy gap decreases with the system size, this tends to indicate that this phase is indeed realized at the thermodynamical limit. It is also important to notice that the momentum sectors involved in the four-fold degenerate manifold depend on the cluster shape and can be predicted in complete analogy to the Fractional Quantum Hall and Fractional Chern insulator states [165, 166].

In Fig. 4.2 a) we investigate the energy splitting of the four ground states as we switch on a finite J_χ coupling. At $J_\chi = 0$ the long-range order in the spin chirality is spectrally encoded in the presence of two states per topological sector, where the two states have to be at the same momentum, but differ in the spatial reflection quantum number (if the sample allows this symmetry). As is shown in Fig. 4.2 a), the two states per sector split very rapidly upon switching on $J_\chi \neq 0$. We can understand the action of J_χ regarding the scalar chirality in analogy to the effect of a longitudinal magnetic field on the two degenerate ground states in a ferromagnetic Ising model in the ordered phase, where the magnetic field immediately selects one of the two ordered states. As we show later based on overlaps, the chiral spin liquid thus selected by J_χ is of the same type as the one stabilised in the $J_1 - J_\chi$ model alone, and is connected to the TRS symmetric situation in the absence of J_χ .

In Fig. 4.2 b) we investigate the effect of a deviation from the $J_2 = J_3$ condition (in the absence of J_χ) by fixing $J_2 = 0.5$ and varying J_3 . One observes that the four-fold ground state degeneracy is rapidly lifted when J_3 deviates more than about $0.05 \sim 0.1$ from 0.5. Interestingly the line $0 < J_2 = J_3 < 1$ is the classical transition line between a magnetically ordered $\mathbf{q} = 0$ ground state for $J_3 < J_2$ and the non-coplanar magnetically ordered *cuboc1* phase for $J_3 > J_2$ [38]. Below we will show that also the overlaps with the variational wave functions are large only in the direct vicinity of this classical transition line. A deeper understanding of the classical ground state configurations on that line and of the effect of quantum fluctuations on that manifold might thus lead to an identification of the crucial ingredients required to predict and uncover chiral spin liquids in TRS Hamiltonians on different lattices. We note in passing that the explicitly TRS breaking Hamiltonian Eq. (4.2.1) with $J_\chi \neq 0$ can be considered as a truncated version of a parent Hamiltonian for the CSL constructed in Refs. [167, 168], similar to the spin Hamiltonian on the square lattice considered in Ref. [46].

In order to finally prove that the two CSLs from Refs. [160, 161] are in the same phase, Fig. 4.3 shows excitation spectra from Exact Diagonalization for a path connecting the

4. Nature of chiral spin liquids on the kagome lattice

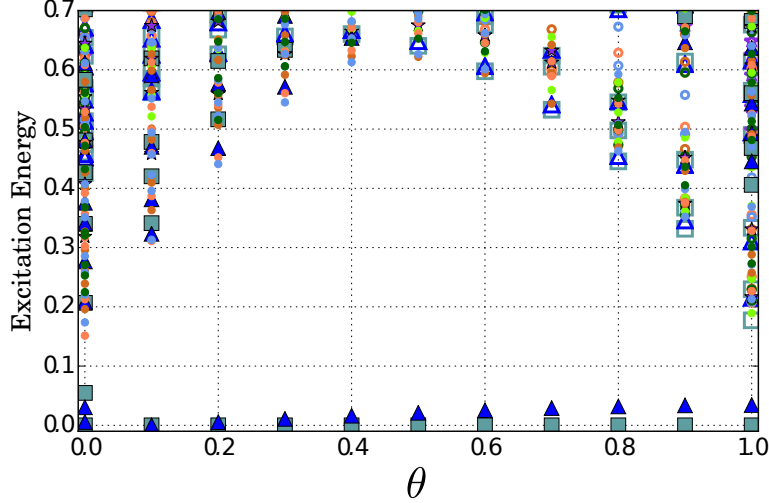


Figure 4.3.: Excitation Spectra for a path in phase space connecting the two CSLs from Refs. [160, 161] on a 30 sites lattice. The excitation spectra remain fully gapped over the whole path thus no phase transition takes place. The parameters in Eq. (4.2.1) are chosen $J_2 = J_3 = 0.5 \cos(\frac{\pi}{2}\theta)$, $J_\chi = \frac{1}{\sqrt{2}} \sin(\frac{\pi}{2}\theta)$ and $J_1 = \cos(\frac{\pi}{2}\theta) + \frac{1}{\sqrt{2}} \sin(\frac{\pi}{2}\theta)$ Turquoise rectangle: $(0, 0)$ [Γ] momentum, even under 180° rotation. Blue up triangle: $(0, \pi)$ [M] momentum, odd under 180° rotation.

two CSLs. We find that no gap is closing and thus the two phases are connected without a phase transition.

4.4. Parton construction and overlaps

As stated earlier on, the CSL can be considered as lattice analogues of the bosonic $\nu = 1/2$ Laughlin state. In recent years substantial activity focused on realizing such states on fractionally filled Chern insulators, so called Fractional Chern Insulators (FCI) [165, 169, 170]. It is thus a natural question whether the CSLs under consideration might also have such an interpretation. The natural bosonic $\nu = 1/2$ FCI state on the kagome lattice [171, 172] however does not have the correct magnetisation since it corresponds to magnetisation $m/m_{\text{sat}} = \pm 2/3$ instead of the required $m = 0$ ¹.

In the absence of a simple FCI candidate wave function we pursue an alternative approach, based on a parton construction. In order to understand and classify the different spin liquids a generalized construction scheme called parton construction has been in-

¹An interesting idea for future study might be to combine a *featureless* Mott insulator wave function with bosonic density $n = 1/3$ (i.e. magnetisation $m = 2/3$) with a $\nu = 1/2$ FCI state.

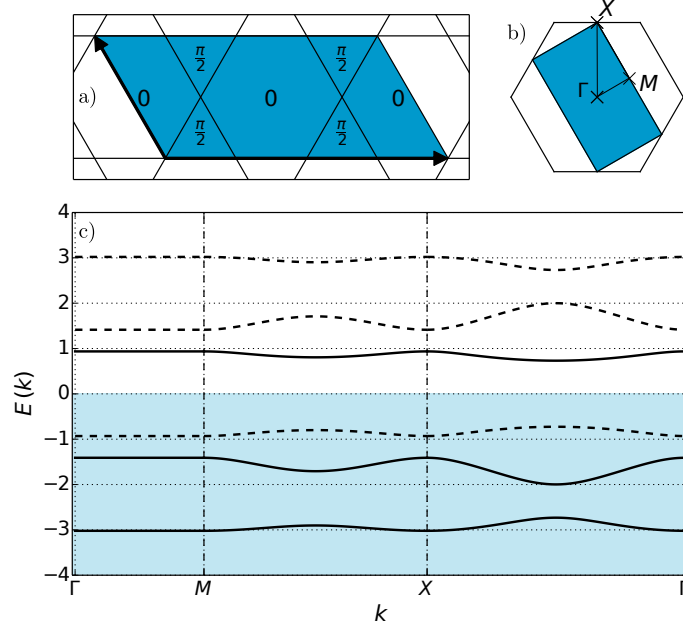


Figure 4.4.: Band structure of the $[\pi/2, 0]$ - model used to generate the pair of model states with positive scalar chirality. **a)** geometry of the unit cell. The mean-field parameters χ_{ij} are chosen such that there are $\pi/2$ fluxes through the triangles and no flux through the hexagons. **b)** Brillouin zone of the model (shaded) and conventional first Brillouin zone of the kagome lattice (hexagon). **c)** Band structure of the model along the path between high symmetry points in the Brillouin zone as drawn in b). The bands are separated by a finite gap. Each solid (dashed) band carries Chern number -1 ($+1$).

roduced by Refs. [106, 173–177] - see [178] for an introduction. The main idea of this technique is to split up each spin operator \mathbf{S}_i at site i into two fermionic parton operators $c_{i,\uparrow}$, $c_{i,\downarrow}$ according to

$$\begin{aligned} S_i^+ &= c_{i,\uparrow}^\dagger c_{i,\downarrow}, \quad S_i^- = c_{i,\downarrow}^\dagger c_{i,\uparrow}, \\ S_i^z &= \frac{1}{2}(c_{i,\uparrow}^\dagger c_{i,\uparrow} - c_{i,\downarrow}^\dagger c_{i,\downarrow}). \end{aligned} \quad (4.4.1)$$

Note that by introducing these operators the Hilbert space is enlarged due to the possibility of doubly occupied or vacant sites. Substituting the parton operators for the spin operators and performing a mean-field approximation by introducing mean-field parameters $\chi_{ij} = \sum_\sigma \langle c_{i\sigma}^\dagger c_{j\sigma} \rangle$ yields (ignoring constants) a tight-binding model of type

$$H_{\text{mean}} = \frac{1}{2} \sum_{i,j,\sigma} \left(\chi_{ij} c_{i\sigma}^\dagger c_{j\sigma} + \text{h.c.} \right). \quad (4.4.2)$$

4. Nature of chiral spin liquids on the kagome lattice

Several of these models have been investigated for the kagome lattice [26–29, 37]. Here we focus on nearest neighbour χ_{ij} only and the norm is chosen to be $|\chi_{ij}| = 1$. Physically different states can be created by choosing χ_{ij} such that different magnetic fluxes thread the triangles and the hexagons of the kagome lattice. Amongst these states we consider states whose parent mean-field models have uniform $\pm\pi/2$ flux through the triangles and zero flux through the hexagons [26, 27, 37]. To do so a magnetic six sites unit cell is needed instead of the standard three sites unit cell of the kagome lattice. In the following we will call these the $[\pm\pi/2, 0]$ - models. On the parton level these wave functions break time and parity symmetry. Thus the projected wave functions are expected to break these symmetries too. Moreover the states constructed from the $[\pi/2, 0]$ - model are related to the states of the $[-\pi/2, 0]$ - model by time-reversal symmetry.

The unit cell geometry, Brillouin zone and band structure of the $[\pi/2, 0]$ - model are shown in Fig. 4.4. All six bands have non-zero Chern numbers as indicated in Fig. 4.4c). To obtain a $S_z = 0$ model state, the three lowest bands are completely filled both for spins up and spins down and an exact Gutzwiller projection is applied to project onto the physical spin subspace. As the filled bands are separated by a finite gap from the empty ones, the spin-spin correlations after projection are expected to decay exponentially with distance, and thus describe a spin disordered state. The Chern number of the filled bands for the $[\pi/2, 0]$ - model ($[-\pi/2, 0]$ - model) is -1 ($+1$). The $[\pi/2, 0]$ - model ($[-\pi/2, 0]$ - model) yields a positive (negative) scalar chirality expectation value for every basic triangle. The average expectation value is the same for the two topological partners within numerical precision and is given by $\langle \mathbf{S}_i \cdot (\mathbf{S}_j \times \mathbf{S}_k) \rangle_{i,j,k \in \Delta, \nabla} = \pm 0.2057 \pm 0.0005$. The long-range chiral-chiral correlations are expected to be the square of this value. Thus we get value of 0.042 for the long-range chiral-chiral correlation functions which is within the same order of magnitude as the correlations computed in Refs. [179, 180].

On the torus there are two independent non contractible loops. Some of the gauge choices which leave the flux through the triangles and hexagons invariant, correspond to different fluxes through these torus loops. Threading flux through these loops corresponds to a Laughlin flux insertion. Thereby different topological states can be generated. These states cannot be distinguished by local observables and therefore are degenerate for local Hamiltonians in the thermodynamic limit. For the chiral spin liquid a two-fold topological ground state degeneracy is expected. Thus, by threading different fluxes through the torus we should only be able to create a two-dimensional space. We numerically computed the Gutzwiller projected wave functions (GPWFs) of the $[\pm\pi/2, 0]$ - models with a fixed gauge. In order to construct the topological partners of these states we additionally thread fluxes through the torus as explained in the previous section. We checked that for each of the $[\pm\pi/2, 0]$ - models, only two linearly independent states can be constructed as expected for a CSL within a numerical accuracy of 10^{-3} , similar as in Ref. [181].

We compare now these four model states with the ground state $|\psi_{\text{ED}}\rangle$ of the Hamiltonian (4.2.1) obtained using Exact Diagonalization. We choose the overlap $\mathcal{O}_{\text{GW}}^{\text{ED}}$ of the ground

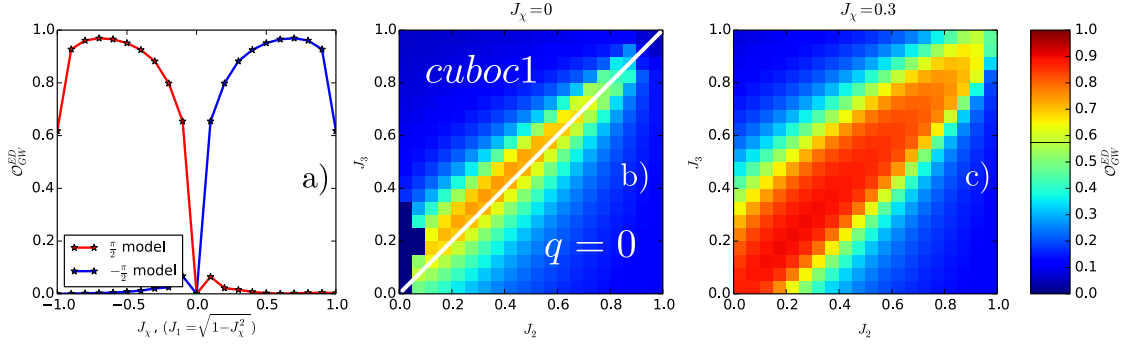


Figure 4.5.: Overlaps $\mathcal{O}_{\text{GW}}^{\text{ED}}$ of GPWFs with ground states from Exact Diagonalization for $J_2 = J_3 = 0$ and $J_1 = \sqrt{1 - J_\chi^2}$ on a 30 sites lattice. The overlaps of the GPWFs of the $\pm\pi/2$ -models are symmetric under changing the sign of J_χ . The maximum overlap is equal to 0.97 and is reached for $J_\chi = \pm 0.7$. The CSL phase extends almost up to the Heisenberg point.

state wave function with the four model states as our figure of merit:

$$\mathcal{O}_{\text{GW}}^{\text{ED}} \equiv \sqrt{\sum_{\alpha} |\langle \psi_{\text{ED}} \rangle \psi_{\text{GW}}^{\alpha}|^2} \quad (4.4.3)$$

Overlaps of the GPWFs with the ground state of the Hamiltonian (4.2.1) for different parameters on a $N_s = 30$ sites sample are shown in Fig. 4.5. The overlaps of our model state with the ground state wave functions of the model of Ref. [161] where $J_2 = J_3 = 0$, $J_1 = \cos \theta$ and $J_\chi = \sin \theta$ are shown in Fig. 4.5(a). We found that overlaps for J_χ between 0.1 and 1 range from 0.62 to 0.97. The overlap of the two GPWFs of the $[-\pi/2, 0]$ -model are by orders of magnitude larger than those of the $[\pi/2, 0]$ -model. For J_χ between -1 and -0.1 the overlaps are exactly the same within numerical precision as for J_χ between 0.1 and 1 but the role of the GPWFs from the $[\pi/2, 0]$ -model and $[-\pi/2, 0]$ -model are exchanged. This is expected since the model with negative J_χ should have a positive scalar chirality and therefore only little overlap with the variational states from the $[-\pi/2, 0]$ -model with negative chirality and vice versa.

For the time-reversal symmetric model with $J_\chi = 0$, our variational wave functions have substantial overlap only close to the line $J_2 = J_3$, in agreement with the energy spectroscopy results discussed above [Fig. 4.5(b)]. In this region the overlaps reach up to 0.72 for $N_s = 30$.

As can be seen in Fig. 4.5 c) for $J_\chi = 0.3$ and for $J_\chi = 0.6$ (not shown), the region of the CSL broadens significantly when J_χ is increased from zero. For $J_\chi = 0.3$ (resp. $J_\chi = 0.6$) the overlaps on the classical transition line for $J_2 = J_3$ between 0 and 0.7 range from 0.8 to 0.9 (resp. from 0.85 to 0.95).

4.5. Conclusion

We showed that the two recently found realizations of chiral spin liquids on the kagome lattice [160, 161] are indeed related and can be described by Gutzwiller projected parton wave functions. This yields an intuitive microscopic picture of the CSL phase stabilized in these models. The ansatz wave functions we chose have been shown to describe a CSL on the kagome lattice [26, 27, 37]. We constructed a pair of Gutzwiller projected parton CSL wave functions for each sign of the scalar chirality. We suggested that these states describe the CSL ground state found on the kagome lattice. To prove that indeed these wave functions describe the novel CSL phases found in Refs. [160, 161] we computed overlaps of these variational wave functions with the ground state wave functions computed by Exact Diagonalization. Substantial overlaps were found in regions of the phase diagram where the CSL is expected. By further investigation of excitation spectra, we showed that the CSL phase in Ref. [160] is only present on the transition line between a chiral *cuboc1* and a coplanar $q = 0$ phase of the classical phase diagram [38]. This could serve as a guiding principle for finding CSL phases in other models and on others lattices. Being related to the Laughlin state, these states should exhibit anyonic excitations. Their investigations will be pursued in a future work.

Note added

While completing the present manuscript we became aware of parallel work reaching similar conclusions using complementary methods [179, 180].

Acknowledgments

We acknowledge inspiring discussions with H.-H. Tu and A.B. Nielsen. AW acknowledges support through the Austrian Science Fund project I-1310-N27 (DFG FOR1807). AS acknowledges support through the Austrian Science Fund SFB FoQus (F-4018-N23). This work was supported by the Austrian Ministry of Science BMWF as part of the Konjunkturpaket II of the Focal Point Scientific Computing at the University of Innsbruck.

Chiral Spin Liquid and Quantum Criticality in Extended $S = 1/2$ Heisenberg Models on the Triangular Lattice

This chapter has been published as:

Alexander Wietek and Andreas M. Läuchli. “Chiral spin liquid and quantum criticality in extended $S = \frac{1}{2}$ Heisenberg models on the triangular lattice”. In: *Phys. Rev. B* 95.3 (2017). DOI: 10.1103/PhysRevB.95.035141. arXiv: 1604.07829 [cond-mat.str-el]

The numerical simulations and the development of simulation software has been performed by the author of this thesis. He also wrote substantial parts of the paper.

Abstract

We investigate the J_1 - J_2 Heisenberg model on the triangular lattice with an additional scalar chirality term and show that a chiral spin liquid is stabilized in a sizeable region of the phase diagram. This topological phase is situated in between a coplanar 120° Néel ordered and a non-coplanar tetrahedrally ordered phase. Furthermor we discuss the nature of the spin-disordered intermediate phase in the J_1 - J_2 model. We compare the ground states from Exact Diagonalization with a Dirac spin liquid wave function and propose a scenario where this wave function describes the quantum critical point between the 120° magnetically ordered phase and a putative \mathbb{Z}_2 spin liquid.

5.1. Introduction

The emergence of quantum spin liquids in frustrated quantum magnetism is an exciting phenomenon in contemporary condensed matter physics [89]. These novel states of matter exhibit fascinating properties such as long-range ground state entanglement [42, 183] or

5. Chiral Spin Liquid on the Triangular Lattice

anyonic braiding statistics of quasiparticle excitations, relevant for a potential implementation of topological quantum computation [6]. Only very recently such phases have been found to be stabilized in realistic local spin models [30, 31, 33, 42, 44, 140, 160–162, 167, 184–188].

Triangular lattice Heisenberg models are a paradigm of frustrated magnetism. Although the Heisenberg model with only nearest neighbour interaction is known to stabilize a regular 120° Néel order [25, 80, 189, 190] adding further interaction terms may increase frustration and induce magnetic disorder to the system. Experimentally, several materials with triangular lattice geometry do not exhibit any sign of magnetic ordering down to lowest temperatures [17–20]. These include for example the organic Mott insulators like $\kappa - (\text{BEDT} - \text{TTF})_2\text{Cu}_2(\text{CN})_3$ [19, 20] or $\text{EtMe}_3\text{Sb}[\text{Pd}(\text{dmit})_2]_2$ [17, 18] and are thus candidates realizing spin liquid physics.

Historically Kalmeyer and Laughlin [24] introduced the *chiral spin liquid* (CSL) state on the triangular lattice. This state closely related to the celebrated Laughlin wave function of the fractional quantum Hall effect has recently been shown to be the ground state of several extended Heisenberg models on the kagome lattice [140, 160–162]. The question arises whether a CSL can indeed be realized on the triangular lattice as originally proposed. In a recent study [185] this was shown for $\text{SU}(N)$ models for $N \geq 3$. In this letter we provide conclusive evidence that indeed the CSL is stabilized in a spin-1/2 Heisenberg model upon adding a further scalar chirality term $J_\chi \mathbf{S}_i \cdot (\mathbf{S}_j \times \mathbf{S}_k)$ similar as in Refs. [140, 161, 184, 185]. Such a term can be realized as a lowest order effective Heisenberg Hamiltonian of the Hubbard model upon adding Φ flux through the elementary plaquettes [161, 191, 192], either via a magnetic field or by introducing artificial gauge fields in possible cold atoms experiments [193, 194]. The coupling constants then relate to the Hubbard model parameters t and U as $J_1 \sim t^2/U$ and $J_\chi \sim \Phi t^3/U^2$ where J_1 (resp. J_χ) is the nearest neighbour Heisenberg (resp. scalar chirality) coupling.

Another open question in frustrated magnetism of the triangular lattice is the nature of the intermediate phase in the phase diagram of the $S = 1/2$ Heisenberg model with added next-nearest neighbour couplings around $J_2/J_1 \approx 1/8$. Several authors [80–82] found a spin disordered state. Recently several numerical studies [113, 195–199] proposed that a topological spin liquid state of some kind might be realized in this regime. The exact nature of this phase yet remains unclear. In this Letter we advocate the presence of a $O(4)^*$ quantum critical point [200–203] separating the 120° Néel order from a putative \mathbb{Z}_2 spin liquid. The diverging correlation length at this quantum critical point and the neighbouring first order phase transition into the stripy collinear magnetic ordered phase render the unambiguous identification of the intermediate spin liquid phase challenging however.

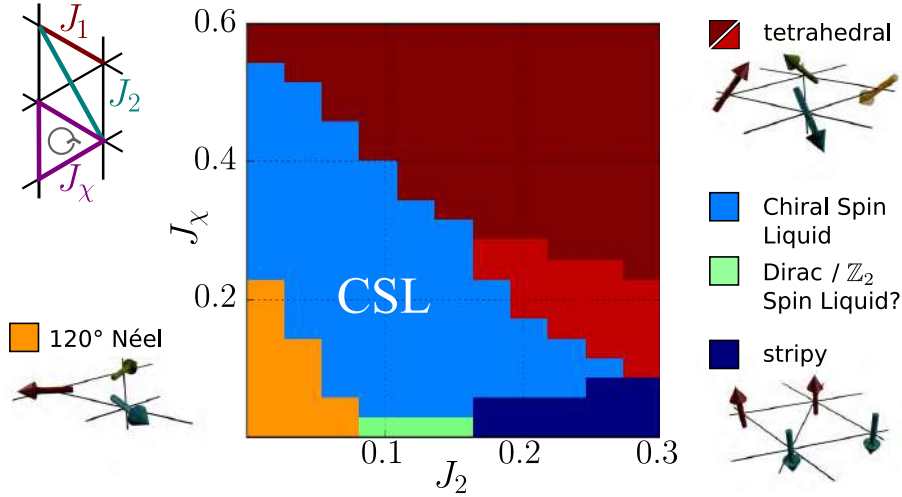


Figure 5.1.: Approximate $T = 0$ phase diagram of the J_1 - J_2 - J_χ model on the triangular lattice, c.f. Eq. (5.2.1). The extent of phases is inferred from excitation spectra from ED on a periodic 36 sites triangular simulation cluster, see main text for details.

5.2. Model

We investigate the Heisenberg model with nearest and next-nearest neighbour interactions with an additional uniform scalar chirality term on the triangular lattice

$$\mathcal{H} = J_1 \sum_{\langle i,j \rangle} \mathbf{S}_i \cdot \mathbf{S}_j + J_2 \sum_{\langle\langle i,j \rangle\rangle} \mathbf{S}_i \cdot \mathbf{S}_j + J_\chi \sum_{i,j,k \in \Delta} \mathbf{S}_i \cdot (\mathbf{S}_j \times \mathbf{S}_k) \quad (5.2.1)$$

where we set $J_1 \equiv 1$ and consider $J_2, J_\chi \geq 0$. Amongst a 120° Néel order, a stripy and a tetrahedral magnetic order we find a CSL being realized in an extended region of the phase diagram in Fig. 5.1. A first study of the classical phase diagram for $J_\chi = 0$ [80] found a three sublattice 120° Néel ordered ground state for $J_2 < 1/8$ whereas for $1/8 < J_2 < 1$ a two-parameter family of magnetic ground states with a four-site unit cell was found [81]. Two high-symmetry solutions within this manifold are a two-sublattice collinear stripy magnetic order breaking lattice rotation symmetry and a tetrahedral non-coplanar state with a uniform scalar spin chirality on all triangles. Taking into account quantum fluctuations by applying spin-wave theory, large- S perturbation theory and ED studies [80–82] the degeneracy is lifted by an *order-by-disorder* mechanism. The true quantum ground state for $J_2 \gtrsim 0.18$ exhibits stripy Néel order. Yet the behaviour of the system close to the classical phase transition point $J_2 = 1/8$ has not been fully understood.

5.3. Phase diagram

We performed ED calculations on a $N_s = 36$ sites simulation cluster with periodic boundary conditions to investigate ground state properties and order parameters of the model (5.2.1). We have also checked selected results on smaller clusters, but the $N_s = 36$ cluster is particularly well suited because this single cluster can harbour all phases which we were able to detect.

We present the approximate phase diagram in Fig. 5.1 based on the quantum numbers of the ground state level and the first excited state. The ground state is always in the $\Gamma.A1$ representation (except in the stripy phase where $\Gamma.A1$ and the two $\Gamma.E2$ sectors are almost degenerate). The symmetry sector of the first excited state determines the phase. *Orange*: $S = 1 K.A1$ (120° Néel) *Light blue*: $S = 0 \Gamma.E2b$ (CSL), *Green*: $S = 0 \Gamma.E2a, \Gamma.E2b$ degenerate (Dirac/ \mathbb{Z}_2 spin liquid), *Dark Blue*: $S = 0 \Gamma.A1, \Gamma.E2a, \Gamma.E2b$ degenerate (stripy magnetic order), *Dark red/Light red*: $S = 1 M.A / S = 0 \Gamma.E2a$ (tetrahedral magnetic order) For the magnetically ordered phases these quantum numbers follow from a standard tower of states symmetry analysis [204, 205], see supp. mat. [206] for details. The spectral phase diagram is further corroborated by the analysis of relevant order parameters and variational energies of model wave functions, c.f. Fig. 5.2, where the agreement is striking.

We find three magnetically ordered phases, a 120° Néel order [25], a stripy order [80–82], and a non-coplanar tetrahedral order [58, 184, 207]. The structure factor $\mathcal{S}(q) = |\sum_j e^{iq(x_j - x_0)} \langle \mathbf{S}_j \cdot \mathbf{S}_0 \rangle|^2 / N_s$ is peaked at the Brillouin zone points K for 120° Néel and at M for stripy and tetrahedral order [58]. To distinguish between the latter we computed a nematic order parameter

$$\mathcal{N} = \sum_{(i,j) \parallel (0,1)} \langle (\mathbf{S}_0 \cdot \mathbf{S}_1) (\mathbf{S}_i \cdot \mathbf{S}_j) \rangle_c \quad (5.3.1)$$

indicative for the stripy phase and the summed scalar chirality correlations

$$\mathcal{X} = \sum_{(i,j,k) \in \Delta} \langle \chi_{(0,1,2)} \cdot \chi_{(i,j,k)} \rangle \quad (5.3.2)$$

where $\chi_{(i,j,k)} = \mathbf{S}_i \cdot (\mathbf{S}_j \times \mathbf{S}_k)$, indicative for tetrahedral order. The regions where these quantities are large in magnitude agree very well with the phase boundaries derived from tower of states analysis, cf. Fig. 5.2. For the tetrahedral order the $S = 1 M.A$ level is lowest energy level in the tower of states, depicted dark red in Fig 5.1. Close to the stripy phase we observe that the first excited level is a $S = 0 \Gamma.E2a$ level, shown as the light red region in Fig. 5.1. We believe that this level is an artifact of the finite size sample and is related to the order by disorder mechanism. In neither of the ground state correlation functions we can see a difference between the light red region and the red region and thus conclude that also this region belongs to the same tetrahedral phase.

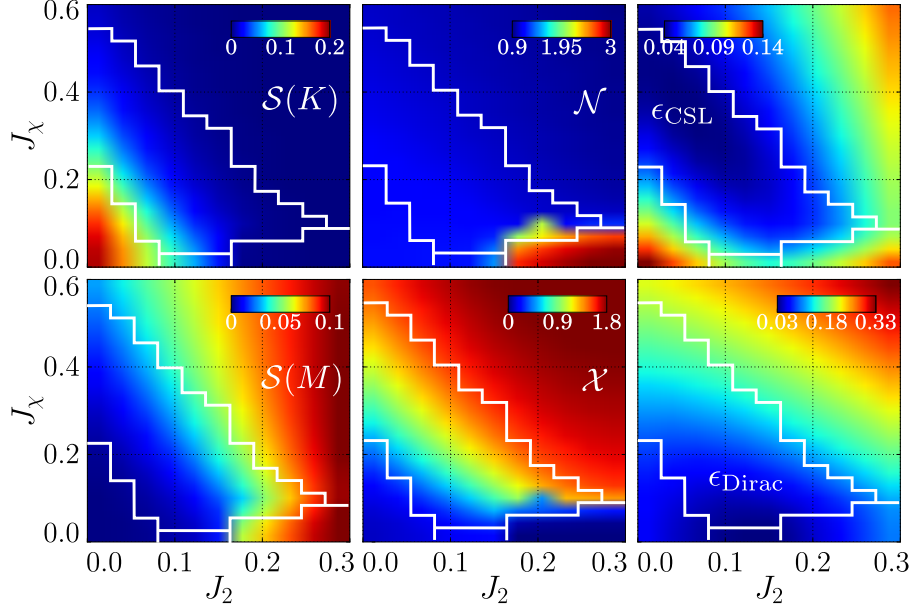


Figure 5.2.: Order parameters and variational energies of model wave functions. *Left:* static spin structure factor $\mathcal{S}(q)$, evaluated at K and M point. *Middle:* nematic order parameter \mathcal{N} as in Eq. (5.3.1) and (disconnected) scalar chirality correlation \mathcal{X} as in Eq. (5.3.2) *Right:* Variational energies $\epsilon = (E_{\text{model}} - E_{\text{ED}})/E_{\text{ED}}$ for the chiral and Dirac spin liquid.

5.4. Chiral Spin Liquids

are spin disordered chiral topological states. Hallmark features of this phase are the topology dependent ground state degeneracy, long-range entanglement, abelian anyonic excitations and gapless chiral edge modes. Several instances of this phase have recently been found in local spin models [44, 140, 160–162, 167, 184–188, 208]. It has been understood that a representative lattice model wave function for the CSL is provided by Gutzwiller projected parton wave functions (GPWF) with a completely filled parton band with Chern number ± 1 [105, 140, 178, 185, 209]. We observe no strong magnetic structure peak in between the 120° Néel order and the tetrahedral, cf. Fig. 5.2. Therefore a spin disordered state is formed in a sizeable intermediate region. The summed scalar chirality correlations \mathcal{X} in Fig. 5.2 are relatively large in this regime compliant with the fact that here a CSL with a uniform chirality is formed. We will now show conclusive evidence that this is indeed the case. We do so by constructing two GPWFs describing the two topological sectors of the chiral spin liquid on the torus and by computing their overlaps with the two lowest lying exact eigenstates from ED, similarly as in refs. [140, 185].

In Fig. 5.3 we show energy spectra for a horizontal cut in the phase diagram at $J_x = 0.24$.

5. Chiral Spin Liquid on the Triangular Lattice

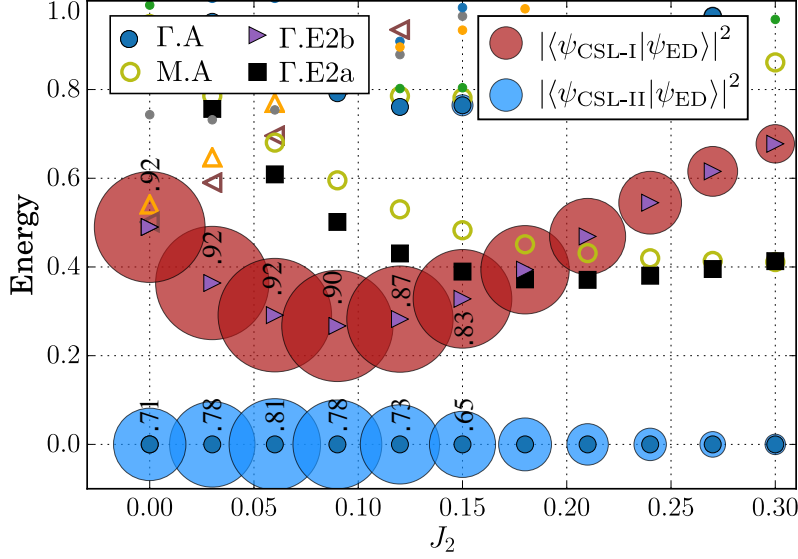


Figure 5.3.: Excitation spectra of the model (5.2.1) from ED for $J_\chi = 0.24$ and overlaps with the two CSL wave functions on a 36 site cluster. Full (empty) symbols denote even (odd) spin levels, different types of symbols denote different space-group representations. The numbers denote the summed overlaps $\mathcal{O}_{\text{GW-ED}}^\alpha$ as in Eq. (5.4.1). We find overlaps up to 0.92.

The first excited level above the ground state for $J_2 \lesssim 0.16$ belongs to the irreducible representation $\Gamma.E2b$. The region where this representation is the first excited state is colored light blue in Fig. 5.1. The parton tight binding model for the GPWFs we choose has a two-site unit cell on the triangular lattice with $\pi/2$ flux through the triangles. This yields a bandstructure with two bands with Chern numbers ± 1 . The ground state of this tight binding model at half filling is given by filling the orbitals of the lower band. After Gutzwiller projection such a state has been shown to yield a CSL wave function [140, 185, 210, 211]. To construct the topological partner of the CSL wave function the phases in the tight-binding model before projection can be tuned such that locally the flux through each triangle remains $\pi/2$ while the flux through incontractible loops around the torus changes. The set of fluxes can be chosen arbitrarily, yet after Gutzwiller projection these states only form a two dimensional space. This can be verified by computing the overlap matrix for several GPWFs with different fluxes through the torus. Indeed we find that thereby the rank of the overlap matrix is 2 with a numerical precision of $\sim 10^{-3}$ [210]. We chose two out of these wave functions spanning the CSL subspace and compute the overlaps with the lowest two numerical eigenstates from ED. We find that these two model wave functions $|\psi_{\text{GW}}^\alpha\rangle$ yield very high overlaps

$$\mathcal{O}_{\text{GW-ED}}^\alpha \equiv \left| \langle \psi_{\text{ED}}^0 | \psi_{\text{GW}}^\alpha \rangle \right|^2 + \left| \langle \psi_{\text{ED}}^1 | \psi_{\text{GW}}^\alpha \rangle \right|^2 \quad (5.4.1)$$

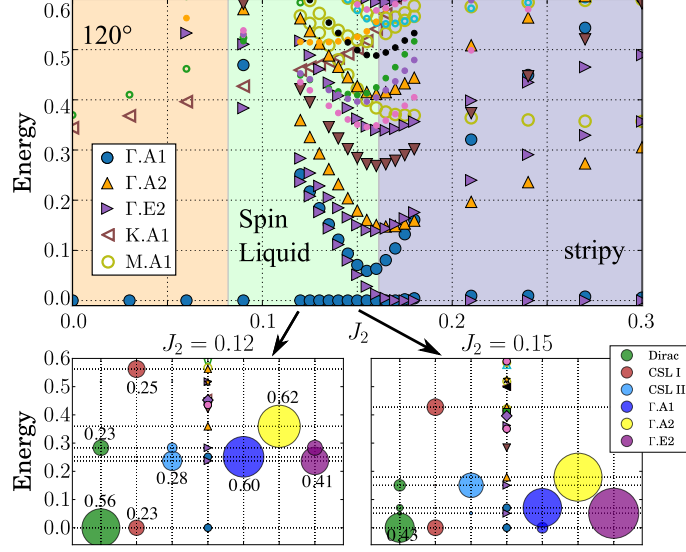


Figure 5.4.: ED spectra for $J_\chi = 0$ and spectral decomposition of several model wave functions for $J_2 = 0.12$ and $J_2 = 0.15$. Full (empty) symbols correspond to even (odd) spin. The diameter of the poles is proportional to the square overlap $|\langle \psi_{ED} \rangle \psi_{Model}|^2$. Besides the CSL and Dirac spin liquid wave functions the three wave functions denoted by $\Gamma.A1$, $\Gamma.A2$ and $\Gamma.E2b$ are the ground states in the respective symmetry sectors at $J_2 = 0.3$.

with the two lowest lying eigenstates of ED of up to 0.92 ¹. In Fig. 5.3 we plot the square overlap $|\langle \psi_{ED}^n \rangle \psi_{CSL}^\alpha|^2$ with the respective exact eigenstate (n) as the diameter of the red ($\alpha = 1$) and light blue ($\alpha = 2$) circles. The overlaps are large where the first excited state is in the $\Gamma.E2b$ representation and quickly decay afterwards. This region coincides approximately with the region where the CSL model wave function has a low variational energy in the upper right panel of Fig. 5.2. We note that the CSL phase in this phase diagram is located near a tetrahedral magnetic phase, reminiscent of a recent study of a frustrated honeycomb spin model [184]. It would be interesting to investigate the nature of the phase transitions from the tetrahedral [184] and the 120° Néel phases into the CSL. Finally a recent purely variational study [211] also found evidence for a CSL in our model for selected values of J_2 and J_χ .

¹Note that both our model wave functions do not have a fixed (angular-) momentum and thus overlap with both exact eigenstates. The fluxes of these two wave functions have been chosen such that one state has mainly overlap with the first excited state and the other mainly with the ground state.

5.5. Spin disordered state in the J_1-J_2 Heisenberg model

We now turn to the time-reversal invariant J_1-J_2 line with $J_\chi = 0$. A number of recent numerical works [113, 195–198] involving flavors of variational Monte Carlo (VMC) [113, 195] and Density Matrix Renormalization Group (DMRG) techniques [196–198] found a spin disordered region between the 120° magnetic order region and the stripy magnetic order at larger J_2/J_1 . Multiple candidate phases for this intermediate parameter range have been proposed, without a consensus so far. Whereas Ref. [196] proposes a gapped spin liquid phase, Ref. [195] proposes an extended gapless ASL state. In Ref. [198] it was argued that a CSL and a \mathbb{Z}_2 spin liquid are competing in the low energy sector in the intermediate region $0.07 \lesssim J_2 \lesssim 0.15$. Ref [113] compared variational energies of several \mathbb{Z}_2 spin liquids based on Gutzwiller projected wave functions. Interestingly they find that among all of these wave functions the lowest energy is not attained by a state with \mathbb{Z}_2 structure, but rather by a model whose band structure features gapless Dirac-like excitations before projection (see supp. mat. [206] and Refs. [113, 212]). After projection this state is called *Dirac Spin Liquid* (DSL) and Ref. [113] finds an extended gapless region described by a dressed wave function of the DSL kind.

In order to shed light on this open question we present the detailed energy spectrum of the $N_s = 36$ site cluster along the $J_\chi = 0$ line in the top panel of Fig. 5.4. In the small J_2 region the first few levels are in agreement with the tower of state expectations for the 120° Néel state [25], and similarly at the largest J_2 values shown for the stripy collinear magnetic order [82]².

Focusing on the intermediate region $0.08 \lesssim J_2 \lesssim 0.16$ we would expect to see an approximate four-fold ground state degeneracy in either a non-chiral \mathbb{Z}_2 spin liquid or two time-reversal related copies of a CSL as in Refs. [140, 160]. This is not the case for our system size. An additional complication comes from the observation that some of the low-lying levels in the spin liquid region seem to be states which become the ground state or low-lying levels in the stripy collinear region across the first order transition around $J_2 \sim 0.16$. This illustrated by calculating overlaps of several low-lying eigenstates at $J_2 = 0.3$ with the eigenstates at $J_2 = 0.12$ ($J_2 = 0.15$) displayed in the lower left (right) panel of Fig. 5.4.

Given the rather low variational energy of the DSL and to a lesser extent of the CSL model wave functions as shown in the right part of Fig. 5.2 (and for the DSL in Refs. [113, 195]) we also compute the decomposition of these model wave functions onto the exact ED eigenstates for $J_2 = 0.12$ and $J_2 = 0.15$, as shown in the lower part of Fig. 5.4. At $J_2 = 0.12$ the ground state has a sizeable overlap with the DSL model wave function of 0.56. Furthermore when going up to energies of about 0.6, we can also find four states which have non-vanishing overlap with the two different topological sectors of the CSL model wave functions, although the integrated weight is lower than for the DSL state.

²Some additional levels are visible remnants of the order by disorder mechanism [82]

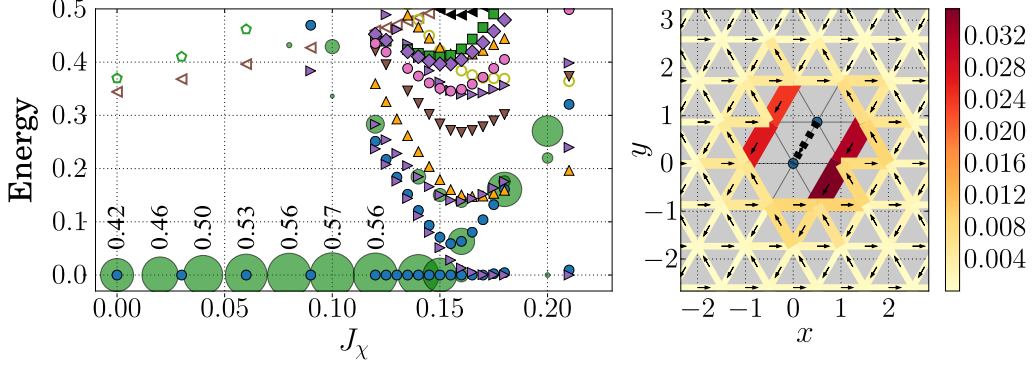


Figure 5.5.: Overlaps of DSL wave function with ED eigenstates and decay of spin-spin and twist-twist correlation functions $\langle (\mathbf{S}_0 \times \mathbf{S}_1) \cdot (\mathbf{S}_i \times \mathbf{S}_j) \rangle$ of the DSL from VMC on a 144 sites lattice. The maximum ground state overlap is attained at $J_2 = 0.1$. The correlations decay algebraically over distance.

This might explain the findings of Ref. [198] and is due to the reported CSL stabilized at finite but small J_χ . In the future one should also explore overlaps with a \mathbb{Z}_2 spin liquid model wave function in order to address the propensity to this kind of spin liquid on an equal footing the other model wave functions.

We have then explored the overlap of the exact ED ground state with the DSL model wave function in a larger range of J_2 couplings and observe the overlap to be maximal in the vicinity of the putative 120° Néel to spin liquid quantum phase transition around $J_2 \sim 0.08$ in Fig. 5.5. Motivated by this observation we have explored correlation functions in the DSL model wave function and we find likely power-law correlation functions which peak at the K point in reciprocal space (consistent with Refs. [113, 195]). We also investigated the spin vector chirality (twist) correlations and find them to exhibit likely power-law correlations with a real space pattern in agreement with the (ordered) pattern in the 120° Néel ordered phase cf. Fig. 5.5.

These nontrivial observations motivate us to conjecture that the DSL wave function should not be considered as a model wave function for an extended ASL region, but instead as a lattice wave function correctly describing the long-distance properties the quantum critical point out of the 120° Néel state into a spin liquid. The $O(4)^*$ theory [200–202] is a strong contender describing this transition. Let us put this advocated picture into a broader context: It is believed that Gutzwiller projected wave functions of partons with $SU(N)$ symmetry and a band structure with n_D Dirac points capture some aspects (see e.g. [213]) of a lattice realization of QED₃: i.e. $N_f = N \times n_D$ two-component Dirac fermions coupled to a compact $U(1)$ gauge field in $2 + 1$ D.

It has been shown that in the limit of sufficiently large N_f there are no relevant operators in the theory [111, 112], and therefore this wave function is representative for an extended

5. Chiral Spin Liquid on the Triangular Lattice

ASL region at large N_f . For small $N_f < N_f^c$ on the other hand one expects QED₃ to become confining in general. The DSL wave function with its power-law decaying correlation functions could then describe a (multi)critical conformal field theory fixed point in between confining phases. The precise value for N_f^c is not known, although recent work [214] bounds $N_f^c \lesssim 10$. In the particular case of the DSL on the triangular lattice we have $N = 2$ and $n_D = 2$ resulting in $N_f = 4$, substantially lower than the presently known bound. There is also an earlier observation in Ref. [215] that a different $N_f = 4$ DSL on the honeycomb lattice describes rather accurately the deconfined quantum critical point [216] between collinear Néel order and a VBS phase, giving further evidence that $N_f = 4$ DSLs should perhaps be seen as an approximate fixed point wave functions for exotic quantum critical points.

The quantum critical scenario naturally comes with divergent correlation lengths, which could be an explanation for the so far missing clear ground state degeneracy both in DMRG and ED. Using couplings frustrating both the 120° and the stripy Néel orders, it might be possible to widen the spin-liquid region and to reduce the correlation lengths to numerically accessible scales, allowing to identify the spin liquid unambiguously. It would also be interesting to understand whether the CSL touches the $J_\chi = 0$ line at the quantum critical point.

5.6. Conclusion

We established the phase diagram of an extended Heisenberg model on the triangular lattice. Amongst several magnetic orderings we found a chiral spin liquid phase in an extended region. For the spin disordered region for $J_\chi = 0$ we found that the DSL has sizeable overlap with ED ground states. We proposed a scenario where this wave function is the quantum critical wave function at a transition from magnetic 120° Néel order into a putative spin liquid phase.

Acknowledgments

We thank F. Becca, Y. Iqbal, S. Sachdev, M. Schuler, P. Strack and S. Whitsitt for discussions. We acknowledge support by the Austrian Science Fund through DFG-FOR1807 (I-1310-N27) and the SFB FoQus (F-4018-N23). The computations for this manuscript have been carried out on VSC3 of the Vienna Scientific Cluster and on the LEOIIIe cluster of the Focal Point Scientific Computing at the University of Innsbruck.

Chiral Spin Liquids in Triangular-Lattice $SU(N)$ Fermionic Mott Insulators with Artificial Gauge Fields

This chapter has been published as:

Pierre Nataf, Miklós Lajkó, Alexander Wietek, Karlo Penc, Frédéric Mila, and Andreas M. Läuchli. “Chiral Spin Liquids in Triangular-Lattice $SU(N)$ Fermionic Mott Insulators with Artificial Gauge Fields”. In: *Phys. Rev. Lett.* 117.16 (2016). DOI: 10.1103/PhysRevLett.117.167202. arXiv: 1601.00958 [cond-mat.quant-gas]

We describe the author’s contribution to the project and present the published manuscript. We studied the $SU(N)$ Heisenberg model with an additional imaginary ring exchange term on the triangular lattice,

$$H = J \sum_{\langle i,j \rangle} P_{ij} + iK_3 \sum_{(i,j,k)} (P_{ijk} + \text{H.c.}), \quad (6.0.1)$$

where P_{ij} denotes the two-site exchange operator on N colors,

$$P_{ij} |\dots \alpha_i \dots \alpha_j \dots \rangle = |\dots \alpha_j \dots \alpha_i \dots \rangle, \quad \alpha_i \in 1, \dots, N. \quad (6.0.2)$$

Analogously, P_{ijk} denotes three-site cyclic exchange operator on the elementary triangles of the triangular lattice. As explained in the paper, such a model can be realized in the Mott insulating regime of an $SU(N)$ Hubbard model with external magnetic field. Experimentally such a system can be realized in ultracold atoms experiments with earth alkaline atoms [217–224]. In the $SU(2)$ case, P_{ij} corresponds to the Heisenberg exchange operator ($S_i^+ S_j^- + S_i^- S_j^+$) and the ring exchange term $i(P_{ijk} - P_{kji})$ to the scalar chirality interaction $\mathbf{S}_i \cdot (\mathbf{S}_j \times \mathbf{S}_k)$. Hence, the model Eq. (6.0.1) may be regarded as a generalization of the model Eq. (5.2.1) studied in chapter 5. In our research manuscript, we conclude that a chiral spin liquid is stabilized in an extended region of the phase diagram for $N = 3, \dots, 9$.

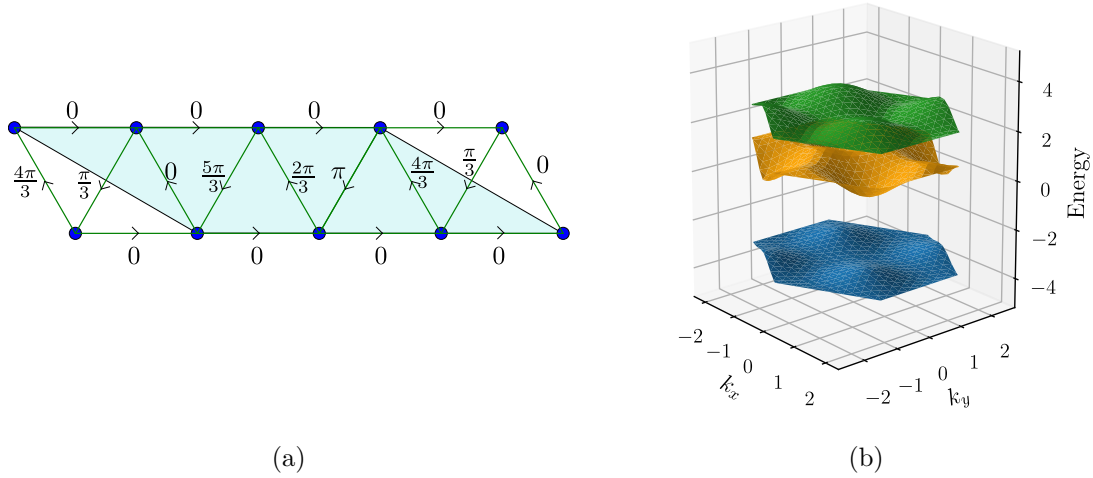


Figure 6.1.: Parton ansatz and band structure for the $SU(3)$ chiral spin liquid. (a) Geometry of the unit cell for the $\pi/3$ model and choice of Peierls phases. There is $\pi/3$ flux through each triangle. The periodicity of the unit cell has been chosen in order to fit this unit cell onto simulation clusters of Exact Diagonalization. (b) Band structure of the $\pi/3$ model. The three bands are gapped and carry Chern numbers -1, -1, 2 from bottom to top.

The contribution by the author of this thesis was to construct model CSL wave functions for the $SU(N)$ chiral spin liquid and compute their overlap with the numerical ground states. The coefficients of the CSL have been evaluated in the conventional real space computational basis. The model has been studied further using Exact Diagonalization with a novel technique that allows for directly working with irreducible representations of the $SU(N)$ symmetry group [225] by Pierre Nataf and Frédéric Mila. Variational energies and further properties of model CSL wave functions have been studied by Miklós Lajkó and Karlo Penc. The project was conceived by Andreas M. Läuchli and the numerical edge spectra together with their analytical prediction have been computed by him.

6.1. Construction of the $SU(N)$ chiral spin liquid

In order to construct the CSL model wave functions, we apply the general parton construction explained in section 1.2.3. We consider a fermionic tight binding model on the triangular lattice. We choose an ansatz with π/N flux through each triangle. This corresponds to $2\pi/N$ flux per unit cell. We will call this the π/N model. For defining this model a N -site unit cell is used. The geometry of the unit cell for the $N = 3$ and $N = 4$ CSL and the choice of the Peierls phases are shown in Figs. 6.1 and 6.2.

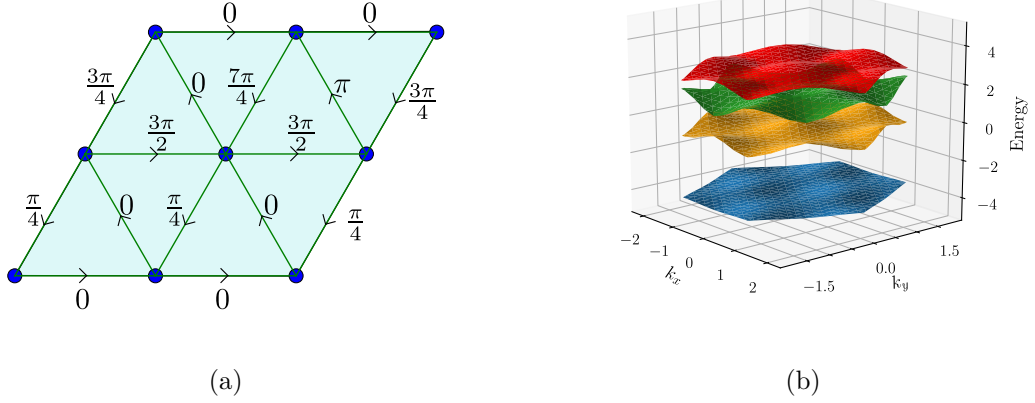


Figure 6.2.: Parton ansatz and band structure for the $SU(4)$ chiral spin liquid. (a) Geometry of the unit cell for the $\pi/4$ model and choice of Peierls phases. There is $\pi/4$ flux through each triangle. The periodicity of the unit cell has been chosen in order to fit this unit cell onto simulation clusters of Exact Diagonalization. (b) Band structure of the $\pi/4$ model. The three bands are gapped and carry Chern numbers $-1, -1, -1, 3$ from bottom to top.

The parton ansatz breaks time-reversal symmetry and yields N bands, which are well separated from each other. Moreover, the lowest $N - 1$ bands carry Chern number ± 1 whereas the top band carries Chern number $\mp(N - 1)$. We fill the lowest band with fermions of N colors to obtain the parton ground state $|\psi_0\rangle$ and perform a Gutzwiller projection,

$$|\psi_{\text{GPWF}}\rangle = P_{\text{GW}} |\psi_0\rangle. \quad (6.1.1)$$

To compute the coefficients of this wave function, the formula Eq. (2.2.31) is straightforwardly generalized to the case of N colors instead of the two up and down spins in the $SU(2)$ case. By shifting the reciprocal space we can insert flux through the torus. This way, we are able to construct a family of wave functions, depending on the amount of flux inserted. The overlap matrix is of rank 3 in the $SU(3)$ case, and of rank 4 in the $SU(4)$ case, with a numerical precision of about 0.01. Consequently, we have been able to construct N orthonormal wave functions spanning the subspace of the CSL. These wave functions are then compared to the ground state wave functions from Exact Diagonalization in Fig. 3 of the paper.

Chiral Spin Liquids in Triangular-Lattice $SU(N)$ Fermionic Mott Insulators with Artificial Gauge Fields

Pierre Nataf,¹ Miklós Lajkó,² Alexander Wietek,³ Karlo Penc,^{4,5} Frédéric Mila,¹ and Andreas M. Läuchli³

¹*Institute of Physics, Ecole Polytechnique Fédérale de Lausanne (EPFL), CH-1015 Lausanne, Switzerland*

²*Institute for Solid State Physics, University of Tokyo, Kashiwa 277-8581, Japan*

³*Institut für Theoretische Physik, Universität Innsbruck, A-6020 Innsbruck, Austria*

⁴*Institute for Solid State Physics and Optics, Wigner Research Centre for Physics, Hungarian Academy of Sciences, H-1525 Budapest, P.O.B. 49, Hungary*

⁵*MTA-BME Lendület Magneto-optical Spectroscopy Research Group, 1111 Budapest, Hungary*

(Received 29 January 2016; published 11 October 2016)

We show that, in the presence of a $\pi/2$ artificial gauge field per plaquette, Mott insulating phases of ultracold fermions with $SU(N)$ symmetry and one particle per site generically possess an extended chiral phase with intrinsic topological order characterized by an approximate ground space of N low-lying singlets for periodic boundary conditions, and by chiral edge states described by the $SU(N)_1$ Wess-Zumino-Novikov-Witten conformal field theory for open boundary conditions. This has been achieved by extensive exact diagonalizations for N between 3 and 9, and by a parton construction based on a set of N Gutzwiller projected fermionic wave functions with flux π/N per triangular plaquette. Experimental implications are briefly discussed.

DOI: 10.1103/PhysRevLett.117.167202

The search for unconventional quantum states of matter in realistic models of strongly correlated systems has been an extremely active field of research over the last 25 years. Mott insulating phases in which charge degrees of freedom are gapped have been argued to potentially host several families of quantum spin liquids ranging from resonating valence bond \mathbb{Z}_2 quantum spin liquids [1–3] to $U(1)$ algebraic spin liquids [4–6] and chiral spin liquids (CSLs) [7–15]. The topological properties of these phases have attracted a lot of attention due to their potential impact on the implementation of quantum computers [16].

Cold atoms open new perspectives in that respect. In particular, alkaline rare earths allow one to realize $SU(N)$ Mott phases with N as large as 10 [17–24], and if a chiral phase can be stabilized, its low-energy theory is expected to be the $SU(N)$ level $k=1$ Chern-Simons theory. The possibility to destroy long-range order in $SU(N)$ generalizations of the $SU(2)$ antiferromagnet on bipartite lattices has long been known [4,25], but the first proposal of a chiral phase in the context of $SU(N)$ models of cold atoms goes back to the work of Hermele *et al.* [26,27], who showed that a mean-field approach leads to the stabilization of chiral phases on the square lattice in the limit of large N and a large number of particles per site m with N/m integer and ≥ 5 . The same mean field applied to $SU(6)$ on the honeycomb lattice with one particle per site has also led to the prediction of a chiral state, with a competing plaquette state very close in energy [28]. More recently, Ref. [29] suggested the stabilization of $SU(N)$ CSLs on the square lattice using static synthetic gauge fields, based on a slave-rotor mean-field approach. In all these cases, the results

call for further investigation with methods that go beyond mean-field theory.

In this Letter, we show that the ground state of the Mott phase of N -color fermions on the triangular lattice with one particle per site is a $SU(N)$ CSL in a large parameter range if the system is subject to a static artificial gauge field with flux $\pi/2$ per triangular plaquette. The starting point is the $SU(N)$ Hubbard Hamiltonian

$$H = -t \sum_{\langle i,j \rangle} \sum_{\alpha=1}^N (e^{i\phi_{ij}} c_{i,\alpha}^\dagger c_{j,\alpha} + \text{H.c.}) + U \sum_{i,\alpha < \beta} n_{i,\alpha} n_{i,\beta}. \quad (1)$$

If the phases ϕ_{ij} are chosen in a such a way that the (gauge-invariant) flux through each triangular plaquette is equal to Φ , then, at a filling of one particle per site, and for large enough U/t , the effective model is an $SU(N)$ Heisenberg model with local spins in the fundamental representation of $SU(N)$ endowed with real pairwise permutations and complex three-site permutations. The Hamiltonian is a generalization of the $SU(2)$ model with scalar chirality [30,31] and is defined by

$$H = J \sum_{\langle i,j \rangle} P_{ij} + K_3 \sum_{\langle i,j,k \rangle} (e^{i\Phi} P_{ijk} + \text{H.c.}), \quad (2)$$

where the sum over (i,j,k) runs over all triangular plaquettes, and P_{ij} and P_{ijk} are circular permutation operators. To second order, the amplitude of the pairwise permutation is simply given by $J = 2t^2/U$, while the 3-site permutation appears at third order in perturbation theory with $K_3 = 6t^3/U^2$. The cases $\Phi = 0$ and $\Phi = \pi$ with purely real positive [32] and negative [33] three-site

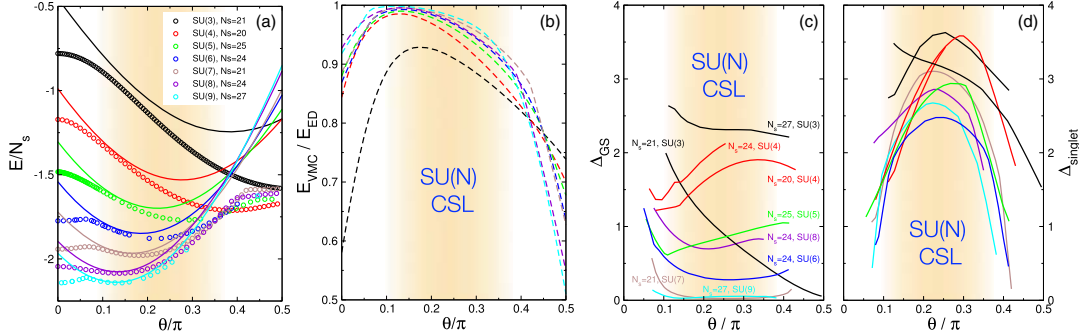


FIG. 1. Panel (a) Ground state energy per site as a function of θ for various N and N_s . Open symbols (full lines) denote ED (VMC) results. (b) Quality of the VMC wave function as measured by the ratio $E_{\text{VMC}}/E_{\text{ED}}$. (c) Energy splitting among the expected N singlet states forming the ground space manifold of a $SU(N)$ CSL. (d) Energy gap from the ground state to the first excited singlet state which is not part of the expected ground space manifold.

permutation have been addressed earlier. In this Letter, we concentrate on the case of a purely imaginary three-site permutation $\Phi = \pi/2$ described by the Hamiltonian

$$H = \cos\theta \sum_{(i,j)} P_{ij} + \sin\theta \sum_{(i,j,k)} (iP_{ijk} + \text{H.c.}), \quad (3)$$

with the parametrization $J = \cos\theta$ and $K_3 = \sin\theta$. We will discuss the experimental prospects of realizing this Hamiltonian towards the end of the Letter. It is interesting to note that parent Hamiltonians for $SU(N)$ chiral spin liquids have been proposed recently [34,35]. While there are some structural similarities, it is not obvious that the spatially compact and physically more realistic Hamiltonian Eq. (3) features CSL phases. It is the goal of this Letter to provide compelling numerical evidence, based on large-scale exact diagonalizations (EDs) and Gutzwiller projected parton wave functions, that the above Heisenberg Hamiltonian indeed features extended regions of $SU(N)$ CSLs for all values of $N = 3$ to 9 considered here.

Exact diagonalizations.—We start by investigating finite periodic triangular lattice clusters as a function of θ for various values of N . We focus on the range $\theta \in [0, \pi/2]$ in the following. $\theta > \pi/2$ is likely to be dominated by ferromagnetism, while $\theta < 0$ yields the time-reversed, but otherwise identical physics as $-\theta$. For small values of $N = 3, 4$ we used the standard ED approach employing all the space group symmetries, while only considering the individual color conservation, corresponding to an Abelian subgroup of $SU(N)$. For all other N a recently developed ED approach by two of the authors [36], exploiting the $SU(N)$ symmetry at the expense of spatial symmetries, is currently the only way to address these systems within ED. Depending on N , the largest system sizes N_s range from 21 to 27 lattice sites.

In Fig. 1(a) we plot the ED results for the energy per site of the ground state as a function of θ for all considered N

(open symbols). While the curves for $N \lesssim 5$ look rather smooth at first sight, it is visible that the energy per site displays kinks around $\theta/\pi \sim 0.05 - 0.1$ and at $\theta/\pi \sim 0.35 - 0.4$ for $N = 6$ to 9. For comparison we plot the energy expectation value of parameter-free Gutzwiller projected CSL model wave functions for all values of N (full lines). We will discuss the properties of these wave functions in a moment. Interestingly, these model wave functions have very competitive energies, especially in the θ region slightly above the first kink. For a quantitative comparison we show in Fig. 1(b) the ratio of the variational energy divided by the ED ground state energy. It is impressive that for N beyond 3 the best ratio exceeds 0.98 for the system sizes considered. So the picture so far is that the small and large θ regimes for all considered N are most likely other phases, while the intermediate region could harbor CSLs.

$SU(N)$ CSLs are intrinsically topologically ordered: They exhibit a nontrivial ground state degeneracy on the torus [27,37] and fractional excitations. The ground state degeneracy on the torus is expected to be N for these particular states with N different Abelian anyons [26,27]. In our numerical simulations, we can detect this degeneracy by investigating the low-energy spectrum on samples with a total number of lattice sites N_s that is an integer multiple of N . In Fig. 1(c) we display the energy spread Δ_{GS} of these N expected ground states for different N as a function of θ . As a general trend we observe that the splitting reduces significantly as we increase N . On the other hand, several samples still show a substantial splitting. Naively one would expect a simple exponential suppression of the splitting with system size; however, in the related context of fractional Chern insulators a more subtle dependence of the ground space splitting on the actual shape of the clusters has been observed and rationalized [48]. We think that similar considerations apply here as well.

Finally we also measure the gap Δ_{singlet} from the absolute ground state to the first singlet level that is not part of the expected ground state manifold. This is a measure for the excitation gap in the gapped CSL states. In Fig. 1(d), one observes an approximate dome-shaped behavior of this gap for all N , and furthermore this gap seems to depend only weakly on N . The approximate region in θ where the N -fold ground state degeneracy splitting is small compared to the excitation gap (for large N) is indicated as a shaded region in all the panels, and indicates a rough stability region for the $SU(N)$ CSLs on the triangular lattice. One should note, however, that the precise extent of the CSLs for small N is an open question at this point.

Variational parton approach.—An appealing way to describe the $SU(N)$ CSLs is to use a parton-based mean field approach [26,27,49–54], complemented with a Gutzwiller projection. The idea is to fractionalize the elementary spin degree of freedom into fermionic spinons (partons) with N colors. For an exact description, a dynamical gauge field needs to enforce the physical constraint of one fermion per site. At the mean-field level, however, it is sufficient to specify the band structure and filling of the fermionic spinons. In the $SU(N)$ CSLs of interest here, the spinon band structure consists of N bands, where the lowest band is completely filled for all N colors and separated by a gap from the other bands. In addition, this band is required to have Chern number ± 1 . For the triangular lattice we use a Hofstadter-type tight-binding Hamiltonian with a uniform flux of π/N per triangular plaquette [55], fulfilling the requirements on the band structure. This mean-field state can now be turned into a valid spin wave function by the application of an exact Gutzwiller projection, enforcing the presence of exactly one fermionic spinon per site. Such a wave function can be handled by variational Monte Carlo (VMC) techniques, and in particular one can easily calculate the energy of the Hamiltonian Eq. (3) on rather large lattices. The VMC energies displayed in Figs. 1(a) and 1(b) have been obtained this way [37].

The next question is how the VMC approach is able to account for the nontrivial ground state degeneracy on the torus. It turns out that by threading flux through the noncontractible loops around the torus, one is able to span an N -dimensional subspace of Gutzwiller projected wave functions, with almost identical local properties on finite lattices. From the viewpoint of topological order, this corresponds to a charge pumping procedure, where one cycles through the N different ground states by threading a different anyonic flux through the interior of the torus. These concepts have recently been explored in the context of $SU(2)$ CSL on several lattices [56–58]. We have checked in Fig. 2 that the subspace of wave functions spanned by using 30 different boundary conditions at the mean-field level leads to a robust rank- N overlap matrix, therefore corroborating the expectation of an N -fold degenerate

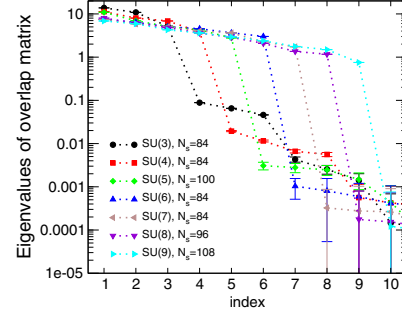


FIG. 2. VMC ground space degeneracy: ordered sequence of eigenvalues of the overlap matrix of Gutzwiller projected wave functions with 30 random values of threaded flux. The overlap matrix has precisely N large eigenvalues for an $SU(N)$ CSL.

ground state manifold in the thermodynamic limit also at the VMC level.

Since the variational energies for $SU(3)$ turned out not to be very competitive, as shown in Figs. 1(a) and 1(b), we explicitly calculated the overlaps of individual ED eigenstates of the Hamiltonian Eq. (3) with the three orthogonal Gutzwiller wave functions obtained on the same system size. In Fig. 3 we plot the summed squared overlap of all three wave functions (area of filled circles) with the ED eigenstates (crosses) as a function of θ . Here we consider a $N_s = 12$ site system, where the momenta of the three ED ground states in the CSL phase are at the zone center (one) and at the corners of the Brillouin zone (twofold degenerate). Around $\theta = 0$, the $SU(3)$ triangular lattice Heisenberg model is in a three-sublattice color ordered state [59,60]; however, in the region around $\theta/\pi \sim 0.25$, the three lowest ED eigenstates indeed have sizeable overlap

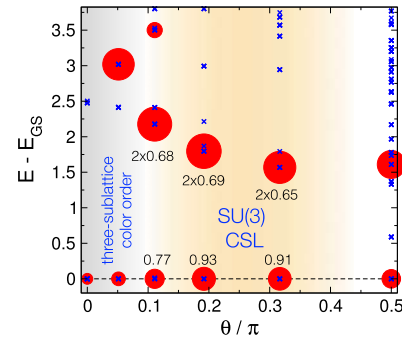


FIG. 3. Summed squared overlaps of the VMC model wave functions with ED eigenstates for $N = 3$ and $N_s = 12$. The blue crosses denote ED eigenstates, while the area of the filled red circles denotes the total squared overlap on those eigenstates. Around $\theta/\pi \approx 0.25$, the summed overlaps on the lowest three ED eigenstates (degeneracy $1 + 2$) account for over 75% of the total weight, while the ground state alone is at 90%.

with the VMC model wave functions, thereby underlining the presence of an $SU(3)$ CSL for sufficiently large values of θ also for $N = 3$.

Edge states.—Another hallmark of chiral topological phases is the presence of chiral edge modes in the energy spectrum of systems with a boundary. It has been understood that the characteristic energy level structure of the edge excitations as a function of the momentum along the boundary serves as a fingerprint of the type of topological order realised in the bulk [61]. The $SU(N)$ CSLs considered here are expected to exhibit a chiral edge energy spectrum described by the $SU(N)_1$ Wess-Zumino-Novikov-Witten (WZNW) conformal field theory (CFT) [27]. This is the same CFT that governs the low-energy spectrum of well-studied one-dimensional critical $SU(N)$ spin chains [34,35,62,63].

In order to test this hypothesis numerically we choose to emulate a disk geometry by considering the specific $N_s = 19$ site triangular lattice with open boundary conditions depicted in the left panel of Fig. 4. Such a lattice might actually be built in future ultracold atom experiments with optical lattices and a tight confining potential. This sample still has a sixfold rotation axis about the central site, yielding an angular momentum quantum number which we use to plot the energy spectrum. The energy spectrum of the disc has no topological ground state degeneracy, but features gapless edge modes which typically propagate only in one direction. The precise multiplet structure of the edge modes depends on the anyonic sector. In our setup, this sector can be simply labeled as $a = (N_s \bmod N)$. In Table I of the Supplemental Material [37], we have compiled the $SU(N)_1$ WZNW CFT predictions for the different irreducible representations of $SU(N)$ which appear at a given excitation energy, here qualitatively

labeled by the excess angular momentum $l - l_0$. In the remaining panels of Fig. 4 we display the actual ED energy spectrum of the Hamiltonian Eq. (3) for a fixed value of $\theta/\pi = 0.25$ for $N = 3$ up to 8 as a function of the angular momentum $l - l_0$. For all N one can clearly identify a branch of chiral excitations propagating to the right. The analytical predictions are indicated by the dimensions of the $SU(N)$ irreducible representations. For all N the numerical data for the first three sectors ($l - l_0 = 0, 1, 2$) are in full agreement with the analytical predictions. The splitting between the multiplets at a given value of l is expected to vanish as N_s grows, and the spectrum should become linear with a certain edge state velocity. The observed structure of the edge excitations confirms the $SU(N)_1$ WZNW CFT predictions and thus strengthens the case for Abelian $SU(N)$ CSLs in the model Hamiltonian Eq. (3).

Experimental considerations.—With the recent realization of the Mott-crossover regime in 3D optical lattices with fermionic Ytterbium atoms [64,65] the future for strongly correlated $SU(N)$ quantum magnetism is shining bright. Our proposal for triangular lattices builds on ingredients that have been demonstrated separately: the possibility to realize Mott insulators in optical lattices, and to create static artificial gauge fields in an optical lattice (for alkaline atoms) [66,67]. Besides, working with the triangular lattice is a big advantage because the 3-site permutation term is the first and only term to appear to third order in perturbation theory starting from the Hubbard model with one particle per site, by contrast to, e.g., the square and honeycomb lattice, where they appear at order 4 and 6, respectively, and are not the first corrections. The chiral phase typically appears for $\theta \approx 0.3$, which, using the perturbation expressions of $J = 2t^2/U$ and $K_3 = 6t^3/U^2$, corresponds to $t/U \approx 0.1$. This might be small enough to be still in the

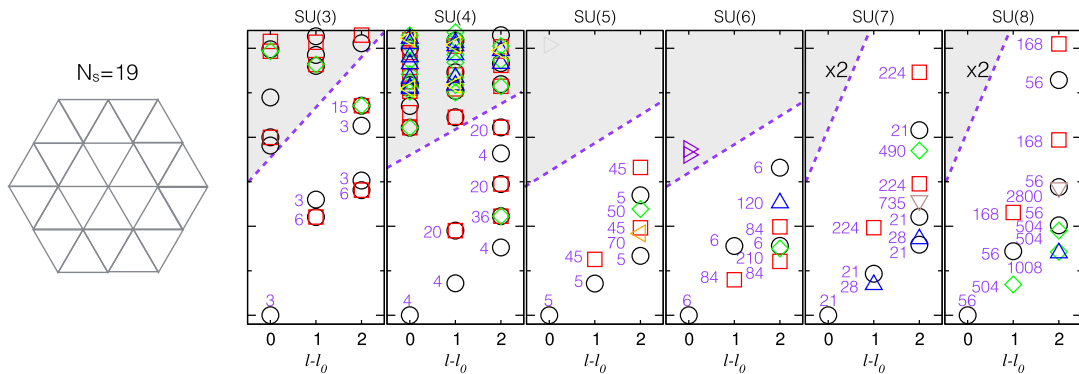


FIG. 4. Edge states in $SU(N)$ CSLs: the leftmost panel displays the $N_s = 19$ site triangular cluster with open boundary conditions used. In the various other panels we exhibit the low energy spectrum as a function of the angular momentum around the central site (l_0 denotes the ground state angular momentum). The chiral edge states are clearly visible, with a characteristic $SU(N)$ multiplet structure, which corresponds to a particular sector of a chiral $SU(N)_1$ Wess-Zumino-Novikov-Witten conformal field theory. The analytical predictions are indicated by the dimensions of the $SU(N)$ multiplets and can be found in Table I of the Supplemental Material [37].

Mott insulating phase, and to ensure that higher order corrections are negligible. In future studies one might also relax the $\pi/2$ flux per plaquette condition, and explore the extent of the expected stability region of the $SU(N)$ CSL phases.

Several interesting questions need to be addressed in future work. For example, is it possible to directly engineer the required three site exchange terms in Hamiltonian Eq. (3) using sophisticated quantum optics schemes? There is hope that the current activity on lattice gauge-theory implementations will bring techniques to address this question. Another intriguing question regards the detection of $SU(N)$ CSL edge states in actual experiments, using for example spectroscopic techniques for small droplets or braiding protocols for the Abelian anyons [27].

The authors acknowledge P. Corboz, M. Hermele, T. Quella, A. Sterdyniak, H.-H. Tu, and Hongyu Yang for useful discussions. This work has been supported by the Swiss National Science Foundation, the JSPS KAKENHI Grant No. 2503802, the Hungarian OTKA Grant No. K106047, by the Austrian Science Fund FWF (F-4018-N23 and I-1310-N27/DFG-FOR1807), and by the National Science Foundation under Grant No. NSF PHY11-25915.

-
- [1] D. S. Rokhsar and S. A. Kivelson, *Phys. Rev. Lett.* **61**, 2376 (1988).
- [2] R. Moessner and S. L. Sondhi, *Phys. Rev. Lett.* **86**, 1881 (2001).
- [3] A. Ralko, M. Ferrero, F. Becca, D. Ivanov, and F. Mila, *Phys. Rev. B* **71**, 224109 (2005).
- [4] I. Affleck and J. B. Marston, *Phys. Rev. B* **37**, 3774 (1988).
- [5] Y. Ran, M. Hermele, P. A. Lee, and X.-G. Wen, *Phys. Rev. Lett.* **98**, 117205 (2007).
- [6] P. Corboz, M. Lajkó, A. M. Läuchli, K. Penc, and F. Mila, *Phys. Rev. X* **2**, 041013 (2012).
- [7] V. Kalmeyer and R. B. Laughlin, *Phys. Rev. Lett.* **59**, 2095 (1987).
- [8] X. G. Wen, F. Wilczek, and A. Zee, *Phys. Rev. B* **39**, 11413 (1989).
- [9] X. G. Wen, *Phys. Rev. B* **40**, 7387 (1989).
- [10] D. F. Schroeter, E. Kapit, R. Thomale, and M. Greiter, *Phys. Rev. Lett.* **99**, 097202 (2007).
- [11] L. Messio, B. Bernu, and C. Lhuillier, *Phys. Rev. Lett.* **108**, 207204 (2012).
- [12] S. Bieri, M. Serbyn, T. Senthil, and P. A. Lee, *Phys. Rev. B* **86**, 224409 (2012).
- [13] Y.-C. He, D. N. Sheng, and Y. Chen, *Phys. Rev. Lett.* **112**, 137202 (2014).
- [14] S.-S. Gong, W. Zhu, and D. N. Sheng, *Sci. Rep.* **4**, 6317 (2014).
- [15] B. Bauer, L. Cincio, B. P. Keller, M. Dolfi, G. Vidal, S. Trebst, and A. W. W. Ludwig, *Nat. Commun.* **5**, 5137 (2014).
- [16] C. Nayak, S. H. Simon, A. Stern, M. Freedman, and S. Das Sarma, *Rev. Mod. Phys.* **80**, 1083 (2008).
- [17] C. Wu, J.-p. Hu, and S.-c. Zhang, *Phys. Rev. Lett.* **91**, 186402 (2003).
- [18] C. Honerkamp and W. Hofstetter, *Phys. Rev. Lett.* **92**, 170403 (2004).
- [19] M. A. Cazalilla, A. F. Ho, and M. Ueda, *New J. Phys.* **11**, 103033 (2009).
- [20] A. V. Gorshkov, M. Hermele, V. Gurarie, C. Xu, P. S. Julienne, J. Ye, P. Zoller, E. Demler, M. D. Lukin, and A. M. Rey, *Nat. Phys.* **6**, 289 (2010).
- [21] F. Scazza, C. Hofrichter, M. Höfer, P. C. De Groot, I. Bloch, and S. Fölling, *Nat. Phys.* **10**, 779 (2014).
- [22] G. Pagano, M. Mancini, G. Cappellini, P. Lombardi, F. Schäfer, H. Hu, X.-J. Liu, J. Catani, C. Sias, M. Inguscio, and L. Fallani, *Nat. Phys.* **10**, 198 (2014).
- [23] X. Zhang, M. Bishof, S. L. Bromley, C. V. Kraus, M. S. Safronova, P. Zoller, a. M. Rey, and J. Ye, *Science* **345**, 1467 (2014).
- [24] M. A. Cazalilla and A. M. Rey, *Rep. Prog. Phys.* **77**, 124401 (2014).
- [25] N. Read and S. Sachdev, *Phys. Rev. Lett.* **62**, 1694 (1989).
- [26] M. Hermele, V. Gurarie, and A. M. Rey, *Phys. Rev. Lett.* **103**, 135301 (2009).
- [27] M. Hermele and V. Gurarie, *Phys. Rev. B* **84**, 174441 (2011).
- [28] G. Szirmai, E. Szirmai, A. Zamora, and M. Lewenstein, *Phys. Rev. A* **84**, 011611 (2011).
- [29] G. Chen, K. R. A. Hazzard, A. M. Rey, and M. Hermele, *Phys. Rev. A* **93**, 061601 (2016).
- [30] O. I. Motrunich, *Phys. Rev. B* **73**, 155115 (2006).
- [31] D. Sen and R. Chitra, *Phys. Rev. B* **51**, 1922 (1995).
- [32] H.-H. Lai, *Phys. Rev. B* **87**, 205111 (2013).
- [33] H.-H. Lai, *Phys. Rev. B* **87**, 205131 (2013).
- [34] H.-H. Tu, A. E. Nielsen, and G. Sierra, *Nucl. Phys.* **B886**, 328 (2014).
- [35] R. Bondesan and T. Quella, *Nucl. Phys.* **B886**, 483 (2014).
- [36] P. Nataf and F. Mila, *Phys. Rev. Lett.* **113**, 127204 (2014).
- [37] See Supplemental Material at <http://link.aps.org/supplemental/10.1103/PhysRevLett.117.167202> for further information concerning the variational Monte Carlo simulations, the analogy with the Quantum Hall effect, and the $SU(N)_1$ predictions for the chiral edge state. This includes Refs. [26,27,38–47].
- [38] B. Halperin, *Helv. Phys. Act.* **56**, 75 (1983).
- [39] Y. Hatsugai, K. Ishibashi, and Y. Morita, *Phys. Rev. Lett.* **83**, 2246 (1999).
- [40] X. G. Wen, F. Wilczek, and A. Zee, *Phys. Rev. B* **39**, 11413 (1989).
- [41] J.-W. Mei and X.-G. Wen, *Phys. Rev. B* **91**, 125123 (2015).
- [42] Y. Zhang, T. Grover, and A. Vishwanath, *Phys. Rev. Lett.* **107**, 067202 (2011).
- [43] Y. Zhang, T. Grover, A. Turner, M. Oshikawa, and A. Vishwanath, *Phys. Rev. B* **85**, 235151 (2012).
- [44] Y. Zhang and A. Vishwanath, *Phys. Rev. B* **87**, 161113 (2013).
- [45] P. Corboz, M. Lajkó, A. M. Läuchli, K. Penc, and F. Mila, *Phys. Rev. X* **2**, 041013 (2012).
- [46] T. Li and F. Yang, *Phys. Rev. B* **81**, 214509 (2010).
- [47] J.-W. Mei and X.-G. Wen, arXiv:1407.0869.
- [48] A. M. Läuchli, Z. Liu, E. J. Bergholtz, and R. Moessner, *Phys. Rev. Lett.* **111**, 126802 (2013).

6. Chiral Spin Liquids in $SU(N)$ Fermionic Mott Insulators

PRL **117**, 167202 (2016)

PHYSICAL REVIEW LETTERS

week ending
14 OCTOBER 2016

- [49] G. Baskaran, Z. Zou, and P. Anderson, *Solid State Commun.* **63**, 973 (1987).
- [50] G. Baskaran and P. W. Anderson, *Phys. Rev. B* **37**, 580 (1988).
- [51] I. Affleck, Z. Zou, T. Hsu, and P. W. Anderson, *Phys. Rev. B* **38**, 745 (1988).
- [52] E. Dagotto, E. Fradkin, and A. Moreo, *Phys. Rev. B* **38**, 2926 (1988).
- [53] X.-G. Wen and P. A. Lee, *Phys. Rev. Lett.* **76**, 503 (1996).
- [54] T. Senthil and M. P. A. Fisher, *Phys. Rev. B* **62**, 7850 (2000).
- [55] Note that at this stage the flux per plaquette is unrelated to the flux per plaquette in the original Fermi-Hubbard Hamiltonian Eq. (1).
- [56] Y. Zhang, T. Grover, and A. Vishwanath, *Phys. Rev. B* **84**, 075128 (2011).
- [57] H.-H. Tu, Y. Zhang, and X.-L. Qi, *Phys. Rev. B* **88**, 195412 (2013).
- [58] A. Wietek, A. Sterdyniak, and A. M. Läuchli, *Phys. Rev. B* **92**, 125122 (2015).
- [59] A. Läuchli, F. Mila, and K. Penc, *Phys. Rev. Lett.* **97**, 087205 (2006).
- [60] B. Bauer, P. Corboz, A. M. Läuchli, L. Messio, K. Penc, M. Troyer, and F. Mila, *Phys. Rev. B* **85**, 125116 (2012).
- [61] X. G. Wen, *Quantum Field Theory of Many-Body Systems: From the Origin of Sound to an Origin of Light and Electrons* (Oxford University Press, Oxford, 2004).
- [62] B. Sutherland, *Phys. Rev. B* **12**, 3795 (1975).
- [63] I. Affleck, *Nucl. Phys.* **B265**, 409 (1986).
- [64] S. Taie, R. Yamazaki, S. Sugawa, and Y. Takahashi, *Nat. Phys.* **8**, 825 (2012).
- [65] C. Hofrichter, L. Riegger, F. Scazza, M. Höfer, D. R. Fernandes, I. Bloch, and S. Fölling, *Phys. Rev. X* **6**, 021030 (2016).
- [66] M. Aidelsburger, M. Atala, M. Lohse, J. T. Barreiro, B. Paredes, and I. Bloch, *Phys. Rev. Lett.* **111**, 185301 (2013).
- [67] H. Miyake, G. A. Siviloglou, C. J. Kennedy, W. C. Burton, and W. Ketterle, *Phys. Rev. Lett.* **111**, 185302 (2013).

SU(N) J-Q model on the square lattice with multi-column representations

Topfpflanzen, bitte gehts spazieren.

JOSEF HADER, *Topfpflanzen, Hey!*

Abstract

In this preliminary Quantum Monte Carlo study, we consider the antiferromagnetic SU(N) Heisenberg model with an additional four-spin term, often called the J - Q model [97]. We allow for representations of SU(N) with a single row and multiple columns, corresponding to higher spin- S in the SU(2) Heisenberg model. This model is expected to exhibit a phase transition from a Néel state to a valence bond solid (VBS) state in two dimensions, where the VBS state in the four-column representation is a putative symmetry-protected topologically (SPT) ordered state. We show results on the evaluation of the strange correlator for the detection of SPT order in one dimension and investigate the two-dimensional “ Q -only” model with only four-spin interactions. We give an estimate of the critical value N_{crit} for the transition to the VBS state in the Q -only model.

7.1. Introduction

Exotic new states of matter, such as quantum spin liquids, may arise in strongly interacting systems when fluctuations of local moments become dominant and determine the behavior of the system [89]. Apart from geometrical frustration or low-dimensionality, higher local symmetry may also increase quantum fluctuations. This was proposed by Read and Sachdev [226, 227], who suggested investigating generalizations of the Heisenberg model with internal SU(2) symmetry to a larger symmetry group, SU(N). In the

7. $SU(N)$ J - Q model on the square lattice with multi-column representations

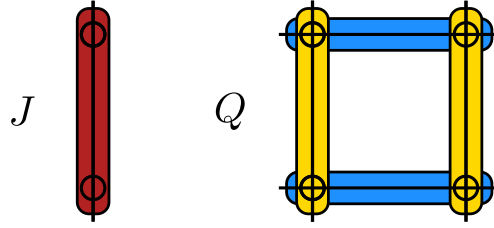
antiferromagnetic $SU(2)$ case, the ground state is Néel ordered for bipartite lattices [55]. However, Read and Sachdev [226, 227] showed that in the $N \rightarrow \infty$ limit a valence bond solid (VBS) state is realized and gave an estimate at which value N a phase transition can be expected, depending on the representation of $SU(N)$ chosen at every site. Numerically, these values have been determined exactly by recent Quantum Monte Carlo (QMC) studies for the square lattice [228–230].

Different local representations correspond to different values of the spin- S in the $SU(2)$ case. Irreducible representations of $SU(N)$ are typically described by their Young diagrams. Here, we only consider the symmetric representations with a single row and multiple columns. The number of columns is denoted by n_c . The exact form of this VBS in the $N \rightarrow \infty$ limit is determined by the representation of $SU(N)$ chosen locally [226, 227]. For the two-dimensional square lattice, the value of $n_c \pmod{4}$ decides which kind of VBS is realized. If $n_c = 1, 3 \pmod{4}$ a columnar VBS is realized, $n_c = 2 \pmod{4}$ yields a nematic VBS. Interestingly, the case $n_c = 0 \pmod{4}$ admits a spin disordered state without spontaneous symmetry breaking but with possible symmetry-protected topological (SPT) order. This may be considered as a two-dimensional analog of the famous Haldane phase in the spin-1 Heisenberg chain [231]. SPT order has recently also attracted attention in the field of measurement-based quantum computation, where several SPT states in two dimensions have been proven to allow for universal quantum computation [232, 233]. As of today, only few examples of two-dimensional SPT phases emerging from local, interacting models are known [234, 235], and often these models feature complicated interactions. Hence, providing evidence for the emergence of this kind of ordering in a simple local model would be highly desirable.

For detecting SPT order in one and two dimensions, the so-called *strange correlator* has been proposed recently [236]. Essentially, studying its behavior allows for differentiating between trivial short-range entangled states and non-trivial SPT phases. The strange correlator has already been evaluated numerically for the Haldane spin-1 chain [237], where a saturation of the strange correlator to a constant value is observed. Ultimately, we are interested in computing the strange correlator for the two-dimensional possibly SPT-ordered VBS state. In section 7.3 we show numerical results from QMC on the evaluation of the strange correlator for the generalized $SU(N)$ chain in the two-column representation. For $N = 2$ this corresponds to the original Haldane chain.

To study the nature of the phase transition between an ordered Néel state and a VBS state a continuous parameter would be desirable. The parameter N is essentially discrete. Although a generalization to continuous N has been proposed [238], another route of inducing a phase transition is to add further interaction terms that favor VBS states. In this context, the so-called J - Q model with an additional four-site exchange term has been proposed [97]. Moreover, the phase transition between the Néel state and the VBS state in the model is expected to provide an example of *deconfined criticality* [216, 239], a novel exotic kind of quantum phase transition beyond Landau's theories.

Figure 7.1.: Interactions of the J - Q model. The Q -terms are defined on pairs of neighboring sites on the elementary square plaquettes of the lattice.



We are thus interested in the J - Q models for generalized $SU(N)$ interactions in two dimensions. In section 7.4 we present results on the Q -only model on the square lattice for the $SU(N)$ representations with $n_c = 1, 2, 3, 4$. We compute spin correlations using QMC to differentiate between ordered and disordered states. This preliminary study shows, for which values of N a phase transition between the Néel state and the VBS states may be observed using QMC simulations.

7.2. Model

We are interested in studying the $SU(N)$ antiferromagnetic Heisenberg model with an additional four-spin term,

$$H = -J \sum_{\langle ij \rangle} B_{ij} - Q \sum_{(ij)(kl)} B_{ij} B_{kl}. \quad (7.2.1)$$

The second sum runs over pairs of nearest-neighbor bonds on an elementary square plaquette of the lattice as shown in Fig. 7.1. The operator B_{ij} is the generalization of the Heisenberg operator for $SU(2)$ and is defined by

$$B_{ij} = -\frac{1}{N} \sum_{\alpha, \beta=1}^N S_i^{\alpha\beta} \tilde{S}_j^{\beta\alpha}. \quad (7.2.2)$$

Here, the operators $S_i^{\alpha\beta}$ denote generators of the $SU(N)$ algebra, satisfying the commutation relations,

$$[S_i^{\alpha\beta}, S_j^{\mu\nu}] = \delta_{ij} (\delta_{\beta\mu} S_i^{\alpha\nu} - \delta_{\alpha\nu} S_i^{\mu\beta}). \quad (7.2.3)$$

The model is considered for different representations of the generators $S_i^{\alpha\beta}$, corresponding to higher spin- S in Heisenberg $SU(2)$ models. Moreover, for bipartite lattices there are two choices for the Heisenberg operator B_{ij} . We can either choose the same representation of generators on each sublattice or choose the conjugate representation,

$$\tilde{S}_i^{\alpha\beta} = -S_i^{\beta\alpha}, \quad (7.2.4)$$

on one of the two sublattices. The latter choice is then called the *antiferromagnetic* Heisenberg $SU(N)$ operator, as opposed to the ferromagnetic Heisenberg $SU(N)$ operator with the same representation on all sublattices [61]. The antiferromagnetic model

7. $SU(N)$ J - Q model on the square lattice with multi-column representations

is sign-problem free and can, therefore, be efficiently simulated with QMC techniques. We note, that the Heisenberg $SU(N)$ model considered in chapter 6 can be considered as the ferromagnetic Heisenberg model in the fundamental representation¹. A convenient method of constructing symmetric representations² of the $SU(N)$ algebra is given by the Schwinger-boson construction [240]. Let

$$a_{i\alpha}, a_{i\alpha}^\dagger, \quad \alpha = 1, \dots, N, \quad (7.2.5)$$

be bosonic operators fulfilling the canonical commutation relations and set

$$S_i^{\alpha\beta} = a_{i\alpha}^\dagger a_{i\beta}. \quad (7.2.6)$$

The operators $S_i^{\alpha\beta}$ satisfy the $SU(N)$ commutation relations Eq. (7.2.3) and conserve the total number of bosons per site,

$$\sum_{\alpha=1}^N a_{i\alpha}^\dagger a_{i\alpha} \equiv n_c = 1, 2, \dots \quad (7.2.7)$$

These operators are now used to derive the representation matrices for the symmetric representations of $SU(N)$ on the finite dimensional spaces with fixed number of Schwinger-bosons. The representation with $n_c = 1$ corresponds to the fundamental representation. In general, the representation on the subspace with n_c bosons corresponds to the symmetric representation of $SU(N)$ with a Young diagram with a single row and n_c columns.

7.3. Strange correlator of $SU(N)$ Heisenberg chains

For detecting SPT phases in one and two dimensions the behavior of so-called the *strange correlator* can be investigated. It is defined between two real-space coordinates \mathbf{r} and \mathbf{r}' by [236]

$$C(\mathbf{r}, \mathbf{r}') = \frac{\langle \Omega | \phi(\mathbf{r}) \phi(\mathbf{r}') | \Psi_0 \rangle}{\langle \Omega | \Psi_0 \rangle}, \quad (7.3.1)$$

where $\phi(\mathbf{r})$ is some local operator. Here, $|\Psi_0\rangle$ denotes the wave function under investigation, such as, for example, a ground state wave function. $|\Omega\rangle$ denotes a SPT-trivial state with short-range correlations, such as a product state of the form

$$|\Omega\rangle = \bigotimes_{i=1}^{N_s} |\sigma_i\rangle, \quad (7.3.2)$$

where N_s denotes the number of lattice sites and $|\sigma_i\rangle$ a state for a local spin. According to Ref. [236], for a gapped, non-trivial short-range entangled state, $C(\mathbf{r}, \mathbf{r}')$ will either

¹The term *ferromagnetic* can be confusing here. A ferromagnetic $SU(N)$ Heisenberg bond with negative coupling constant actually induces antiferromagnetic correlations and vice versa.

²By *symmetric* representations we denote the single row, multiple column representations of $SU(N)$.

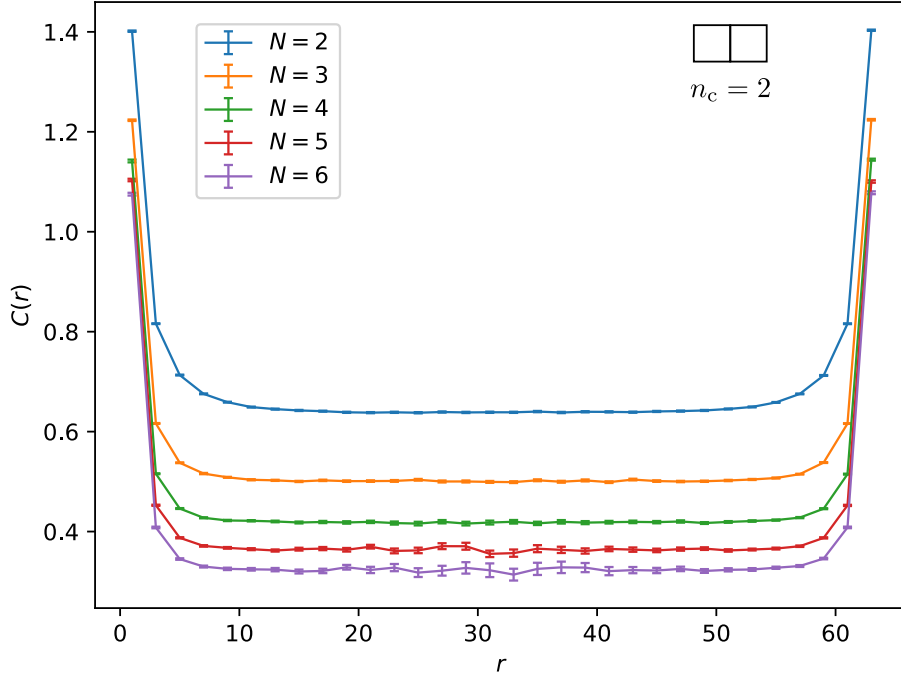


Figure 7.2.: Strange correlator $C(\mathbf{r}) = C(\mathbf{r}, \mathbf{0})$ as in Eq. (7.3.8) for the $SU(N)$ antiferromagnetic Heisenberg chain on a 64-site chain lattice in the $n_c = 2$ representation. The case $N = 2$ corresponds to the Heisenberg spin-1 chain. The imaginary time in Eq. (7.3.8) is set to $\tau = 100$. For all values of N considered, the strange correlator saturates to a constant, indicating SPT order. The error bars represent the standard errors.

converge to a constant or show algebraic decay for $|\mathbf{r} - \mathbf{r}'| \rightarrow \infty$ in one and two dimensions. Gapped, SPT-trivial states are expected to exhibit exponential decay of the strange correlator. The strange correlator has been evaluated exactly for various relevant model wavefunctions in Refs. [236, 237, 241].

We consider the $SU(N)$ antiferromagnetic Heisenberg model as in Eq. (7.2.1) without a Q -term on a one-dimensional chain lattice. We choose periodic boundary conditions. Although in one dimension also several other order parameters exist for detecting non-trivial SPT order [242–244], we compute the strange correlator for the $SU(N)$ generalization of the spin-1 Heisenberg chain. Essentially, the string order parameters proposed by Refs. [242–244] do not allow for a straightforward generalization in two dimensions. The strange correlator for the ground state of a system can be computed by QMC using a ground state projector technique, as demonstrated by Ref. [237]. There, the strange correlator for the $SU(2)$ spin chain with spin $S = 1$ has successfully been computed. The

7. SU(N) J - Q model on the square lattice with multi-column representations

local operator ϕ has been chosen as the off-diagonal exchange operator,

$$\phi(\mathbf{r})\phi(\mathbf{r}') = \frac{1}{2}(S_{\mathbf{r}}^+ S_{\mathbf{r}'}^- + S_{\mathbf{r}}^- S_{\mathbf{r}'}^+), \quad (7.3.3)$$

and the trivial product state as

$$|\Omega\rangle = \bigotimes_{i=1}^{N_s} |0\rangle. \quad (7.3.4)$$

For the generic SU(N) case, we consider the off-diagonal local operators,

$$\phi(\mathbf{r})\phi(\mathbf{r}') = O_{\mathbf{r}\mathbf{r}'} = \frac{1}{N} \sum_{\alpha \neq \beta} S_{\mathbf{r}}^{\alpha\beta} S_{\mathbf{r}'}^{\beta\alpha}, \quad (7.3.5)$$

and the product states

$$|\Omega\rangle = |\Omega_0\rangle = \bigotimes_{i=1}^{N_s} |\sigma_i\rangle, \text{ where } |\sigma_i\rangle = a_0^\dagger a_1^\dagger |\emptyset\rangle. \quad (7.3.6)$$

a_i^\dagger denote the Schwinger-boson operators as in Eq. (7.2.6). Note, that the state $a_0^\dagger a_1^\dagger |\emptyset\rangle$ in the Schwinger-boson representation corresponds to the state $|0\rangle$ in the S^z basis for SU(2).

For an arbitrary wave function $|\Omega_0\rangle$, not orthogonal to the true ground state $\langle\Psi_0|\Omega_0\rangle \neq 0$, the imaginary time evolved state,

$$\exp(-\tau H) |\Omega_0\rangle \rightarrow |\Psi_0\rangle \text{ for } \tau \rightarrow \infty, \quad (7.3.7)$$

converges to the ground state $|\Psi_0\rangle$ of H . τ denotes the imaginary time variable. Hence, we consider the following strange correlator:

$$C(\mathbf{r}) = \lim_{\tau \rightarrow \infty} \langle\Omega|O_{\mathbf{r}\mathbf{0}} \exp(-\tau H)|\Omega_0\rangle / \langle\Omega|\exp(-\tau H)|\Omega_0\rangle. \quad (7.3.8)$$

This quantity agrees with Eqs. (7.3.3) and (7.3.4) for $N = 2$ and can be evaluated for finite τ using the world-line QMC technique. For an introduction and review see [245, 246]. We employ a non-reversible worm algorithm in the continuous imaginary time integral representation [126, 247, 248]. We extended an existing implementation available at [249] to the generic SU(N) case. In order to simulate representations with multiple columns, we apply a variant of the algorithm proposed in Ref. [138]. The results of our computations are shown in Fig. 7.2. We thermalized the system with 10^7 QMC sweeps and measured 10^8 sweeps. Convergence in imaginary time has been confirmed, also by investigating two different states $|\Omega_0\rangle$ at $\tau = 0$. On small lattices, we compared our results to numerically exact data from Exact Diagonalization. We find, that the strange correlator for higher N also saturates to a constant value. For gapped systems, this implies SPT order. We computed conventional spin correlation functions which clearly exhibit an exponential decay in the correlation function for small values of N ³. This indicates a gapped state, which together with the long-ranged strange correlator implies SPT-order also for higher values of N .

³The spin correlation functions decay faster for higher values of N . Hence, differentiating between algebraic and exponential decay becomes challenging due to finite statistical errors.

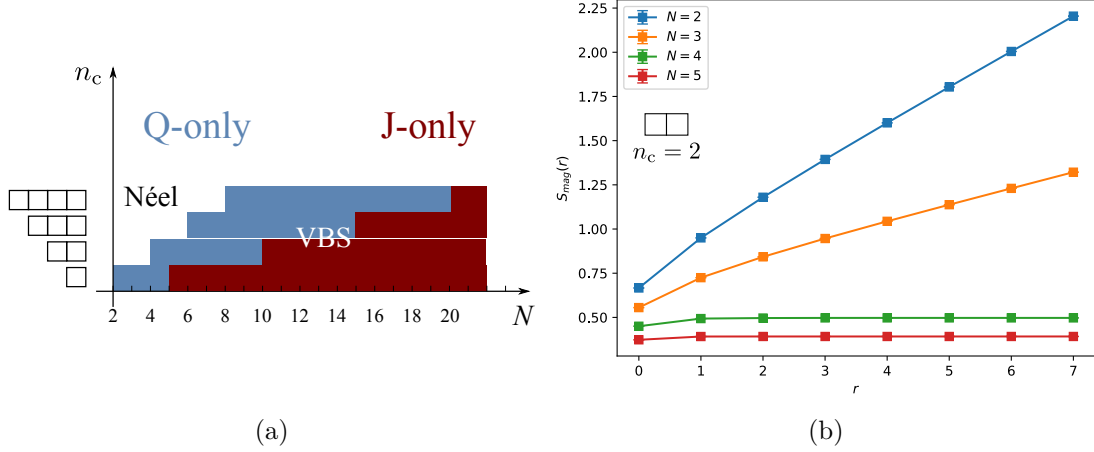


Figure 7.3.: (a): Supposable phase diagram of the Q -only model and the J -only model. (b): Summed spin correlation functions $S_{\text{mag}}(\mathbf{r})$ of the Q -only model on a 16×16 square lattice as defined in Eq. (7.4.3) for $n_c = 2$ across the diagonal of a 16×16 square lattice. Asymptotic linear behavior is expected for long-range order whereas convergence to a constant is due to exponential (or fast algebraic) decay. The error bars represent the standard errors.

7.4. Spin disordered states in Q -only model

We now consider the two-dimensional square lattice case. In order to finally establish the full phase diagram of the model Eq. (7.2.1) we here consider the extremal points $J = 1, Q = 0$ and $J = 0, Q = 1$. The pure Heisenberg case $J = 1, Q = 0$ has already been studied for $n_c = 1, 2, 3$ by Refs. [228–230]. Their findings suggest that a disordered state is stabilized for $N = 5$ if $n_c = 1$, $N = 10$ if $n_c = 2$ and likely $N = 15$ if $n_c = 3$. This agrees well with the analytical estimate by Read and Sachdev [226, 227] who proposed a critical value $n_c/N_{\text{crit}} = 0.19$ in the $n_c \rightarrow \infty$ limit. This prediction yields a critical value of $N \approx 20$ for $n_c = 4$.

The full $SU(N)$ J - Q model for $n_c = 1$ and $N = 2, 3, 4$ has been investigated in Ref. [250]. The points of phase transition for the parameter

$$q \equiv Q/(J + Q) \quad (7.4.1)$$

between the Néel state and the VBS state have been determined using QMC. The critical values found are $q_{\text{crit}} = 0.9585$ for $N = 2$, $q_{\text{crit}} = 0.3353$ for $N = 3$ and $q_{\text{crit}} = 0.0829$ for $N = 4$.

In this preliminary study, we now considered the Q -only version of Eq. (7.2.1) with

7. $SU(N)$ J - Q model on the square lattice with multi-column representations

$J = 0, Q = 1$. We computed the diagonal spin correlations,

$$C_{\text{mag}}(\mathbf{r}) = \frac{1}{N} \left\langle \sum_{\alpha=1}^N S_{\mathbf{r}}^{\alpha\alpha} S_{\mathbf{0}}^{\alpha\alpha} \right\rangle, \quad (7.4.2)$$

across the diagonal of a $L \times L = 16 \times 16$ square lattice for $n_c = 1, 2, 3, 4$. To differentiate between long-range order and exponential (or fast algebraic) decay we consider the summed correlations,

$$S_{\text{mag}}(\mathbf{r}) = \sum_{\mathbf{r}'=\mathbf{0}}^{\mathbf{r}} C_{\text{mag}}(\mathbf{r}'). \quad (7.4.3)$$

Our results for the case $n_c = 2$ are shown in Fig. 7.3b. For our simulation, we used 10^5 thermalization sweeps and 10^6 measurement sweeps. The temperature has been set to $T = 1/L = 1/16$. Long-range order implies an asymptotic linear growth of $S_{\text{mag}}(\mathbf{r})$, whereas saturation to a constant value suggests exponential (or fast algebraic) decay. We find long-range order for $N \leq 3$ if $n_c = 2$. Further preliminary computations suggest Néel order for $N \leq 5$ if $n_c = 3$ and $N \leq 7$ if $n_c = 4$. These findings are summarized in Fig. 7.3a. Nevertheless, in order to determine the exact critical value N_{crit} a more refined analysis should be performed. Especially, the system size dependence of the spin correlations should be investigated in a further study. Our results implicate, that a phase transition between a Néel ordered state and a VBS state with the continuous parameter $q = Q/(J + Q)$ should be observable in the blue region in Fig. 7.3a.

7.5. Conclusion and Outlook

We considered the antiferromagnetic J - Q model for generalized $SU(N)$ spins with multiple-column representations. As a preparational step, we measured the strange correlator using world-line QMC for the $SU(N)$ generalization of the Heisenberg spin-1 chain, exhibiting SPT order in one dimension. We then showed first results on the spin correlation functions of the Q -only model on the two-dimensional square lattice. Our results yield an approximate phase diagram for the number of columns n_c of the $SU(N)$ representation and the value N .

In order to consolidate our results, we will compute the spin correlations of the Q -only model also for different system sizes. Furthermore, the phase transition from the Néel phase to the VBS state for varying the parameter $q = Q/(J + Q)$ will be investigated in a further study. Moreover, computing nematic and columnar order parameters as in Ref. [230] could determine the nature of the VBS states for $n_c = 1, 2, 3$. The case $n_c = 4$ is of particular interest since it supposedly exhibits SPT order in two dimensions. To provide evidence for this kind of order, the strange correlator can be evaluated, as performed for the one-dimensional case in this chapter.

Acknowledgements

I am very grateful to Synge Todo for accepting me as an exchange student in his group to work on this project. I greatly enjoyed the hospitality of him and his group during my stay as well as the scientific collaboration. I would also like to especially thank Hidemaro Suwa for discussions and help with the QMC method. Moreover, I am very grateful for the financial support by Andreas Läuchli and the Marietta Blau Stipendium. The computations in this chapter have been carried out on the LEOIIIe cluster of the Focal Point Scientific Computing at the University of Innsbruck.

Conclusion and Outlook

*Words are flowing out
 Like endless rain into a paper cup
 They slither while they pass
 They slip away across the universe.*

THE BEATLES, *Across The Universe*

The development and implementation of several numerical methods allowed us to investigate interesting problems in frustrated quantum magnetism. The Exact Diagonalization code employing sublattice coding techniques and distributed memory parallelization presented in chapter 3 allowed for numerically exact evaluation of ground state properties with system sizes up to 50 spin-1/2 particles, so far the largest feasible system size.

Using this software we were able to provide conclusive evidence for the emergence of chiral spin liquids in several two-dimensional frustrated quantum magnets in chapters 4 to 6 (Refs. [140, 182, 185]). Moreover, we established approximate phase diagrams in these models and investigated the nature of the phase transitions. Especially, we proposed a scenario for the J_1 - J_2 model on the triangular lattice where a Dirac spin liquid might describe the quantum critical point of the transition from the 120° Néel ordered state to a putative \mathbb{Z}_2 spin liquid. Our findings on the chiral spin liquids on the triangular lattice have also recently been confirmed by an independent DMRG study [251].

We employed energy level spectroscopy (see Appendix B and Ref. [57]) methods, directly computed ground state properties from ED and compared with model spin liquid wave functions derived from Gutzwiller projection, cf. section 2.2. To investigate properties of the Gutzwiller projected wave functions also a Variational Monte Carlo simulation code has been developed.

The methods we developed are now readily applicable to various other problems. As an extension of the projects in chapters 4 to 6, where the emergence of an Abelian $SU(2)_1$

8. Conclusion and Outlook

(resp. $SU(N)_1$) chiral spin liquid was shown, it would be interesting to investigate systems possibly realizing non-Abelian topological order. Various candidate systems have already been proposed [168, 252–254]. In the course of these projects, it might be interesting also to compute modular matrices of the ground state manifold [255, 256] or Wilson Loop observables (see e.g. [257]).

Dynamical properties of frustrated magnets are often directly accessible in experiments. The dynamical spin structure factor of a sample, for example, can be measured by Neutron scattering experiments [50]. It would, therefore, be desirable to compare measurements in the laboratory to numerical data derived from a model Hamiltonian. For this purpose, the Exact Diagonalization software can be extended by implementing the continuous fraction expansion method [258]. Moreover, to study non-equilibrium dynamics of quantum magnets, time evolution of wave functions can also be implemented by Krylov subspace methods [259, 260].

Another important direction of research is to investigate experimental signatures of chiral spin liquids. Examples include the quantized spin Hall conductivity measurements [261] or thermal Hall conductivity measurements [262]. The spin Hall conductivity can be obtained by computing the many-body Chern number [261]. A similar topological invariant for the thermal Hall conductivity is not known so far. Yet, the behavior of the system at low temperatures may be predicted by investigating boundary modes [263]. Hence, a comparison of thermal conductivities derived numerically from the Kubo formula with these analytical results would be highly interesting. Moreover, certain dynamical signatures for topological order have been proposed [264] and a numerical investigation of those processes could yield new insight into the dynamical behavior of quantum spin liquids.

Experimentally, several materials have been found as candidates for realizing spin liquid behavior. First-principle calculations are often capable of providing approximate low-energy effective Hamiltonians for these systems, see e.g. [265]. Recently, studies on the compound α - RuCl_3 suggested a possible spin liquid behavior at low temperatures [266, 267] and effective Hamiltonians have been derived [268]. Also, effective Hamiltonians for Herbertsmithite including Dzyaloshinskii-Moriya interactions have been proposed and investigated [269]. Applying energy level spectroscopy and evaluation of ground state properties from Exact Diagonalization might yield novel insights for these systems.

The preliminary results on the $SU(N)$ Heisenberg models on the square lattice with an additional four-site Q -term in chapter 7 suggest a phase transition from a long-range Néel ordered state to a paramagnetic state. In the case of the fundamental representation of $SU(N)$ it has already been shown that the disordered state is a Valence Bond solid [270]. For the representations with multiple columns, we still need to evaluate observables to precisely determine their nature. Also, the critical point separating those phases can be evaluated by further computations. The four-column case is expected to exhibit symmetry protected topological order [230]. This kind of order has rarely been observed in local models in two dimensions. We plan on establishing this order by computing the strange

correlator [236, 237] in this system, as already done in chapter 7 for the case of the $SU(N)$ Haldane chains.

During this thesis many tools have been developed in collaboration with Michael Schuler for constructing lattice geometries and models, computing their symmetries and visualizing the results of numerical computations, such as energy spectra or correlation functions. Also, parsers for several formats of data structures common in quantum many-body computations have been written. This collection Python scripts has been put into a form of a Python package and is by now well documented. It also includes a flexible Exact Diagonalization code as a C++ extension which can be used in a user-friendly and didactic way. We think that these tools might be of broader interest to the numerical community and plan on making the source code publicly accessible as an open-source code called *QuantiPy*.

Appendices

Appendices A and B are part of lecture notes for the autumn school *Quantum Materials: Experiments and Theory* held at Forschungszentrum Jülich from 12. - 16. September 2016. The full manuscript is available as:

Alexander Wietek, Michael Schuler, and Andreas M. Läuchli. “Studying Continuous Symmetry Breaking using Energy Level Spectroscopy”. In: *arXiv E-prints* (2017). arXiv: 1704.08622 [cond-mat.str-el]

Representation theory for space groups

For finite discrete groups such as the space group of a finite lattice the full set of irreducible representations (irreps) can be worked out. Let us first discuss some basic groups. Let's consider a $n \times n$ square lattice with periodic boundary conditions and a translationally invariant Hamiltonian like the Heisenberg model on it. In the following we will set the lattice spacing to $a = 1$. The discrete symmetry group we consider is $\mathcal{T} = \mathbb{Z}_n \times \mathbb{Z}_n$ corresponding to the group of translations on this lattice. This is an Abelian group of order n^2 . Its representations can be labeled by the momentum vectors $\mathbf{k} = (\frac{2\pi i}{n}, \frac{2\pi j}{n})$, $i, j \in \{0, \dots, n-1\}$ which just correspond to the reciprocal Bloch vectors defined on this lattice. Put differently, the vectors \mathbf{k} are the reciprocal lattice points of the lattice spanned by the simulation torus of our $n \times n$ square lattice. The character $\chi_{\mathbf{k}}$ of the \mathbf{k} -representation is given by

$$\chi_{\mathbf{k}}(\mathbf{t}) = e^{i\mathbf{k} \cdot \mathbf{t}} \quad (\text{A.0.1})$$

where $\mathbf{t} \in \mathcal{T}$ is the vector of translation. This is just the usual Bloch factor for translationally invariant systems.

Let us now consider a (symmorphic) space group of the form $\mathcal{D} = \mathcal{T} \times \text{PG}$ as the discrete symmetry group of the lattice where PG is the pointgroup of the lattice. For a model on a $n \times n$ square lattice this could for example be the dihedral group of order 8, D_4 , consisting of fourfold rotations together with reflections. The representation theory and the character tables of these point groups are well-established. An example for such character tables can be found in Tab. A.1 for the dihedral group D_6 ¹. Since \mathcal{D} is now a product of the translation and the point group we could think that the irreducible representations of \mathcal{D} are simply given by the product representations $(\mathbf{k} \otimes \rho)$ where \mathbf{k} labels a momentum representation and ρ an irrep of PG. But here is a small yet important caveat. We have to be careful since \mathcal{D} is only a semidirect product of groups as translations and pointgroup symmetries do not necessarily commute. This alters the representation theory for this

¹We follow the labeling scheme for point group representations according to Mulliken [271].

A. Representation theory for space groups

D_6	1	$2C_6$	$2C_3$	C_2	$3\sigma_d$	$3\sigma_v$
A1	1	1	1	1	1	1
A2	1	1	1	1	-1	-1
B1	1	-1	1	-1	1	-1
B2	1	-1	1	-1	-1	1
E1	2	1	-1	-2	0	0
E2	2	-1	-1	2	0	0

Table A.1.: Character table for pointgroup D_6 .

product of groups and the irreps of \mathcal{D} are not just simply the products of irreps of \mathcal{T} and PG. Instead the full set of irreps for this group is given by $(\mathbf{k} \otimes \rho_{\mathbf{k}})$ where $\rho_{\mathbf{k}}$ is an irrep of the so called *little group* $L_{\mathbf{k}}$ of \mathbf{k} defined as

$$L_{\mathbf{k}} = \{g \in \text{PG}; g(\mathbf{k}) = \mathbf{k}\} \quad (\text{A.0.2})$$

which is just the stabilizer of \mathbf{k} in PG. For example, all pointgroup elements leave $\mathbf{k} = (0, 0)$ invariant, thus the little group of $\mathbf{k} = (0, 0)$ is the full pointgroup PG. In general, this does not hold for other momenta and only a subgroup of PG will be the little group of \mathbf{k} . In Fig. B.1 we show the \mathbf{k} -points of a 6×6 triangular lattice together with its little groups as an example. The K point in the Brillouin zone has a D_3 little group, the M point a D_2 little group. Having discussed the representation theory for (symmorphic) space groups we state that the characters of these representations are simply given by

$$\chi_{(\mathbf{k}, \rho_{\mathbf{k}})}(\mathbf{t}, p) = e^{i\mathbf{k} \cdot \mathbf{t}} \chi_{\rho_{\mathbf{k}}}(p) \quad (\text{A.0.3})$$

where $\mathbf{t} \in \mathcal{T}$, $p \in \text{PG}$ and $\chi_{\rho_{\mathbf{k}}}$ denotes the character of the representation $\rho_{\mathbf{k}}$ of the little group $L_{\mathbf{k}}$.

Tower of States analysis

Symmetry analysis

In the analysis of excitation spectra from Exact Diagonalization on finite size simulation clusters the *tower of states* analysis, short TOS, is a powerful tool to detect spontaneous symmetry breaking. As we have seen in section 1.1.1 explicitly for the Heisenberg anti-ferromagnet, symmetry breaking implies degenerate ground states in the thermodynamic limit. On finite size simulation clusters this degeneracy is in general not an exact degeneracy. We rather expect a certain scaling of the energy differences in the thermodynamic limit. We distinguish two cases:

- **Discrete symmetry breaking:** In this case we have a degeneracy of finitely many states in the thermodynamic limit. The ground state splitting Δ on finite size clusters scales as $\Delta \sim \exp(-N/\xi)$, where N is the number of sites in the system.
- **Continuous symmetry breaking:** The ground state in the thermodynamic limit is infinitely degenerate. The states belonging to this degenerate manifold collapse as $\Delta \sim 1/N$ on finite size clusters as we have seen in section 1.1.1. It is important to understand that these states are not the Goldstone modes of continuous symmetry breaking. Both the degenerate ground state and the Goldstone modes appear as low energy levels on finite size clusters but have different scaling behaviours.

The scaling of these low energy states can now be investigated on finite size clusters. More importantly also their quantum numbers such as momentum, pointgroup representation or total spin can be predicted [204, 205, 272]. The detection of correct scaling behaviour together with correctly predicted quantum numbers yields very strong evidence that the system spontaneously breaks symmetry in the way that has been anticipated. This is the TOS method. In the following we will discuss how to predict the quantum numbers for discrete as well as continuous symmetry breaking. The main mathematical tool we use is the character-formula from basic group representation theory.

B. Tower of States analysis

Lattice Hamiltonians like a Heisenberg model often have a discrete symmetry group arising from translational invariance, pointgroup invariance or some discrete local symmetry, like a spinflip symmetry. In this chapter we will first discuss the representation theory and the characters of the representations of space groups on finite lattices. We will then see how this helps us to predict the representations of the degenerate ground states in discrete as well as continuous symmetry breaking.

Predicting irreducible representations in spontaneous symmetry breaking

Spontaneous symmetry breaking at $T = 0$ occurs when the ground state $|\psi_{\text{GS}}\rangle$ of H in the thermodynamic limit is not invariant under the full symmetry group \mathcal{G} of H . We will call a specific ground state $|\psi_{\text{GS}}\rangle$ a *prototypical state* and the *ground state manifold* is defined by

$$V_{\text{GS}} = \text{span} \left\{ |\psi_{\text{GS}}^i\rangle \right\} \quad (\text{B.0.1})$$

where $|\psi_{\text{GS}}^i\rangle$ is the set of degenerate ground states in the thermodynamic limit. This ground state manifold space can be finite or infinite dimensional depending on the situation. For breaking a discrete finite symmetry this ground state manifold will be finite dimensional, for breaking continuous $\text{SO}(3)$ spin rotational symmetry¹ as in section 1.1.1 it is infinite dimensional in the thermodynamic limit. For every symmetry $g \in \mathcal{G}$ we denote by O_g the symmetry operator acting on the Hilbert space. The ground state manifold becomes degenerate in the thermodynamic limit and we want to calculate the quantum numbers of the ground states in this manifold. Another way of saying this is that we want to compute the irreducible representations of \mathcal{G} to which the ground states belong to. For this we look at the action Γ of the symmetry group \mathcal{G} on V_{GS} defined by

$$\Gamma : \mathcal{G} \rightarrow \text{Aut}(V_{\text{GS}}) \quad (\text{B.0.2})$$

$$g \mapsto \left(\langle \psi_{\text{GS}}^i | O_g | \psi_{\text{GS}}^j \rangle \right)_{i,j} \quad (\text{B.0.3})$$

This is a representation of \mathcal{G} on V_{GS} , so every group element $g \in \mathcal{G}$ is mapped to an invertible matrix on V_{GS} . In general this representation is reducible and can be decomposed into a direct sum of irreducible representations

$$\Gamma = \bigoplus_{\rho} n_{\rho} \rho \quad (\text{B.0.4})$$

These irreducible representations ρ are the quantum numbers of the eigenstates in the ground state manifold and n_{ρ} are its respective multiplicities (or degeneracies). Therefore these irreps constitute the TOS for spontaneous symmetry breaking [204]. To compute

¹The actual symmetry group of Heisenberg antiferromagnets is usually $\text{SU}(2)$. For simplicity we only consider the subgroup $\text{SO}(3)$ in these notes which yields the same predictions for the case of sublattices with even number of sites (corresponding to integer total sublattice spin).

the multiplicities we can use a central result from representation theory, the *character formula*

$$n_\rho = \frac{1}{|\mathcal{G}|} \sum_{g \in \mathcal{G}} \overline{\chi_\rho(g)} \text{Tr}(\Gamma(g)) \quad (\text{B.0.5})$$

where $\chi_\rho(g)$ is the character of the representation ρ and $\text{Tr}(\Gamma(g))$ denotes the trace over the representation matrix $\Gamma(g)$ as defined in Eq. (B.0.2). Often we have the case that

$$\langle \psi_{\text{GS}} | O_g | \psi'_{\text{GS}} \rangle = \begin{cases} 1 & \text{if } O_g | \psi'_{\text{GS}} \rangle = | \psi_{\text{GS}} \rangle \\ 0 & \text{otherwise} \end{cases} \quad (\text{B.0.6})$$

With this we can simplify Eq. (B.0.5) to what we call the *character-stabilizer formula*

$$n_\rho = \frac{1}{|\text{Stab}(|\psi_{\text{GS}}\rangle)|} \sum_{g \in \text{Stab}(|\psi_{\text{GS}}\rangle)} \chi_\rho(g) \quad (\text{B.0.7})$$

where

$$\text{Stab}(|\psi_{\text{GS}}\rangle) \equiv \{g \in \mathcal{G} : O_g | \psi_{\text{GS}} \rangle = | \psi_{\text{GS}} \rangle\} \quad (\text{B.0.8})$$

is the stabilizer of a prototypical state $|\psi_{\text{GS}}\rangle$ ². We see that for applying the character-stabilizer formula in Eq. (B.0.7) only two ingredients are needed:

- the stabilizer $\text{Stab}(|\psi_{\text{GS}}\rangle)$ of a prototypical state $|\psi_{\text{GS}}\rangle$ in the ground state manifold
- the characters of the irreducible representations of the symmetry group \mathcal{G}

We want to remark that in the case of $\mathcal{G} = \mathcal{D} \times \mathcal{C}$ where \mathcal{D} is a discrete symmetry group such as the spacegroup of a lattice and \mathcal{C} is a continuous symmetry group such as $\text{SO}(3)$ rotations for Heisenberg spins the Eqs. (B.0.5) and (B.0.7) include integrals over Lie groups additionally to the sum over the elements of the discrete symmetry group \mathcal{D} . Furthermore also the characters for Lie groups like $\text{SO}(3)$ are well-known. For an element $R \in \text{SO}(3)$ the irreducible representations are labeled by the spin S and its characters are given by

$$\chi_S(R) = \frac{\sin \left[\left(S + \frac{1}{2} \right) \phi \right]}{\sin \frac{\phi}{2}} \quad (\text{B.0.9})$$

where $\phi \in [0, 2\pi]$ is the angle of rotation of the spin rotation R .

²In some cases, the orbit of the prototypical state $G \cdot |\psi_{\text{GS}}\rangle = \{g \in G : O_g | \psi_{\text{GS}} \rangle\}$ does not span the full set of degenerate ground states $|\psi_{\text{GS}}^i\rangle$. In this case, we have to find a set of prototypical states with different orbits, such that the union of these orbits spans the full ground state manifold. Then, Eq. (B.0.7) has to be applied to each prototypical state, individually, and the final multiplicity is the sum of the individual results.

SU(2) symmetry breaking in square Heisenberg model

We now give a first example how the TOS method can be applied to predict the structure of the tower of states for magnetically ordered phases. We look at the Néel state of the antiferromagnet on the bipartite square lattice with sublattices A and B . A prototypical state in the ground state manifold is given by

$$|\psi\rangle = |\uparrow\downarrow\uparrow\downarrow\cdots\rangle \quad (\text{B.0.10})$$

where all spins point up on sublattice A and down on sublattice B . The symmetry group $\mathcal{G} = \mathcal{D} \times \mathcal{C}$ of the model we consider is a product between discrete translational symmetry $\mathcal{D} = \mathbb{Z}_2 \times \mathbb{Z}_2 = \{1, t_x, t_y, t_{xy}\}$ and spin rotational symmetry $\mathcal{C} = \text{SO}(3)$. We remark that we restrict our translational symmetry group to $\mathcal{D} = \mathbb{Z}_2 \times \mathbb{Z}_2$ instead of $\mathcal{D}' = \mathbb{Z} \times \mathbb{Z}$ because the Néel state transforms trivially under two-site translations $(t_x)^2, (t_y)^2$. Thus, only the representations of \mathcal{D}' trivial under two-site translations are relevant; these are exactly the representations of \mathcal{D} . Put differently we only have to consider the translations in the unitcell of the magnetic structure which in the present case can be chosen as a 2-by-2 cell. Furthermore, we will for now neglect pointgroup symmetries like rotations and reflections of the lattice to simplify calculations. At the end of this section we give results where also these symmetry elements are incorporated.

The ground state manifold V_{GS} we consider are the states related to $|\psi\rangle$ by an element of the symmetry group \mathcal{G} , i.e.

$$V_{\text{GS}} = \{O_g |\psi\rangle; g \in \mathcal{G}\} \quad (\text{B.0.11})$$

The symmetry elements in \mathcal{G} that leave our prototypical state $|\psi\rangle$ invariant are given by two sets of elements:

- No translation in real space or a diagonal t_{xy} translation together with a spin rotation $R_z(\alpha)$ around the z -axis with an arbitrary angle α .
- Translation by one site, t_x or t_y , followed by a rotation $R_a(\pi)$ of 180° around an axis $a \perp z$ perpendicular to the z -axis.

So the stabilizer of our prototype state $|\psi\rangle$ is given by

$$\text{Stab}(|\psi\rangle) = \{1 \times R_z(\alpha)\} \cup \{t_{xy} \times R_z(\alpha)\} \cup \{t_x \times R_a(\pi)\} \cup \{t_y \times R_a(\pi)\} \quad (\text{B.0.12})$$

The representations of the discrete symmetry group can be labeled by four momenta $\mathbf{k} \in \{(0, 0), (0, \pi), (\pi, 0), (\pi, \pi)\}$ with corresponding characters

$$\chi_{\mathbf{k}}(t) = e^{i\mathbf{k} \cdot \mathbf{t}}$$

where \mathbf{t} denotes the translation vector corresponding to t . The continuous symmetry group we consider is the Lie group $\text{SO}(3)$. Its representations are labeled by the total spin S . The character of the spin- S representation is given by

$$\chi_S(R) = \frac{\sin \left[\left(S + \frac{1}{2} \right) \phi \right]}{\sin \frac{\phi}{2}}$$

where $\phi \in [0, 2\pi]$ is the angle of rotation of the element $R \in \text{SO}(3)$. We see that spin rotations with different axes but same rotational angle give rise to the same character. The representations of the total symmetry group $\mathcal{G} = \mathcal{D} \times \mathcal{C}$ are now just the product representations of \mathcal{D} and \mathcal{C} . Therefore also the characters of representations of \mathcal{G} are the product of characters of \mathcal{D} and \mathcal{C} . We label these representations by (\mathbf{k}, S) where \mathbf{k} denotes the lattice momentum and S the total spin. To derive the multiplicities of the representations (\mathbf{k}, S) in the ground state manifold, we now apply the character-stabilizer formula, Eq. (B.0.7). In the case of the square antiferromagnet this yields

$$n_{(\mathbf{k}, S)} = e^{i\mathbf{k} \cdot \mathbf{0}} \frac{1}{4 |R_z(\alpha)|} \int_0^{2\pi} d\alpha \chi_S(R_z(\alpha)) + e^{i\mathbf{k} \cdot (\mathbf{e}_x + \mathbf{e}_y)} \frac{1}{4 |R_z(\alpha)|} \int_0^{2\pi} d\alpha \chi_S(R_z(\alpha)) \quad (\text{B.0.13})$$

$$+ e^{i\mathbf{k} \cdot \mathbf{e}_x} \frac{1}{4 |R_a(\pi)|} \int_0^{2\pi} da \chi_S(R_a(\pi)) + e^{i\mathbf{k} \cdot \mathbf{e}_y} \frac{1}{4 |R_a(\pi)|} \int_0^{2\pi} da \chi_S(R_a(\pi)) \quad (\text{B.0.14})$$

We compute

$$|R_z(\alpha)| = |R_a(\pi)| = \int_0^{2\pi} d\phi = 2\pi$$

$$\frac{1}{2\pi} \int_0^{2\pi} d\alpha \chi_S(R_z(\alpha)) = \frac{1}{2\pi} \int_0^{2\pi} d\alpha \frac{\sin \left[\left(S + \frac{1}{2} \right) \alpha \right]}{\sin \frac{\alpha}{2}} = \frac{1}{2\pi} \int_0^{2\pi} d\alpha \sum_{l=-S}^S e^{il\alpha} = 1 \quad (\text{B.0.15})$$

and

$$\frac{1}{2\pi} \int_0^{2\pi} da \chi_S(R_a(\pi)) = \frac{1}{2\pi} \int_0^{2\pi} da \frac{\sin \left[\left(S + \frac{1}{2} \right) \pi \right]}{\sin \frac{\pi}{2}} = (-1)^S \quad (\text{B.0.16})$$

Putting this together gives the final result for the multiplicities of the representations in the tower of states

$$n_{((0,0), S)} = \frac{1}{4} \left(1 \cdot 1 + 1 \cdot 1 + 1 \cdot (-1)^S + 1 \cdot (-1)^S \right) = \begin{cases} 1 & \text{if } S \text{ even} \\ 0 & \text{if } S \text{ odd} \end{cases} \quad (\text{B.0.17})$$

$$n_{((\pi, \pi), S)} = \frac{1}{4} \left(1 \cdot 1 + 1 \cdot 1 - 1 \cdot (-1)^S - 1 \cdot (-1)^S \right) = \begin{cases} 0 & \text{if } S \text{ even} \\ 1 & \text{if } S \text{ odd} \end{cases} \quad (\text{B.0.18})$$

$$n_{((0, \pi), S)} = \frac{1}{4} \left(1 \cdot 1 - 1 \cdot 1 + 1 \cdot (-1)^S - 1 \cdot (-1)^S \right) = 0 \quad (\text{B.0.19})$$

$$n_{((\pi, 0), S)} = \frac{1}{4} \left(1 \cdot 1 - 1 \cdot 1 - 1 \cdot (-1)^S + 1 \cdot (-1)^S \right) = 0 \quad (\text{B.0.20})$$

B. Tower of States analysis

Tab. B.1 lists the computed multiplicities of the irreducible representations where additionally the D_4 point group was considered in the symmetry analysis. These irreps and their multiplicities exactly agree with the irreps and multiplicities in the TOS of the square lattice Heisenberg model from ED in Fig. 1.3. The spectroscopic predictions together with the numerical data thus constitute a firm and solid evidence of Néel order.

S	$\Gamma.A1$	$M.A1$
0	1	0
1	0	1
2	1	0
3	0	1

Table B.1.: Multiplicities of irreducible representations in the TOS for the Néel Antiferromagnet on a square lattice.

Magnetic order in triangular lattice geometries

On the triangular lattice several magnetic orders can be stabilized. The Heisenberg nearest neighbour model has been shown to have a 120° Néel ordered ground state where spins on neighbouring sites align in an angle of 120° [80, 81]. Upon adding further second nearest neighbour interactions J_2 to the Heisenberg nearest neighbour model with interaction strength J_1 it was shown that the ground state exhibits *stripy order* for $J_2/J_1 \gtrsim 0.18$ [82]. Here spins are aligned ferromagnetically along one direction of the triangular lattice and antiferromagnetically along the other two. Interestingly, it was shown that a phase exists between these two magnetic orders whose exact nature is unclear until today. Several articles propose that in this region an exotic *quantum spin liquid* is stabilized [113, 195, 196, 198]. In a recent proposal two of the authors established an approximate phase diagram of an extended Heisenberg model with further scalar chirality interactions $J_\chi \mathbf{S}_i \cdot (\mathbf{S}_j \times \mathbf{S}_k)$ [182] on elementary triangles. The Hamiltonian of this model is given by

$$H = J_1 \sum_{\langle i,j \rangle} \mathbf{S}_i \cdot \mathbf{S}_j + J_2 \sum_{\langle\langle i,j \rangle\rangle} \mathbf{S}_i \cdot \mathbf{S}_j + J_\chi \sum_{i,j,k \in \Delta} \mathbf{S}_i \cdot (\mathbf{S}_j \times \mathbf{S}_k) \quad (\text{B.0.21})$$

Amongst the already known 120° Néel and stripy phases an exotic *Chiral Spin Liquid* and a magnetic *tetrahedrally ordered* phase were found. Here we will only discuss the magnetic orders appearing in this model. The non-coplanar tetrahedral order has a four-site unitcell where four spins align such that they span a regular tetrahedron. In this chapter we discuss the tower of states for the three magnetic phases in this model.

First of all Fig. B.1 shows the simulation cluster used for the Exact Diagonalization calculations in [182]. We chose a $N = 36 = 6 \times 6$ sample with periodic boundary conditions. This sample allows to resolve the momenta Γ , K and M , amongst several others in the

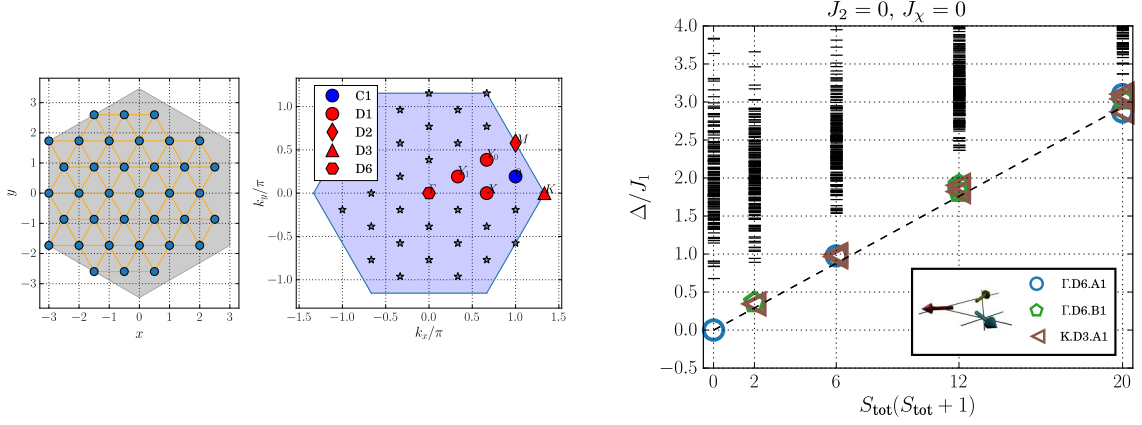


Figure B.1.: (Left): Simulation cluster for the Exact Diagonalization calculations. (Center): Brillouin zone of the triangular lattice with the momenta which can be resolved with this choice of the simulation cluster. Different symbols denote the little groups of the corresponding momentum. (Right): TOS for the 120° Néel order on the triangular lattice. The symmetry sectors and multiplicities fulfill the predictions from the symmetry analysis (See Tab. B.2). One should note, that the multiplicities grow with S_{tot} for non-collinear states.

Brillouin zone. The K and M momenta are the ordering vectors for the 120° , stripy and tetrahedral order. Furthermore, this sample features full sixfold rotational as well as reflection symmetries (the latter only in the absence of the chiral term, i.e. $J_\chi = 0$). Its pointgroup is therefore given by the dihedral group of order 12, D_6 . The little groups of the individual \mathbf{k} vectors are also shown in Fig. B.1. For our tower of states analysis we now want to consider the discrete symmetry group

$$\mathcal{D} = \mathcal{T} \times D_6 \quad (\text{B.0.22})$$

where \mathcal{T} is the translational group of the magnetic unitcell. The full set of irreducible representations of this symmetry group is given by the set $(\mathbf{k} \otimes \rho_{\mathbf{k}})$ where \mathbf{k} denotes the momentum and $\rho_{\mathbf{k}}$ is an irrep of the little group associated to \mathbf{k} . The points Γ , K and M give rise to the little groups D_6 , D_3 and D_2 (the dihedral groups of order 12, 8, and 4), respectively. For the stripy and tetrahedral order we can choose a 2×2 magnetic unitcell, and a 3×3 unitcell for the 120° Néel order. The spin rotational symmetry gives rise to the continuous symmetry group

$$\mathcal{C} = \text{SO}(3) \quad (\text{B.0.23})$$

We can therefore label the full set of irreps as $(\mathbf{k}, \rho_{\mathbf{k}}, S)$ where S denotes the total spin S representation of $\text{SO}(3)$. Similarly to the previous chapter we now want to apply the character-stabilizer formula, Eq. (B.0.7), to determine the multiplicities of the represen-

B. Tower of States analysis

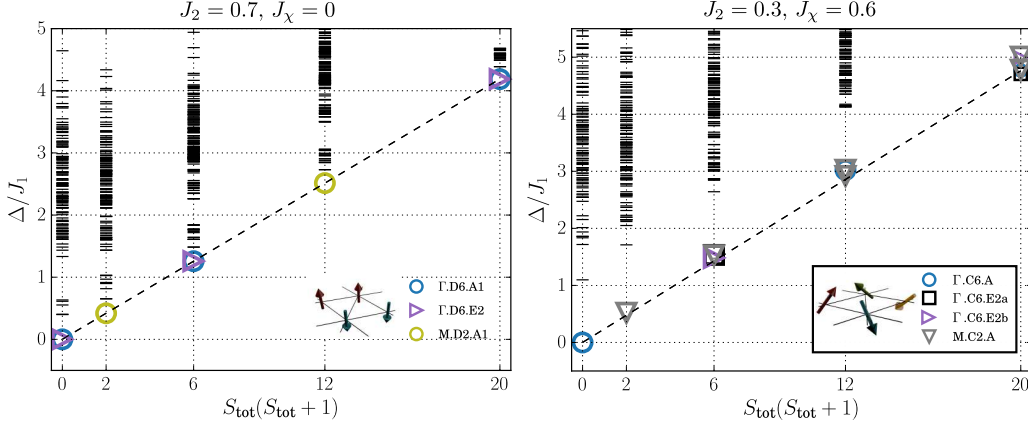


Figure B.2.: (Left): TOS for the stripy phase on the triangular lattice. The multiplicities for each even/odd S_{tot} are constant for collinear phases. (Right): TOS for the tetrahedral order on the triangular lattice.

tations forming the tower of states. The characters of the irreps $(\mathbf{k}, \rho_{\mathbf{k}}, S)$ are given by

$$\chi_{(\mathbf{k}, \rho_{\mathbf{k}}, S)}(t, p, R) = e^{i\mathbf{k}\cdot\mathbf{t}} \chi_{\rho_{\mathbf{k}}}(p) \frac{\sin\left[\left(S + \frac{1}{2}\right)\phi\right]}{\sin\frac{\phi}{2}} \quad (\text{B.0.24})$$

where again $\phi \in [0, 2\pi]$ is the angle of rotation of the spin rotation R . The characters of the pointgroup D_6 are given in Tab. A.1. We skip the exact calculations which follow closely the calculations performed in the previous chapter, although now pointgroup symmetries are additionally taken into account. The results are summarized in Tab. B.2. We remark

	120° Néel			stripy order			tetrahedral order			
S	$\Gamma.A1$	$\Gamma.B1$	$K.A1$	$\Gamma.A1$	$\Gamma.E2$	$M.A$	$\Gamma.A$	$\Gamma.E2a$	$\Gamma.E2b$	$M.A$
0	1	0	0	1	1	0	1	0	0	0
1	0	1	1	0	0	1	0	0	0	1
2	1	0	2	1	1	0	0	1	1	1
3	1	2	2	0	0	1	1	0	0	2

Table B.2.: Multiplicities of irreducible representations in the Anderson tower of states for the three magnetic orders on the triangular lattice defined in the main text.

that the tetrahedral order is stabilized only for $J_x \neq 0$ where the model in Eq. (B.0.21) does not have reflection symmetry any more since the term $\mathbf{S}_i \cdot (\mathbf{S}_j \times \mathbf{S}_k)$ does not preserve this symmetry. Therefore we used only the pointgroup C_6 of sixfold rotation in the calculations of the tower of states for this phase.

If we compare these results to Figs. B.1, B.2 we see that these are exactly the representations appearing in the TOS from Exact Diagonalization for certain parameter values J_2

and J_χ . This is a strong evidence that indeed $\text{SO}(3)$ symmetry is broken in these models in a way described by the 120° Néel, stripy and tetrahedral magnetic prototype states.

It is worth noting, that the sum of the multiplicities is constant with S_{tot} for collinear phases, e.g. the stripy order shown here, whereas it is increasing for non-collinear orders.

Bibliography

- [1] D. C. Tsui, H. L. Stormer, and A. C. Gossard. “Two-Dimensional Magnetotransport in the Extreme Quantum Limit”. In: *Phys. Rev. Lett.* 48.22 (1982). DOI: 10.1103/PhysRevLett.48.1559.
- [2] H. L. Stormer et al. “Fractional Quantization of the Hall Effect”. In: *Phys. Rev. Lett.* 50.24 (1983). DOI: 10.1103/PhysRevLett.50.1953.
- [3] H.L. Stormer. “Two-dimensional electron correlation in high magnetic fields”. In: *Phys. B* 177.1 (1992). DOI: 10.1016/0921-4526(92)90138-I.
- [4] Xiao-Gang Wen. “Topological orders and edge excitations in fractional quantum Hall states”. In: *Adv. Phys.* 44.5 (1995). DOI: 10.1080/00018739500101566. eprint: arXiv:cond-mat/9506066.
- [5] R. G. Clark et al. “Experimental determination of fractional charge e/q for quasi-particle excitations in the fractional quantum Hall effect”. In: *Phys. Rev. Lett.* 60.17 (1988). DOI: 10.1103/PhysRevLett.60.1747.
- [6] Chetan Nayak et al. “Non-Abelian anyons and topological quantum computation”. In: *Rev. Mod. Phys.* 80.3 (2008). DOI: 10.1103/RevModPhys.80.1083. arXiv: arXiv:0707.1889 [cond-mat.str-el].
- [7] J. I. Cirac and P. Zoller. “Quantum Computations with Cold Trapped Ions”. In: *Phys. Rev. Lett.* 74.20 (1995). DOI: 10.1103/PhysRevLett.74.4091.
- [8] H. Häffner, C.F. Roos, and R. Blatt. “Quantum computing with trapped ions”. In: *Phys. Rep.* 469.4 (2008). DOI: 10.1016/j.physrep.2008.09.003. arXiv: arXiv:0809.4368 [quant-ph].
- [9] J. G. Bednorz and K. A. Müller. “Possible high T_c superconductivity in the Ba-La-Cu-O system”. In: *Z. Phys. B: Condens. Matter* 64.2 (1986). DOI: 10.1007/BF01303701.
- [10] P. W. Anderson. “New Approach to the Theory of Superexchange Interactions”. In: *Phys. Rev.* 115.1 (1959). DOI: 10.1103/PhysRev.115.2.

Bibliography

- [11] P. W. Anderson. “The Resonating Valence Bond State in La₂CuO₄ and Superconductivity”. In: *Science* 235.4793 (1987). DOI: 10.1126/science.235.4793.1196.
- [12] H. Bethe. “Zur Theorie der Metalle”. In: *Z. Phys.* 71.3 (1931). DOI: 10.1007/BF01341708.
- [13] David A. Huse. “Ground-state staggered magnetization of two-dimensional quantum Heisenberg antiferromagnets”. In: *Phys. Rev. B* 37.4 (1988). DOI: 10.1103/PhysRevB.37.2380.
- [14] J. Oitmaa and D. D. Betts. “The ground state of two quantum models of magnetism”. In: *Can. J. Phys.* 56.7 (1978). DOI: 10.1139/p78-120.
- [15] J. D. Reger and A. P. Young. “Monte Carlo simulations of the spin-1/2 Heisenberg antiferromagnet on a square lattice”. In: *Phys. Rev. B* 37.10 (1988). DOI: 10.1103/PhysRevB.37.5978.
- [16] Tian-Heng Han et al. “Fractionalized excitations in the spin-liquid state of a kagome-lattice antiferromagnet”. In: *Nature* 492.7429 (2012). DOI: 10.1038/nature11659. arXiv: arXiv:1307.5047 [cond-mat.str-el].
- [17] Minoru Yamashita et al. “Highly Mobile Gapless Excitations Quantum Spin Liquid”. In: *Science* 328 (2010). DOI: 10.1126/science.1188200.
- [18] T. Itou et al. “Quantum spin liquid in the spin-1/2 triangular antiferromagnet EtMe₃Sb[Pd(dmit)₂]₂”. In: *Phys. Rev. B* 77.10 (2008). DOI: 10.1103/PhysRevB.77.104413.
- [19] Y. Kurosaki et al. “Mott Transition from a Spin Liquid to a Fermi Liquid in the Spin-Frustrated Organic Conductor κ -(ET)₂Cu₂(CN)₃”. In: *Phys. Rev. Lett.* 95.17 (2005). DOI: 10.1103/PhysRevLett.95.177001. arXiv: arXiv:cond-mat/0504273 [cond-mat.str-el].
- [20] Y. Shimizu et al. “Spin Liquid State in an Organic Mott Insulator with a Triangular Lattice”. In: *Phys. Rev. Lett.* 91.10 (2003). DOI: 10.1103/PhysRevLett.91.107001. arXiv: arXiv:cond-mat/0307483 [cond-mat.str-el].
- [21] Danna E. Freedman et al. “Site Specific X-ray Anomalous Dispersion of the Geometrically Frustrated Kagomé Magnet, Herbertsmithite, ZnCu₃(OH)₆Cl₂”. In: *J. Am. Chem. Soc.* 132.45 (2010). DOI: 10.1021/ja1070398.
- [22] P.W. Anderson. “Resonating valence bonds: A new kind of insulator?” In: *Mater. Res. Bull.* 8.2 (1973). DOI: 10.1016/0025-5408(73)90167-0.
- [23] X. G. Wen, Frank Wilczek, and A. Zee. “Chiral spin states and superconductivity”. In: *Phys. Rev. B* 39.16 (1989). DOI: 10.1103/PhysRevB.39.11413.
- [24] V. Kalmeyer and R. B. Laughlin. “Equivalence of the resonating-valence-bond and fractional quantum Hall states”. In: *Phys. Rev. Lett.* 59.18 (1987). DOI: 10.1103/PhysRevLett.59.2095.

- [25] B. Bernu, C. Lhuillier, and L. Pierre. “Signature of Néel order in exact spectra of quantum antiferromagnets on finite lattices”. In: *Phys. Rev. Lett.* 69.17 (1992). DOI: 10.1103/PhysRevLett.69.2590.
- [26] M. B. Hastings. “Dirac structure, RVB, and Goldstone modes in the kagomé anti-ferromagnet”. In: *Phys. Rev. B* 63.1 (2000). DOI: 10.1103/PhysRevB.63.014413.
- [27] Ying Ran et al. “Projected-Wave-Function Study of the Spin-1/2 Heisenberg Model on the Kagomé Lattice”. In: *Phys. Rev. Lett.* 98.11 (2007). DOI: 10.1103/PhysRevLett.98.117205.
- [28] Michael Hermele et al. “Properties of an algebraic spin liquid on the kagome lattice”. In: *Phys. Rev. B* 77.22 (2008). DOI: 10.1103/PhysRevB.77.224413.
- [29] Yasir Iqbal et al. “Gapless spin-liquid phase in the kagome spin- $\frac{1}{2}$ Heisenberg anti-ferromagnet”. In: *Phys. Rev. B* 87.6 (2013). DOI: 10.1103/PhysRevB.87.060405.
- [30] Subir Sachdev. “Kagome- and triangular-lattice Heisenberg antiferromagnets: Ordering from quantum fluctuations and quantum-disordered ground states with unconfined bosonic spinons”. In: *Phys. Rev. B* 45.21 (1992). DOI: 10.1103/PhysRevB.45.12377.
- [31] R. Moessner and S. L. Sondhi. “Resonating Valence Bond Phase in the Triangular Lattice Quantum Dimer Model”. In: *Phys. Rev. Lett.* 86.9 (2001). DOI: 10.1103/PhysRevLett.86.1881.
- [32] L. Balents, M. P. A. Fisher, and S. M. Girvin. “Fractionalization in an easy-axis Kagome antiferromagnet”. In: *Phys. Rev. B* 65.22 (2002). DOI: 10.1103/PhysRevB.65.224412.
- [33] G. Misguich, D. Serban, and V. Pasquier. “Quantum Dimer Model on the Kagome Lattice: Solvable Dimer-Liquid and Ising Gauge Theory”. In: *Phys. Rev. Lett.* 89.13 (2002). DOI: 10.1103/PhysRevLett.89.137202.
- [34] Fa Wang and Ashvin Vishwanath. “Spin-liquid states on the triangular and Kagomé lattices: A projective-symmetry-group analysis of Schwinger boson states”. In: *Phys. Rev. B* 74.17 (2006). DOI: 10.1103/PhysRevB.74.174423.
- [35] Yuan-Ming Lu, Ying Ran, and Patrick A. Lee. “ \mathbb{Z}_2 spin liquids in the $S=1/2$ Heisenberg model on the kagome lattice: A projective symmetry-group study of Schwinger fermion mean-field states”. In: *Phys. Rev. B* 83.22 (2011). DOI: 10.1103/PhysRevB.83.224413.
- [36] Yasir Iqbal, Federico Becca, and Didier Poilblanc. “Projected wave function study of \mathbb{Z}_2 spin liquids on the kagome lattice for the spin- $\frac{1}{2}$ quantum Heisenberg anti-ferromagnet”. In: *Phys. Rev. B* 84.2 (2011). DOI: 10.1103/PhysRevB.84.020407.
- [37] J. B. Marston and C. Zeng. “Spin-Peierls and spin-liquid phases of Kagomé quantum antiferromagnets”. In: *J. Appl. Phys.* 69.8 (1991). DOI: 10.1063/1.347830.

Bibliography

- [38] Laura Messio, Bernard Bernu, and Claire Lhuillier. “Kagome Antiferromagnet: A Chiral Topological Spin Liquid?” In: *Phys. Rev. Lett.* 108.20 (2012). DOI: 10.1103/PhysRevLett.108.207204.
- [39] Laura Messio, Claire Lhuillier, and Grégoire Misguich. “Time reversal symmetry breaking chiral spin liquids: Projective symmetry group approach of bosonic mean-field theories”. In: *Phys. Rev. B* 87.12 (2013). DOI: 10.1103/PhysRevB.87.125127.
- [40] Kun Yang, L. K. Warman, and S. M. Girvin. “Possible spin-liquid states on the triangular and kagomé lattices”. In: *Phys. Rev. Lett.* 70.17 (1993). DOI: 10.1103/PhysRevLett.70.2641.
- [41] A.Yu. Kitaev. “Fault-tolerant quantum computation by anyons”. In: *Ann. Phys.* 303.1 (2003). DOI: 10.1016/S0003-4916(02)00018-0.
- [42] Alexei Kitaev. “Anyons in an exactly solved model and beyond”. In: *Ann. Phys.* 321.1 (2006). January Special Issue. DOI: 10.1016/j.aop.2005.10.005.
- [43] Daniel S. Rokhsar and Steven A. Kivelson. “Superconductivity and the Quantum Hard-Core Dimer Gas”. In: *Phys. Rev. Lett.* 61.20 (1988). DOI: 10.1103/PhysRevLett.61.2376.
- [44] Ronny Thomale et al. “Parent Hamiltonian for the chiral spin liquid”. In: *Phys. Rev. B* 80.10 (2009). DOI: 10.1103/PhysRevB.80.104406.
- [45] Darrell F. Schroeter et al. “Spin Hamiltonian for which the Chiral Spin Liquid is the Exact Ground State”. In: *Phys. Rev. Lett.* 99.9 (2007). DOI: 10.1103/PhysRevLett.99.097202.
- [46] Anne E. B. Nielsen, Germán Sierra, and J. Ignacio Cirac. “Local models of fractional quantum Hall states in lattices and physical implementation”. In: *Nat. Commun.* 4 (2013). DOI: 10.1038/ncomms3864.
- [47] D. Ceperley, G. V. Chester, and M. H. Kalos. “Monte Carlo simulation of a many-fermion study”. In: *Phys. Rev. B* 16.7 (1977). DOI: 10.1103/PhysRevB.16.3081.
- [48] Steven R. White. “Density matrix formulation for quantum renormalization groups”. In: *Phys. Rev. Lett.* 69.19 (1992). DOI: 10.1103/PhysRevLett.69.2863.
- [49] Román Orús. “A practical introduction to tensor networks: Matrix product states and projected entangled pair states”. In: *Ann. Phys.* 349 (2014). DOI: 10.1016/j.aop.2014.06.013.
- [50] Claudine Lacroix, Philippe Mendels, and Frédéric Mila, eds. *Introduction to Frustrated Magnetism*. Vol. 164. Springer Series in Solid-State Sciences. Berlin, Heidelberg: Springer Berlin Heidelberg, 2011. ISBN: 978-3-642-10588-3. DOI: 10.1007/978-3-642-10589-0.

- [51] Lars Onsager. “Crystal Statistics. I. A Two-Dimensional Model with an Order-Disorder Transition”. In: *Phys. Rev.* 65.3-4 (1944). DOI: 10.1103/PhysRev.65.117.
- [52] P. W. Anderson. “An Approximate Quantum Theory of the Antiferromagnetic Ground State”. In: *Phys. Rev.* 86.5 (1952). DOI: 10.1103/PhysRev.86.694.
- [53] P. Azaria, B. Delamotte, and D. Mouhanna. “Spontaneous symmetry breaking in quantum frustrated antiferromagnets”. In: *Phys. Rev. Lett.* 70.16 (1993). DOI: 10.1103/PhysRevLett.70.2483.
- [54] M. Louis Néel. “Propriétés magnétiques des ferrites ; ferrimagnétisme et antiferromagnétisme”. In: *Ann. Phys. (France)* 12.3 (1948). DOI: 10.1051/anphys/194812030137.
- [55] W. Marshall. “Antiferromagnetism”. In: *Proc. R. Soc. A* 232.1188 (1955). DOI: 10.1098/rspa.1955.0200.
- [56] Elliott Lieb and Daniel Mattis. “Ordering Energy Levels of Interacting Spin Systems”. In: *J. Math. Phys.* 3.4 (1962). DOI: 10.1063/1.1724276.
- [57] Alexander Wietek, Michael Schuler, and Andreas M. Läuchli. “Studying Continuous Symmetry Breaking using Energy Level Spectroscopy”. In: *arXiv E-prints* (2017). arXiv: 1704.08622 [cond-mat.str-el].
- [58] L. Messio, C. Lhuillier, and G. Misguich. “Lattice symmetries and regular magnetic orders in classical frustrated antiferromagnets”. In: *Phys. Rev. B* 83.18 (2011). DOI: 10.1103/PhysRevB.83.184401.
- [59] “Field theories with « Superconductor » solutions”. In: *Il Nuovo Cimento* 19.1 (1961). DOI: 10.1007/BF02812722.
- [60] Jeffrey Goldstone, Abdus Salam, and Steven Weinberg. “Broken Symmetries”. In: *Phys. Rev.* 127.3 (1962). DOI: 10.1103/PhysRev.127.965.
- [61] Assa Auerbach. *Interacting Electrons and Quantum Magnetism*. Graduate Texts in Contemporary Physics. Springer New York, 1994. ISBN: 978-1-4612-6928-1. DOI: 10.1007/978-1-4612-0869-3.
- [62] Ryogo Kubo. “The Spin-Wave Theory of Antiferromagnetics”. In: *Phys. Rev.* 87.4 (1952). DOI: 10.1103/PhysRev.87.568.
- [63] S. Toth and B. Lake. “Linear spin wave theory for single-Q incommensurate magnetic structures”. In: *J. Phys.: Condens. Matter* 27.16 (2015). DOI: 10.1088/0953-8984/27/16/166002. arXiv: arXiv:1402.6069v1.
- [64] Elliott H. Lieb. “The classical limit of quantum spin systems”. In: *Commun. Math. Phys.* 31.4 (1973). DOI: 10.1007/BF01646493.

Bibliography

- [65] N. D. Mermin and H. Wagner. “Absence of Ferromagnetism or Antiferromagnetism in One- or Two-Dimensional Isotropic Heisenberg Models”. In: *Phys. Rev. Lett.* 17.22 (1966). DOI: 10.1103/PhysRevLett.17.1133.
- [66] Frédéric Mila. *Frustrated Spin Systems*. Ed. by P. Coleman E. Pavarini, E. Koch. Many-Body. Vol. 5. Forschungszentrum Julich, 2015.
- [67] R. Moessner and J. T. Chalker. “Properties of a Classical Spin Liquid: The Heisenberg Pyrochlore Antiferromagnet”. In: *Phys. Rev. Lett.* 80.13 (1998). DOI: 10.1103/PhysRevLett.80.2929.
- [68] G. H. Wannier. “Antiferromagnetism. The Triangular Ising Net”. In: *Phys. Rev.* 79.2 (1950). DOI: 10.1103/PhysRev.79.357.
- [69] R.M.F. Houtappel. “Order-disorder in hexagonal lattices”. In: *Physica* 16.5 (1950). DOI: 10.1016/0031-8914(50)90130-3.
- [70] I. Syozi. “Statistics of Kagome Lattice”. In: *Prog. Theor. Phys.* 6.3 (1951). DOI: 10.1143/ptp/6.3.306.
- [71] Kenzi Kano and Shigeo Naya. “Antiferromagnetism. The Kagome Ising Net”. In: *Prog. Theor. Phys.* 10.2 (1953). DOI: 10.1143/ptp/10.2.158.
- [72] John Cardy. *Scaling and renormalization in statistical physics*. Vol. 5. Cambridge University Press, 1996. ISBN: 9780521499590.
- [73] Nikolai Nikolajewitsch Bogoljubow. In: *Physik. Abhandl. Sowjetunion* 6, 1, 113, 229 (1962).
- [74] P. C. Hohenberg. “Existence of Long-Range Order in One and Two Dimensions”. In: *Phys. Rev.* 158.2 (1967). DOI: 10.1103/PhysRev.158.383.
- [75] Axel Gelfert and Wolfgang Nolting. “The absence of finite-temperature phase transitions in low-dimensional many-body models: a survey and new results”. In: *J. Phys.: Condens. Matter* 13.27 (2001). DOI: 10.1088/0953-8984/13/27/201.
- [76] Sidney Coleman. “There are no Goldstone bosons in two dimensions”. In: *Commun. Math. Phys.* 31.4 (1973). DOI: 10.1007/BF01646487.
- [77] Efstratios Manousakis. “The spin-1/2 Heisenberg antiferromagnet on a square lattice and its application to the cuprous oxides”. In: *Rev. Mod. Phys.* 63.1 (1991). DOI: 10.1103/RevModPhys.63.1.
- [78] Kenn Kubo and Tatsuya Kishi. “Existence of Long-Range Order in the XXZ Model”. In: *Phys. Rev. Lett.* 61.22 (1988). DOI: 10.1103/PhysRevLett.61.2585.
- [79] Anders W. Sandvik. “Critical Temperature and the Transition from Quantum to Classical Order Parameter Fluctuations in the Three-Dimensional Heisenberg Antiferromagnet”. In: *Phys. Rev. Lett.* 80.23 (1998). DOI: 10.1103/PhysRevLett.80.5196.

- [80] Th. Jolicoeur et al. “Ground-state properties of the $S=1/2$ Heisenberg antiferromagnet on a triangular lattice”. In: *Phys. Rev. B* 42.7 (1990). DOI: 10.1103/PhysRevB.42.4800.
- [81] Andrey V. Chubukov and Th. Jolicoeur. “Order-from-disorder phenomena in Heisenberg antiferromagnets on a triangular lattice”. In: *Phys. Rev. B* 46.17 (1992). DOI: 10.1103/PhysRevB.46.11137.
- [82] P. Lecheminant et al. “ J_1 - J_2 quantum Heisenberg antiferromagnet on the triangular lattice: A group-symmetry analysis of order by disorder”. In: *Phys. Rev. B* 52.9 (1995). DOI: 10.1103/PhysRevB.52.6647. arXiv: arXiv:cond-mat/9504077.
- [83] J. T. Chalker, P. C. W. Holdsworth, and E. F. Shender. “Hidden order in a frustrated system: Properties of the Heisenberg Kagomé antiferromagnet”. In: *Phys. Rev. Lett.* 68.6 (1992). DOI: 10.1103/PhysRevLett.68.855.
- [84] Andrey Chubukov. “Order from disorder in a kagome antiferromagnet”. In: *J. Appl. Phys.* 73.10 (1993). DOI: 10.1063/1.353624.
- [85] S. T. Bramwell, M. J P Gingras, and J. N. Reimers. “Order by disorder in an anisotropic pyrochlore lattice antiferromagnet”. In: *J. Appl. Phys.* 75.10 (1994). DOI: 10.1063/1.355676.
- [86] J. Villain et al. “Order as an effect of disorder”. In: *J. Phys. (France)* 41.11 (1980). DOI: 10.1051/jphys:0198000410110126300.
- [87] E. F. Shender. “Antiferromagnetic garnets with fluctuationally interacting sublattices”. In: *Sov. Phys. JETP* 56.1 (1982).
- [88] R. B. Laughlin. “Anomalous Quantum Hall Effect: An Incompressible Quantum Fluid with Fractionally Charged Excitations”. In: *Phys. Rev. Lett.* 50.18 (1983). DOI: 10.1103/PhysRevLett.50.1395.
- [89] Leon Balents. “Spin liquids in frustrated magnets”. In: *Nature* 464.7286 (2010). DOI: 10.1038/nature08917.
- [90] Lucile Savary and Leon Balents. “Quantum spin liquids: a review”. In: *Rep. Prog. Phys.* 80.1 (2017). DOI: 10.1088/0034-4885/80/1/016502. arXiv: 1601.03742.
- [91] Yi Zhou, Kazushi Kanoda, and Tai-Kai Ng. “Quantum spin liquid states”. In: *Rev. Mod. Phys.* 89.2 (2017). DOI: 10.1103/RevModPhys.89.025003.
- [92] Ian Affleck and J. Brad Marston. “Large- n limit of the Heisenberg-Hubbard model: Implications for high- T_c superconductors”. In: *Phys. Rev. B* 37.7 (1988). DOI: 10.1103/PhysRevB.37.3774.
- [93] J. Brad Marston and Ian Affleck. “Large- n limit of the Hubbard-Heisenberg model”. In: *Phys. Rev. B* 39.16 (1989). DOI: 10.1103/PhysRevB.39.11538.

Bibliography

- [94] Elliott Lieb, Theodore Schultz, and Daniel Mattis. “Two soluble models of an antiferromagnetic chain”. In: *Ann. Phys.* 16.3 (1961). DOI: 10.1016/0003-4916(61)90115-4.
- [95] M. B. Hastings. “Lieb-Schultz-Mattis in higher dimensions”. In: *Phys. Rev. B* 69.10 (2004). DOI: 10.1103/PhysRevB.69.104431. arXiv: 0305505 [cond-mat].
- [96] Elliott H. Lieb and Derek W. Robinson. “The finite group velocity of quantum spin systems”. In: *Commun. Math. Phys.* 28.3 (1972). DOI: 10.1007/BF01645779.
- [97] Anders W. Sandvik. “Evidence for Deconfined Quantum Criticality in a Two-Dimensional Heisenberg Model with Four-Spin Interactions”. In: *Phys. Rev. Lett.* 98.22 (2007). DOI: 10.1103/PhysRevLett.98.227202.
- [98] Franz J. Wegner. “Duality in Generalized Ising Models and Phase Transitions without Local Order Parameters”. In: *J. Math. Phys.* 12.10 (1971). DOI: 10.1063/1.1665530.
- [99] Steven Kivelson. “Statistics of holons in the quantum hard-core dimer gas”. In: *Phys. Rev. B* 39.1 (1989). DOI: 10.1103/PhysRevB.39.259.
- [100] B. Bernu et al. “Exact spectra, spin susceptibilities, and order parameter of the quantum Heisenberg antiferromagnet on the triangular lattice”. In: *Phys. Rev. B* 50.14 (1994). DOI: 10.1103/PhysRevB.50.10048.
- [101] L. Hulthén. *Über das Austauschproblem eines Kristalles*. Arkiv för matematik, astronomi och fysik. Almqvist & Wiksell, 1938.
- [102] M. Karbach et al. “Approach to the spin-1/2 quantum Heisenberg model”. In: *Phys. Rev. B* 48.18 (1993). DOI: 10.1103/PhysRevB.48.13666.
- [103] Martin C. Gutzwiller. “Effect of Correlation on the Ferromagnetism of Transition Metals”. In: *Phys. Rev. Lett.* 10.5 (1963). DOI: 10.1103/PhysRevLett.10.159.
- [104] Claudius Gros. “Physics of projected wavefunctions”. In: *Ann. Phys.* 189.1 (1989). DOI: 10.1016/0003-4916(89)90077-8.
- [105] Xiao-Gang Wen. “Quantum orders and symmetric spin liquids”. In: *Phys. Rev. B* 65.16 (2002). DOI: 10.1103/PhysRevB.65.165113.
- [106] G. Baskaran and P. W. Anderson. “Gauge theory of high-temperature superconductors and strongly correlated Fermi systems”. In: *Phys. Rev. B* 37.1 (1988). DOI: 10.1103/PhysRevB.37.580.
- [107] D. J. Thouless et al. “Quantized Hall Conductance in a Two-Dimensional Periodic Potential”. In: *Phys. Rev. Lett.* 49.6 (1982). DOI: 10.1103/PhysRevLett.49.405.
- [108] Xiao-Gang Wen. “Vacuum degeneracy of chiral spin states in compactified space”. In: *Phys. Rev. B* 40.10 (1989). DOI: 10.1103/PhysRevB.40.7387.

- [109] Vadim Kalmeyer and R. B. Laughlin. “Theory of the spin liquid state of the Heisenberg antiferromagnet”. In: *Phys. Rev. B* 39.16 (1989). DOI: 10.1103/PhysRevB.39.11879.
- [110] Walter Rantner and Xiao-Gang Wen. “Electron Spectral Function and Algebraic Spin Liquid for the Normal State of Underdoped High Tc Superconductors”. In: *Phys. Rev. Lett.* 86.17 (2001). DOI: 10.1103/PhysRevLett.86.3871.
- [111] Michael Hermele, T. Senthil, and Matthew P. A. Fisher. “Algebraic spin liquid as the mother of many competing orders”. In: *Phys. Rev. B* 72.10 (2005). DOI: 10.1103/PhysRevB.72.104404.
- [112] Michael Hermele et al. “Stability of $U(1)$ spin liquids in two dimensions”. In: *Phys. Rev. B* 70.21 (2004). DOI: 10.1103/PhysRevB.70.214437.
- [113] Yasir Iqbal et al. “Spin liquid nature in the Heisenberg $J_1 - J_2$ triangular antiferromagnet”. In: *Phys. Rev. B* 93.14 (2016). DOI: 10.1103/PhysRevB.93.144411. arXiv: arXiv:1601.06018 [cond-mat.str-el].
- [114] Youcef Saad. *Numerical methods for large eigenvalue problems*. Manchester University Press, 1992. ISBN: 978-1-61197-072-2. DOI: 10.1137/1.9781611970739.
- [115] Cornelius Lanczos. “An iteration method for the solution of the eigenvalue problem of linear differential and integral operators”. In: *J. Res. Natl. Bur. Stand.* 45.4 (1950). DOI: 10.6028/jres.045.026.
- [116] Grégoire Allaire and Sidi Mahmoud Kaber. *Numerical Linear Algebra*. Vol. 55. Texts in Applied Mathematics. Springer Verlag New York, 2008. ISBN: 978-0-387-34159-0. DOI: 10.1007/978-0-387-68918-0.
- [117] J. Kuczyński and H. Woźniakowski. “Estimating the Largest Eigenvalue by the Power and Lanczos Algorithms with a Random Start”. In: *SIAM J. Matrix Anal. Appl.* 13.4 (1992). DOI: 10.1137/0613066. arXiv: 1106.1622.
- [118] Horst D. Simon. “Analysis of the symmetric Lanczos algorithm with reorthogonalization methods”. In: *Linear Algebra Appl.* 61 (1984). DOI: 10.1016/0024-3795(84)90025-9.
- [119] C. C. Paige. “Computational Variants of the Lanczos Method for the Eigenproblem”. In: *IMA J. Appl. Math.* 10.3 (1972). DOI: 10.1093/imamat/10.3.373.
- [120] C.C. Paige. “Accuracy and effectiveness of the Lanczos algorithm for the symmetric eigenproblem”. In: *Linear Algebra Appl.* 34 (1980). DOI: 10.1016/0024-3795(80)90167-6.
- [121] Jane Cullum and Ralph A. Willoughby. “A survey of Lanczos procedures for very large real ‘symmetric’ eigenvalue problems”. In: *J. Comput. Appl. Math.* 12 (1985). DOI: 10.1016/0377-0427(85)90006-8.

Bibliography

- [122] E.M. Lifshitz L.D. Landau. *L.D. Landau, E.M. Lifshitz, Lehrbuch der Theoretischen Physik, vol. III, Quantenmechanik, 8th edn.* Akademie-Verlag, Berlin, 1988.
- [123] “Stanislaw Ulam 1909-1984”. In: *Los Alamos Science* 15.Special Issue (1987).
- [124] Walter R. Gilks, Sylvia Richardson, and David Spiegelhalter. *Markov chain Monte Carlo in practice.* CRC press, 1995. ISBN: 9780412055515.
- [125] Nicholas Metropolis et al. “Equation of State Calculations by Fast Computing Machines”. In: *J. Chem. Phys.* 21.6 (1953). DOI: 10.1063/1.1699114.
- [126] Hidemaro Suwa and Syngae Todo. “Markov Chain Monte Carlo method without detailed balance”. In: *Phys. Rev. Lett.* 105.12 (2010). DOI: 10.1103/PhysRevLett.105.120603.
- [127] Ulli Wolff. “Monte Carlo errors with less errors”. In: *Comput. Phys. Commun.* 156.2 (2004). DOI: 10.1016/S0010-4655(03)00467-3. arXiv: 0306017 [hep-lat].
- [128] Vinay Ambegaokar and Matthias Troyer. “Estimating errors reliably in Monte Carlo simulations of the Ehrenfest model”. In: *Am. J. Phys.* 78.2 (2010). DOI: 10.1119/1.3247985. arXiv: 0906.0943.
- [129] Martin C. Gutzwiller. “Correlation of Electrons in a Narrow s Band”. In: *Phys. Rev.* 137.6A (1965). DOI: 10.1103/PhysRev.137.A1726.
- [130] Takashi Yanagisawa. “Lattice distortions and stripes in the underdoped region of high- T_c cuprates”. In: *J. Phys. A: Math. Gen.* 36.35 (2003). DOI: 10.1088/0305-4470/36/35/318.
- [131] H. Q. Lin. “Exact diagonalization of quantum-spin models”. In: *Phys. Rev. B* 42.10 (1990). DOI: 10.1103/PhysRevB.42.6561.
- [132] Alexander Weiße. “Divide and conquer the Hilbert space of translation-symmetric spin systems”. In: *Phys. Rev. E* 87.4 (2013). DOI: 10.1103/PhysRevE.87.043305. arXiv: arXiv:1210.1701.
- [133] Schulz, H.J., Ziman, T.A.L., and Poilblanc, D. “Magnetic Order and Disorder in the Frustrated Quantum Heisenberg Antiferromagnet in Two Dimensions”. In: *J. Phys. (France)* 6.5 (1996). DOI: 10.1051/jp1:1996236.
- [134] Jörg Schulenburg. *SPINPACK*. 2017. URL: <https://www-e.uni-magdeburg.de/jschulen/spin/> (visited on 09/18/2017).
- [135] Mitsuaki Kawamura et al. “Quantum Lattice Model Solver $\mathcal{H}\Phi$ ”. In: *Comput. Phys. Commun.* 217 (2017). DOI: 10.1016/j.cpc.2017.04.006. arXiv: 1703.03637.
- [136] Message Passing Forum. *MPI: A Message-Passing Interface Standard*. Tech. rep. Knoxville, TN, USA, 1994.
- [137] *SHM_OVERVIEW(7) Linux Programmer’s Manual*. 4.13. 2017.

- [138] Syngae Todo and Kiyoshi Kato. “Cluster Algorithms for General- S Quantum Spin Systems”. In: *Phys. Rev. Lett.* 87.4 (2001). DOI: 10.1103/PhysRevLett.87.047203.
- [139] Andreas M. Läuchli, Julien Sudan, and Roderich Moessner. “The $S = 1/2$ Kagome Heisenberg Antiferromagnet Revisited”. In: *arXiv E-prints* (2016). arXiv: 1611.06990.
- [140] Alexander Wietek, Antoine Sterdyniak, and Andreas M. Läuchli. “Nature of chiral spin liquids on the kagome lattice”. In: *Phys. Rev. B* 92.12 (2015). DOI: 10.1103/PhysRevB.92.125122. arXiv: 1503.03389 [cond-mat.str-el].
- [141] P. Nikolic and T. Senthil. “Physics of low-energy singlet states of the Kagome lattice quantum Heisenberg antiferromagnet”. In: *Phys. Rev. B* 68.21 (2003). DOI: 10.1103/PhysRevB.68.214415.
- [142] Rajiv R. P. Singh and David A. Huse. “Ground state of the spin-1/2 kagome-lattice Heisenberg antiferromagnet”. In: *Phys. Rev. B* 76.18 (2007). DOI: 10.1103/PhysRevB.76.180407.
- [143] Didier Poilblanc and Grégoire Misguich. “Competing valence bond crystals in the kagome quantum dimer model”. In: *Phys. Rev. B* 84.21 (2011). DOI: 10.1103/PhysRevB.84.214401.
- [144] Sylvain Capponi et al. “ $p6$ chiral resonating valence bonds in the kagome antiferromagnet”. In: *Phys. Rev. B* 87.16 (2013). DOI: 10.1103/PhysRevB.87.161118.
- [145] P. W. Leung and Veit Elser. “Numerical studies of a 36-site *kagome* antiferromagnet”. In: *Phys. Rev. B* 47.9 (1993). DOI: 10.1103/PhysRevB.47.5459.
- [146] P. Lecheminant et al. “Order versus disorder in the quantum Heisenberg antiferromagnet on the *kagomé* lattice using exact spectra analysis”. In: *Phys. Rev. B* 56.5 (1997). DOI: 10.1103/PhysRevB.56.2521.
- [147] C. Waldtmann et al. “First excitations of the spin 1/2 Heisenberg antiferromagnet on the kagome lattice”. In: *Eur. Phys. J. B* 2.4 (1998). DOI: 10.1007/s100510050274.
- [148] Sylvain Capponi, Andreas Läuchli, and Matthieu Mambrini. “Numerical contractor renormalization method for quantum spin models”. In: *Phys. Rev. B* 70.10 (2004). DOI: 10.1103/PhysRevB.70.104424.
- [149] H. C. Jiang, Z. Y. Weng, and D. N. Sheng. “Density Matrix Renormalization Group Numerical Study of the Kagome Antiferromagnet”. In: *Phys. Rev. Lett.* 101.11 (2008). DOI: 10.1103/PhysRevLett.101.117203.
- [150] David Schwandt, Matthieu Mambrini, and Didier Poilblanc. “Generalized hard-core dimer model approach to low-energy Heisenberg frustrated antiferromagnets: General properties and application to the kagome antiferromagnet”. In: *Phys. Rev. B* 81.21 (2010). DOI: 10.1103/PhysRevB.81.214413.

Bibliography

- [151] Simeng Yan, David A. Huse, and Steven R. White. “Spin-Liquid Ground State of the $S = 1/2$ Kagome Heisenberg Antiferromagnet”. In: *Science* 332.6034 (2011). DOI: 10.1126/science.1201080.
- [152] Andreas M Läuchli. “Introduction to Frustrated Magnetism: Materials, Experiments, Theory”. In: ed. by Claudine Lacroix, Philippe Mendels, and Frédéric Mila. Berlin, Heidelberg: Springer Berlin Heidelberg, 2011. Chap. Numerical Simulations of Frustrated Systems, pp. 481–511. DOI: 10.1007/978-3-642-10589-0_{_}18.
- [153] Hong-Chen Jiang, Zhenghan Wang, and Leon Balents. “Identifying topological order by entanglement entropy”. In: *Nat. Phys.* 8.12 (2012). DOI: 10.1038/nphys2465.
- [154] Stefan Depenbrock, Ian P. McCulloch, and Ulrich Schollwöck. “Nature of the Spin-Liquid Ground State of the $S = 1/2$ Heisenberg Model on the Kagome Lattice”. In: *Phys. Rev. Lett.* 109.6 (2012). DOI: 10.1103/PhysRevLett.109.067201.
- [155] Satoshi Nishimoto, Naokazu Shibata, and Chisa Hotta. “Controlling frustrated liquids and solids with an applied field in a kagome Heisenberg antiferromagnet”. In: *Nat. Commun.* 4 (2013).
- [156] Bryan K. Clark et al. “Striped Spin Liquid Crystal Ground State Instability of Kagome Antiferromagnets”. In: *Phys. Rev. Lett.* 111.18 (2013). DOI: 10.1103/PhysRevLett.111.187205.
- [157] Sylvain Capponi et al. “Numerical study of magnetization plateaus in the spin- $\frac{1}{2}$ kagome Heisenberg antiferromagnet”. In: *Phys. Rev. B* 88.14 (2013). DOI: 10.1103/PhysRevB.88.144416.
- [158] Tsutomu Momoi, Kenn Kubo, and Koji Niki. “Possible Chiral Phase Transition in Two-Dimensional Solid ^3He ”. In: *Phys. Rev. Lett.* 79.11 (1997). DOI: 10.1103/PhysRevLett.79.2081.
- [159] A. Läuchli, G. Schmid, and M. Troyer. “Phase diagram of a spin ladder with cyclic four-spin exchange”. In: *Phys. Rev. B* 67.10 (2003). DOI: 10.1103/PhysRevB.67.100409.
- [160] Shou-Shu Gong, Wei Zhu, and D. N. Sheng. “Emergent Chiral Spin Liquid: Fractional Quantum Hall Effect in a Kagome Heisenberg Model”. In: *Sci. Rep.* 4 (2014).
- [161] B. Bauer et al. “Chiral spin liquid and emergent anyons in a Kagome lattice Mott insulator”. In: *Nat. Commun.* 5.5137 (2014). DOI: 10.1038/ncomms6137.
- [162] Yin-Chen He, D. N. Sheng, and Yan Chen. “Chiral Spin Liquid in a Frustrated Anisotropic Kagome Heisenberg Model”. In: *Phys. Rev. Lett.* 112.13 (2014). DOI: 10.1103/PhysRevLett.112.137202.
- [163] Yin-Chen He and Yan Chen. “Distinct Spin Liquids and Their Transitions in Spin- $1/2$ XXZ Kagome Antiferromagnets”. In: *Phys. Rev. Lett.* 114.3 (2015). DOI: 10.1103/PhysRevLett.114.037201.

- [164] Michael Freedman et al. “A class of P,T-invariant topological phases of interacting electrons”. In: *Ann. Phys.* 310.2 (2004). DOI: <http://dx.doi.org/10.1016/j.aop.2004.01.006>.
- [165] N. Regnault and B. Andrei Bernevig. “Fractional Chern Insulator”. In: *Phys. Rev. X* 1.2 (2011). DOI: 10.1103/PhysRevX.1.021014.
- [166] A. M. Läuchli et al. “Hierarchy of Fractional Chern Insulators and Competing Compressible States”. In: *Phys. Rev. Lett.* 111.12 (2013). DOI: 10.1103/PhysRevLett.111.126802.
- [167] Anne E. B. Nielsen, J. Ignacio Cirac, and Germán Sierra. “Laughlin Spin-Liquid States on Lattices Obtained from Conformal Field Theory”. In: *Phys. Rev. Lett.* 108.25 (2012). DOI: 10.1103/PhysRevLett.108.257206.
- [168] Martin Greiter, Darrell F. Schroeter, and Ronny Thomale. “Parent Hamiltonian for the non-Abelian chiral spin liquid”. In: *Phys. Rev. B* 89.16 (2014). DOI: 10.1103/PhysRevB.89.165125.
- [169] D. N. Sheng et al. “Fractional quantum Hall effect in the absence of Landau levels”. In: *Nat. Commun.* 2 (2011). DOI: 10.1038/ncomms1380.
- [170] Titus Neupert et al. “Fractional Quantum Hall States at Zero Magnetic Field”. In: *Phys. Rev. Lett.* 106.23 (2011). DOI: 10.1103/PhysRevLett.106.236804.
- [171] J.-W. Mei, E. Tang, and X.-G. Wen. “Chiral spin states in polarized kagome spin systems with spin-orbit coupling”. In: *ArXiv e-prints* (2011). arXiv: 1102.2406 [cond-mat.str-el].
- [172] K. Kumar, K. Sun, and E. Fradkin. “Chern-Simons theory of the magnetization plateaus of the spin-1/2 quantum XXZ Heisenberg model on Kagome Lattice”. In: *ArXiv e-prints* (2014). arXiv: 1409.2171 [cond-mat.str-el].
- [173] G. Baskaran, Z. Zou, and P.W. Anderson. “The resonating valence bond state and high-Tc superconductivity ? A mean field theory”. In: *Solid State Communications* 63.11 (1987). DOI: [http://dx.doi.org/10.1016/0038-1098\(87\)90642-9](http://dx.doi.org/10.1016/0038-1098(87)90642-9).
- [174] Ian Affleck et al. “SU(2) gauge symmetry of the large- U limit of the Hubbard model”. In: *Phys. Rev. B* 38.1 (1988). DOI: 10.1103/PhysRevB.38.745.
- [175] Elbio Dagotto, Eduardo Fradkin, and Adriana Moreo. “SU(2) gauge invariance and order parameters in strongly coupled electronic systems”. In: *Phys. Rev. B* 38.4 (1988). DOI: 10.1103/PhysRevB.38.2926.
- [176] Xiao-Gang Wen and Patrick A. Lee. “Theory of Underdoped Cuprates”. In: *Phys. Rev. Lett.* 76.3 (1996). DOI: 10.1103/PhysRevLett.76.503.
- [177] T. Senthil and Matthew P. A. Fisher. “ Z_2 gauge theory of electron fractionalization in strongly correlated systems”. In: *Phys. Rev. B* 62.12 (2000). DOI: 10.1103/PhysRevB.62.7850.

Bibliography

- [178] Xiao Gang Wen. *Quantum Field Theory of Many-Body Systems: From the Origin of Sound to an Origin of Light and Electrons*. Oxford: Oxford Univ. Press, 2004.
- [179] Wen-Jun Hu et al. “Variational Monte Carlo study of a chiral spin liquid in the extended Heisenberg model on the kagome lattice”. In: *Phys. Rev. B* 91.4 (2015). DOI: 10.1103/PhysRevB.91.041124.
- [180] Shou-Shu Gong et al. “Global phase diagram of competing ordered and quantum spin-liquid phases on the kagome lattice”. In: *Phys. Rev. B* 91.7 (2015). DOI: 10.1103/PhysRevB.91.075112.
- [181] J.-W. Mei and X.-G. Wen. “Modular matrices from universal wave function overlaps in Gutzwiller-projected parton wave functions”. In: *ArXiv e-prints* (2014). arXiv: 1409.5427 [cond-mat.str-el].
- [182] Alexander Wietek and Andreas M. Läuchli. “Chiral spin liquid and quantum criticality in extended $S = \frac{1}{2}$ Heisenberg models on the triangular lattice”. In: *Phys. Rev. B* 95.3 (2017). DOI: 10.1103/PhysRevB.95.035141. arXiv: 1604.07829 [cond-mat.str-el].
- [183] Michael Levin and Xiao-Gang Wen. “Detecting Topological Order in a Ground State Wave Function”. In: *Phys. Rev. Lett.* 96.11 (2006).
- [184] Ciarán Hickey et al. “Haldane-Hubbard Mott Insulator: From Tetrahedral Spin Crystal to Chiral Spin Liquid”. In: *Phys. Rev. Lett.* 116.13 (2016). DOI: 10.1103/PhysRevLett.116.137202.
- [185] Pierre Nataf et al. “Chiral Spin Liquids in Triangular-Lattice $SU(N)$ Fermionic Mott Insulators with Artificial Gauge Fields”. In: *Phys. Rev. Lett.* 117.16 (2016). DOI: 10.1103/PhysRevLett.117.167202. arXiv: 1601.00958 [cond-mat.quant-gas].
- [186] Krishna Kumar, Kai Sun, and Eduardo Fradkin. “Chiral spin liquids on the kagome lattice”. In: *Phys. Rev. B* 92.9 (2015). DOI: 10.1103/PhysRevB.92.094433.
- [187] Gregory Gorohovsky, Rodrigo G. Pereira, and Eran Sela. “Chiral spin liquids in arrays of spin chains”. In: *Phys. Rev. B* 91.24 (2015). DOI: 10.1103/PhysRevB.91.245139.
- [188] Tobias Meng et al. “Coupled-wire construction of chiral spin liquids”. In: *Phys. Rev. B* 91.24 (2015). DOI: 10.1103/PhysRevB.91.241106.
- [189] Luca Capriotti, Adolfo E. Trumper, and Sandro Sorella. “Long-Range Néel Order in the Triangular Heisenberg Model”. In: *Phys. Rev. Lett.* 82.19 (1999). DOI: 10.1103/PhysRevLett.82.3899.
- [190] Steven R. White and A. L. Chernyshev. “Néel Order in Square and Triangular Lattice Heisenberg Models”. In: *Phys. Rev. Lett.* 99.12 (2007). DOI: 10.1103/PhysRevLett.99.127004.

- [191] Diptiman Sen and R. Chitra. “Large- U limit of a Hubbard model in a magnetic field: Chiral spin interactions and paramagnetism”. In: *Phys. Rev. B* 51.3 (1995). DOI: 10.1103/PhysRevB.51.1922.
- [192] Olexei I. Motrunich. “Orbital magnetic field effects in spin liquid with spinon Fermi sea: Possible application to κ -(ET) $_2$ Cu $_2$ (CN) $_3$ ”. In: *Phys. Rev. B* 73.15 (2006). DOI: 10.1103/PhysRevB.73.155115.
- [193] M. Aidelsburger et al. “Realization of the Hofstadter Hamiltonian with Ultracold Atoms in Optical Lattices”. In: *Phys. Rev. Lett.* 111.18 (2013). DOI: 10.1103/PhysRevLett.111.185301.
- [194] Hirokazu Miyake et al. “Realizing the harper hamiltonian with laser-assisted tunneling in optical lattices”. In: *Phys. Rev. Lett.* 111.18 (2013). DOI: 10.1103/PhysRevLett.111.185302. arXiv: 1308.1431.
- [195] Ryui Kaneko, Satoshi Morita, and Masatoshi Imada. “Gapless Spin-Liquid Phase in an Extended Spin 1/2 Triangular Heisenberg Model”. In: *J. Phys. Soc. Jpn.* 83.9 (2014). DOI: 10.7566/JPSJ.83.093707. arXiv: arXiv:1407.0318 [cond-mat.str-el].
- [196] Zhenyue Zhu and Steven R. White. “Spin liquid phase of the $S = \frac{1}{2} J_1 - J_2$ Heisenberg model on the triangular lattice”. In: *Phys. Rev. B* 92.4 (2015). DOI: 10.1103/PhysRevB.92.041105. arXiv: arXiv:1502.04831 [cond-mat.str-el].
- [197] S. N. Saadatmand, B. J. Powell, and I. P. McCulloch. “Phase diagram of the spin $-\frac{1}{2}$ triangular $J_1 - J_2$ Heisenberg model on a three-leg cylinder”. In: *Phys. Rev. B* 91.24 (2015). DOI: 10.1103/PhysRevB.91.245119.
- [198] Wen-Jun Hu et al. “Competing spin-liquid states in the spin- $\frac{1}{2}$ Heisenberg model on the triangular lattice”. In: *Phys. Rev. B* 92.14 (2015). DOI: 10.1103/PhysRevB.92.140403. arXiv: arXiv:1504.00654 [cond-mat.str-el].
- [199] Ryan V. Mishmash et al. “Theory of a Competitive Spin Liquid State for Weak Mott Insulators on the Triangular Lattice”. In: *Phys. Rev. Lett.* 111.15 (2013). DOI: 10.1103/PhysRevLett.111.157203.
- [200] Andrey V. Chubukov, T. Senthil, and Subir Sachdev. “Universal magnetic properties of frustrated quantum antiferromagnets in two dimensions”. In: *Phys. Rev. Lett.* 72.13 (1994). DOI: 10.1103/PhysRevLett.72.2089. arXiv: 9311045 [cond-mat].
- [201] Andrey V. Chubukov, Subir Sachdev, and T. Senthil. “Quantum phase transitions in frustrated quantum antiferromagnets”. In: *Nucl. Phys. B* 426.3 (1994). DOI: 10.1016/0550-3213(94)90023-X.
- [202] Seth Whitsitt and Subir Sachdev. “Transition from the Z_2 spin liquid to anti-ferromagnetic order: Spectrum on the torus”. In: *Phys. Rev. B* 94.8 (2016). DOI: 10.1103/PhysRevB.94.085134.

Bibliography

- [203] Alex Thomson and Subir Sachdev. “Spectrum of conformal gauge theories on a torus”. In: *ArXiv e-prints* (2016). arXiv: 1607.05279 [cond-mat].
- [204] Claire Lhuillier and Grégoire Misguich. “Frustrated Quantum Magnets”. In: *High Magnetic Fields: Applications in Condensed Matter Physics and Spectroscopy*. Ed. by C. Berthier, L. P. Lévy, and G. Martinez. Berlin, Heidelberg: Springer Berlin Heidelberg, 2001, pp. 161–190. DOI: 10.1007/3-540-45649-X_6. arXiv: arXiv:cond-mat/0502464 [cond-mat.str-el].
- [205] Ioannis Rousochatzakis, Andreas M. Läuchli, and Frédéric Mila. “Highly frustrated magnetic clusters: The kagomé on a sphere”. In: *Phys. Rev. B* 77.9 (2008). DOI: 10.1103/PhysRevB.77.094420. arXiv: arXiv:0711.3231 [cond-mat.other].
- [206] See Supplemental Material at <https://journals.aps.org/prb/supplemental/10.1103/PhysRevB.95.035141> for further information concerning details on the Exact Diagonalization calculations, the tower of states analysis and the Gutzwiller projected Dirac spin liquid.
- [207] Kenn Kubo and Tsutomu Momoi. “Ground state of a spin system with two- and four-spin exchange interactions on the triangular lattice”. In: *Z. Phys. B: Condens. Matter* 103.3 (1997). DOI: 10.1007/s002570050403.
- [208] Tigran A. Sedrakyan, Leonid I. Glazman, and Alex Kamenev. “Spontaneous Formation of a Nonuniform Chiral Spin Liquid in a Moat-Band Lattice”. In: *Phys. Rev. Lett.* 114.3 (2015). DOI: 10.1103/PhysRevLett.114.037203.
- [209] Samuel Bieri, Claire Lhuillier, and Laura Messio. “Projective symmetry group classification of chiral spin liquids”. In: *Phys. Rev. B* 93.9 (2016). DOI: 10.1103/PhysRevB.93.094437.
- [210] Jia-Wei Mei and Xiao-Gang Wen. “Modular matrices from universal wave-function overlaps in Gutzwiller-projected parton wave functions”. In: *Phys. Rev. B* 91.12 (2015). DOI: 10.1103/PhysRevB.91.125123.
- [211] Wen-Jun Hu, Shou-Shu Gong, and D. N. Sheng. “Variational Monte Carlo study of chiral spin liquid in quantum antiferromagnet on the triangular lattice”. In: *Phys. Rev. B* 94.7 (2016). DOI: 10.1103/PhysRevB.94.075131.
- [212] Yuan-Ming Lu. “Symmetric Z_2 spin liquids and their neighboring phases on triangular lattice”. In: *Phys. Rev. B* 93.16 (2016). DOI: 10.1103/PhysRevB.93.165113.
- [213] Tiamhock Tay and Olexei I. Motrunich. “Failure of Gutzwiller-type wave function to capture gauge fluctuations: Case study in the exciton Bose liquid context”. In: *Phys. Rev. B* 83.23 (2011). DOI: 10.1103/PhysRevB.83.235122.
- [214] Tarun Grover. “Entanglement Monotonicity and the Stability of Gauge Theories in Three Spacetime Dimensions”. In: *Phys. Rev. Lett.* 112.15 (2014). DOI: 10.1103/PhysRevLett.112.151601.

- [215] A. F. Albuquerque et al. “Phase diagram of a frustrated quantum antiferromagnet on the honeycomb lattice: Magnetic order versus valence-bond crystal formation”. In: *Phys. Rev. B* 84.2 (2011). DOI: 10.1103/PhysRevB.84.024406.
- [216] T. Senthil et al. “Deconfined Quantum Critical Points”. In: *Science* 303.5663 (2004). DOI: 10.1126/science.1091806.
- [217] Congjun Wu, Jiang-ping Hu, and Shou-cheng Zhang. “Exact SO(5) Symmetry in the Spin-3/2 Fermionic System”. In: *Phys. Rev. Lett.* 91.18 (2003). DOI: 10.1103/PhysRevLett.91.186402.
- [218] Carsten Honerkamp and Walter Hofstetter. “Ultracold Fermions and the SU(N) Hubbard Model”. In: *Phys. Rev. Lett.* 92.17 (2004). DOI: 10.1103/PhysRevLett.92.170403.
- [219] M. A. Cazalilla, A. F. Ho, and M. Ueda. “Ultracold gases of ytterbium: ferromagnetism and Mott states in an SU(6) Fermi system”. In: *New J. Phys.* 11.10 (2009).
- [220] A. V. Gorshkov et al. “Two-orbital SU(N) magnetism with ultracold alkaline-earth atoms”. In: *Nat. Phys.* 6.4 (2010). DOI: 10.1038/nphys1535.
- [221] F. Scazza et al. “Observation of two-orbital spin-exchange interactions with ultracold SU(N)- symmetric fermions”. In: *Nat. Phys.* 8 (2014). DOI: 10.1038/nphys3061.
- [222] Guido Pagano et al. “A one-dimensional liquid of fermions with tunable spin”. In: *Nat. Phys.* 10.3 (2014). DOI: 10.1038/nphys2878.
- [223] X. Zhang et al. “Spectroscopic observation of SU(N)-symmetric interactions in Sr orbital magnetism.” In: *Science* 345.6203 (2014). DOI: 10.1126/science.1254978.
- [224] Miguel A. Cazalilla and Ana Maria Rey. “Ultracold Fermi gases with emergent SU(N) symmetry”. In: *Rep. Prog. Phys.* 77.12 (2014).
- [225] Pierre Nataf and Frédéric Mila. “Exact Diagonalization of Heisenberg SU(N) Models”. In: *Phys. Rev. Lett.* 113.12 (2014). DOI: 10.1103/PhysRevLett.113.127204.
- [226] N. Read and Subir Sachdev. “Some features of the phase diagram of the square lattice SU(N) antiferromagnet”. In: *Nucl. Phys. B* 316.3 (1989). DOI: 10.1016/0550-3213(89)90061-8.
- [227] N. Read and Subir Sachdev. “Spin-Peierls, valence-bond solid, and Néel ground states of low-dimensional quantum antiferromagnets”. In: *Phys. Rev. B* 42.7 (1990). DOI: 10.1103/PhysRevB.42.4568.
- [228] Kenji Harada, Naoki Kawashima, and Matthias Troyer. “Néel and Spin-Peierls Ground States of Two-Dimensional SU(N) Quantum Antiferromagnets”. In: *Phys. Rev. Lett.* 90.11 (2003). DOI: 10.1103/PhysRevLett.90.117203.

Bibliography

- [229] Naoki Kawashima and Yuta Tanabe. “Ground States of the $SU(N)$ Heisenberg Model”. In: *Phys. Rev. Lett.* 98.5 (2007). DOI: 10.1103/PhysRevLett.98.057202.
- [230] Tsuyoshi Okubo et al. “ $SU(N)$ Heisenberg model with multicolumn representations”. In: *Phys. Rev. B* 92.13 (2015). DOI: 10.1103/PhysRevB.92.134404.
- [231] F. D. M. Haldane. “Nonlinear Field Theory of Large-Spin Heisenberg Antiferromagnets: Semiclassically Quantized Solitons of the One-Dimensional Easy-Axis Néel State”. In: *Phys. Rev. Lett.* 50.15 (1983). DOI: 10.1103/PhysRevLett.50.1153.
- [232] Dominic V. Else et al. “Symmetry-Protected Phases for Measurement-Based Quantum Computation”. In: *Phys. Rev. Lett.* 108.24 (2012). DOI: 10.1103/PhysRevLett.108.240505.
- [233] Andrew S. Darmawan, Gavin K. Brennen, and Stephen D. Bartlett. “Measurement-based quantum computation in a two-dimensional phase of matter”. In: *New J. Phys.* 14.1 (2012). DOI: 10.1088/1367-2630/14/1/013023.
- [234] Xie Chen, Zheng-Xin Liu, and Xiao-Gang Wen. “Two-dimensional symmetry-protected topological orders and their protected gapless edge excitations”. In: *Phys. Rev. B* 84.23 (2011). DOI: 10.1103/PhysRevB.84.235141.
- [235] Yi-Zhuang You et al. “Quantum phase transitions between bosonic symmetry-protected topological states without sign problem: Nonlinear sigma model with a topological term”. In: *Phys. Rev. B* 93.12 (2016). DOI: 10.1103/PhysRevB.93.125101.
- [236] Yi-Zhuang You et al. “Wave Function and Strange Correlator of Short-Range Entangled States”. In: *Phys. Rev. Lett.* 112.24 (2014). DOI: 10.1103/PhysRevLett.112.247202.
- [237] Keola Wierschem and Pinaki Sengupta. “Strange correlations in spin-1 Heisenberg antiferromagnets”. In: *Phys. Rev. B* 90.11 (2014). DOI: 10.1103/PhysRevB.90.115157.
- [238] K. S. D. Beach et al. “ $SU(N)$ Heisenberg model on the square lattice: A continuous- N quantum Monte Carlo study”. In: *Phys. Rev. B* 80.18 (2009). DOI: 10.1103/PhysRevB.80.184401.
- [239] T. Senthil et al. “Quantum criticality beyond the Landau-Ginzburg-Wilson paradigm”. In: *Phys. Rev. B* 70.14 (2004). DOI: 10.1103/PhysRevB.70.144407.
- [240] J. Schwinger. *ON ANGULAR MOMENTUM*, Atomic Energy Commission Report NoNYO-3071. Jan. 1952. DOI: 10.2172/4389568.
- [241] K. Wierschem and K. S. D. Beach. “Detection of symmetry-protected topological order in AKLT states by exact evaluation of the strange correlator”. In: *Phys. Rev. B* 93.24 (2016). DOI: 10.1103/PhysRevB.93.245141.

- [242] Marcel den Nijs and Koos Rommelse. “Preroughening transitions in crystal surfaces and valence-bond phases in quantum spin chains”. In: *Phys. Rev. B* 40.7 (1989). DOI: 10.1103/PhysRevB.40.4709.
- [243] Masaaki Nakamura and Synge Todo. “Order Parameter to Characterize Valence-Bond-Solid States in Quantum Spin Chains”. In: *Phys. Rev. Lett.* 89.7 (2002). DOI: 10.1103/PhysRevLett.89.077204.
- [244] Kasper Duivenvoorden and Thomas Quella. “Discriminating string order parameter for topological phases of gapped $SU(N)$ spin chains”. In: *Phys. Rev. B* 86.23 (2012). DOI: 10.1103/PhysRevB.86.235142.
- [245] H. G. Evertz. “The loop algorithm”. In: *Adv. Phys.* 52.1 (2003). DOI: 10.1080/0001873021000049195.
- [246] Synge Todo. “Loop Algorithm”. In: *Strongly Correlated Systems: Numerical Methods*. Ed. by Adolfo Avella and Ferdinando Mancini. Berlin, Heidelberg: Springer Berlin Heidelberg, 2013, pp. 153–184. DOI: 10.1007/978-3-642-35106-8_6.
- [247] Olav F. Syljuåsen and Anders W. Sandvik. “Quantum Monte Carlo with directed loops”. In: *Phys. Rev. E* 66.4 (2002). DOI: 10.1103/PhysRevE.66.046701.
- [248] Naoki Kawashima and Kenji Harada. “Recent Developments of World-Line Monte Carlo Methods”. In: *J. Phys. Soc. Jpn.* 73.6 (2004). DOI: 10.1143/JPSJ.73.1379.
- [249] Synge Todo. *worms: a simple worm code*. <https://github.com/wistaria/worms>. 2014.
- [250] Kenji Harada et al. “Possibility of deconfined criticality in $SU(N)$ Heisenberg models at small N ”. In: *Phys. Rev. B* 88.22 (2013). DOI: 10.1103/PhysRevB.88.220408.
- [251] Shou-Shu Gong et al. “Global phase diagram and quantum spin liquids in a spin- $\frac{1}{2}$ triangular antiferromagnet”. In: *Phys. Rev. B* 96.7 (2017). DOI: 10.1103/PhysRevB.96.075116.
- [252] Tarun Grover and T. Senthil. “Non-Abelian Spin Liquid in a Spin-One Quantum Magnet”. In: *Phys. Rev. Lett.* 107.7 (2011). DOI: 10.1103/PhysRevLett.107.077203.
- [253] Po-Hao Huang et al. “Non-Abelian topological spin liquids from arrays of quantum wires or spin chains”. In: *Phys. Rev. B* 93.20 (2016). DOI: 10.1103/PhysRevB.93.205123.
- [254] Michael Hermele and Victor Gurarie. “Topological liquids and valence cluster states in two-dimensional $SU(N)$ magnets”. In: *Phys. Rev. B* 84.17 (2011). DOI: 10.1103/PhysRevB.84.174441.
- [255] Yi Zhang et al. “Quasiparticle statistics and braiding from ground-state entanglement”. In: *Phys. Rev. B* 85.23 (2012). DOI: 10.1103/PhysRevB.85.235151.

Bibliography

- [256] Alexei Kitaev and John Preskill. “Topological Entanglement Entropy”. In: *Phys. Rev. Lett.* 96.11 (2006). DOI: 10.1103/PhysRevLett.96.110404.
- [257] Yin-Chen He et al. “Kagome Chiral Spin Liquid as a Gauged $U(1)$ Symmetry Protected Topological Phase”. In: *Phys. Rev. Lett.* 115.26 (2015). DOI: 10.1103/PhysRevLett.115.267209.
- [258] E. R. Gagliano and C. A. Balseiro. “Dynamical Properties of Quantum Many-Body Systems at Zero Temperature”. In: *Phys. Rev. Lett.* 59.26 (1987). DOI: 10.1103/PhysRevLett.59.2999.
- [259] Tae Jun Park and J. C. Light. “Unitary quantum time evolution by iterative Lanczos reduction”. In: *J. Chem. Phys.* 85.10 (1986). DOI: 10.1063/1.451548.
- [260] Carlo B. Krimphoff. “Quench Dynamics of closed quantum Many-Body Systems”. PhD thesis. Leopold-Franzens-Universität Innsbruck, 2017.
- [261] F. D. M. Haldane and Daniel P. Arovas. “Quantized spin currents in two-dimensional chiral magnets”. In: *Phys. Rev. B* 52.6 (1995). DOI: 10.1103/PhysRevB.52.4223.
- [262] Hosho Katsura, Naoto Nagaosa, and Patrick A. Lee. “Theory of the Thermal Hall Effect in Quantum Magnets”. In: *Phys. Rev. Lett.* 104.6 (2010). DOI: 10.1103/PhysRevLett.104.066403.
- [263] Kentaro Nomura et al. “Cross-Correlated Responses of Topological Superconductors and Superfluids”. In: *Phys. Rev. Lett.* 108.2 (2012). DOI: 10.1103/PhysRevLett.108.026802.
- [264] Kaden R. A. Hazzard et al. “Quantum correlations and entanglement in far-from-equilibrium spin systems”. In: *Phys. Rev. A* 90.6 (2014). DOI: 10.1103/PhysRevA.90.063622.
- [265] Youhei Yamaji et al. “First-Principles Study of the Honeycomb-Lattice Iridates Na_2IrO_3 in the Presence of Strong Spin-Orbit Interaction and Electron Correlations”. In: *Phys. Rev. Lett.* 113.10 (2014). DOI: 10.1103/PhysRevLett.113.107201.
- [266] K. W. Plumb et al. “ α - RuCl_3 : A spin-orbit assisted Mott insulator on a honeycomb lattice”. In: *Phys. Rev. B* 90.4 (2014). DOI: 10.1103/PhysRevB.90.041112.
- [267] A. Banerjee et al. “Proximate Kitaev quantum spin liquid behaviour in a honeycomb magnet”. In: *Nat. Mater.* (2016). DOI: 10.1038/nmat4604.
- [268] Andreas Koitzsch et al. *Low temperature enhancement of ferromagnetic Kitaev correlations in α - RuCl_3* . 2017.
- [269] Ioannis Rousochatzakis et al. “Dzyaloshinskii-Moriya anisotropy and nonmagnetic impurities in the $s = \frac{1}{2}$ kagome system $\text{ZnCu}_3(\text{OH})_6\text{Cl}_2$ ”. In: *Phys. Rev. B* 79.21 (2009). DOI: 10.1103/PhysRevB.79.214415.

- [270] Jie Lou, Anders W. Sandvik, and Naoki Kawashima. “Antiferromagnetic to valence-bond-solid transitions in two-dimensional $SU(N)$ Heisenberg models with multispin interactions”. In: *Phys. Rev. B* 80.18 (2009). DOI: 10.1103/PhysRevB.80.180414.
- [271] Robert S. Mulliken. “Report on Notation for the Spectra of Polyatomic Molecules”. In: *J. Chem. Phys.* 23.11 (1955). DOI: 10.1063/1.1740655.
- [272] Grégoire Misguich and Philippe Sindzingre. “Detecting spontaneous symmetry breaking in finite-size spectra of frustrated quantum antiferromagnets”. In: *J. Phys.: Condens. Matter* 19.14 (2007). DOI: 10.1088/0953-8984/19/14/145202. arXiv: arXiv:cond-mat/0607764 [cond-mat.str-el].

List of Publications

Alexander Wietek, Antoine Sterdyniak, and Andreas M. Läuchli. “Nature of chiral spin liquids on the kagome lattice”. In: *Phys. Rev. B* 92.12 (2015). DOI: 10.1103/PhysRevB.92.125122. arXiv: 1503.03389 [cond-mat.str-el]

Pierre Nataf, Miklós Lajkó, Alexander Wietek, Karlo Penc, Frédéric Mila, and Andreas M. Läuchli. “Chiral Spin Liquids in Triangular-Lattice $SU(N)$ Fermionic Mott Insulators with Artificial Gauge Fields”. In: *Phys. Rev. Lett.* 117.16 (2016). DOI: 10.1103/PhysRevLett.117.167202. arXiv: 1601.00958 [cond-mat.quant-gas]

Alexander Wietek and Andreas M. Läuchli. “Chiral spin liquid and quantum criticality in extended $S = \frac{1}{2}$ Heisenberg models on the triangular lattice”. In: *Phys. Rev. B* 95.3 (2017). DOI: 10.1103/PhysRevB.95.035141. arXiv: 1604.07829 [cond-mat.str-el]

Alexander Wietek, Michael Schuler, and Andreas M. Läuchli. “Studying Continuous Symmetry Breaking using Energy Level Spectroscopy”. In: *arXiv E-prints* (2017). arXiv: 1704.08622 [cond-mat.str-el]

Eidesstattliche Erklärung

Ich erkläre hiermit an Eides statt durch meine eigenhändige Unterschrift, dass ich die vorliegende Arbeit selbständig verfasst und keine anderen als die angegebenen Quellen und Hilfsmittel verwendet habe. Alle Stellen, die wörtlich oder inhaltlich den angegebenen Quellen entnommen wurden, sind als solche kenntlich gemacht.

Die vorliegende Arbeit wurde bisher in gleicher oder ähnlicher Form noch nicht als Dissertation eingereicht.

Innsbruck, den

Alexander Wietek, M.Sc., M.Sc.